Université de Montréal

The Effects of Additives and Chemical Modification on the Solution Properties of Thermo-Sensitive Polymers

par
Na Xue

Département de chimie
Faculté des arts et des sciences

Thèse présentée à la Faculté des études supérieures et postdoctorales
en vue de l'obtention du grade de Philosophiae Doctor (Ph.D.)
en chimie

April, 2015

Résumé

Cette thèse concerne l'étude de phase de séparation de deux polymères thermosensibles connus-poly(*N*-isopropylacylamide) (PNIPAM) et poly(2-isopropyl-2-oxazoline) (PIPOZ). Parmi des études variées sur ces deux polymères, il y a encore deux parties de leurs propriétés thermiques inexplicites à être étudiées. Une partie concerne l'effet de consolvant de PNIPAM dans l'eau et un autre solvant hydromiscible. L'autre est l'effet de propriétés de groupes terminaux de chaînes sur la séparation de phase de PIPOZ.

Pour ce faire, nous avons d'abord étudié l'effet de l'architecture de chaînes sur l'effet de cosolvant de PNIPAMs dans le mélange de méthanol/eau en utilisant un PNIPAM en étoile avec 4 branches et un PNIPAM cyclique comme modèles. Avec PNIPAM en étoile, l'adhérence de branches PNIPAM de à un cœur hydrophobique provoque une réduction de T_c (la température du point de turbidité) et une enthalpie plus faible de la transition de phase. En revanche, la T_c de PNIPAM en étoile dépend de la masse molaire de polymère. La coopérativité de déhydratation diminue pour PNIPAM en étoile et PNIPAM cyclique à cause de la limite topologique.

Une étude sur l'influence de concentration en polymère sur l'effet de cosolvant de PNIPAM dans le mélange méthanol/eau a montré qu'une séparation de phase liquide-liquide macroscopique (MLLPS) a lieu pour une solution de PNIPAM dans le mélange méthanol/eau avec la fraction molaire de méthanol entre 0.127 et 0.421 et la concentration en PNIPAM est constante à 10 $g.L^{-1}$. Après deux jours d'équilibration à température ambiante, la suspension turbide de PNIPAM dans le mélange méthanol/eau se sépare en deux phases dont une phase possède beaucoup plus de PNIPAM que l'autre.

Un diagramme de phase qui montre la MLLPS pour le mélange PNIPAM/eau/méthanol a été établi à base de données expérimentales. La taille et la morphologie de gouttelettes dans la phase riche en polymère condensée dépendent de la fraction molaire de méthanol. Parce que la présence de méthanol influence la tension de surface des gouttelettes liquides, un équilibre lent de la séparation de phase pour PNIPAM/eau/méthanol système a été accéléré et une séparation de phase liquide-liquide macroscopique apparait.

Afin d'étudier l'effet de groupes terminaux sur les propriétés de solution de PIPOZ, deux PIPOZs téléchéliques avec groupe perfluorodécanyle (FPIPOZ) ou groupe octadécyle (C_{18}PIPOZ) comme extrémités de chaîne ont été synthétisés. Les valeurs de T_c des polymères téléchéliques ont beaucoup diminué par rapport à celle de PIPOZ. Des micelles stables se forment dans des solutions aqueuses de polymères téléchéliques. La micellization et la séparation de phase de ces polymères dans l'eau ont été étudiées. La séparation de phase de PIPOZs téléchéliques suit le mécanisme de MLLPS. Des différences en tailles de gouttelettes formées à l'intérieur de solutions de deux polymères ont été observées. Pour étudier profondément les différences dans le comportement d'association entre deux polymères téléchéliques, les intensités des signaux de polymères correspondants et les temps de relaxation T_1, T_2 ont été mesurés. Des valeurs de T_2 de protons correspondants aux IPOZs sont plus hautes.

Mots-clés : transition de phase, séparation de phase liquide-liquide, téléchélique, relaxation RMN

Abstract

This thesis focused on the phase separation of two well-known thermoresponsive polymers, namely PNIPAM (poly(*N*-isopropylacrylamide)) and PIPOZ (poly(2-isopropyl-2-oxazoline). Despite various studies of the two polymers, two aspects of their thermal properties remained unclear and needed to be investigated. One is the cononsolvency effect of PNIPAM in water and a second water miscible solvent. The other is the effect of the end group properties on the phase separation of PIPOZ.

With this in mind, we first studied the effect of the chain architecture on the cononsolvency of PNIPAM in water/methanol mixture, employing a 4-arm star shape PNIPAM and a cyclic PNIPAM as model. Tethering PNIPAM arms to a hydrophobic core resulted in a reduced T_c (cloud point temperature) and a lower phase transition enthalpy change. The T_c of the star shape PNIPAM was inversely dependent on the polymer molecular weight. The dehydration cooperativity was depressed for the star PNIPAM and cyclic PNIPAM due to topological constraints.

A study of the effect of polymer concentration on the cononsolvency of PNIPAM in water/methanol mixture revealed a macroscopic liquid-liquid phase separation (MLLPS) for PNIPAM in water/methanol mixtures of methanol molar fraction ranging from 0.127 to 0.421 at a polymer concentration of 10 $g \cdot L^{-1}$. The turbid suspension of PNIPAM/water/methanol separated into a polymer rich phase coexisting with a polymer poor solution phase after equilibration for two days at room temperature. The phase diagram showing the MLLPS for the PNIPAM/water/methanol mixtures was constructed based on experimental data. The droplets in the condensed polymer rich phase showed a dependence on the methanol molar fraction. Methanol affects the surface tension of the liquid droplets. The slow equilibrium kinetics of PNIPAM phase separation was sped up and a macroscopic liquid-liquid phase separation realized.

In order to study the effect of end groups on the solution properties of PIPOZ, two telechelic PIPOZ end capped with perfluorodecanyl groups (FPIPOZ) and octadecyl groups (C_{18}PIPOZ), respectively, were synthesized. The T_c values of the telechelic polymers were greatly reduced after end-functionalization. Stable micelles formed in aqueous solutions of

the telechelic polymers. The micellization and phase separation of the telechelic polymers in water were studied. The phase separation of the telechelic PIPOZs in water followed a liquid-liquid phase separation mechanism. Differences in the sizes of droplets formed inside of the two polymer solutions were observed. To further investigate the differences in the association behaviour between the two telechelic polymer, NMR signal intensities and T_1 and T_2 relaxation times were examined. Higher ^{1}H T_2 values were obtained for the IPOZ unit in FPIPOZ than that in C_{18}PIPOZ, indicating a higher mobility of the main chain in the FPIPOZ micelles than that in the C_{18}PIPOZ micelles. Together with the ^{13}C NMR and ^{19}F NMR relaxation studies, we obtained better knowledge of the association properties of the telechelic PIPOZ in water. NMR relaxation studies proved to be efficient way of probing the solution behaviour of the polymers.

Keywords : Phase transition, liquid-liquid phase separation, telechelic, NMR relaxation.

Table of contents

List of tables

List of figures

List of schemes

List of abbrevations

ATRP	atom transfer radical polymerization
cac	critical aggregation concentration
CMC	critical micelle concentration
c-PNIPAM	cyclic PNIPAM
CROP	cationic ring opening polymerization
CTA	chain transfer agent
Đ	dispersity
DLS	dynamic light scattering
DMAP	4-dimethylaminopyridine
DPMK	di(phenylmethyl) potassium
E_a	acitivation energy
HEUR	hydrophobically modified ethoxylated urethane
HPLC	high performance liquid chromatography
HS-DSC	high sensitive differential scanning microcalorimeter
IPDU	isophorone diurethane
LCST	lower critical solution temperature
l-PNIPAM-Cl	linear PNIPAM carrying Cl end groups
l-PNIPAM-N3	linear PNIPAM having azide group at one end
LS	light scattering
MLLPS	macroscopic liquid liquid phase separation
NIPAM	*N*-isopropylacrylamide
NMR	Nuclear magnetic resonance
PEO	polyethyleneglycol
PEOZ	poly(2-ethyl-2-oxazoline)
PGSE	pulse-gradient spin-echo
PIPOZ	poly(2-isopropyl-2-oxazoline)
PMMA	poly(methylmethacrylate)
PMOZ	poly(2-methyl-2-oxazoline)
PNIPAM	poly(*N*-isopropylacrylamide)

PNIPAM-arm	precursor PNIPAM for *s*-PNIPAM
PNonOZ	poly(2-nonyl-2-oxazoline)
POZ	poly(2-alkyl-oxazoline)
PPhOZ	poly(2-phenyl-2-oxazoline
PVME	poly(vinylmethylether)
PVP	polyvinylpyridine
RAFT	reversible addition-fragmentation chain-transfer
R_g	radius of gyration
R_H	hydrodynamic radius
ROP	ring opening polymerization
SANS	small angle neutron scattering
SDS	sodium dodecyl sulfate
SEC	size exclusion chromatography
SLS	static light scattering
s-PNIPAM	star-shaped PNIPAM
T_1	longitudinal relaxation time
T_2	transverse relaxation time
T_c	cloud point temperature
τ_c	correlation time
TMPS	trimethylsilyl propionic acid sodium salt
UCST	upper critical solution temperature
χ_m	methanol volume fraction

Acknowledgment

I would like to thank my supervisor, Professor Françoise Winnik, for giving me the precious opportunity to carry out this research in her lab. This work would not have been possible without her support, encouragement, profound knowledge, great patience, and invaluable experience. I appreciated the helpful advice and frequent discussions, which helped to advance my research.

This work wouldn't have been possible without the financial support from the Chemistry Department, Faculty of Arts and Science; Université de Montréal; Natural Sciences and Engineering Research Council (NSERC); and the China Scholarship Council (CSC).

I would like to thank Professor Julian Zhu for many fruitful discussions, helpful advice on the NMR studies. I appreciated his great patience and profound knowledge.

I would like to thank our collaborator, Professor Toshifumi Satoh, at Hokkaido University for the supply of the star polymer.

I am thankful to my colleagues at the Université de Montréal for their invaluable friendship and collaboration, especially Dr. Xing-Ping Qiu, who helped me a lot with the synthesis of the polymers.

I would like to express my sincere appreciation to Dr. Cedric Malveau for helping me set up the NMR experiments and useful advice.

I would like to thank my family for their constant support and care during my studies.

Chapter 1. Introduction and Literature Review

1.1 Thermoresponsive smart materials — PNIPAM and PIPOZ

Poly(*N*-isopropylacrylamide) (PNIPAM) is an attractive temperature responsive polymer that has been extensively studied over the past few decades. Its aqueous solution turns turbid around 32 ºC, the cloud point temperature. This reversible response to temperature changes makes PNIPAM useful in numerous applications such as optical filters, optical switches, adsorbents, drug-release devices, water purification devices, hair shading, protein immobilization, and immunoassay procedures.[1-5] Hydrogels of cross linked PNIPAM or PNIPAM based systems are used as nonfouling surface coatings, drug release/delivery vehicles, enzyme stabilizers and sensors.[6-8]

Besides the practical applications, PNIPAM solutions have also been the subject of extensive theoretical studies from the viewpoint of polymer physics and model simulation in order to understand the coil to globule collapse. Scarpa et al.[9] were the first to report in 1967 the inverse temperature solubility of PNIPAM in aqueous solution with a lower critical solution temperature (LCST) at 31 °C. The phenomenon was explained as follows: A strong interaction between water molecules is essential thermodynamically for controlling the conformations of polymer chains in aqueous solutions. PNIPAM segments of specific orientation form hydrogen bonds with the already partially ordered water molecules in aqueous solution. The hydrogen bonds between the polar amide group of the PNIPAM segments and the arranged water molecules lead to a reorientation of water molecules around the nonpolar groups. Clathrate-like clusters of water surround the hydrophobic isopropyl group of the PNIPAM side chain resulting in decreased entropy upon mixing. This phenomenon is known as the hydrophobic effect. At temperatures above the LCST, the entropy term overwhelms the exothermic enthalpy of the hydrogen bond formed between the amide group of PNIPAM and water molecules. The mixing free energy change becomes positive and phase separation happens. Large aggregates form, through hydrophobic interactions, between the dehydrated PNIPAM chains. [10, 11] The number of hydrating water molecules around each NIPAM segment was determined by dielectric relaxation measurements below the LCST.[12] This number decreases sharply when the PNIPAM aqueous

solution is heated above LCST. Studies of the phase transition of PNIPAM aqueous solutions via light scattering reveals the coil-to-globule transition as shown in **Scheme 1.1**. The PNIPAM chain collapses at LCST through hydrogen bonding between polymer-polymer instead of polymer-water.

Stable milky suspensions are obtained above the LCST of PNIPAM in dilute aqueous solutions. The size of PNIPAM aggregates, the so-called mesoglobules, formed at temperatures above the LCST was found to be in the submicron region. The conformation of chains before and after phase transition was studied in dilute solutions by static and dynamic light scattering in order to obtain detailed information of phase transition dynamics.[13] A report by Wu et al.[14] revealed that the coil-to-globule phase transition of PNIPAM in dilute aqueous solution has two distinct kinetic stages with two characteristic transition times (0.1 ms and 0.8 ms, respectively). The first stage can be attributed to the nucleation and initial growth of some "pearls" (contracted segments) along the chain, while the second stage includes the merging and coarsening of the "pearls".

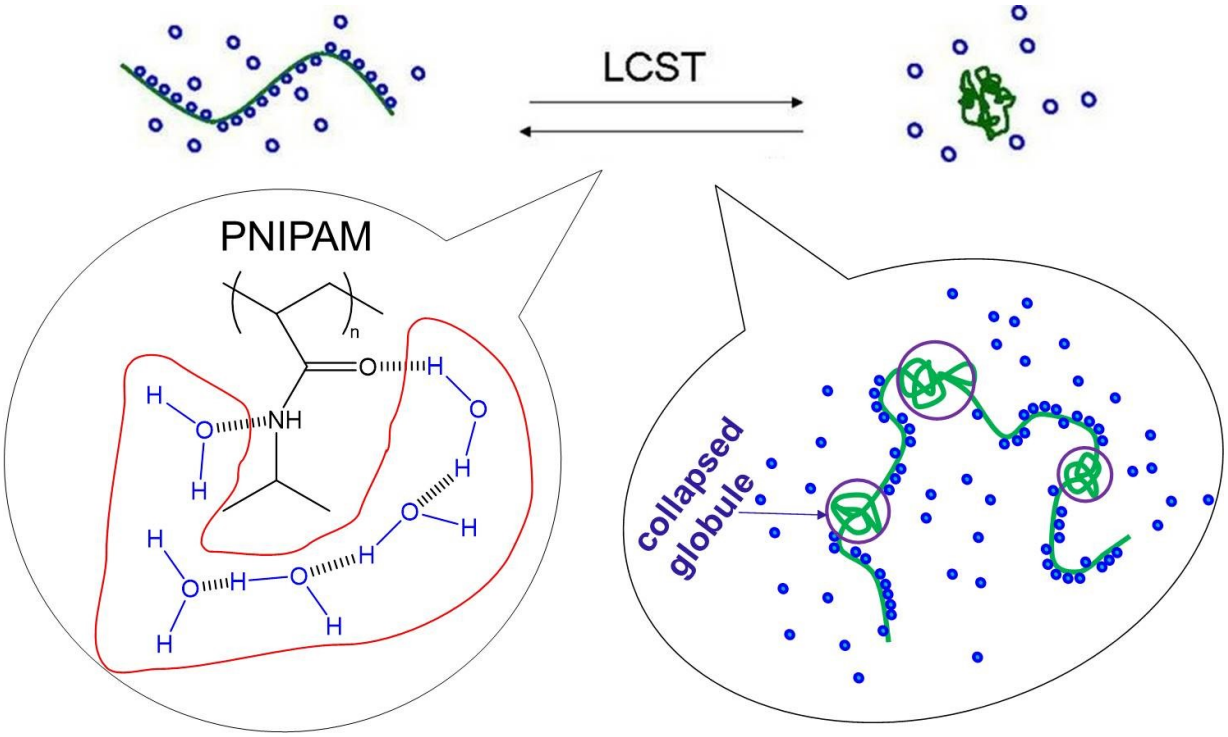

Scheme 1.1 Representation of the phase transition of PNIPAM in water.

A theory by Tanaka et al.[15] has put forward the importance of the cooperative character of the PNIPAM hydration. The formation of one hydrogen bond between water and PNIPAM

chain facilitates the formation of another hydrogen bond of water to an amide. A sequence of water molecules dehydrate cooperatively, when the temperature is increased above the cloud point temperature of PNIPAM as shown in **Scheme 1.1**. A sharp transition around the cloud point temperature is predicted by Tanaka's theory. Factors influencing the PNIPAM phase transition were considered, including addition of a second water miscible solvent, salts, concentration, molar mass, etc.

The effect of polymer concentration on the cloud point temperature (T_c) of PNIPAM in water has been investigated by Tong et al.[16] A drop about 3 ºC was detected when the concentration of polymer increased from 5.8 to 700 $g \cdot L^{-1}$ for PNIPAM with molar mass of 49.4 kDa (**Figure 1.1a**). The T_c decreased from 35.2 ºC to 30.9 ºC for PNIPAM with 2.1 kDa when concentration of polymer increased from 3.7 to 73.9 $g \cdot L^{-1}$ as reported by Otake et al.[17] (**Figure 1.1b**). Van Mele et al.[18] reported a constant value of LCST for PNIPAM regardless of the polymer molar mass at the same polymer concentration (i.e. 500 $g \cdot L^{-1}$). In all these studied PNIPAM/water binary systems, steady suspensions of phase separated solutions were observed above the LCST of PNIPAM.

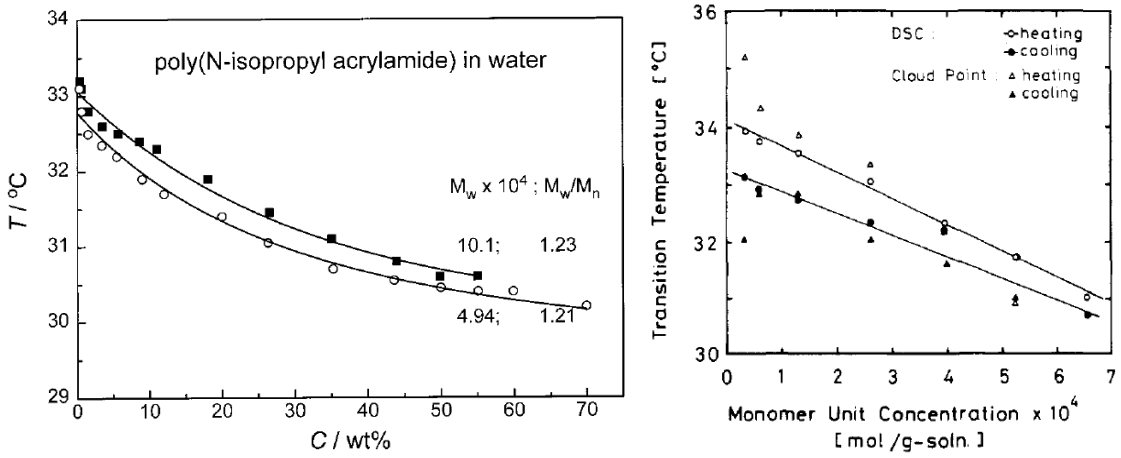

(a) (b)

Figure 1.1 (a) The cloud point temperature of PNIPAM in water as a function of polymer concentration (filled square, M_n = 101 kDa; open circle M_n = 49.4 kDa.). (Reprinted with permission from Ref 16. Copyright 1999 American Chemical Society.) (b) The cloud point temperature of PNIPAM in water as a function of monomer concentration (M_n = 2.1 kDa). (Reprinted with permission from Ref 17. Copyright 1990 American Chemical Society.)

Recently, a structural isomer of PNIPAM, poly(2-isopropyl-2-oxazoline) (PIPOZ) (**Scheme 1.2**) is gaining increasing attention.[19, 20] PIPOZ aqueous solutions possess a cloud

point temperature around 40 ºC.[21, 22] In addition the polymer is non-toxic and biodegradable making it a promising material for biomedical and pharmaceutical applications. The LCST of PIPOZ was tuned by changes in end group polarity[23], by the addition of salts,[24] and by the polymer composition.[25] Schlaad reviewed the synthesis of polyoxazolines with a special focus on the synthesis of biohybrids. A review by Hoogenboom highlights the bioapplications of polyoxazolines.[26]

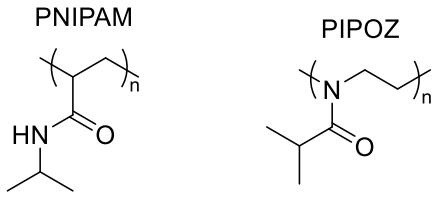

Scheme 1.2 Structure of PNIPAM and PIPOZ.

Like its structural isomer PNIPAM, PIPOZ is highly soluble in water at room temperature, although the ternary amide in the PIPOZ main chain acts only as a proton receptor and is not effective in undergoing hydrogen bonding with water contrary to the secondary amide group of PNIPAM. PIPOZ is sometimes considered to be a pseudopeptide in view of the presence of amide group in the main chain. The tertiary nature of the polyamides and the lack of chiral centers in the PIPOZ main chain are the reasons why it cannot form distinct secondary structures via hydrogen bonding like polyleucine. Nevertheless, the polarity in the main chain and short isopropyl side chain of PIPOZ still make it water soluble. Studies of the solution properties of PIPOZ are limited when compared to PNIPAM, due to the difficulty in the ROP (ring opening polymerization) synthesis of long PIPOZ chain. Still, PIPOZ as a biocompatible polymer was introduced into some amphiphilic systems as hydrophilic and nontoxic segment. Based on the high sensitivity of the cloud point temperature of poly(*N*-alkyl-2-oxazoline) on the side chain length, block copolymers of PIPOZ and poly(*N*-alkyl-2-oxazoline)s with different side chain length were synthesized. Solution properties of these copolymers and homopolymers were examined taking into account factors such as addition of a second solvent or salts[27] and chain length.[24]

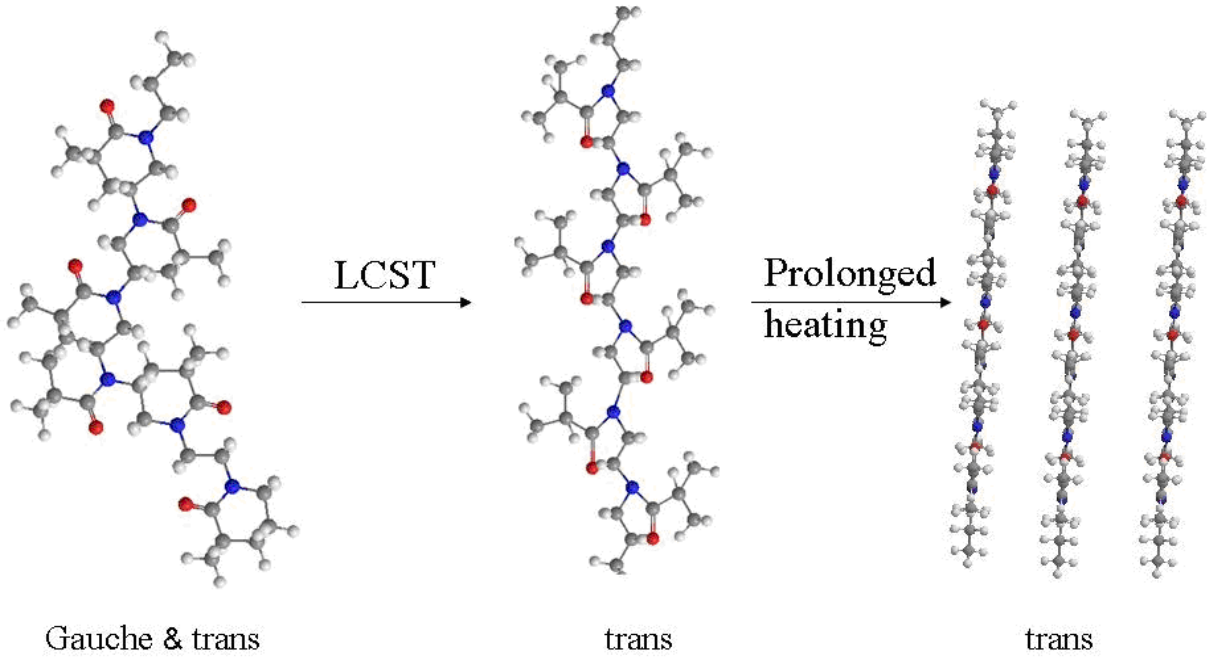

Scheme 1.3 Change in conformation of PIPOZ segment in aqueous solutions.

The heat-induced phase transition of PIPOZ in aqueous solution is fully reversible when solutions are kept above LCST for a short time (< 2 h).[28] Micrometer-sized particles composed of fiber meshes and nanofibers have been reported in studies of PIPOZ aqueous solutions subjected to a longer heating treatment.[29, 30] Based on XRD and TEM results, the authors proposed a mechanism for the crystallization process in the solution. The PIPOZ crystallization occurred through a combined mechanism involving the hydrophobic interaction between side chains and alignment of the acrylamide group. The evolution of the morphologies of the particles formed in PIPOZ aqueous solution at 60 ºC was studied by Diehl et al.[28] by conventional and cryogenic scanning electron microscopy. A bicontinuous polymer network-like structure was observed in PIPOZ solution after heating at 60 ºC for 0.5 h arising from phase separation into a polymer-rich phase and a polymer-poor phase. The bicontinuous phase collapses into individual particles composed of a porous fiber mesh after heating for 4 h at 60 ºC. Nanofibers form preferentially on the surface and eventually wrap the hollow particles like a ball of wool. The size and density of the porous fiber meshes were related to the concentrations of solutions and temperature. A liquid-liquid phase transition mechanism above the LCST was proposed by Katsumoto et al.[31] for the phase separation of PIPOZ in water. A polymer rich phase and polymer lean phase coexist in the phase separated PIPOZ

aqueous solution as observed by optical microscopy. The changes of polymer chain conformation (**Scheme 1.3**) in the phase separation and subsequent crystallization process for PIPOZ in hot water solution were observed by IR.

1.2 Effects of additives on the solution properties of PNIPAM and PIPOZ

Addition of various cosolutes can affect the phase behaviour of PNIPAM and PIPOZ through non-covalent bonding with the polymer or by changing the water structure. The behaviour of the polymer in solution is a result of the balance of interactions between its segments and between the segments and the solvent molecules. Any component whose hydration sphere is not compatible with the polymer depresses the LCST. If the third component has the same activity in both separating phases, the LCST increases.

1.2.1 Effect of addition of a water-miscible solvent on the solution properties of PNIPAM in water

The phase transition of aqueous PNIPAM solutions can be affected by added solvents. Addition of a certain amount of water miscible solvent (methanol, ethanol, THF, DMSO etc.) to a clear aqueous solution of PNIPAM results in a turbid solution. The phase separated solution becomes clear again by cooling the mixtures below a certain temperature. Both water and methanol are good solvents for PNIPAM at room temperature. However, PNIPAM does not dissolve in the mixture of the two solvents. The phenomenon is known as cononsolvency. The solvent pair is called cononsolvent of PNIPAM. **Figure 1.2** shows the phase diagram of PNIPAM in water/methanol mixture as an example. At 20 ºC, a clear solution is obtained when the methanol volume fraction is below 27% in the PNIPAM/water/methanol system. Increasing the methanol volume fraction to 27–65% leads to a cloud solution. This becomes clear again upon further increasing the methanol volume fraction.

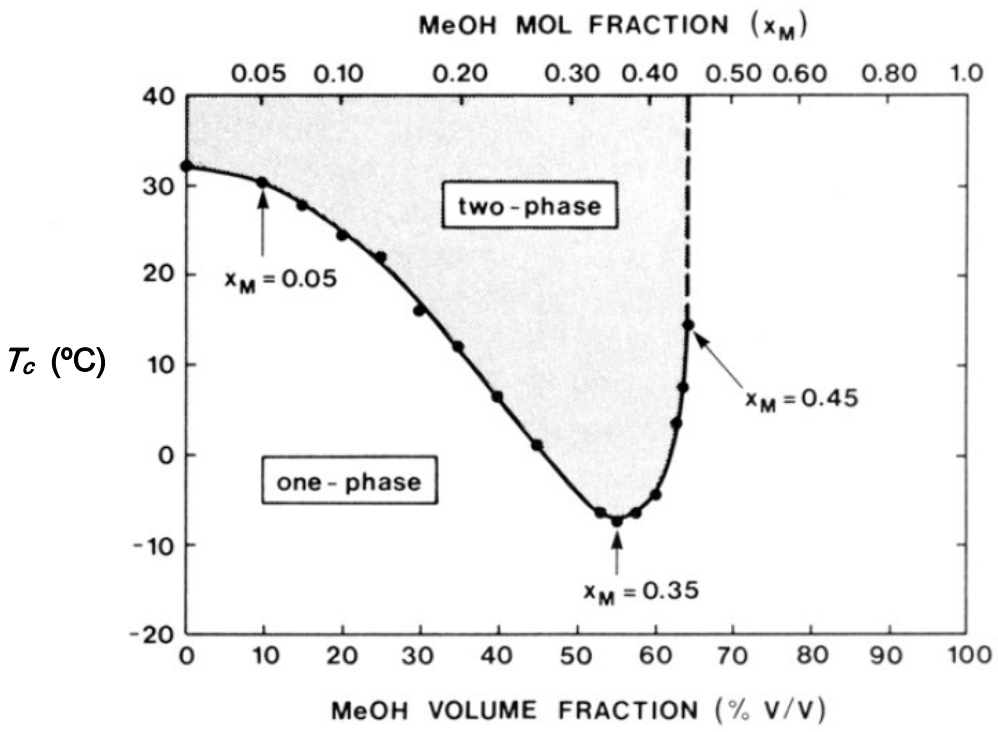

Figure 1.2 Phase diagram of PNIPAM in water/methanol. (Reprinted with permission from Ref 32. Copyright 1990 American Chemical Society.)

Different theories were proposed to interpret the phenomenon. The phase separation of PNIPAM in water-methanol mixture can be described by the changes in the balance between hydrogen bonding and hydrophobic interactions. Addition of methanol to the aqueous solution of PNIPAM destroys the hydrated water layer around PNIPAM chain. The competition between water molecules and the second solvent molecules in forming hydrogen bond along the PNIPAM main chain causes the dehydration of the polymer. The competition reaches maximum when the volume fraction of methanol is ~ 0.55 corresponding to the minimum of the phase diagram.

Wu et al.[33] explained the LCST type phase transition in water/methanol mixture using the water/methanol cluster network theory. The formation of methanol-water complex in the water-methanol mixed solvent was suggested as the reason for the sudden dehydration of PNIPAM. The formation of pentagon clusters through hydrogen bonding between water and methanol molecules caused the dehydration of PNIPAM chains. The minimum of the phase diagram occurred at the point where water and methanol molecules formed stable clathrate structures. Pang's study confirmed the formation of complex structures between solvent

molecules.[34] The addition of methanol reduced the interaction between PNIPAM chain and solvents. They found that the cluster structure of the free water molecules was not affected by added methanol molecules; however the number of such structures decreased as a result of the strong interaction between the two species via hydrogen bonding. Schild et al.[35] used the Flory-Huggins ternary solution theory to explain the cononsolvency in terms of a change in the water-ethanol interaction parameter in the PNIPAM solution. The local contact between the polymer and solvent caused a perturbation of the binary interaction parameter. Tanaka et al.[36] introduced a mechanism which combined the cooperativity in hydration of the PNIPAM chain and the competition of methanol and water in hydrogen bonding to the polymer. The formation of hydrogen bond of one water molecule with the PNIPAM chain displaced the isopropyl group and made it easy for the hydrogen bonding of a second water molecule. As a result, a sequence of water molecules formed along the PNIPAM chain. Added methanol molecules competed with water in the formation of hydrogen bonds. When the sequence of water molecules along the PNIPAM chain was not long enough to retain cooperativity, the chain was dehydrated and the LCST reached its minimum. The cooperativity in hydrogen bonding and competition between water and methanol led to the re-entrant curvature of the phase diagram of PNIPAM. Using molecular dynamics, Walter et al.[37] investigated the cononsolvency phenomenon by molecular simulation and found that the methyl group of methanol was oriented towards the bulk solvent in the outer region of the solvent shell of PNIPAM, which caused the PNIPAM and solvent shell to become hydrophobic and collapse in the water/methanol mixture. Hao et al.[38] studied the origin of cononsolvency in THF/water mixture and concluded that the composition fluctuation which reaches the maximum at about 20 mol% THF content, induced PNIPAM cononsolvency. At the composition fluctuation maximum, neither the hydrogen bonding with water nor the Van der Waals interaction with THF was adequate to solubilize PNIPAM.

What is the effect of polymer concentration on the LCST of PNIPAM in mixtures of water/methanol? Most studies of the cononsolvency phenomenon of PNIPAM were conducted for dilute polymer solutions. So far, only a few reports are found on the phase transition in more concentrated solutions of PNIPAM in mixed solution of methanol and water. Tao's[39] study about PNIPAM at polymer concentration up to 150 $g \cdot L^{-1}$ reported a

macroscopic phase separation in the mixed solution of water and methanol. Two liquid phases were observed in the concentrated PNIPAM/water/methanol system with certain solvent composition. A very clear polymer-poor phase coexisted with a viscous polymer-rich phase. The phase demixing boundary was determined as the composition at which phase separation began. A ternary interaction parameter was considered in the PNIPAM/water/methanol system to explain the formation of ternary complexes.

A liquid-liquid phase demixing was also reported for other polymers.[40, 41] The polymer concentration has been reported to affect the solution properties of PVP, PMMA etc. in mixed solvents. Three liquid phases have been observed in a PVME/water/THF system.[40] The concentration of PVME used in their work varied from 50 to 900 $g \cdot L^{-1}$. The liquid-liquid phase demixing of poly(methacrylic acid) in methacrylic acid and water mixtures was reported and the values of the parameters of the ternary version of the Cahn-Hilliard equation of spinodal decomposition were determined.[41] The phase separation process of PMMA in mixed solvents of water/acetone or water/THF was studied by a solvent shifting process (also called the "Ouzo process") in which water (nonsolvent) was added to a solution of PMMA/solvent system.[42] Nanoparticles or microparticles were observed depending on the initial PMMA concentration and water/solvent ratio in the mixtures. The boundary between the Ouzo region of compositions (PMMA nanoparticles only), from the "non-Ouzo" region (nano- and microparticles) were determined and appeared to have no relation with the spinodal decomposition line of the ternary solutions.

A study on the phase transition of PNIPAM in water/methanol mixture, taking into account the polymer concentration effect will contribute to a better understanding of the phase transition mechanism of PNIPAM. Chapter 3 of the thesis will present the phase transition behaviour of highly concentrated solutions of PNIPAM in methanol/water. The effect of other parameters such as the architecture and the polymer concentration on mixed polymer solutions are still poorly understood. The effect of polymer architecture on LCST of PNIPAM in mixed solvent of methanol and water will be addressed in Chapter 2.

1.2.2 Effect of addition of water-miscible solvents on the solution properties of PIPOZ

There are only a few reports about the effect of addition of water-miscible solvents on the LCST phase transition of PIPOZ water solutions. The LCST of aqueous PIPOZ solution was tuned by addition of ethanol as reported by Lambermont-Thijs et al.[43] The minimum LCST appeared for an ethanol composition of 5 wt% in the PIPOZ/water/ethanol mixture. However THF and water mixed solvent were a cosolvent for PIPOZ.[44]

A UCST (upper critical solution temperature) was observed for PPhOZ (poly(2-phenyl-2-oxazoline) in ethanol by Schubert et al.[45] (Structure shown in **Scheme 1.4**). Addition of water to the ethanol solution of PPhOZ resulted in an increase in solubility of the polymer with a maximum in 6 ~ 25 wt% of water in ethanol. The hydrogen bonding of water with amide groups of PPhOZ formed a hydration shell around the polymer. $PEOZ_{80}$-stat-$PPhOZ_{20}$ (the subscript indicates mole percent of monomer) exhibited both LCST and UCST transitions in a water/ethanol mixture with 40 wt% ethanol.[46] A UCST was also observed for copolymers of PEOZ (poly(2-ethyl-2-oxazoline) and PNonOZ (poly(2-nonyl-2-oxazoline) in water/ethanol solvent mixtures.[47]

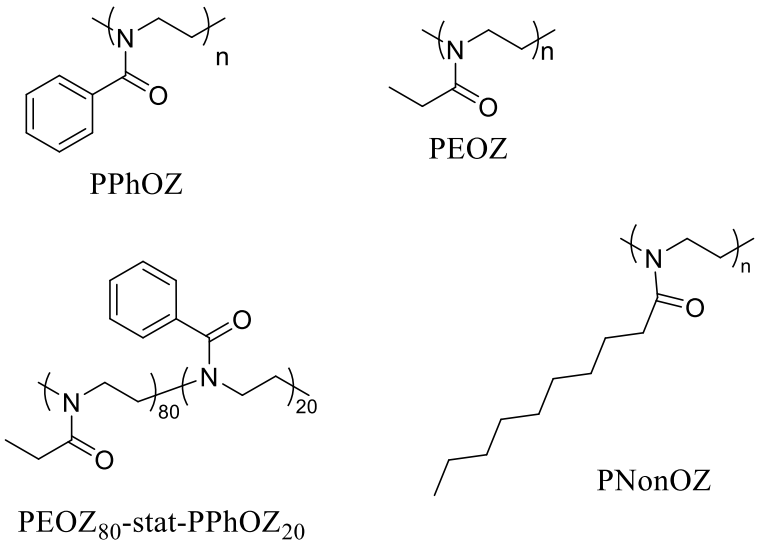

Scheme 1.4 Structures of PPhOZ, $PEOZ_{80}$-stat-$PPhOZ_{20}$, PEOZ and PNonOZ.

1.2.3 Effect of other additives – salts, surfactant

Besides these water-miscible solvents, salts are also known to influence the LCST. Before discussing the effect of salts on the solution behaviour of polymer, there are a few concepts that need to be clarified. The Hofmeister series is a classification of ions in the order of their ability to salt-out or salt-in proteins. Anions appear to have a larger effect than cations, and usually follow the order:

$$F^- \approx SO_4^{2-} > HPO_4^{2-} > OAc^- > Cl^- > NO_3^- > Br^- > ClO_3^- > I^- > ClO_4^- > SCN^-$$

The order of cations is usually given as:

$$NH_4^+ > K^+ > Na^+ > Li^+ > Mg^{2+} > Ca^{2+} > [C(NH_2)_3]^+$$

The salts in the left part of these series decrease the solubility of nonpolar molecules. The process is known as salting-out. The salting-in process refers to the increase of the solubility of nonpolar molecules by the later salts in the series. The ions that contribute to the stability of water - water interactions and intramolecular interactions in polymers, are defined as kosmotropic ions. On the contrary, chaotropic ions disrupt the hydrogen bond between water molecules and polymer-water molecules.

The effect of a series of salts on the LCST of PNIPAM was studied by Cremer et al.[48], among others. The anions studied followed the Hofmeister series. The phase transition of PNIPAM was found to be directly correlated with the hydration entropy of the strongly hydrated anion at adequate concentration. The weakly hydrated anions exhibited salting-out effects. Bergbreiter et al.[14] investigated the effect of a series of sodium salts on the LCST of PNIPAM as a function of polymer molecular weight and polymer concentration. In concentrated solutions of strongly hydrated kosmotropic anions, the phase transition of PNIPAM consisted of two separate steps for higher molecular weight samples. The first step was found to be sensitive to the polymer molecular weight and the solution concentration, which was not observed in the second step. Interaction between the chaotropic anions and the polymer was also found to be affected by the molecular weight of PNIPAM. Wang et al.[49] studied the effect of salts on the reentrant behaviour of PNIPAM in water-methanol system. SCN^- and ClO_4^- depressed the reentrant transition, while other anions enhanced the transition.

Bloksma et al.[24] investigated the effect of addition of a range of Hofmeister salts on the LCST of PIPOZ as shown **Figure 1.3**. SCN^-, ClO_4^- , and I^- showed a salting in effect, i.e., the cloud points increased with increasing salt concentration, while Cl^-, OAc^-, and SO_4^{2-} , caused a salting-out effect. The order of salting in to salting-out effect nicely followed the Hofmeister series: $SCN^- > ClO_4^- > I^- > Cl^- > OAc^- > SO_4^{2-}$.

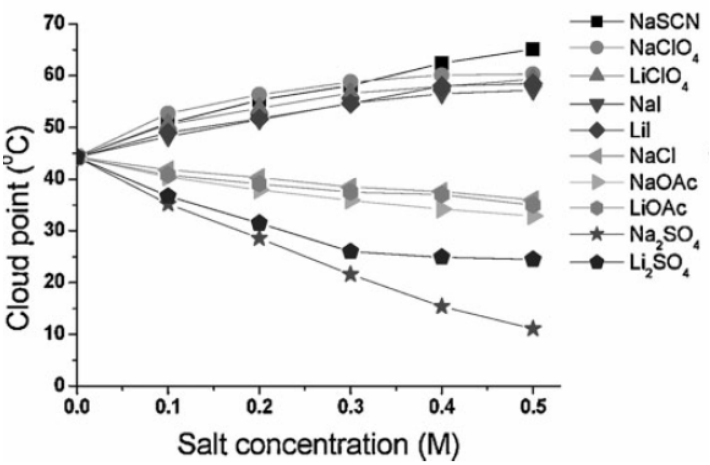

Figure 1.3 Influence of salts on the cloud points of PIPOZ. (Reprinted with permission from Ref 24. Copyright 2010 WILEY-VCH Verlag GmbH & Co. KGaA, Weinheim)

Eliassaf et al.[50] were the first to report the effect of surfactant addition on phase transition of PNIPAM employing the sodium dodecyl sulfate (SDS). The solution viscosity increased and the phase transition temperature was elevated with the addition of 1% of SDS. Schild and Tirrell[51] used different fluorescent probes to investigate the PNIPAM/SDS system and observed that the critical aggregation concentrations (cac) were essentially the same in most cases. Meewes et al.[52] observed that the phase transition of PNIPAM was completely prevented when SDS concentration reached 250 $mg \cdot L^{-1}$. Addition of SDS and dodecyltrimethylammonium chloride into aqueous solutions of PIPOZ caused an increase of LCST.[19]

1.3 Effect of end group modification on the solution properties of PNIPAM and PIPOZ

1.3.1 Synthesis of telechelic and semitelechelic amphiphilic polymers

A telechelic polymer is defined by IUPAC as a "prepolymer capable of entering into further polymerization via its reactive endgroups". Depending on the number of functionality, telechelic polymers can be classified as mono-, di- and multi- functional telechelics. In this work, only linear polymers are considered, we simply use the common name telechelic and semitelechelic to differentiate the di- and mono- end functional polymers. Amphiphilic telechelic polymers refer to polymers containing water soluble segments in the middle of the chain and hydrophobes at the chain ends which tend to associate with each other in water. The first report of telechelic polymers can be traced back to the 1970s when telechelic PVP and PEO were used as emulsifiers and thickeners.[53] Most research interests have been devoted to tune the properties of telechelics by changing the chain length and structure of the central hydrophilic chain and of the hydrophobic chain ends, which provides the basis for applications as associative thickeners,[53] sieving media for DNA sequencing,[54] and drug delivery vehicles. The rheological behavior of telechelic polymers has been reviewed recently by Chassenieux.[55] The association behaviour of end-hydrophobically-modified PEO and poly(acrylamide) are reviewed by Grassl et al.[56] An extensively studied class of amphiphilic telechelic polymers are the hydrophobically end-functionalized PEO through urethane or ester linkages with hydrophobic alkyl end groups of various length and structure.[57-62] The typical synthesis routes of amphiphilic telechelic and semitelechelic PEO, PNIPAM and PIPOZ having interesting structures and stimuli responses will be discussed in this section.

1.3.1.1 Synthesis of telechelic and semitelechelic PEO

i) Alkyl isocyanate attached to α,ω-dihydroxyl PEO through urethane linkage

In the early studies, telechelic PEOs were prepared by reacting short PEO chains with isophorone diisocyanate or isophorone diurethane (IPDU) to extend the chain length and to attach end groups.[63, 64, 65] These commercially available telechelic polymers, end capped with alkyl group via urethane linker, were known as HEUR (hydrophobically-modified ethoxylated

urethane) polymers (structure shown in **Scheme 1.5**). In the beginning, the classic step-growth reaction was employed to produce HEUR polymers with broad molecular weight distribution.

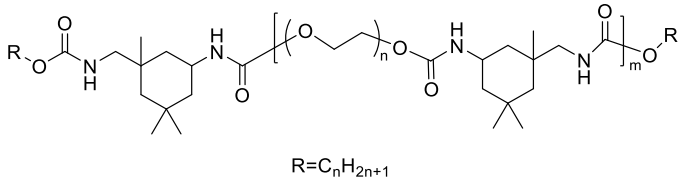

Scheme 1.5 Structure of HEUR.

The HEUR polymers containing only two urethane linkers were obtained by modification of prepared PEO bearing hydroxyl groups at both ends. Hydrocarbons with variable chain length have been attached to the PEO chain ends as shown in **Table 1.1**. The prevalent synthetic approach follows a two-step procedure, whereby, first, isocyanates present in excess are linked to the PEO terminal hydroxyl groups. In the second step, isocyanate-modified PEO is subjected to purification treatment to remove diurea and diurethane products due to the excess of isocyanates.[66, 67] Gourier et al.[68] and Beaudoin et al.[69] synthesized α,ω-di-functionalized PEOs by addition of an alkyl (C_{16} or C_{12}) isocyanate to α,ω-dihydroxylated PEO in the presence of 1,4-diazobicyclo[2.2.2]octane in toluene at 30 °C as shown in **Scheme 1.6**.

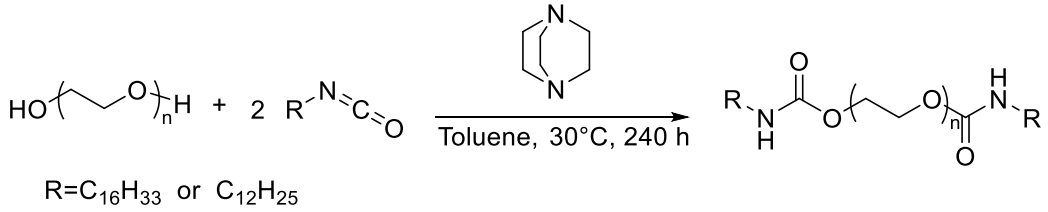

Scheme 1.6 Synthesis of telechelic PEO using alkyl isocyanates.

ii) Alkyl acid reaction with α,ω-dihydroxyl PEO

The drawback of the above method lies in the fact that even though isocyanate is in large excess in the first step of the modification procedure, it is difficult to completely avoid polycondensation leading to formation of polymers of twice the initial molecular weight. To minimize this issue, a one pot synthesis was proposed, which involved in situ generation of a hydrophobic anhydride by reaction of a carboxylic acid or an alcohol with N,N-

dicyclohexylcarbodiimide, leading to complete modification of hydroxyl end groups. Laflèche et al.[70] modified the PEO by reaction of the terminal hydroxyl groups with hexadecylchloric acid.

iii) Alkyl tosylate reaction with α,ω-potassium dialkylate-PEO

Beaudoin et al.[71] synthesized α,ω-dioctadecyl-PEO and α,ω-dihexadecyl-PEO with M_n = 32 kDa which had the same structure as described in a previous report.[69] A different synthetic method was employed, in which telechelic PEOs were prepared using alkyl tosylate intermediates in two steps as shown in **Scheme 1.7**. First, PEO with hydroxyl end groups reacted slowly with di(phenylmethyl) potassium (DPMK) to yield α,ω-potassium dialkylate-PEO. Then dodecyl tosylate or octadecyl tosylate was introduced to obtain the final product. The telechelic PEOs with end group functionalization degree above 0.9 prepared by the alkyl tosylates method was obtained in 1 day, while it took more than 5 days to generate the telechelic PEOs with end group functionalization degree above 0.9 prepared by the alkyl isocyanate method. Using alkyl tosylates to attach hydrophobic end groups reduced the reaction time and avoided polycondensation, but there were more steps involved and it was complicated to prepare the DPMK.

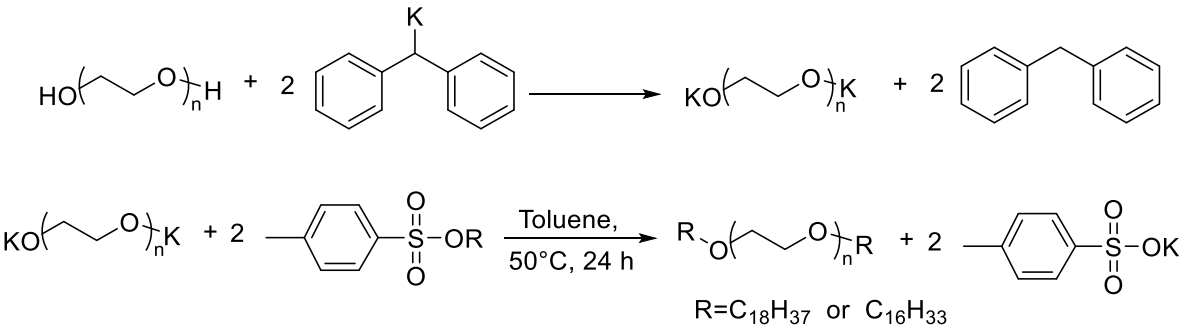

Scheme 1.7 Synthesis of telechelic PEO using alkyl tosylates.

iv) PEO-sodium alcoholate reaction with alkyl bromide

Renou et al.[72] synthesized semitelechelic PEO by reacting the PEO-sodium alcoholate with alkyl bromide in THF (Williamson reaction). The product PEOs had a methyl group at α- end and long alkyl chains of a variety length at the ω- end. The semi-telechelic PEO was synthesized the same way as the telechelic PEO by controlling the ratio of polymer and end group modifier.[71]

Table 1.1 A summary of the methods used for the synthesis of telechelic α,ω- difunctional PEO

Synthesis method	α,ω - functionality	M_n (kDa)	$Đ$
urethane linkages	$-C_{18}H_{37}$	4[59]	1.05
	$-C_{18}H_{37}$	20[58]	-
	$-C_{16}H_{33}$	51, 67.6, 84.3, 100.4[60]	1.7
	$-C_{16}H_{33}$ $-C_{18}H_{37}$	20, 35 35[61]	<1.2
	$-C_{18}H_{37}$	1, 2, 4[57]	1.1
Alkyl-isocyanate reaction with HO-PEO-OH	$-C_8H_{17}$, $-C_{12}H_{25}$, $-C_{18}H_{37}$	4[66]	1.1
	$-C_{12}H_{25}$, $-C_{16}H_{33}$	12, 20 32[68]	<1.1
	$-C_{16}H_{33}$	32[69]	1.02
$C_{16}H_{33}Cl$ reaction with HO-PEO–OH	$-C_{16}H_{33}$	10[70]	<1.1
Alkyl tosylates reaction with KO-PEO–OK	$-C_{18}H_{37}$, $-C_{12}H_{25}$	35, 6, 10, 20, 35[71]	-
PEO-sodium alcoholate reaction with alkyl bromides	$-C_{12}H_{25}$, $-C_{14}H_{29}$, $-C_{16}H_{33}$, $-C_{18}H_{37}$, $-C_{20}H_{42}$, $-C_{22}H_{45,}$ $-CH_3$	4.5[72]	1.05

1.3.1.2 Synthesis of telechelic and semitelechelic PNIPAM

Telechelic PNIPAMs capped with hydrophobic groups at each end were synthesized by RAFT (Reversible addition−fragmentation chain-transfer) polymerization. The synthesis method of PNIPAM was summarized in **Table 1.2**.

i) End groups induced by modified CTA

Telechelic PNIPAM end-capped with various end groups were synthesized by preparing a chain transfer agent (CTA) containing desired end groups. Kujawa et al.[73] synthesized a series of $C_{18}H_{37}$- end capped PNIPAMs by RAFT polymerization using the CTA

2 as shown in **Scheme 1.8**. The CTA 2 was prepared by a modified ketoform reaction yielding the carboxyl-terminated trithiocarbonate 1, followed by a carbonyldiimidazole-mediated amidation of the terminal carboxyl group with *n*-octadecylamine. RAFT polymerizations of NIPAM were then conducted to obtain telechelic PNIPAM 3 with various molecular weight and low dispersity index (< 1.2). Specially prepared CTAs with various structures have been used to synthesize telechelic PNIPAMs, such as 4'-(4-methylphenyl)-2,2':6',2"-terpyridine- 4'-yl-benzyl dithiobenzoate,[74] butyl phthalimidomethyl trithiocarbonate,[75] tetrathiafulvalene trithiocarbonate,[76] 4-(tert-butyl)phenyl 2-(((ethylthio)carbonothioyl)thio)-2-methylpropanoate,[77] and 1,4-bis(n-butylsulfanylthiocarbonylsulfanylmethyl)benzene.[78]

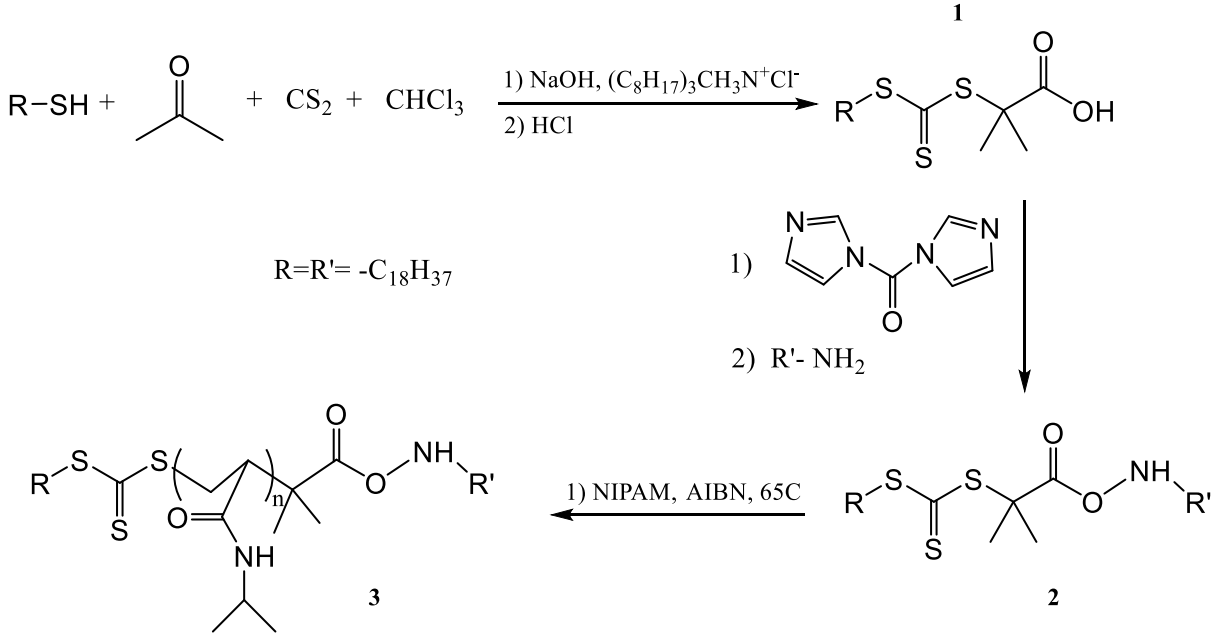

Scheme 1.8 Synthetic route of the C_{18}-PNIPAM-C_{18} by RAFT. (Adapted with permission from Ref 73. Copyright 2006 American Chemical Society.)

ii) Alkyl iodides or ethers reaction with HS-PNIPAM-SH

The methodology employed above to synthesize hydrophobically end capped telechelic PNIPAMs has the disadvantage of preparation of a different CTA for each type of end group. A more efficient pathway to synthesize telechelic PNIPAMs has been reported by Qiu et al.[79] The telechelic PNIPAM was prepared by coupling the alkyl iodides or ethers to the precursor polymer (HS-PNIPAM-SH) carrying mercaptan functions at each end. This strategy has been

used to synthesize dicholesteryl-PNIPAM as shown in **Scheme 1.9**.[80] The HS-PNIPAM-SH 2 was prepared by RAFT polymerization of NIPAM using diethylene glycol di(2-(1-isobutyl)sulfanylthiocarbonylsulfanyl-2-methylpropionate) 1 as difunctional CTA, followed by aminolysis with *n*-butyl amine. The telechelic PNIPAM 4 was obtained by the coupling reaction of cholest-5-en-3b-yl 6-iodohexyl ether 3 and precursor polymer 2. The synthetic method in **Scheme 1.9** was employed to synthesize a α,ω-diazobenzene-PNIPAM in two steps.[79] A HS-PNIPAM-SH precursor polymer was first prepared the same way as shown in **Scheme 1.9**. By reacting with 4-Cyano-4'-(6-iodohexyloxy)azobenzene in sodium dicarbonate DMF solution, azobenzylhexyloxy group was coupled to the thiol end group of the HS-PNIPAM-SH telechelics.

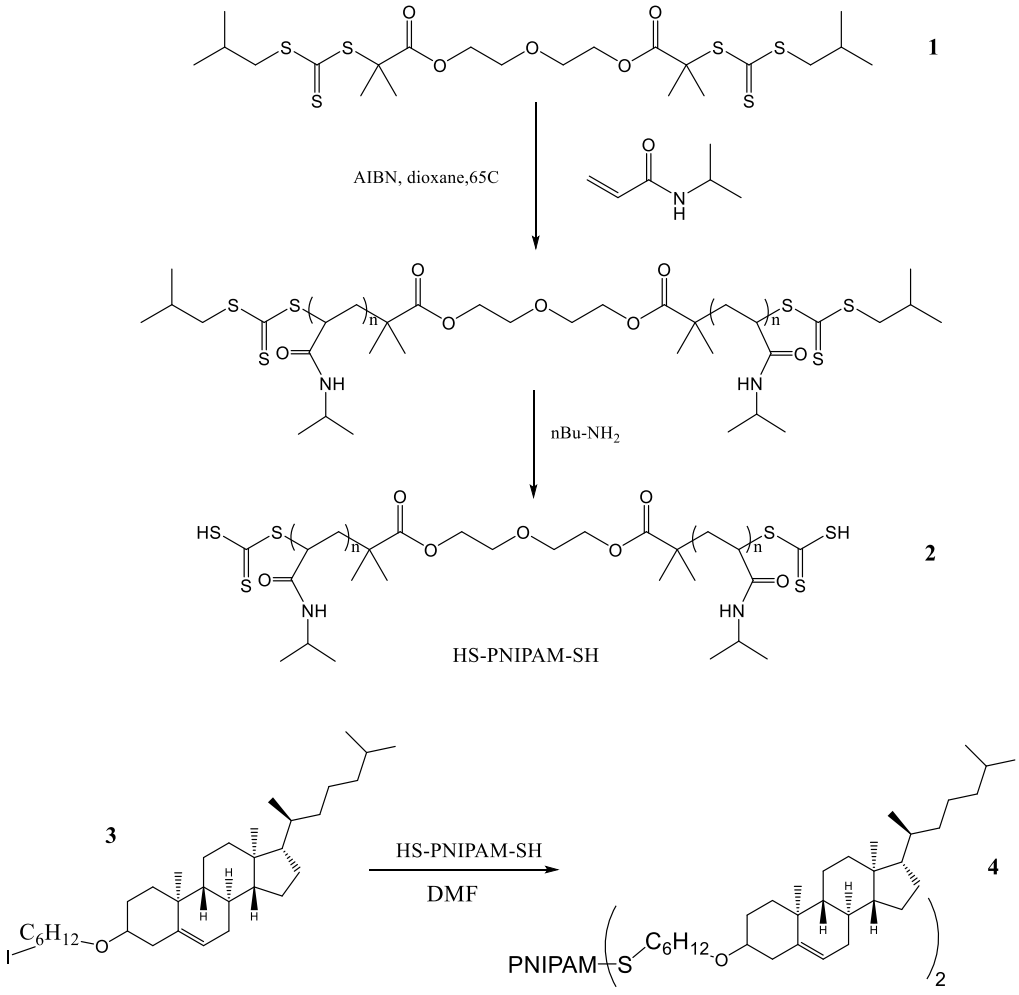

Scheme 1.9 Synthetic route of the telechelic α,ω-di-cholesteryl PNIPAM.

iii) Alkyl end groups attached to PNIPAM main chain by click chemistry

Another efficient method to synthesize end functionalized telechelics is the combination of RAFT polymerization and click chemistry.

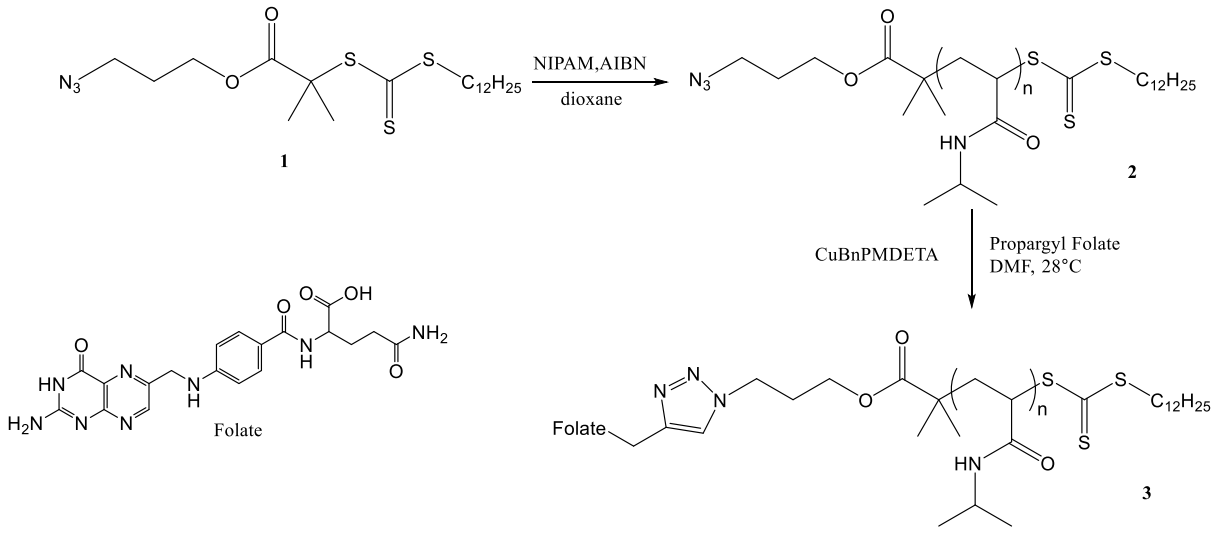

Scheme 1.10 Synthetic route of the α-folate ω-dodecyl telechelic PNIPAM.

The telechelic PNIPAM 2 carrying an azido group at one end and a dodecyl group at the other end was synthesized by RAFT polymerization using 2-dodecylsulfanylthiocarbonylsulfanyl-2-methyl-propionic acid 3-azidopropyl ester as CTA 1 (**Scheme 1.10**).[81] The RAFT polymerization was conducted in dioxane in the presence of AIBN, CTA, NIPAM with N_2 purge and heating for a certain time. The same method was employed to synthesize a telechelic PNIPAM end-capped with an azido and dodecyl groups at each teminus of M_n = 16.3 kDa using the same CTA by Li et al.[82] and Vora et al.,[83] respectively. The azido end group reacted with propargyl folate by click reaction to obtained the α-folate ω-dodecyl telechelic PNIPAM.[82]

Table 1.2 A summary of the methods used for the synthesis of telechelic PNIPAM

Synthesis method	End group functionality	M_n (kDa)	$Đ$
RAFT with modified CTA	α,ω = -$C_{18}H_{37}$	12.4–49[73]	<1.2
	α = terpyridinyl-benzyl; ω = benzyl	1.91–2.86[74]	1.06–1.11
	α = phthalimidomethyl; ω = butyl	10.6[75]	1.07
	α = tetrathiafulvalene; ω = isobutyl	1.7–13.1[76]	1.14–1.3
	α=-$CH(CH_3)_2CO_2$Ph-tBu; ω =-C_2H_5	4–50[77]	1.15–1.46
	α,ω = -C_4H_9	39[78]	1.5
HS-PNIPAM-SH reaction with Alkyl iodides	α,ω = -azobenzyl	10.5[79]	1.08
	α,ω = cholesteryloxyhexyl	8.8–26.1[80]	<1.1
RAFT and click chemistry	α= -$C(CH_3)CO_2C_3H_6N_3$; ω = -$C_{12}H_{25}$	27[81]	1.15
	α = Folate; ω = -$C_{12}H_{25}$	16.3[82]	1.06
	α = -OH; ω = -$C_{12}H_{25}$	4.6[83]	1.10

1.3.1.3 Synthesis of telechelic and semitelechelic POZ

There are only a few reports (**Table 1.3**) on hydrophobically end capped PIPOZ. Generally the poly(2-alkyl-oxazoline) (POZ) was synthesized by cationic ring opening polymerization (CROP), and specific initiators and termination agents were chosen to supply desired hydrophobic end groups. Huber et al.[23] synthesized a PIPOZ oligomer (DP = 25) with nonyl or methyl group at the α- end and a nonyl, piperidine or piperazine group at the ω- end. Nonyltriflate or methyltriflate were used as initiators so that the nonyl or methyl groups remained at one end of the PIPOZ chains. The termination agent piperidine, piperazine or nonylamine were attached to the ω- end of the PIPOZ chain. Both telechelic and semi-telechelic PIPOZ with $C_{18}H_{37}$ group attached to one end or both ends were synthesized by Obeid et al.[84] The semitelechelic PIPOZ with $C_{18}H_{37}$ group at α- end was synthesized by CROP using *n*-octadecyl-4-chlorobenzenesulfonate as initiator and methanolic KOH as termination agent. The telechelic PIPOZ was prepared starting from the semitelechelic PIPOZ and react with *n*-octadecyl isocyanate.

Table 1.3 Synthesis routes for POZ.

Synthesis method	End group functionality	M_n (kDa)	$Đ$
CROP of PIPOZ initiator = alkyltriflate	α = -C_9H_{19} or -CH_3 ω = -C_9H_{19}, piperidine/ piperazine	~3[23]	1.04–1.16
CROP of PIPOZ initiator=octadecyl tosylate	α = -$C_{18}H_{37}$ ω = -$C_{18}H_{37}$ or -OH	7–13[84]	1.06–1.21
CROP of PMOZ initiator = alkyl tosylate terminator = alkyl-piperidine	α = C_8F_{17}-C_2H_4- ω = C_nH_{2n+1}, n=6~18	1.8–2.2[85]	1.15–1.20
CROP of PMOZ Initiator = alkyl iodides Terminator = alkyl amine	α,ω = -$C_{12}H_{25}$ or α,ω = -$C_{18}H_{37}$	2–14[86]	1.1–1.4

A telechelic asymmetric poly(2-methyl-2-oxazoline) (PMOZ) with a perfluoro alkyl group or hydrocarbon alkyl group at the α- end and a piperidine group at ω- end was synthesized by CROP by Nuyken et al.[85] The hydrocarbon or fluorocarbon end group came from the initiator and the piperidine group originated from the termination reagent. The telechelic PMOZ with C_8F_{17}-C_2H_4- group at α- end and a hydrocarbon group C_nH_{2n+1} at ω- end was synthesized as well using the same synthetic route (**Scheme 1.11**). Volet et al.[86] synthesized a range of telechelic poly(2-methyl-2-oxazoline) (PMOZ) end capped with alkyl end groups (-$C_{12}H_{25}$ and -$C_{18}H_{37}$). The alkyl iodides as initiator and alkyl amine as terminator were used to attach alkyl groups to the termini of the PMOZ main chain prepared by CROP as shown in **Scheme 1.12**.

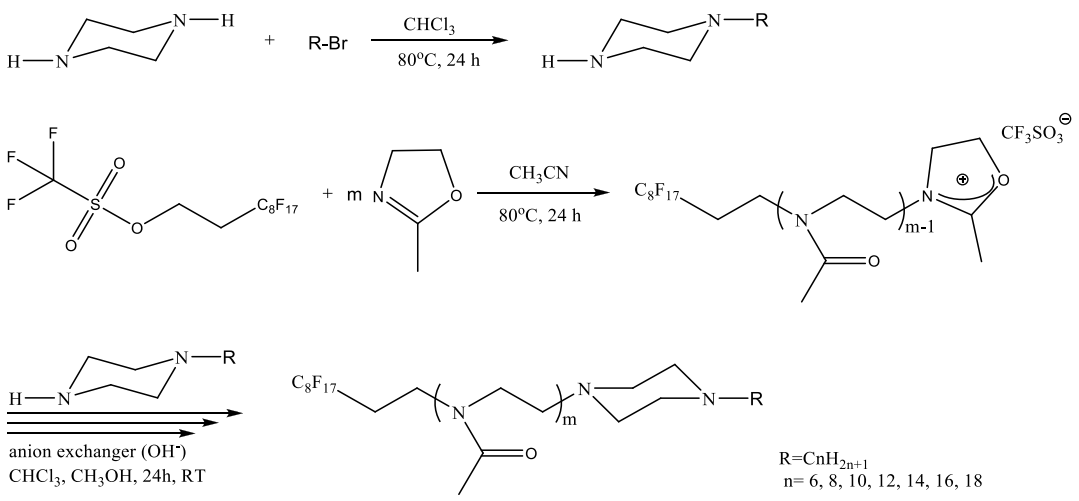

Scheme 1.11 Synthetic route to asymmetric telechelic PMOZ.

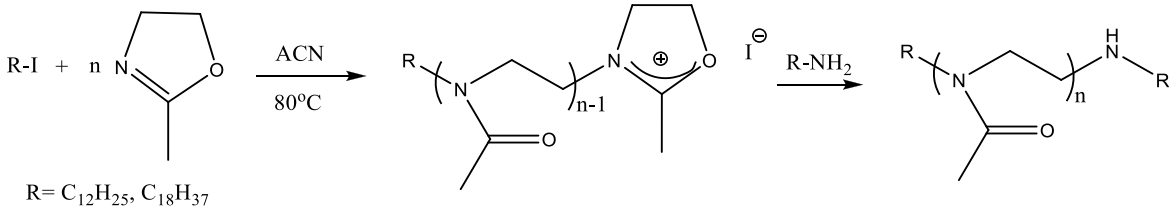

Scheme 1.12 Synthetic route to telechelic PMOZ.

1.3.2 Effects of hydrophilic end groups and of the length of polymer chains on the solution phase transition of amphiphilic polymers

A significant effect of the polymer end groups on the solution behaviour of PNIPAM and PIPOZ has been reported particularly for polymers of low molecular weight.[87, 88] PNIPAM bearing end groups of different hydrophilic/hydrophobic balance have been synthesized,[89] and their solution behaviour has been examined.[87, 88] Smithenry et al.[89] synthesized telechelic PNIPAMs with varying M_n 5.1–32.3 kDa possessing carboxylic acid (-$C(CH_3)(CN)$-C_2H_4COOH) group at both ends. The LCST of carboxylic acid functionalized PNIPAMs in aqueous solutions decreased from 31 to 29 ºC with increasing molecular weight as shown in **Table 1.4**. Xia et al.[90] synthesized four series of PNIPAM with a propionamide or propionate group at the α- end and a chloride group at ω- end and studied the effect of end group hydrophobicity on LCST of PNIPAM. Their study revealed that the shape of the turbidity curves and the enthalpy change of phase transition were affected by the end group hydrophobicity. Sharp transitions and relatively higher LCSTs were observed for PNIPAM

with more hydrophilic end groups (propionamide and isopropionamide group), while PNIPAM with least hydrophilic end group (ethylpropionate- and phenylpropionamide group) exhibited early onsets in their turbidity curves and lower LCST. The molecular weight dependence of the cloud point was found to be more prominent for PNIPAM end modified with the most hydrophilic group. Furyk et al.[91] synthesized three series of PNIPAM with different groups on α- end and a methyl group at ω- end using different initiators. Only a slight molecular weight dependence of LCST was observed within each series and the difference between LCST of PNIPAM carrying different groups was less than 1 ºC, probably due to the high molecular weight of PNIPAMs (18–200 kDa). Wei et al.[92] synthesized asymmetric PNIPAMs (M_n = 10 kDa) with a hydrophobic alkyl chain ($C_{12}H_{25}$- or C_2H_5-) at α-end and a hydrophilic carboxyl acid group or phenylboronic acid group at ω- end. The phase transition of $C_{12}H_{25}$-PNIPAM exhibited a lower LCST and wider transition than that of C_2H_5-PNIPAM. From all these studies, we o conclude that: 1) hydrophilic end group elevate the LCST of PNIPAM, while hydrophobic end groups depress it; 2) the effect of end group modification only interferes when the PNIPAM chain is relatively short; 3) molecular weight dependence is more prominent when the end group is less hydrophobic. A series of PNIPAM having the same M_n (7 kDa) with different end groups (hydroxyethyl, propargyl, chloroethyl, *n*-butyl, *n*-hexyl, and isobutylsulfanylthiosulfanyl) was synthesized by Winnik et al.[93] The LCST ranged from 40.5 to 23.5 ºC as shown in **Table 1.4**. The effect of the end group was more prominent for lower molar mass sample.

There are a few studies of the PIPOZ end functionalized with hydrophilic groups. Meyer et al.[30] synthesized a series of PIPOZ possessing 4-(*N*-Boc-amino)-piperidine at α- end and methyl group at ω- end with varying polymerization degree (DP) 47–174 (M_n 5.3–19.7 kDa). The LCST of charged $PIPOZ^+$ (due to the ammonium in the piperidine group) in saline solution (0.94 wt% NaCl, pH 7) decreased from 38.5 to 35.5 °C when the DP increased from 47 to 174. The larger the polymerization degree, the lower were the hydrophilicity and the LCST. A 3,3-diethoxy-propyl moiety at α- end of PIPOZ (M_n = 9.6 kDa) did not affect the LCST of the PIPOZ compared to PIPOZ carrying methyl groups at α- end with similar molecular weight under identical measurement condition.[94] The authors concluded that chain length was the determinant factor dictating the phase transition of PIPOZ. A hydrophobic

acrylate group at α- end of PIPOZ with DP of 40 reduced the LCST by 5 °C compared with PIPOZ having –OH group at α- end.[95] Huber et al.[23] investigated the effect of end group hydrophilicity on the LCST of PIPOZ oligomers with a DP of 25. Attaching hydrophilic 2-methyl-oxazoline segments (3 monomer units) to the ends of the PIPOZ oligomer resulted in an increase of the LCST from 47 to 53 °C. The more hydrophilic piperazyl end group caused a rise of the LCST of PIPOZ by 1 ºC compared with the less hydrophilic piperidyl end group. Terminal oligoethyleneglycol units also depressed the LCST by 5 °C. The hydrophilic end groups elevated the LCST of PIPOZ. The effect was more prominent for PIPOZ with low molecular weight.

Table 1.4 LCSTs of PNIPAM and PIPOZ end capped with hydrophilic end groups.

Main chain	α- End group	ω- End group	M_n (kDa)	C ($g \cdot L^{-1}$)	LCST (°C)
PNIPAM[89]	$-C(CH_3)(CN)-C_2H_4CO_2H$	$-C(CH_3)(CN)-C_2H_4CO_2H$	5.1–32.3	5	31–29[c]
NIPAM[90]	$-CH_2CH(CH_3)-CONH_2$	Cl	7.5	10	45.3[a]
			11.4		40.7[a]
			19.1		36.3[a]
			57		34.4[a]
	$-CH_2CH(CH_3)CONHCH(CH_3)_2$	Cl	6.5	10	42.9[a]
			11.1		40.3[a]
			20.5		36.0[a]
			58.4		34.1[a]
	$-CH_2CH(CH_3)COOC_2H_5$	Cl	6.1	10	40.6[a]
			9.7		37.8[a]
			21		35.2[a]
			45.1		33.3[a]
	$-CH_2CH(CH_3)CONHC_6H_5$	Cl	7.5	10	37.4[a]
			12.5		35.1[a]
			25		34.2[a]
			49.9		32.8[a]
PNIPAM[96]	$-CH_2CH(CH_3)COOCH3$	Cl	2.8	10	43.0[a]
			5.0		38.9[a]
			6.7		36.4[a]
			15.7		34.6[a]
PNIPAM[91]	$-CH_2C(CH_3)_2CN$	$-OCH_3$	17.8	10	30.83[d]
			55.8		30.40[d]
			170		30.21[d]
			475		30.18[d]
PNIPAM[91]	$-CH_2C(CH_3)(CN)CH_2CH_2CONHC(C_6H_5)_3$	$-OCH_3$	45.8	10	29.74[d]
			93.2		

			144		29.94[d]
			170		29.95[d]
			195		30.18[d]
			384		30.21[d]
					30.27[d]
PNIPAM[92]	$C_{12}H_{25}$-	-COOH	11	0.2	34[a]
	C_2H_5-	-COOH	12	0.2	~37[a]
	$C_{12}H_{25}$-	$-COOCH_2C_6H_4B(OH)_2$	8.5	0.2	~31[a]
	C_2H_5-	$-COOCH_2C_6H_4B(OH)_2$	9.7	0.2	~33[a]
PNIPAM[93]	$-CH_2CH_2OH$	$-CH_2CH_2OH$	7	0.5	40.5[a]
	$-CH_2CH_2Cl$	$-CH_2CH_2Cl$			35[a]
	$-CH_2(CH_2)_2CH_3$	$-CH_2(CH_2)_2CH_3$			32.5[a]
	$-CH_2(CH_2)_4CH_3$	$-CH_2(CH_2)_4CH_3$			27[a]
	$-CH_2-C\equiv CH$	$-CH_2-C\equiv CH$			36.5[a]
	$-SCS_2CH_2CH(CH_3)_2$	$-SCS_2CH_2CH(CH_3)_2$			23.5[a]
PIPOZ[30]	4-(N-Boc-amino)-piperidyl	$-CH_3$	5.3	10	38.5[b]
	4-(N-Boc-amino)-piperidyl	$-CH_3$	19.7	10	35.5[b]
PIPOZ[94]	CH_3-	-OH	9.7	10	37.3[a]
	$-CH_2CH_2CH(OC_2H_5)_2$	-OH	9.6	10	37.5[a]
PIPOZ[95]	CH_3-	acrylate	4.5	1	48.5[a]
	CH_3-	-OH	4.5	1	52[a]
PIPOZ[23]	MOZ_3	MOZ_3-piperidyl	3.2	20	53[a]
	MOZ_3	piperidyl	2.8	20	47[a]
	CH_3-	piperidyl	3.9	20	47[a]
	CH_3-	piperazyl	2.9	20	48[a]
	CH_3-$(O(CH_2)_2)_3$-	piperidyl	4.1	20	42[a]
	CH_3-$(O(CH_2)_2)_3$-	CH_3-$(O(CH_2)_2)_3$-NH-	4.0	20	42[a]

[a] T_c measured by a UV-vis spectrometer.

[b] T_c measured by monitoring the static light scattering intensity.

[c] T_c measured by a right-angle light scattering turbidometer.

[d] T_c measured by monitoring solution clouding through a darkfield condenser using a CCD camera.

Generally, for polymers of similar DP, end group polarity affects more strongly the LCST of PIPOZ than that of PNIPAM. But the differences in end group composition and charge in some cases make it difficult to compare the influence on LCST with various end groups. In order to systemically examine the effect of end group modification on the phase transition behaviour of PIPOZ, a simple structured end groups is necessary. Considering the widely studied telechelic PEO end capped with various length of alkyl groups, alkyl chain might be the proper choice.

1.3.3 Influence of the alkyl end groups on the phase transition of polymer

Introduction of hydrophobic alkyl groups to the termini of the hydrophilic main block induces formation of micelles in most cases. The solution properties of PNIPAM and PIPOZ are greatly changed when the end groups are chemically modified. When dissolved in water, the hydrophilic polymer main chain interacts with water molecules by hydrogen bonding. The entropically unfavorable process of exposing hydrophobic chain ends to water drives the hydrophobic end groups to enter in contact with each other and to reduce the surface energy. When the concentration of the polymer increases, flower-like micelles form with the hydrophobic chain ends in the core of the micelle and the hydrophilic main chain in the corona. The corresponding threshold concentration is known as critical aggregation concentration (cac). The number of polymer chains per micelle is the aggregation number N_{agg}. The cac, N_{agg} and the size of the micelles are the common parameters to characterize polymer micelles.

1.3.3.1 Characterization parameters of micelles formed by telechelic polymers end capped with alkyl end group

One technique to determine the cac is the fluorescence probe method employing probes, such as pyrene. Detailed information about the fluorescence technique is discussed in Section 1.4.3. The cac value of a telechelic polymer micelle is determined by monitoring the intensity ratios of the first and third vibronic bands (I_1/I_3) of the pyrene emission spectrum.

The N_{agg} can be determined by analysis of the pyrene monomer fluorescence decay curves using equation 1.8–1.9 in Section 1.4.3. Another pathway to determine N_{agg} is the fluorescence quenching technique. By adding a quencher into a micelle solution with a fluorescence probe in it and monitoring the fluorescence intensity changes, the N_{agg} can be determined. The average N_{agg} is significantly affected by the concentration of pyrene. The dispersity of polymer, the formation of excimers and the existence of oxygen in solution are the influencing factors of the accuracy of this method.

The cac value can be also determined based on the polymer concentration dependence of the light scattering intensity.[68, 97-99] The light scattering intensity or the I/Kc (I is the scattering intensity, K is the optical constant, and c is polymer concentration) of the telechelic polymer solution increases abruptly upon approaching the cac. The onset concentration of the

intensity increase is defined as the cac of the telechelic polymer. For the telechelic polymer with a cac not very low, the flower-like micelles can be detected by DLS (dynamic light scattering) measurement, and the cac values obtained by light scattering measurement and fluorescence method are comparable. For polymers with very high associativity and very low cac, the flower-like micelles cross-link at concentrations slightly higher than the cac, individual micelles can barely be detected by light scattering and the cac values cannot be measured by light scattering.

The N_{agg} can be deduced from static light scattering either through the Zimm plot in dilute solutions or from analysis of the form factors in concentrated solutions. The apparent molecular weight and radius of gyration are obtained by static light scattering measurements (as shown in Section 1.4), and the N_{agg} is thus obtained. The same information could be obtained by SANS (small angle neutron scattering) in smaller length scales.

The N_{agg} can be also determined by the combination of DLS and viscometry measurement by the expression

$$N_{agg} = \frac{10\pi R_H^3 N_A}{3M\eta} \tag{1.1}$$

where R_H is the hydrodynamic radius determine by DLS, η is the intrinsic viscosity determined by measuring the viscosities of dilute polymer solutions with Ubbelohde viscometers and extrapolating to zero concentration, N_A is Avogadro's number, M is molar mass of the polymer.

The R_H (hydrodynamic radius) and R_g (radius of gyration) of the telechelic polymer micelles were commonly determined by DLS and SLS (static light scattering) respectively. The description of this technique is presented in Section 1.4.

1.3.3.2 Association properties of telechelic PEO, PNIPAM and PIPOZ end-capped with alkyl end groups

To investigate the influence of the alkyl end group properties on the solution behavior of PNIPAM and PIPOZ, we review here the association properties of the most widely studied thermo responsive telechelic PEO in water.

i) Telechelic PEO

PEO end-functionalized with various hydrophobes has been investigated intensively as an associative polymer model.[100] Hydrophobes of various lengths, structures and composition were employed. **Table 1.5** presents an overview of properties of telechelic PEO, PNIPAM and PMOZ micelles in terms of cac and N_{agg}.

The association properties and mechanism of the thermo responsive polymer in dilute solutions induced by introduction of hydrophobic end groups are the interest of our study. The association process of telechelic polymer in aqueous solutions can be generally illustrated by **Scheme 1.13** based on studies about telechelic PEO. Below the cac, a telechelic polymer behaves like a random coil in water. Upon approaching the cac, flower like micelles formed consisting of loops of individual polymer chain via hydrophobic association of end groups. Further increase of the concentration results in network formation through bridging between micelles. In the micelle formation step, different models exist concerning the micelle structure. The closed micelle model treats the flower micelle as an isolated moiety with a constant aggregation number which does not change with concentration. On the contrary, increase of polymer concentration leads to increase of N_{agg} in the open micelle model. Apart from closed loops, dangling chains also participate in building flower micelles in the open micelle model. One essential parameter which is different between for the two models is the N_{agg}.

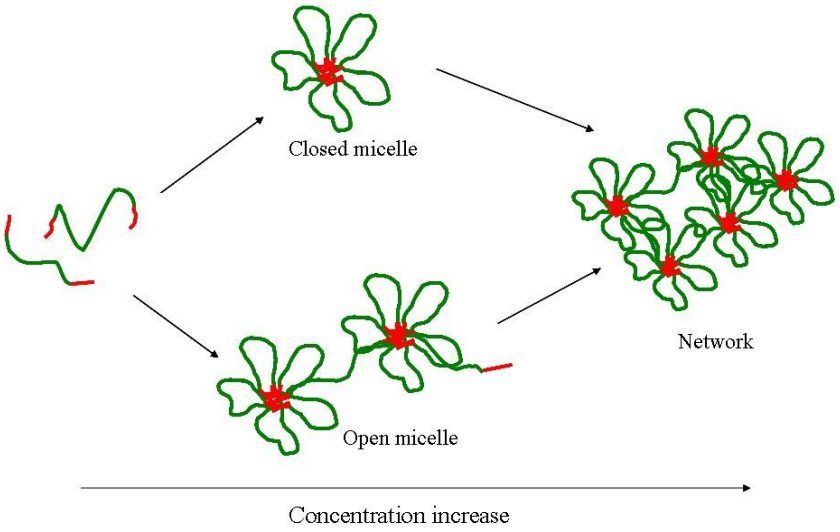

Scheme 1.13 Aggregation pathways for telechelic PEOs.

To understand the association behavior of these polymers, important features which need to be characterized are the aggregation number and influencing factors. The number of studies listed in **Table 1.5** gives an idea of how the length and properties of end groups influence the aggregation number and the cac. However, great discrepancy of these values is inevitable due to the different measuring techniques or experiment conditions. Alami et al.[101] reported a $N_{agg} = 14 \pm 2$ for a telechelic PEO ($M_n = 20$ kDa) end capped with $C_{12}H_{25}$- group in aqueous solutions with polymer concentration 2–7 wt% using pyrene as a probe and dimethylbenzophenone as a quencher. The cac value was determined to be 8 for this polymer measured at a higher pyrene concentration quenched by pyrene excimer formation with polymer concentration of 6 wt%. It's important to emphasize the difficulties in determining the aggregation numbers, and they are only comparable for the association character of telechelic PEOs with the same architecture determined by the same technique.

a. Telechelic PEO end-capped with hydrocarbons

The adequate association model for telechelic PEO in water is still an open issue. A closed association process was proposed by Yekta et al.[102] for the aqueous solutions of telechelic PEO end-capped with $C_{16}H_{33}$- end groups with varying molecular weight ($M_n = 34 – 51$ kDa). The $C_{16}H_{33}$- end groups were attached to the chain ends through an IPDU linkers. N_{agg} values ranging from 9 to 14 were determined by the fluorescence quenching method using pyrene as a probe. The linkers were also shown to participate in the formation of the hydrophobic core of micelles. A report by Pham et al.[103] about a telechelic PEO with the same structure but different end group lengths ($C_{16}H_{33}$- and $C_{18}H_{37}$- groups respectively) confirmed the closed association model. For the polymer concentration ranging from 0.2 to 1.5 $g \cdot L^{-1}$, N_{agg} values were determined to be 20 ± 2 and 33 ± 9 by DLS and viscometry measurements for the $C_{16}H_{33}$- and $C_{18}H_{37}$- end capped PEO, respectively. Generally, the N_{agg} determined by combination of DLS and viscometry measurements are higher than that obtained by fluorescence techniques in dilute solution region. Vorobyova' study [103] for telechelic PEO having the same structure as the former two groups ($C_{18}H_{37}$- groups, $M_n = 35$ kDa, IPDU linker) supported the open association model. N_{agg} was determined to be 12 by fluorescence at polymer concentration 2.1 $g \cdot L^{-1}$, which tended to increase with polymer concentration increasing from 3 to 17 wt%. Beaudoin et al.[69] confirmed the increase in the aggregation

number upon increase in concentration, based on their study of a PEO end capped with $C_{16}H_{33}$- groups (M_n = 32 kDa) via ether linkers.

A study by Kadam et al.[104] revealed that increasing the main chain length led to smaller aggregation number (from 25 to 17) for telechelic $C_{16}H_{33}$- end capped PEO with molecular weight varying from 10 kDa to 20 kDa. Rheological measurements indicated that the association of telechelic PEO in dilute aqueous solutions showed an open association process. Chassenieux et al.[98] studied the effect of molecular weight (M_w = 34 kDa, 18.8 kDa and 8.7 kDa) on the association process of telechelic PEO end capped by $C_{12}H_{25}$- groups by light scattering and viscometry. They concluded that the cac increased with increasing molecular mass. The shortest telechelic PEO studied associated in water following a two-step model. Isolated micelles formed at low concentrations, which interconnected in higher concentrations according to an open association model. The two steps were very distinct probably due to the dispersity of the sample. For the other two high molar mass samples studied, both the close association and open association existed simultaneously. There are studies supporting both the close association model and open association model. No final conclusions could be drawn from the present studies.

The effect of the length of the alkyl end groups on the cac and N_{agg} was studied by Lafleche et al.[105] Their study revealed that with increasing length of alkyl groups, the aggregation number increased and the critical association concentration decreased. No influence of the backbone architecture was observed on these parameters. Francois et al.[106] examined the solubility of telechelic PEOs of varying molar mass (10–35 kDa) and end capped with hydrocarbon groups of varying lengths ($C_{12}H_{25}$-, $C_{16}H_{33}$- and $C_{18}H_{37}$-). Increasing the length of end group led to enhanced formation of micelles and phase separation of PEO with a wider two phase region. The aggregation number increased with increasing end group length. Kim et al.[66] synthesized a series of telechelic PEOs (M_n = 4 kDa) end capped with C_8H_{17}-, $C_{12}H_{25}$- and $C_{18}H_{37}$- respectively through a –NH-COO- linker and studied their solution behaviour. DLS results showed that no micelles were observed in aqueous solutions of telechelic α,ω-dioctyl PEO (C_8H_{17}-PEO), while the α,ω-dioctadecyl PE ($C_{18}H_{37}$-PEO) formed more stable and larger micelles than the α,ω-didodecyl-PEO ($C_{12}H_{25}$-PEO) with a lower cac. The association mechanism was revealed to be a combined result of chain

flexibility and hydrophobicity of molecules. $C_{12}H_{25}$-PEO had the largest flexibility and hydrophobicity as predicted by Molecular Dynamic Simulation, thus more favourable in forming aggregates rather than micelles. C_8H_{17}-PEO did not form micelles due to insufficient chain flexibility. The formation of network was also affected by end group length. The micelles formed by $C_{18}H_{37}$-PEO were more compact and did not readily interact with each other, compared to the $C_{12}H_{25}$-PEO micelles. Networks started to form at concentrations lower than with the $C_{12}H_{25}$-PEO micelles.

b. Telechelic PEO end-capped with fluorocarbons

Besides the mostly studied hydrocarbon groups, fluorinated alkyl groups were also employed to tune the solution behaviour of telechelic PEO due to the stronger hydrophobicity and outstanding chemical and thermal stability. It is conventionally accepted that the hydrophobicity of one CF_2 equals to 1.5 CH_2. Rufier et al.[107] studied the rheological behaviour of a series of PEO end capped with different hydrocarbon and fluorocarbon groups and found macroscopic phase separation in dilute aqueous solutions (above cac) of telechelic PEO containing fluorinated end groups as an evidence of the reinforced hydrophobicity of fluorinated segments.

Séréro et al.[108] synthesized a telechelic PEO (M_n = 10 kDa) end capped with C_8F_{17}-$C_{11}H_{22}$- groups and investigated the structure of flower micelles by SANS. A N_{agg} of ~ 50 was obtained. Tae et al.[109] synthesized a series of telechelic PEOs (M_n = 6 kDa and 10 kDa) with fluorinated alkyl end groups (C_6F_{13}-, C_8F_{17}- and $C_{10}F_{21}$-) and investigated their aggregation behavior in water by rheology and SANS. The N_{agg} was observed to be dependent on the length of the end groups and did not change with concentration. Increasing the length of the end groups resulted in larger N_{agg}. Unlike the case of PEO end capped with hydrocarbon end groups C_8H_{17}-, the short fluorinated alkyl groups C_8F_{17}- end capped PEO associated into flower micelles in water. Flower micelles were observed by Xu et al.[110] for telechelic PEOs (M_n = 35 kDa) end capped with C_6F_{13}- and C_8F_{17}- groups, respectively. The N_{agg} was determined by NMR technique to be 15 and 10 for the two polymers, respectively. An attempt to determine the molecular weight dependence of N_{agg} by fluorescence using pyrene derivative as a probe revealed perturbation of micelles by the fluorescent probe. The authors claimed that flower micelles could only form when the entropic penalty of looping was overcome by

the insolubility of chain ends. Zhou et al.[111] synthesized fluorinated telechelic PEOs (M_n = 10 kDa) end capped with fluorocarbon groups of varying length of (C_3F_7-, C_6F_{13}- and C_8F_{17}-) and measured their cac values by fluorescence method using fluorocarbon modified pyrene probes. The cac values obtained for the three polymers were close to each other, around 0.8 $g \cdot L^{-1}$. A range of C_8F_{17}- end capped telechelic PEO with M_n = 10, 20 and 35 kDa formed flower micelles above cac of each polymer in water as reported by Lammertink et al.[112] A constant N_{agg} of 15 was observed for all three polymers. Increasing the end group length to $C_{10}F_{23}$- led to higher N_{agg} of 25.

ii) Telechelic PNIPAM

Telechelic PNIPAM end capped with octadecyl groups having various molecular weights were synthesized and their assembly behavior in aqueous solution was studied by Kujawa et al.[73, 113, 114] Flower-like micelles were formed in dilute solutions of telechelic PNIPAM with aggregation number around 25, measured by DLS. The LCST of telechelic PNIPAM increased as the mainchain length decreased. A depression of LCST by 8 °C was observed for telechelic PNIPAM compared to homopolymer with the same molecular weight (7.3 kDa). Semi-telechelic PNIPAMs, having alkyl groups with various length (C_3-C_{18}) at one end, were synthesized by Chung et al.[88] The $C_{18}H_{37}$- and $C_{12}H_{25}$- end modified PNIPAMs formed flower like micelle in aqueous solution above their corresponding cac (0.08 $g \cdot L^{-1}$ for $C_{18}H_{37}$-PNIPAM and 3.5 $g \cdot L^{-1}$ for $C_{12}H_{25}$-PNIPAM measured by fluorescence using pyrene as probe), while the C_3H_7-, C_6H_{13}- and C_8H_{17}- end functionalized PNIPAMs associated in water and formed hydrophobic region with loose interaction. No clear cac could be detected for the semi-telechelic PNIPAMs with short alkyl chains (C_3-C_{18}). De et al.[81] synthesized a semi-telechelic PNIPAM (M_n = 2.7 kDa) with $C_{12}H_{25}$- group at α- end and a telechelic asymmetric PNIPAM after attaching a folic acid group to ω- end of the semitelechelic PNIPAM. The LCST values were determined to be 26 ºC and 22 ºC for the semi-telechelic and telechelic PNIPAM respectively, which were much lower than the unmodified PNIPAM. Nojima et al.[115] investigated the solution behavior of telechelic PNIPAM (M_n = 47.5 kDa) end-capped with $C_{18}H_{37}$- chains by static light scattering. The weight average molar mass and radius of gyration were determined by static light scattering. The deviation of radius of gyration, Rg from that predicted for isolated flower micelle and the strong molar mass dependence,

indicated that flower micelles formed even in dilute solutions as low as 1 $g \cdot L^{-1}$ by bridging attractions of the telechelic chains. Koga et al.[116] developed a theoretical model to describe the solution behavior of telechelic PNIPAM (M_n = 22.2 kDa) end capped with $C_{18}H_{37}$- groups. Flower micelles formed in solution at concentration of 10 $g \cdot L^{-1}$ at temperatures between 10 and 20 ºC. The micelle model has a 3-layered core-shell structure with an inner core of hydrophobic end groups, a compact inner shell consisting of partly collapsed PNIPAM chains and an outer layer of freely hydrated PNIPAM chain. The change in concentration did not affect the structure of micelles below the percolation concentration when the network structure formed.

iii) Telechelic POZ

There are few reports on the effect of end group modification on the solution properties of PIPOZ solutions. A $C_{18}H_{37}$ group was used to modify end groups of PIPOZ. Both telechelic and semi-telechelic PIPOZ with $C_{18}H_{37}$ group attached to one end or both ends, respectively were synthesized by Obeid et al.[84] The $C_{18}H_{37}$ group was attached to the ω- end of telechelic PIPOZ by a -CONH- linker, so the architecture of the telechelic was not totally symmetric. Flower-like and star like micelles were formed in aqueous solutions of the telechelic and semi-telechelic polymers, respectively. The N_{agg} of telechelic PIPOZ determined by fluorescence was 14 and 9 for polymer with M_n of 7 and 10 kDa, repectively. The LCST of the telechelic PIPOZ in water decreased by 12 ºC compared to unmodified PIPOZ with $–CH_3$ and –OH at each end. Huber et al.[23] synthesized a PIPOZ oligomer end capped with nonyl groups at both ends and a -NH- linker included in ω- end. A LCST depression of 15 ºC was noted and attributed to the end group modification. Since very few reports can be found concerning the telechelic PNIPAM and PIPOZ, we include the PMOZ (poly(2-methyl-2-oxazoline)) to examine the effect of alkyl end group modification on the solution properties of telechelic amphiphiles. Volet et al.[86] synthesized a range of telechelic poly(2-methyl-2-oxazoline) (PMOZ) end capped with alkyl end groups ($C_{12}H_{25}$- and $C_{18}H_{37}$) of varying molecular weight 2–14 kDa. The cac values of micelles were determined by fluorescence technique and showed molecular weight and end group length dependence. Increasing molar mass from 2 to 14 kDa, the cac of $C_{12}H_{25}$- end functionalized PMOZ increased from 0.08 $g \cdot L^{-1}$ to 0.85 $g \cdot L^{-1}$. The cac of $C_{18}H_{37}$ end capped PMOZ was lower (0.03

g·L^{-1}) than the cac of $C_{12}H_{25}$- end functionalized PMOZ (0.11 g·L^{-1}) having the same molar mass 4 kDa.

To illustrate the effect of end group modification on the association and the phase transition behaviour of PIPOZ, telechelic PIPOZs with identical main chain structures but end capped with both hydrocarbon alkyl chains and fluorocarbon alkyl chains, respectively, was synthesized and studied as model polymers. The solution behaviour of the two telechelic PIPOZs will be discussed in Chapter 4.

Table 1.5 Association parameters of telechelic PEO/PNIPAM/POZ with identical end groups in water.

Polymer	End groups	M_n (kDa)	cac (g·L^{-1})	N_{agg}	linker
PEO[105]	-$C_{12}H_{25}$	4.8–17.2	0.45	10	n.a.
	-$C_{14}H_{28}$		0.13	14	
	-$C_{16}H_{33}$		0.05	18	
	-$C_{18}H_{37}$		0.02	22	
PEO[63]	-$C_{16}H_{33}$	25	0.1–0.2	13–23	IPDU
PEO[117]	-$C_{16}H_{33}$	34	n.a	20	IPDU
PEO[118]	-$C_{12}H_{25}$	8.5	0.14	14	n.a.
PEO[119]	-$C_{12}H_{25}$	9.3	n.a.	17(±3)	n.a.
PEO[68]	-$C_{12}H_{25}$	12	2	20	IPDU
	-$C_{12}H_{25}$	20	7	20	IPDU
	-$C_{16}H_{33}$	32	0.1	15	IPDU
PEO[102]	-$C_{16}H_{33}$	34, 51	n.a.	9,11	IPDU
PEO[101]	-$C_{12}H_{25}$	20.3	n.a.	15–30	n.a.
PEO[120]	-$C_{12}H_{25}$	6	0.3–4	6	-O-
		20	0.46–6.7	11	
		20	2–30	10	
		35	3–60	7	
PEO[121]	-$C_{12}H_{25}$	5.7	0.1	n.a.	-O-
		9.88	1.2		
		20.8	25		

PEO[122]	-$C_{16}H_{33}$	51	n.a.	11(±1)	IPDU
PEO[108]	-$C_8F_{17}C_{11}H_{23}$	10	n.a.	~50	IPDU
PEO[123]	-$C_{16}H_{33}$	35	0.2	20(±2)	-CONH-
PEO[123]	-$C_{18}H_{37}$	35	0.2	33(±9)	-CONH-
PEO[124]	-C_8H_{17} -$C_{12}H_{25}$ -$C_{18}H_{37}$	16.7 26.2 37.65	16.16 3.33 0.017	n.a.	n.a.
PEO[111]	$H(CF_2)_8CH_2$-	10	0.8	n.a.	IPDU
PEO[111]	$C_{12}H_{25}O$-	10	0.078	-	IPDU
PEO[111]	$C_{12}H_{25}O$-	20	0.83	-	IPDU
PEO[125]	$C_8F_{17}C_{11}H_{23}O$-	-	-	49(±6)	IPDU
PEO[69]	-$C_{16}H_{33}$	32	1	17(±2)	-CONH-
PEO[126]	$C_8F_{17}C_{11}H_{23}$-	10	n.a.	49(±6)	IPDU
PEO[126]	$C_8F_{17}C_{11}H_{23}$-	20	n.a.	35(±3)	IPDU
PEO[71]	$C_{12}H_{25}O$-	10	2	n.a	n.a
PEO[71]	$C_{12}H_{25}O$-	20	7	n.a	n.a
PEO[71]	$C_{12}H_{25}O$-	35	19	n.a	n.a
PEO[109]	-$C_2H_4(CF_2)_n$, n=6,8,10	6, 10, 20	n.a.	16–26	IPDU
PEO[127]	-C_8H_{17}	35	10	n.a	-CONH-
PEO[127]	-$C_{12}H_{25}$	35	5	n.a	-CONH-
PEO[127]	-$C_{18}H_{37}$	35	0.1	n.a	-CONH-
PEO[97]	-$C_{16}H_{33}$	50	0.2–0.5	8–21	-CONH-
PEO[128]	-$C_{12}H_{25}$, -$C_{16}H_{33}$, -$C_{20}H_{42}$	~25	0.28–1.83	5–7	diisocynate
PEO[106]	-$C_{12}H_{25}$ -$C_{16}H_{33}$	6–35 32	0.9–19 1	n.a.	n.a. -CONH-
PEO[129]	-$C_{18}H_{37}$	35	0.04	n.a.	-CONH-
PEO[66]	-$C_{12}H_{25}$,	4	1.2	13	-CONH-

	$-C_{18}H_{37}$	4	0.4	10	-CONH-
PEO[104]	$-C_{15}H_{31}$	10	n.a.	18–26	IPDC
	$-C_{15}H_{31}$	20		14–19	IPDC
PNIPAM[113]	$-C_{18}H_{37}$	37	n.a.	25 (±3)	CS3, -CONH-
PNIPAM[114]	$-C_{18}H_{37}$	12	0.006	27–39	CS3, -CONH-
		22	0.01	24–32	CS3, -CONH-
		49	0.024	16–22	CS3, -CONH-
PNIPAM[79]	Azobenzene-C_6H_{13}-	n.a.	0.056	29	-S-
PMOZ[86]	$-C_{12}H_{25}$,	2.4–14	0.08–0.85	~30	—
	$-C_{18}H_{37}$	4.5–7.3	0.03–0.1		
PIPOZ[84]	$-C_{18}H_{37}$	7	0.006	14 (±2)	—, -OCONH-
		10	0.009	9 (±1)	

1.4 Techniques

1.4.1 NMR

NMR spectroscopy is a versatile and powerful technique to correlate the variation of the molecular structure with the dynamics of molecules in solutions. Studies of the micellization and aggregation of polymers in solutions have been reported earlier.[130-132] ^{1}H NMR spectroscopy is the most commonly employed technique to investigate the molecular dynamics of the phase transitions. However, the dynamic changes of segments manifested by line shape and peak position are limited by the resolution of the spectrometer and therefore a complementary measurement was needed: a study of the relaxation times of corresponding segments. Depending on the nature of the relaxation, shielding anisotropy, spin diffusion, dipolar interactions etc., relaxation times provide information about the molecular dynamics on various time scales. Spin-lattice relaxation times T_1 are sensitive to motions on the 10^{-7} to 10^{-9} s time scale and can be tuned by varying temperature. The value of T_1 decreases as mobility increases in the slow motional limit and increases as mobility increases under extreme narrowing conditions, with the minimum value at mobility comparable to Larmor frequency. Typically, for different chemical groups along a hydrocarbon chain, only one

single ^1H T_1 value exists because of ^1H spin diffusion. The contribution of spin diffusion is reduced when the phase transition occurs.

The phase transition of PNIPAM in D_2O solution has been studied by monitoring the ^1H NMR spectra as a function of temperature by Díez-Peña etc.[66] The peak of DOH shifted and splitted into two peaks corresponding to free water and water expelled by the hydrogel, respectively, as the temperature increased above the LCST. A ^1H NMR study of PNIPAM solutions and gels was reported by Tokuhiro et al.[133] The methylene and methine protons in the PNIPAM gels do not show appreciable change throughout the phase transition. On the other hand, the intensity of the isopropyl methyl protons signal, decreased substantially with temperature even beyond the collapse temperature of the gel. Proton T_1 relaxation time of PNIPAM in D_2O solution (35 $mg \cdot L^{-1}$) was also determined in their study. Temperature dependence of ^1H T_1 for PNIPAM in D_2O solution exhibited differences between the behavior of the side chain and main chain proton. The T_1 values for the methyl protons and methine proton in the isopropyl group increased with increasing temperature. The temperature dependence of T_1 values for main chain methylene and methine proton was completely opposite to the side chain groups. A study by Ohta et al[134] measured the T_1 and T_2 relaxation times for PNIPAM as a function of temperature and pressure. Another study by Zeng[135] and coworkers about PNIPAM solutions revealed a decrease in T_1 relaxation time of methylene and methine proton and an increase in methyl proton with increasing temperature, which indicates that the side chain methyl group motion slow down and that of the main chain speed up. The phase separation in PNIPAM/water system was investigated by ^{13}C and ^1H NMR in their research. T_1 and T_2 of polyampholyte hydrogel poly(methylacrylic acidacryloyloxyethyl trimethylammonium chloride)[P(MA-DAC)] was determined by Lu et al. under different conditions.[136] The molecular mobility of polyampholyte hydrogel was characterized by changes in T_2. The mobility of mainchain methylene group proton of PNIPAM and proton of different end group was investigated for D_2O solutions of PNIPAM end-capped with different groups.[137] The kinetic behaviour of phase transition of PNIPAM was studied by ^1H NMR. The chain mobility as revealed by T_2, the mobile fraction of PNIPAM chain as revealed by signal intensity and the self-diffusion coefficient were examined as function of temperature and time by Yushmanov et al.[138] A faster collapse and intermolecular aggregation and a

slower redistribution of the individual chains among and within the globular and mobile states, were suggested. The mobility of PNIPAM protons for PNIPAM microgel in SDS solutions was studied by Andersson[139] through monitoring ^{1}H NMR relaxation times of different groups in PNIPAM.

In addition to the most commonly used ^{1}H NMR spectroscopy, ^{19}F NMR has some advantages in studying fluorinated molecules due to the strong signal of ^{19}F and much less interference from the environment. The strong hydrophobicity of fluorocarbon groups makes the ^{19}F NMR a useful technique to study the micellization of fluorinate polymers.[130] Because of the high sensitivity of ^{19}F peaks, low background signal, and biocompatibility, fluoropolymers have attracted increasing attention as paramagnetic contrast agents in ^{19}F MRI as an alternative of the Gd^{III}-assisted ^{1}H MRI techniques, in applications like monitoring drug delivery, imaging of lung and vascular injury, visualization of cellular therapeutic[140-143], etc. ^{19}F NMR spectroscopy has been reported to examine the association and network formation of telechelic fluorinated PEG with C_6F_{13} and C_8F_{17} end groups.[130] Another study about the association of an asymmetric telechelic poly(*N*-acylethyleneimine) end-capped with a fluorocarbon and a hydrocarbon chain by ^{19}F NMR spectroscopy has been reported.[144] The T_2 relaxation values observed for the fluorocarbon end group in the aggregated state were taken as an indication of the formation of segregated hydrocarbon and fluorocarbon micellar compartments. A study of an amphiphilic copolymer of the water soluble poly(sodium acrylate) grafted by 8% hydrophobic C_7F_{15}-CH_2- side chains by ^{19}F NMR spectroscopy revealed a slow exchange of the polymer chains among different states of aggregation and a fast exchange of individual side chains among aqueous and hydrophobic environments within the same aggregate.[145]

NMR spectroscopy has been proved to be a convenient technique to study the association dynamics of fluorocarbons. As has been reported, besides ^{13}C nuclear spins, chemical shift of ^{19}F nuclear spins of fluorinated molecules was significantly shifted by environment.[146-148] A systematic study, using the above mentioned NMR techniques of the temperature sensitive telechelic fluorinated PIPOZ in aqueous solutions below and above its LCST, would be beneficial for a more comprehensive understanding of the phase separation process happened in its aqueous solutions. It will be presented in Chapter 5 of this thesis.

1.4.2 Light Scattering

Structural information on the size, shape, and interactions of polymer chains in solution can be obtained using light scattering experiments. The initial studies employing light scattering apparatus focused on determining the apparent weight average molecular weight of PNIPAM. DLS and SLS were first employed to detect a coil-to-globule transition in a dilute PNIPAM solutions by Wu et al.[149] Light scattering has been a common used technique to characterize the structures of polymers in solutions. I will only introduce here the information we can obtain by light scattering without any practical application examples.

The weight average molecular weight $M_{w,app}$, the z-average root-mean-square radius of gyration R_g, and the second virial coefficient $A_{2,}$ can be obtained by static light scattering. These parameters are derived by collecting the average scattered light intensity as a function of scattering angle θ and polymer concentration c,

$$\frac{Kc}{R} = \frac{1}{M_{w,app}}\left[1 + 2A_2 M_{w,app} c + \ldots\right]\left[1 + \frac{R_g^2}{3} q^2\right] \tag{1.2}$$

The optical constant $K = 4\pi^2 n^2 (\mathrm{d}n/\mathrm{d}c)^2 / N_A \lambda_0^4$, where n is the refractive index of the solvent, $\mathrm{d}n/\mathrm{d}c$ is the specific refractive index increment, N_A is Avogadro's number, and λ_0 is the wavelength of the incident light in vacuum, $q = (4\pi n/\lambda_0)\sin(\theta/2)$. From the slopes and intercept of the double extrapolated lines of Kc/R to $c \rightarrow 0$ and $q \rightarrow 0$, the three parameters are determined.

In dynamic light scattering, monochromatic light travels through a solution containing scattering particles. The fluctuations in time of the scattered light intensity are measured at different scattering vectors q. These fluctuations typically occur on the microsecond to second time scales and can be traced to the Brownian motion of molecules in dilute polymer solutions. The intensity autocorrelation function at an instant time τ can be expressed by

$$G_{(2)}(\tau) = \langle I(t) I(t+\tau) \rangle \tag{1.3}$$

The Siegert equation relates the second-order autocorrelation function with the first-order autocorrelation function $g_{(1)}(\tau)$ with

$$g_{(2)}(\tau) = 1 + \left|g_{(1)}(\tau)\right|^2 \tag{1.4}$$

$$g_{(1)}(\tau) = \exp\left(-\left|q\right|^2 D_0 \tau\right) \tag{1.5}$$

The translational diffusion coefficient D_0 is thus obtained by analyzing the autocorrelation function using different method (CONTIN for polydispersed sample or Guinier for narrow dispersion) from a dynamic light scattering experiment. R_H, is then calculated via the Stokes-Einstein equation:

$$R_H = \frac{k_B T}{6\pi\eta_s D_0} \tag{1.6}$$

where k_B is the Boltzmann constant, η_s is the viscosity of the solvent (water), and T is the absolute temperature.

The shape of particles especially for comparatively small particles (size 10−100 nm) can be evaluated by the form factor $\rho = R_g/R_H$. ρ for a Gaussian chain is predicted to be around 1.50, 1 for a hollow sphere, and 0.775 for a homogeneous sphere. For smaller particles < 50 nm, beyond the length scale of light scattering experiments, the form factor ρ only provides an indicative, and ambiguous, determination of the particle shape.

1.4.3 Fluorescence

Fluorescence probe methods are a widely used to determine the cac and N_{agg} by employing fluorescence probes, e.g. pyrene. The high environmental sensitivity of the intensity ratios of the first and third vibronic bands (I_1/I_3) in the pyrene emission spectrum and shifts of excitation and emission spectra, makes it efficient in probing the partition of pyrene between water and the segregated core of the telechelic amphiphilic polymer micelles. The cac values determined for hydrophobically end–capped polymers are usually very low (about 10^{-6} mol of hydrophobic groups per liter) compared to the cmc (critical micelle concentration) of low molecular weight surfactants. The small value of the cac makes it difficult to determine the onset of aggregation from the shift in the partition equilibrium of the probe. In addition, unlike low molecular weight surfactants, the I_1/I_3 decreases upon micellization of telechelic polymer over a broad range of concentrations (from 10^{-7} to 2×10^{-5} mol·L^{-1})[128].

N_{agg} can be determined by analysis of fluorescence decay curves.[102, 150, 151] The probability (P_n) of finding a pyrene molecule in a given micelle following Poisson quenching kinetics

$$P_n = \frac{\langle n \rangle^n e^{-\langle n \rangle}}{n!} \tag{1.7}$$

where <*n*> is the average number of pyrene molecules in a micelle. The pyrene monomer fluorescence decay function $I_M(t)$ is given by the expression

$$I_M(t) = I_M(0)\exp\left\{-t/\tau - \langle n \rangle\left[1-\exp(-kt)\right]\right\} \tag{1.8}$$

In this equation, $I_M(t)$ and $I_M(0)$ are the fluorescence intensities at time t and 0, and τ is the fluorescence lifetime of pyrene in the micelle with low pyrene concentration. The term t/τ indicates the exponential decay of pyrene in micelles containing only one pyrene molecule. The second term corresponds to the contribution to the total fluorescence intensity from the micelles which contain two or more pyrene molecules, and *k* is the rate coefficient for intramicellar excimer formation. N_{agg} is determined from a plot of <*n*> vs pyrene concentration by the equation

$$[\text{micelle}] = [C_{polymer} - cac]/N_{agg} \tag{1.9}$$

where $C_{polymer}$ is the polymer concentration. However, the N_{agg} value obtained by this method depends somewhat on the probe and the polymer concentration. The average N_{agg} is significantly affected by the concentration of pyrene. The dispersity of polymer, the formation of excimers and the existence of oxygen in solution are the influencing factors of the accuracy of this method.

Another widely used pathway to determine N_{agg} is fluorescence quenching technique. By adding a quencher into the micelle solutions with fluorescence probe in it and monitoring the fluorescence intensity changes, the N_{agg} can be determined by the expression

$$\ln\frac{I_0}{I} = \frac{[Q]}{[M]} \tag{1.10}$$

$$N_{agg} = \frac{[R]}{[M]} \tag{1.11}$$

where, [Q], [M] and [R] are the concentration of quencher, micelle and polymer respectively.

1.5 Objectives

(1) The solution behaviour of PNIPAM in mixtures of water and a water-miscible organic solvent will be systematically explored.

The phase separation of linear PNIPAM has been widely studied in aqueous solution and in the mixture of water and a water miscible solvent. There are only few reports, however, about the solution properties of PNIPAM of different architecture. The solution behaviour of PNIPAM has been studied from different viewpoints. In all these theories, the orientation of chain segments is important to examine the solution behaviour of PNIPAM. PNIPAMs of different architectures are employed, for which the orientation of chain segments are constrained by space limitation. In the beginning, we study their solution behaviour in water and water-methanol mixtures hoping to gain a better knowledge of the phenomena.

(2) The effect of polymer concentration on the cononsolvency phenomena of PNIPAM in methanol/water system is examined to obtain information on the structure and composition of the phase separated PNIPAM.

Most studies of the cononsolvency phenomenon of PNIPAM were conducted in dilute solvent mixtures, and stable milky solutions were observed with proper compositions of solvent mixture. So far, there is only one study on the phase transition of PNIPAM in methanol and water mixture with high polymer concentration. Macroscopic phase separation of the PNIPAM/water/methanol was reported in that study and two liquid phases were observed at proper solvent ratio. The mechanism of the macroscopic phase separation and influencing factors remain unknown. The present work on the phase separation of PNIPAM in methanol/water mixture with adequate polymer concentration will contribute to a better understanding of the phase transition mechanism of PNIPAM.

(3) The effect of end group modification on the solution behaviour of thermo sensitive PIPOZ in water is studied.

The telechelic amphiphilic polymers, end capped with alkyl groups of sufficient hydrophobicity and flexibility, associate into flower-like micelles in water. The solution

properties and phase transition behaviour of the telechelic PEO and PNIPAM have been studied by fluorescence, light scattering, NMR etc. The characterization parameters of the micelles (cac, N_{agg} etc.) were found to deviate greatly from each other due to the difference in polymer chemical structure and limitation of different characterization techniques. There are only few studies about the solution properties of telechelic PEO with fluorocarbon groups and the N_{agg} value in general is reported to be higher than that of hydrocarbon end-capped telechelic PEO with similar end group hydrophobicity. The difference in association properties between telechelic polymers end capped with hydrocarbons and fluorocarbons having identical structures has not been examined yet. Two telechelic PIPOZ with hydrocarbon and fluorocarbon end groups are synthesized to study the problem. The effect of end group modification on the phase transition of PIPOZ is studied as well by NMR Relaxation technique. The changes in relaxation times provide information about the chemical environment and molecular dynamics of polymer chain. It is an efficient tool to monitor the phase separation process without contaminating the original solution of polymer.

1.6 References

1. Asher, S. A.; Weissman, J. M.; Sunkara, H. B. WO9820388A1, 1998.
2. Leipzig, N.; Wijekoon, A. WO2013112863A1, 2013.
3. Mikos, A. G. WO2013086523A2, 2013.
4. Samain, H. WO2013093773A1, 2013.
5. Folan, M.; Horgan, F.; Turkington, M. US20130018258A1, 2013.
6. Pelton, R. *Adv. Colloid Interface Sci.* **2000,** 85, 1-33.
7. Kikuchi, A.; Okano, T. *Adv. Drug Delivery Rev.* **2002,** 54, 53-77.
8. Stile, R. A.; Healy, K. E. *Biomacromolecules* **2001,** 2, 185-94.
9. Scarpa, J. S.; Mueller, D. D.; Klotz, I. M. *J. Am. Chem. Soc.* **1967,** 89, 6024-30.
10. Schild, H. G. *Prog. Polym. Sci.* **1992,** 17, 163-249.
11. Shibayama, M.; Mizutani, S.-y.; Nomura, S. *Macromolecules* **1996,** 29, 2019-24.
12. Ono, Y.; Shikata, T. *J. Am. Chem. Soc.* **2006,** 128, 10030-1.
13. Wu, C.; Wang, X. *Phys. Rev. Lett.* **1998,** 80, 4092-4.
14. Ye, X.; Lu, Y.; Shen, L.; Ding, Y.; Liu, S.; Zhang, G.; Wu, C. *Macromolecules* **2007,** 40, 4750-2.
15. Okada, Y.; Tanaka, F. *Macromolecules* **2005,** 38, 4465-71.
16. Tong, Z.; Zeng, F.; Zheng, X.; Sato, T. *Macromolecules* **1999,** 32, 4488-90.
17. Otake, K.; Inomata, H.; Konno, M.; Saito, S. *Macromolecules* **1990,** 23, 283-9.
18. Van Durme, K.; Van Assche, G.; Van Mele, B. *Macromolecules* **2004,** 37, 9596-605.
19. Uyama, H.; Kobayashi, S. *Chem. Lett.* **1992,** 21, 1643-6.
20. Uyama, H.; Kobayashi, S. *Chem. Lett.* **1992**, 1643-6.
21. Park, J.-S.; Kataoka, K. *Macromolecules* **2007,** 40, 3599-609.

22. Huber, S.; Jordan, R. *Colloid Polym. Sci.* **2007,** 286, 395-402.
23. Huber, S.; Hutter, N.; Jordan, R. *Colloid Polym. Sci.* **2008,** 286, 1653-61.
24. Bloksma, M. M.; Bakker, D. J.; Weber, C.; Hoogenboom, R.; Schubert, U. S. *Macromol. Rapid Commun.* **2010,** 31, 724-8.
25. Hoogenboom, R.; Thijs, H. M. L.; Jochems, M. J. H. C.; van Lankvelt, B. M.; Fijten, M. W. M.; Schubert, U. S. *Chem. Commun.* **2008**, 5758-60.
26. Hoogenboom, R. *Angew. Chem. Int. Ed.* **2009,** 48, 7978-94.
27. ten Brummelhuis, N.; Secker, C.; Schlaad, H. *Macromol. Rapid Commun.* **2012,** 33, 1690-4.
28. Diehl, C.; Černoch, P.; Zenke, I.; Runge, H.; Pitschke, R.; Hartmann, J.; Tiersch, B.; Schlaad, H. *Soft Matter* **2010,** 6, 3784.
29. Demirel, A. L.; Meyer, M.; Schlaad, H. *Angew. Chem. Int. Ed.* **2007,** 46, 8622-4.
30. Meyer, M.; Antonietti, M.; Schlaad, H. *Soft Matter* **2007,** 3, 430-1.
31. Katsumoto, Y.; Tsuchiizu, A.; Qiu, X.; Winnik, F. M. *Macromolecules* **2012,** 45, 3531-41.
32. Winnik, F. M.; Ringsdorf, H.; Venzmer, J. *Macromolecules* **1990,** 23, 2415-6.
33. Zhang, G.; Wu, C. *J. Am. Chem. Soc.* **2001,** 123, 1376-80.
34. Pang, J.; Yang, H.; Ma, J.; Cheng, R. *J. Phys. Chem. B* **2010,** 114, 8652-8.
35. Howard G. Schild, M. M., and David A. Tirrell. *Macromolecules* **1991,** 24, 948-52
36. Tanaka, F.; Koga, T.; Kojima, H.; Winnik, F. M. *Macromolecules* **2009,** 42, 1321-30.
37. Walter, J.; Sehrt, J.; Vrabec, J.; Hasse, H. *J. Phys. Chem. B* **2012,** 116, 5251-9.
38. Hao, J.; Cheng, H.; Butler, P.; Zhang, L.; Han, C. C. *J. Chem. Phys.* **2010,** 132, 154902.
39. Tao, C.-T.; Young, T.-H. *Polymer* **2005,** 46, 10077-84.
40. Bergé, B.; Koningsveld, R.; Berghmans, H. *Macromolecules* **2004,** 37, 8082-90.
41. Saxena, R.; Caneba, G. T. *Polym. Eng. Sci.* **2002,** 42, 1019-31.
42. Aubry, J.; Ganachaud, F.; Cohen Addad, J. P.; Cabane, B. *Langmuir* **2009,** 25, 1970-9.
43. Lambermont-Thijs, H. M. L.; Kuringen, H. P. C. v.; Put, J. P. W. v. d.; Schubert, U. S.; Hoogenboom, R. *Polymers* **2010,** 2, 188-99.
44. Demirel, A. L.; Meyer, M.; Schlaad, H. *Angew. Chem. Int. Ed.* **2007,** 46, 8622-4.
45. Fik, C. P.; Konieczny, S.; Pashley, D. H.; Waschinski, C. J.; Ladisch, R. S.; Salz, U.; Bock, T.; Tiller, J. C. *Macromol. Biosci.* **2014,** 14, 1569-79.
46. Ulbricht, J.; Jordan, R.; Luxenhofer, R. *Biomaterials* **2014,** 35, 4848-61.
47. Lambermont-Thijs, H. M. L.; Hoogenboom, R.; Fustin, C. A.; Bomal-D'Haese, C.; Gohy, J. F.; Schubert, U. S. *J. Polym. Sci., Part A: Polym. Chem.* **2009,** 47, 515-22.
48. Zhang, Y.; Furyk, S.; Bergbreiter, D. E.; Cremer, P. S. *J. Am. Chem. Soc.* **2005,** 127, 14505-10.
49. Wang, T.; Liu, G.; Zhang, G.; Craig, V. S. J. *Langmuir* **2012,** 28, 1893-9.
50. Eliassaf, J. *J. Appl. Polym. Sci.* **1978,** 22, 873-4.
51. Schild, H. G.; Tirrell, D. A. *Langmuir* **1991,** 7, 665-71.
52. Meewes, M.; Ricka, J.; De Silva, M.; Nyffenegger, R.; Binkert, T. *Macromolecules* **1991,** 24, 5811-6.
53. In *ACS Symposium Series 462*, Donald N. Schulz, J. E. G., Ed. American Chemical Society: Washington, DC, 1989.
54. Menchen, S.; Johnson, B.; Winnik, M. A.; Xu, B. *Chem. Mater.* **1996,** 8, 2205-8.

55. Chassenieux, C.; Nicolai, T.; Benyahia, L. *Curr. Opin. Colloid Interface Sci.* **2011,** 16, 18-26.
56. Tanaka, F.; Edwards, S. F. *Macromolecules* **1992,** 25, 1516-23.
57. Choi, Y.-W.; Park, J.; Park, Y.; Kim, K.; Lee, Y.; Sohn, D. *J. Phys. Chem. B* **2007,** 111, 12959-63.
58. Pellens, L.; Vermant, J.; Mewis, J. *Macromolecules* **2005,** 38, 1911-8.
59. Nicolai, T.; Benyahia, L. *Macromolecules* **2005,** 38, 9794-802.
60. Hough, L. A.; Ou-Yang, H. D. *Phys. Rev. E* **2006,** 73, 031802.
61. Meng, X. *J. Rheol.* **2006,** 50, 189.
62. Nakaya?Yaegashi, K. *J. Rheol.* **2008,** 52, 359.
63. Wang, Y.; Winnik, M. A. *Langmuir* **1990,** 6, 1437-9.
64. Plazek, D. *J. Rheol.* **2000,** 44, 929.
65. Suzuki, S.; Uneyama, T.; Inoue, T.; Watanabe, H. *Macromolecules* **2012,** 45, 888-98.
66. Kim, M.; Choi, Y.-W.; Sim, J.-H.; Choo, J.; Sohn, D. *J. Phys. Chem. B* **2004,** 108, 8269-77.
67. Meng, X.-X.; Russel, W. B. *Macromolecules* **2004,** 38, 593-600.
68. Gourier, C.; Beaudoin, E.; Duval, M.; Sarazin, D.; Maı; amp; x; tre, S.; François, J. *J. Colloid Interface Sci.* **2000,** 230, 41-52.
69. Beaudoin, E.; Borisov, O.; Lapp, A.; Billon, L.; Hiorns, R. C.; François, J. *Macromolecules* **2002,** 35, 7436-47.
70. Laflèche, F.; Durand, D.; Nicolai, T. *Macromolecules* **2003,** 36, 1331-40.
71. Beaudoin, E.; Hiorns, R. C.; Borisov, O.; François, J. *Langmuir* **2003,** 19, 2058-66.
72. Renou, F. d. r.; Nicolai, T.; Nicol, E.; Benyahia, L. *Langmuir* **2008,** 25, 515-21.
73. Kujawa, P.; Segui, F.; Shaban, S.; Diab, C.; Okada, Y.; Tanaka, F.; Winnik, F. M. *Macromolecules* **2005,** 39, 341-8.
74. Zhou, G.; Harruna, I. I. *Macromolecules* **2005,** 38, 4114-23.
75. Postma, A.; Davis, T. P.; Li, G.; Moad, G.; O'Shea, M. S. *Macromolecules* **2006,** 39, 5307-18.
76. Bigot, J.; Charleux, B.; Cooke, G.; Delattre, F. o.; Fournier, D.; Lyskawa, J.; Stoffelbach, F. o.; Woisel, P. *Macromolecules* **2009,** 43, 82-90.
77. Schmidt, B. V. K. J.; Hetzer, M.; Ritter, H.; Barner-Kowollik, C. *Macromolecules* **2011,** 44, 7220-32.
78. Wang, W.; Troll, K.; Kaune, G.; Metwalli, E.; Ruderer, M.; Skrabania, K.; Laschewsky, A.; Roth, S. V.; Papadakis, C. M.; Müller-Buschbaum, P. *Macromolecules* **2008,** 41, 3209-18.
79. Ishii, N.; Obeid, R.; Qiu, X.-P.; Mamiya, J.-i.; Ikeda, T.; Winnik, F. M. *Mol. Cryst. Liq. Cryst.* **2010,** 529, 60-70.
80. Segui, F.; Qiu, X.-P.; Winnik, F. M. *J. Polym. Sci., Part A: Polym. Chem.* **2008,** 46, 314-26.
81. De, P.; Gondi, S. R.; Sumerlin, B. S. *Biomacromolecules* **2008,** 9, 1064-70.
82. Li, M.; De, P.; Gondi, S. R.; Sumerlin, B. S. *Macromol. Rapid Commun.* **2008,** 29, 1172-6.
83. Vora, A.; Singh, K.; Webster, D. C. *Polymer* **2009,** 50, 2768-74.
84. Obeid, R.; Maltseva, E.; Thünemann, A. F.; Tanaka, F.; Winnik, F. M. *Macromolecules* **2009,** 42, 2204-14.

85. Weberskirch, R.; Preuschen, J.; Spiess, H. W.; Nuyken, O. *Macromol. Chem. Phys.* **2000,** 201, 995-1007.
86. Volet, G.; Deschamps, A.-C. L.; Amiel, C. *J. Polym. Sci., Part A: Polym. Chem.* **2010,** 48, 2477-85.
87. Liu, Z.; Liao, Q.; Yang, D.; Gao, Y.; Luo, X.; Lei, Z.; Li, H. *Des. Monomers Polym.* **2013,** 16, 465-74.
88. Chung, J. E.; Yokoyama, M.; Suzuki, K.; Aoyagi, T.; Sakurai, Y.; Okano, T. *Colloids Surf., B* **1997,** 9, 37-48.
89. Smithenry, D. W.; Kang, M.-S.; Gupta, V. K. *Macromolecules* **2001,** 34, 8503-11.
90. Xia, Y.; Burke, N. A. D.; Stöver, H. D. H. *Macromolecules* **2006,** 39, 2275-83.
91. Furyk, S.; Zhang, Y.; Ortiz-Acosta, D.; Cremer, P. S.; Bergbreiter, D. E. *J. Polym. Sci., A Polym. Chem.* **2006,** 44, 1492-501.
92. Wei, K.; Su, L.; Chen, G.; Jiang, M. *Polymer* **2011,** 52, 3647-54.
93. Qiu, X.; Koga, T.; Tanaka, F.; Winnik, F. *Sci. China Chem.* **2013,** 56, 56-64.
94. Park, J.-S.; Akiyama, Y.; Winnik, F. M.; Kataoka, K. *Macromolecules* **2004,** 37, 6786-92.
95. Park, J.-S.; Akiyama, Y.; Yamasaki, Y.; Kataoka, K. *Langmuir* **2006,** 23, 138-46.
96. Xia, Y.; Yin, X.; Burke, N. A. D.; Stöver, H. D. H. *Macromolecules* **2005,** 38, 5937-43.
97. Dai, S.; Sio, S. T.; Tam, K. C.; Jenkins, R. D. *Macromolecules* **2003,** 36, 6260-6.
98. Chassenieux, C.; Nicolai, T.; Durand, D. *Macromolecules* **1997,** 30, 4952-8.
99. Beaudoin, E.; Gourier, C.; Hiorns, R. C.; François, J. *J. Colloid Interface Sci.* **2002,** 251, 398-408.
100. Dai, S.; Tam, K. C.; Jenkins, R. D. *J. Phys. Chem. B* **2001,** 105, 10189-96.
101. Alami, E.; Almgren, M.; Brown, W.; François, J. *Macromolecules* **1996,** 29, 2229-43.
102. Yekta, A.; Xu, B.; Duhamel, J.; Adiwidjaja, H.; Winnik, M. A. *Macromolecules* **1995,** 28, 956-66.
103. Pham, Q. T.; Russel, W. B.; Thibeault, J. C.; Lau, W. *Macromolecules* **1999,** 32, 5139-46.
104. Kadam, V. S.; Badiger, M. V.; Wadgaonkar, P. P.; Ducouret, G.; Hourdet, D. *Polymer* **2008,** 49, 4635-46.
105. Laflèche, F.; Nicolai, T.; Durand, D.; Gnanou, Y.; Taton, D. *Macromolecules* **2003,** 36, 1341-8.
106. François, J.; Beaudoin, E.; Borisov, O. *Langmuir* **2003,** 19, 10011-8.
107. Rufier, C.; Collet, A.; Viguier, M.; Oberdisse, J.; Mora, S. *Macromolecules* **2008,** 41, 5854-62.
108. Séréro, Y.; Aznar, R.; Porte, G.; Berret, J. F.; Calvet, D.; Collet, A.; Viguier, M. *Phys. Rev. Lett.* **1998,** 81, 5584.
109. Tae, G.; Kornfield, J. A.; Hubbell, J. A.; Lal, J. *Macromolecules* **2002,** 35, 4448-57.
110. Xu, B.; Li, L.; Yekta, A.; Masoumi, Z.; Kanagalingam, S.; Winnik, M. A.; Zhang, K.; Macdonald, P. M.; Menchen, S. *Langmuir* **1997,** 13, 2447-56.
111. Zhou, J.; Zhuang, D.; Yuan, X.; Jiang, M.; Zhang, Y. *Langmuir* **2000,** 16, 9653-61.
112. Lammertink, R. G. H.; Kornfield, J. A. *Macromolecules* **2003,** 36, 9154-61.
113. Kujawa, P.; Watanabe, H.; Tanaka, F.; Winnik, F. M. *Eur. Phys. J. E Soft Matter* **2005,** 17, 129-37.
114. Kujawa, P.; Tanaka, F.; Winnik, F. M. *Macromolecules* **2006,** 39, 3048-55.

115. Nojima, R.; Sato, T.; Qiu, X.; Winnik, F. M. *Macromolecules* **2008,** 41, 292-4.
116. Koga, T.; Tanaka, F.; Motokawa, R.; Koizumi, S.; Winnik, F. M. *Macromolecular Symposia* **2010,** 291-292, 177-85.
117. Yekta, A.; Duhamel, J.; Adiwidjaja, H.; Brochard, P.; Winnik, M. A. *Langmuir* **1993,** 9, 881-3.
118. Persson, K.; Wang, G.; Olofsson, G. *J. Chem. Soc., Faraday Trans.* **1994,** 90, 3555-62.
119. Persson, K.; Bales, B. L. *J. Chem. Soc., Faraday Trans.* **1995,** 91, 2863-70.
120. Alami, E.; Rawiso, M.; Isel, F.; Beinert, G.; Binana-Limbele, W.; François, J., Model Hydrophobically End-Capped Poly(ethylene oxide) in Water. In *Hydrophilic Polymers*, American Chemical Society: 1996; Vol. 248, pp 343-62.
121. François, J.; Maitre, S.; Rawiso, M.; Sarazin, D.; Beinert, G.; Isel, F. *Colloids Surf. A Physicochem. Eng. Asp.* **1996,** 112, 251-65.
122. Xu, B.; Yekta, A.; Li, L.; Masoumi, Z.; Winnik, M. A. *Colloids Surf. A Physicochem. Eng. Asp.* **1996,** 112, 239-50.
123. Pham, Q. T.; Russel, W. B.; Thibeault, J. C.; Lau, W. *Macromolecules* **1999,** 32, 2996-3005.
124. Paeng, K. W.; Kim, B.-S.; Kim, E.-R.; Sohn, D. *Bull. Korean Chem. Soc.* **2000,** 21, 623-7.
125. Séréro, Y.; Jacobsen, V.; Berret, J. F.; May, R. *Macromolecules* **2000,** 33, 1841-7.
126. Calvet, D.; Collet, A.; Viguier, M.; Berret, J.-F.; Séréro, Y. *Macromolecules* **2002,** 36, 449-57.
127. Choi, J.; Sohn, D.; Lee, Y.; Cheong, C. *Macromol. Res.* **2003,** 11, 444-50.
128. Elliott, P. T.; Xing, L.-l.; Wetzel, W. H.; Glass, J. E. *Macromolecules* **2003,** 36, 8449-60.
129. Chestakova, A.; Lau, W.; Kumacheva, E. *Macromolecules* **2004,** 37, 5047-53.
130. Rzaev, Z. M. O.; Dinçer, S.; Pişkin, E. *Prog. Polym. Sci.* **2007,** 32, 534-95.
131. Wanka, G.; Hoffmann, H.; Ulbricht, W. *Macromolecules* **1994,** 27, 4145-59.
132. Zeghal, M.; Auvray, L. *Eur. Phys. J. E* **2004,** 14, 259-68.
133. Tokuhiro, T.; Amiya, T.; Mamada, A.; Tanaka, T. *Macromolecules* **1991,** 24, 2936-43.
134. Ohta, H.; Ando, I.; Fujishige, S.; Kubota, K. *J. Polym. Sci., Part B: Polym. Phys.* **1991,** 29, 963-8.
135. Zeng, F.; Tong, Z.; Feng, H. *Polymer* **1997,** 38, 5539-44.
136. Lu, C.-g.; Xu, K.; Li, W.-b.; Li, P.-c.; Tan, Y.; Wang, P.-x. *Chem. Res. Chin. Univ.* **2013,** 29, 1203-7.
137. Ru, G.; Feng, J. *J. Polym. Sci., Part B: Polym. Phys.* **2011,** 49, 749-55.
138. Yushmanov, P. V.; Furó, I.; Iliopoulos, I. *Macromol. Chem. Phys.* **2006,** 207, 1972-9.
139. Andersson, M.; Maunu, S. L. *Colloid Polym. Sci.* **2006,** 285, 293-303.
140. Richardson, J. C.; Bowtell, R. W.; Mäder, K.; Melia, C. D. *Adv. Drug Delivery Rev.* **2005,** 57, 1191-209.
141. Wolf, W.; Presant, C. A.; Waluch, V. *Adv. Drug Delivery Rev.* **2000,** 41, 55-74.
142. Laukemper-Ostendorf, S.; Scholz, A.; Bürger, K.; Heussel, C. P.; Schmittner, M.; Weiler, N.; Markstaller, K.; Eberle, B.; Kauczor, H.-U.; Quintel, M.; Thelen, M.; Schreiber, W. G. *Magn. Reson. Med.* **2002,** 47, 82-9.
143. Ahrens, E. T.; Flores, R.; Xu, H.; Morel, P. A. *Nat Biotech* **2005,** 23, 983-7.
144. Liu, R.; Fraylich, M.; Saunders, B. R. *Colloid Polym. Sci.* **2009,** 287, 627-43.
145. Matsuyama, A.; Tanaka, F. *J. Chem. Phys.* **1991,** 94, 781-6.

146. Abraham, R. J.; Wileman, D. F.; Bedford, G. R. *J. Chem. Soc., Perkin Trans. 2* **1973**, 1027-35.
147. Muller, N.; Simsohn, H. *J. Phys. Chem.* **1971,** 75, 942-5.
148. Rassing, J. *Adv. Mol. Relax. Pr.* **1972,** 4, 55-86.
149. Wu, C.; Zhou, S. *Macromolecules* **1995,** 28, 8381-7.
150. Kawaguchi, S.; Yekta, A.; Duhamel, J.; Winnik, M. A.; Ito, K. *J. Phys. Chem.* **1994,** 98, 7891-8.
151. Yekta, A.; Duhamel, J.; Brochard, P.; Adiwidjaja, H.; Winnik, M. A. *Macromolecules* **1993,** 26, 1829-36.

Chapter 2. Effect of chain architecture on the phase transitions of star PNIPAM and cyclic PNIPAM in water and in the water/methanol mixture.

2.1 Introduction

Poly(*N*-isopropylacrylamide) (PNIPAM) undergoes a coil-to-globule transition in aqueous solutions above the cloud point temperature (T_c) around 32 ºC, exhibiting promising potentials as a thermo sensitive smart material. Many applications of PNIPAM such as optical filters, optical switches, adsorbents, drug-release devices, water purification devices, hair shading, protein immobilization, and immunoassay procedures have been proposed or patented.[1-5] Hydrogels of cross-linked PNIPAM or PNIPAM-based systems which could be used as nonfouling surface coatings, drug release/delivery vehicles, enzyme stabilizers and sensors, have been extensively studied over the past few decades.[6-8]

The coil-to-globule phase transition of PNIPAM has been interpreted from different viewpoints. The hydrophobic effect is considered essential for the phase transition of PNIPAM in water. When PNIPAM is dissolved in water, clathrate-like clusters of water form surrounding the hydrophobic isopropyl groups, resulting in negative mixing entropy. At temperatures above the LCST, the entropy term overwhelms the exothermic enthalpy of the hydrogen bond formed between the amide group of PNIPAM and water molecules. The mixing free energy change becomes positive and phase separation happens. Large aggregates form through hydrophobic interactions between the dehydrated PNIPAM chains.[9, 10] The number of hydrating water molecules around each NIPAM segment was determined by dielectric relaxation measurement below the LCST.[11] This number decreases sharply when the aqueous solution of PNIPAM is heated to its LCST. A report by Wu et al.[12] revealed that the coil-to-globule phase transition of PNIPAM in dilute aqueous solution has two distinct kinetic stages: the nucleation and initial growth of some “pearls” (contracted segments) along the chain in the first stage, and the merging and coarsening of the “pearls” in the second stage. A theory by Tanaka et al.[13] emphasizes the importance of the cooperative character of the

PNIPAM hydration. The formation of one hydrogen bond with the amide group of PNIPAM chain by water molecule facilitates the formation of another hydrogen bond between water and an amide. A sequence of water molecules dehydrate together cooperatively, when the temperature is increased above the T_c of PNIPAM.

The phase transition of PNIPAM is affected by many factors such as molecular weight,[14] polymer concentration, addition of salts,[12, 15] surfactant[16] or a second water-miscible solvent. The addition of a second good and water miscible solvent within a given solvent composition range results in a depression of the lower critical solution temperature (LCST). This phenomenon is known as cononsolvency. Among the reported solvents (THF,[17] DMF, dioxane, and methanol[18, 19]), methanol has been the most extensively studied cononsolvent for the phase separation of PNIPAM in water. Wu and Zhang[19] studied the phase transition of individual PNIPAM chains in extremely dilute solutions by monitoring the R_g, R_H and light scattering (LS) intensity changes of PNIPAM solutions of different compositions of water/methanol. They attributed the observed re-entrant transition to the formation of water-methanol complexes which are poor solvents for PNIPAM. Pang's study confirmed the formation of complex structures between solvent molecules.[20] They found that the cluster structure of the free water molecules was not affected by added methanol molecules; however the number of such structures decreased as a result of the strong interaction between the two species via hydrogen bonding. Tanaka et al.[21] proposed a mechanism which combined the cooperativity of the hydration of the PNIPAM chain and the competition between methanol and water for formation of hydrogen bonds to the polymer. This mechanism stipulates that a sequence of water molecules bind to the PNIPAM chain cooperatively. The added methanol molecules compete with water molecules in the formation of hydrogen bonds to the polymer. If the sequence of water molecules along the PNIPAM chain is not long enough to retain cooperativity, the chain will dehydrate and the LCST reaches minimum. Walter et al.[22] investigated the cononsolvency phenomenon by molecular simulation and found that the methyl group of methanol is oriented towards the bulk solvent in the outer region of the solvent shell of PNIPAM, which causes the PNIPAM and solvent shell to become hydrophobic and collapse in the water/methanol mixture.

The polymer architecture is an important influencing factor of the thermo properties of PNIPAM. Numerous studies of the star polymers and cyclic polymers showed different physical properties and functions comparing to their linear counterpart.[23-25] Various type of arms (chemical composition and structure) for star polymers find them potential uses in biological and pharmaceutical applications.[23, 24, 26-30] PNIPAM has been widely used as an thermosensitive component in star polymers. An investigation of the effect of polymer architecture on the properties of PNIPAM is important for the design and functionalization of smart materials having a component of PNIPAM. There are a few studies on the solution behaviour of multi-arm star shape PNIPAM prepared by the "core-first" method. A 4-arm star-shaped PNIPAM was synthesized by Gao et al.[31] via ATRP (atom transfer radical polymerization) of NIPAM with zinc(II) tetra-(2-chloropropionylamido) phthalocyanine as the initiator and CuBr/Me_6TREN as the catalyst. The LCST of star PNIPAM was raised significantly compared to the linear PNIPAM and the effect of star architecture on LCST decreased with molecular weight. 7-arm and 21-arm star-shaped PNIPAMs[32] with β-cyclodextrin (β-CD) cores were prepared via a combination of ATRP and click reactions. Opposite molecular weight dependence of the LCST was observed for the 7-arm and 21-arm star-shaped PNIPAMs compared with the linear precursor PNIPAMs. The LCST of linear precursor PNIPAM decreased from 41 to 38 °C. However, the LCST of 7-arm and 21-arm PNIPAM increased from 33 to 36 ºC and 30 to 35 ºC, respectively, when the polymerization degree of the individual arm increased from 10 to 40. The authors explained the increase of LCST with molecular weight by the formation of *n*-cluster of PNIPAM segments at the surface of the β-CD core due to the high grafting density. For the star polymers with high molar mass, the collapse of inner chain segments is stabilized by the outer layer due to much lower chain density. A 4-arm star PNIPAM was prepared by Plummer et al.[33] using the 4-arm RAFT (Reversible addition-fragmentation chain-transfer) agentpentaerythritoltetrakis(3-(*S*-benzyltrithiocarbonyl)propionate. The LCST of the resulting star PNIPAM was greatly depressed by the hydrophobic star core and benzyl end groups originating from the RAFT agent. For the 10 kDa PNIPAM star, the LCST was around 17 ºC, and for the 32 kDa and 52 kDa star polymers, the LCST of them were in the range of 32–33 ºC. The effect of chain architecture and end group was observed to be negligible when the degree of polymerization is larger than 70. The LCST of the linear PNIPAM arms cleaved from the star PNIPAM was

constant (~ 35 ºC) for M_w ranging from 3.2 to 11.7 kDa. Since the structure of the star and linear PNIPAM was not the same in this study (the linear PNIPAM was much shorter), the effect of chain architecture on the LCST could not be evaluated. Pedersen et al.[34] synthesized star PNIPAM with 2, 3, 4, and 6 arms with about 60 repeating unit per arm, and investigated their thermo responsive properties in water by SAXS (small-angle X-ray scattering) and turbidity measurement. The T_c decreased as the polymer concentration increased and as the number of arms increased. The SAXS data were fitted with a Gaussian star form factor, and intermolecular interactions were successfully described by the RPA (random-phase approximation) approach. The effect of PNIPAM architecture and additives on the phase separation of PNIPAM aqueous solution remains unclear.

Cyclic polymers, due to their closed topology, exhibits unique properties, such as smaller hydrodynamic radius, higher glass transition temperature (T_g), and higher density, etc. Potential applications have been developed, such as functional gels composing of multicyclopolymers,[35] cyclic comb polymers with a great tumor accumulation time,[36] thermally stable micelles,[37] polymers with enhanced fluorescence,[38, 39] cyclic polylactide-clay hybrid as support for palladium(0) catalyst.[40] More useful cyclic materials need to be prepared to broaden their applications. There are a few reports of cyclic PNIPAM synthesized through the azide-alkyne Huisgen cycloaddition[41-43] or the anthracene–thiol-based thiolene click reaction.[44] The solutions properties of cyclic PNIPAM were studied and compared with that of their linear counterpart in water. A smaller average aggregation number, smaller hydrodynamic radius and loose structure for cyclic PNIPAM aggregates obtained by a slow heating process were reported by Ye et al.[42] So far, there is no report on the solution behavior of cyclic PNIPAM in water/methanol mixture. More studies are necessary for a better understanding of the aggregation process of cyclic PNIPAM in water and water/methanol mixture.

In this study, a star shape PNIPAM containing four linear PNIPAM arms tethered to a center core and the linear PNIPAM with identical structure and close molecular weight were employed and their solution properties in water/methanol mixture were explored. To elucidate the effect of chain architecture on the cononsolvency of PNIPAM, phase behaviour of a cyclic PNIPAM and its linear precursor polymer in water/methanol mixtures were studied as well.

In order to investigate the effect of methanol addition to the cooperative hydration/dehydration of PNIPAM with different architectures, the thermo responses of the polymers in water were studied by means of LS and DSC. The aim of this study is to gain some insight into the effects of polymer architecture and solution additives on the LCST and chain interactions. To our knowledge, the phase transition of PNIPAM with various chain architectures in water/methanol mixtures has not been reported in the literature. The results of the study are expected to provide a better understanding of the cooperative dehydration of the PNIPAM with various architectures.

2.2 Experimental section

2.2.1 Materials

A linear PNIPAM (PNIPAM-arm) having a molecular weight of 3300 $g \cdot mol^{-1}$ was synthesized by ATRP polymerization; it was used as "arm" to prepare a star PNIPAM. A star PNIPAM (*s*-PNIPAM) consisting of 4 PNIPAM arms attached to a hydrophobic core and a linear PNIPAM (*l*-PNIPAM-Cl) bearing the same end groups as the star PNIPAM were synthesized by click reaction. The synthesis and characterization of the star and linear PNIPAM were published elsewhere.[45] A linear PNIPAM (*l*-PNIPAM-N_3) carrying an azide and a propargyl group at each end and a cyclic PNIPAM (*c*-PNIPAM) prepared by ring closure of the *l*-PNIPAM-N_3 precursor were synthesized and characterized by a colleague in our group.[41] The M_n of the *c*-PNIPAM and *l*-PNIPAM-N_3 was determined to be 12,700 $g \cdot mol^{-1}$ by GPC.

2.2.2 Instrumentation

The phase transition enthalpy of samples was measured using a high sensitive differential scanning microcalorimeter (HS-DSC). Measurements were performed under excess pressure of 25 psi over the temperature range 10–90 °C with the heating rate of 1.0 $^{o}C \cdot min^{-1}$. Polymer concentration was kept at 1.0 $g \cdot L^{-1}$ for the aqueous solution samples. The transition excess heat capacity was calculated by subtracting the transition base line which was approximated by a progress function using the thermogram of a water ~ water scan. The

Van't Hoff enthalpy (ΔH^{VH}) and number of residues in one cooperative unit (n_{CU}) was determined according to Tiktopulo's method.[46]

The turbidimetry analysis in water-methanol mixture was performed using Agilent 8452A diode array spectrophotometer equipped with an Agilent 89090A temperature controller. The stock solutions of PNIPAMs in deionized water (1.0 $g \cdot L^{-1}$) and in methanol (1.0 $g \cdot L^{-1}$) were prepared 1 day prior to mixing and kept at 5 ºC. The solutions for cloud point temperature (T_c) measurements were prepared by weighing and mixing the stock aqueous solutions of PNIPAM and methanol solutions of PNIPAM at different ratios. T_c values of each polymer solutions were determined by detection of the changes in turbidity of the mixed solutions heated at a constant rate (0.2 $ºC \cdot min^{-1}$) at 550 nm.

Dynamic (DLS) and static (SLS) light scattering measurements were performed on a CGS-3 goniometer (ALV GmbH) equipped with a ALV/LSE-5003 multiple-τ digital correlator, a He-Ne laser (λ = 633 nm), and a C25P circulating water bath (Thermo Haake). The solutions examined (0.09 $g \cdot L^{-1}$) were prepared by dilution of a stock solution (1.0 $g \cdot L^{-1}$), filtered through 0.45 μm PVDF filter unit. In DLS experiments, CONTIN analysis was applied to obtain the diffusion coefficient (D_0) of the scattering objects in solution. The corresponding hydrodynamic radii, R_H, were obtained via the Stokes-Einstein equation (2.1):

$$D_0 = \frac{k_B T}{6\pi\eta_s R_H} \tag{2.1}$$

where k_B is the Boltzmann constant, η_s is the viscosity of the solvent (water), and T is the absolute temperature.

In SLS experiments, the apparent weight-average molar mass ($M_{w,app}$) and the *z*-average root-mean square radius of gyration (R_g) of scattering objects in dilute solution are evaluated according to the angular dependence of the excess absolute scattering intensity, known as the excess Rayleigh ratio $R_{(q,c)}$ given by equation (2.2):

$$\frac{Kc}{R(q,c)} \cong \frac{1}{M_{w,app}}(1+\frac{1}{3}R_g^2 q^2) + 2A_2 c \tag{2.2}$$

For large particles with $qR_g > 1$, the Guinier approximation was employed:

$$\frac{Kc}{R(q,c)} \cong \frac{1}{M_{w,app}} \exp(\frac{1}{3} R_g^2 q^2) + 2A_2 c \quad (2.3)$$

where c is the polymer concentration, A_2 is the second virial coefficient, The optical constant $K = 4\pi^2 n^2 (dn/dc)^2 / N\lambda_0^4$, where n is the refractive index of the solvent, dn/dc is the specific refractive index increment, N_A is Avogadro's number, and λ_0 is the wavelength of the incident light in vacuum. The dn/dc value of 0.167 $mL \cdot g^{-1}$ for PNIPAM at 25 °C was used to calculate the $M_{w,app}$. The number of collapsed PNIPAM chains per aggregate (N_{agg}) above T_c is calculated by $M_{w,app} / M_w$. (M_w is the molecular weight of a single PNIPAM chain.)

2.3 Results

Scheme 2.1 shows the structures of the studied polymers. The characteristic parameters of the studied polymers were presented in **Table 2.1**. A slightly lower T_c value was observed for the *s*-PNIPAM than its linear counterpart (*l*-PNIPAM-Cl). And the T_c value of the PNIPAM-arm was much higher than that of the *s*-PNIPAM consisting of 4 PNIPAM-arm. Attaching a hydrophobic ester moiety to one end of the PNIPAM-arm decreased the T_c for 3.1 °C as reported by Chen et al.[45] The much lower T_c of the *s*-PNIPAM (36.7 °C) compared with that of the PNIPAM-arm (51.2 °C) indicated that tethering PNIPAM chains to a hydrophobic core led to a decrease of the T_c. The star shape architecture implicated a negative effect on T_c. The presence of hydrophilic Cl end group raised the T_c of PNIPAM according to the studies of Qiu et al.[47] and Xia et al.[48] The very close T_c of *s*-PNIPAM and that of the *l*-PNIPAM-Cl revealed that the positive effect on T_c of the higher composition of hydrophilic end group Cl in the *s*-PNIPAM balanced out with the negative effect of star shape architecture. The *c*-PNIPAM and the *l*-PNIPAM-N_3 having a similar DP with the *s*-PNIPAM were also discussed to evaluate the effect of different architecture on the phase transition behavior of PNIPAM. A higher T_c value for the *c*-PNIPAM than its linear counterpart *l*-PNIPAM-N_3 was observed[41]. The slightly higher T_c of *c*-PNIPAM than the *l*-PNIPAM-N_3 was attributed to an enhanced cooperativity in the motions of the monomer units — the formation of transient correlated dipoles of amide groups in the *c*-PNIPAM.[49] **Figure A2.7** shows typical temperature-dependent optical transmittance for linear- and star-PNIPAMs with

varying molecular weight. The T_c of studied polymers exhibited a reverse dependence on the molecular weight.

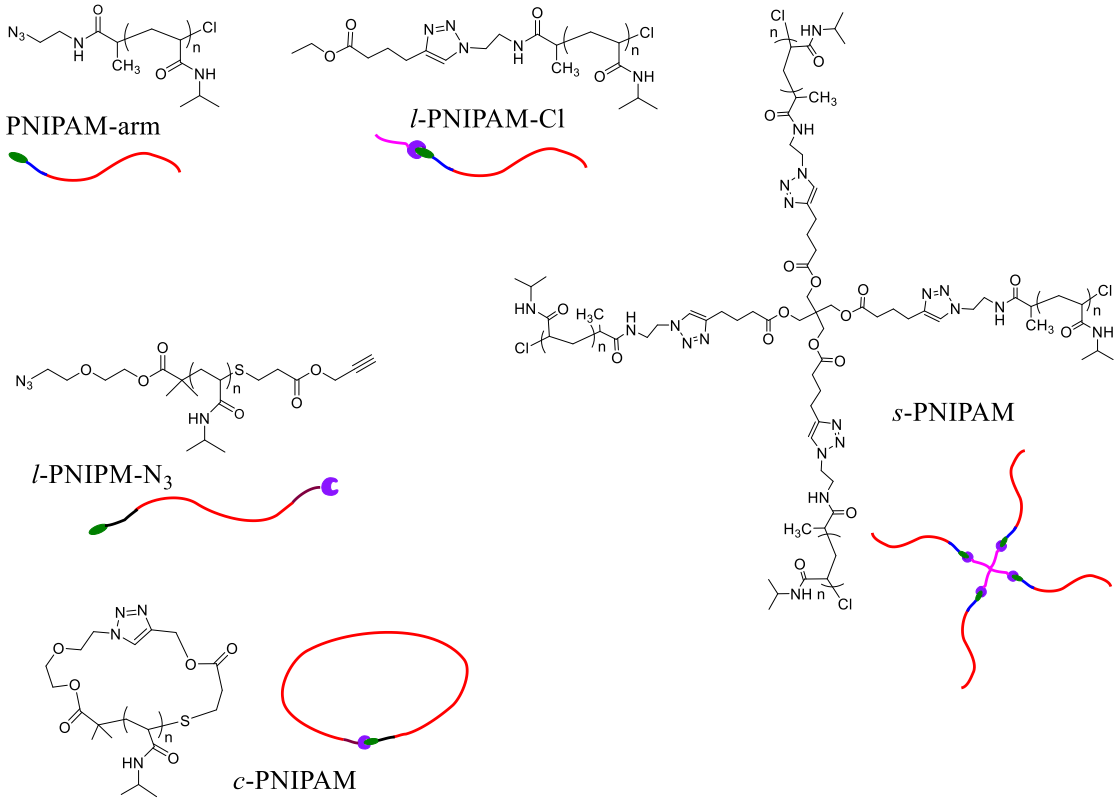

Scheme 2.1 Structures of *s*-PNIPAM, *l*-PNIPAM-Cl, PNIPAM-arm, *l*-PNIPAM-N_3, and *c*-PNIPAM.

Table 2.1 Thermodynamic parameters of the coil-to-globule transition of PNIPAM

Polymer	M_n (g·mol^{-1})	DP[c]	T_c[b]	T_m (°C)	ΔH (kJ·mol^{-1})	ΔH^{VH} (kJ·mol^{-1})	n_{CU}	***n***
s-PNIPAM	14,700[a]	119	36.7	39.64	4.55	798	175	0.66
l-PNIPAM-Cl	13,800[a]	119	37.4	38.82	6.43	775	120	1.0
PNIPAM-arm	3,300[a]	28	51.2	55.4	2.83	293	103	0.28
c-PNIPAM	12,700	109	38.3	41.4	4.39	371	84	1.3
l-PNIPAM-N_3	12,700	109	33.5	36.6	6.07	560	92	1.2

[a.] Reproduced from Ref. 45 (determined by ^{1}H NMR spectrum in D_2O). [b.] Determined by turbidity measurement (heating rate 0.2 °C·min^{-1}; concentration 1.0 g·L^{-1}). T_c defined as the temperature corresponding to 90% transmittance. [c.] Calculated by M_n menus the molar mass of end group and core, and divided by the molar mass of NIPAM monomer.

2.3.1 Phase separation of star PNIPAM in water/methanol mixtures

To examine the influence of chain architecture on the cononsolvency of PNIPAM/water/methanol system, the *s*-PNIPAM, *l*-PNIPAM-Cl, PNIPAM-arm, *c*-PNIPAM, and *l*-PNIPAM-N_3 were investigated. The T_c corresponding to the temperature at 90% transmittance was determined by turbidity measurement. (Phase diagrams with T_c defined at the temperature corresponding to the inflection point in the turbidity curve are shown in **Figure A2.10**). The transmittance curves for the *s*-PNIPAM, *l*-PNIPAM-Cl, and *c*-PNIPAM at different methanol fractions were presented in **Figure 2.2**-**Figure 2.4** (The transmittance curves for the PNIPAM-arm and *l*-PNIPAM-N_3 are shown in **Figure A2.9**). The phase diagrams for the *s*-PNIPAM and *l*-PNIPAM-Cl in water/methanol mixture exhibit re-entrant curvature with a minimum around methanol molar fraction of 0.20 and 0.23, respectively, as shown in **Figure 2.1**. The fact that the phase diagram of the *s*-PNIPAM was closer to that of the *l*-PNIPAM-Cl than that of the arm suggests that the *s*-PNIPAM dehydrates cooperatively. The T_c of the *s*-PNIPAM is lower than that of the *l*-PNIPAM-Cl in water, while the former became higher than the latter and the gap increased with methanol molar fraction in water/methanol mixture. The depth and width of the phase transition were related to the cooperativity parameter and the association constant of the hydrogen bond with methanol according to Tanaka's theoretical study.[13] The deeper and wider the transition, the higher cooperativity and lower association constant of the hydrogen bond with methanol. The more flat phase diagram of the *s*-PNIPAM compared to that of the *l*-PNIPAM-Cl, indicated a lower degree of cooperativity in the dehydration process of the former upon methanol addition. The lower cooperativity of *s*-PNIPAM was a result of the restrained movement of polymer chains due to the rigid structure of the core and the shorter sequence of monomer units in each arm. No cononsolvency phenomenon was observed for the PNIPAM-arm in water/methanol mixture. The very short PNIPAM-arm chain cannot afford an adequate sequence of cooperative hydrogen bonding of solvent molecules along the chain. Increasing methanol fraction simply increased the T_c monotonically for the PNIPAM-arm. These results suggest that, 1) tethering PNIPAM chains to a hydrophobic core results in a higher cooperativity along the polymer chain, which is still lower than its linear counterpart with similar molecular weight, 2) the effect on T_c of end group composition offset the local chain density for star

PNIPAM, and 3) the difference in cooperativity for star and linear shape PNIPAM of similar molecular weight is manifested by the larger gap between the T_c values of the two polymer in water/methanol mixture.

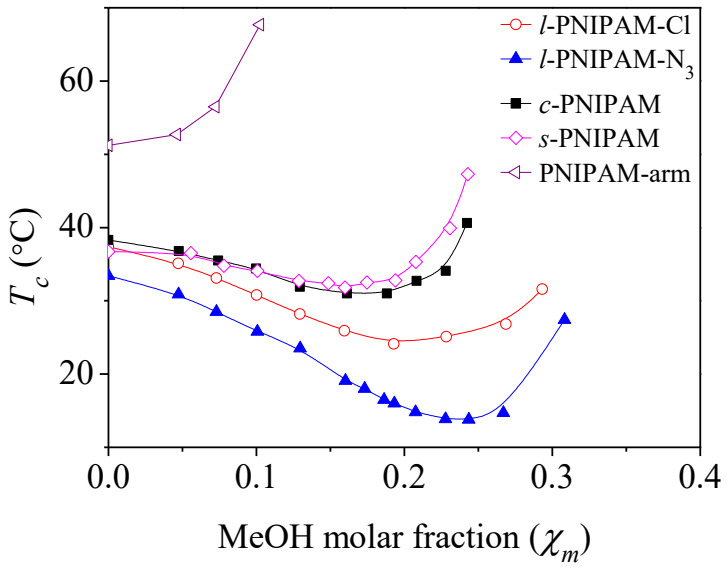

Figure 2.1 Phase diagram of PNIPAMs (1.0 g·L^{-1}) as a function of solvent composition in methanol-water mixtures expressed in methanol (MeOH) molar fraction. T_c was identified as the temperature corresponding to 90% transmittance.

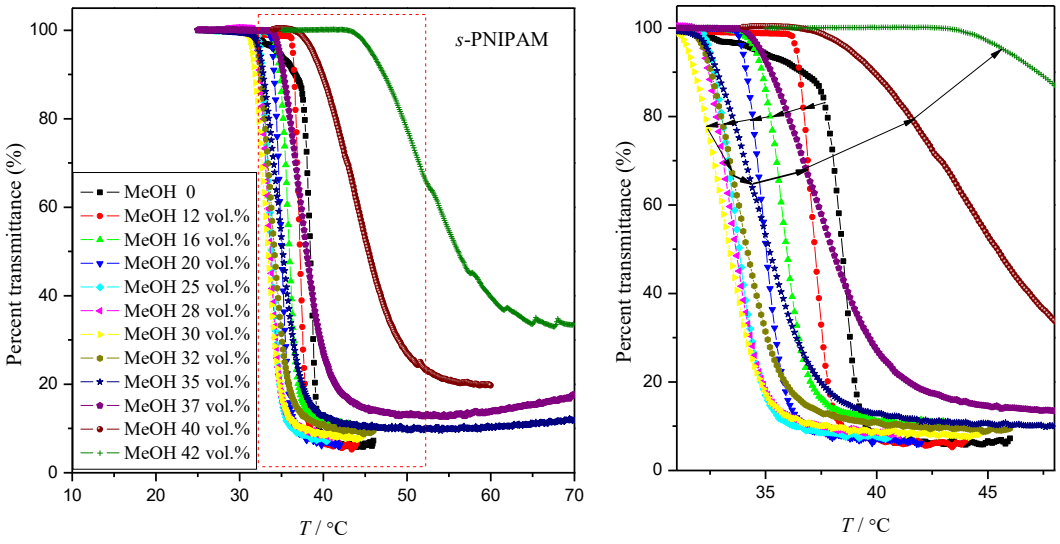

Figure 2.2 Left: Temperature dependencies of the turbidity at a heating rate of 0.2 °C·min^{-1} for *s*-PNIPAM (1.0 g·L^{-1}) in methanol/water mixtures. Right: an enlargement of the region in the red square.

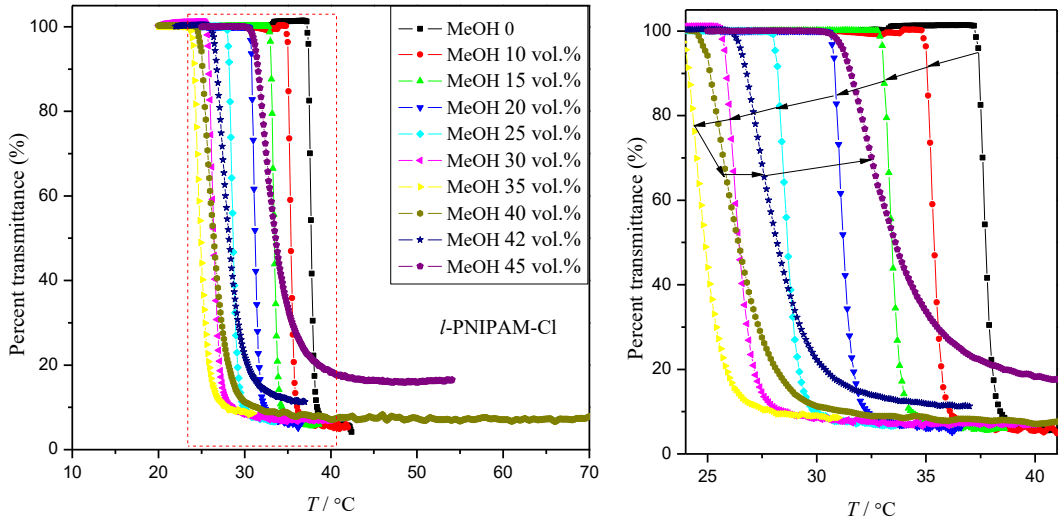

Figure 2.3 Left: Temperature dependencies of the turbidity at a heating rate of 0.2 °C·min^{-1} for *l*-PNIPAM-Cl (1.0 g·L^{-1}) in methanol/water mixtures. Right: an enlargement of the region in the red square.

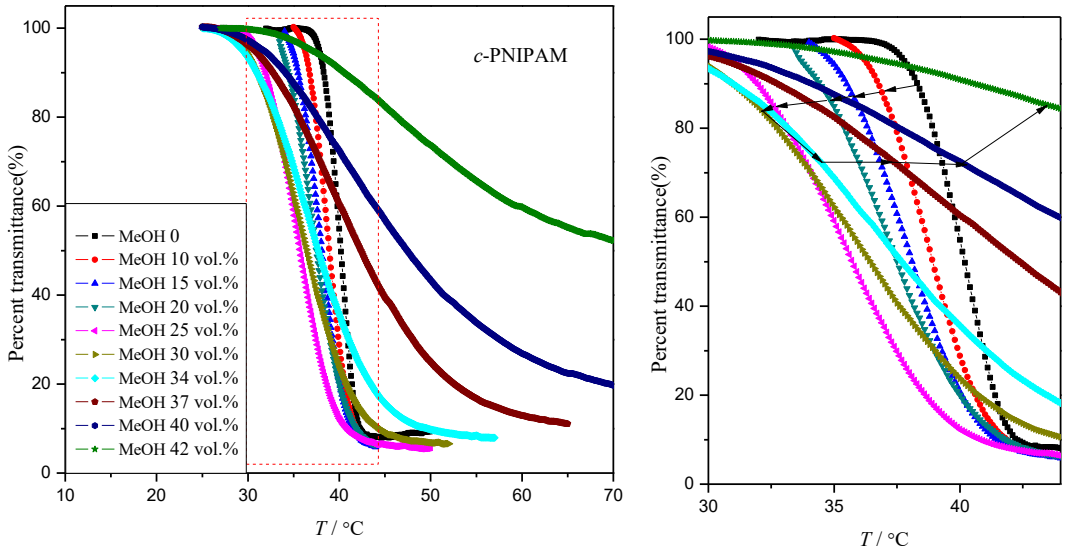

Figure 2.4 Left: Temperature dependencies of the turbidity at a heating rate of 0.2 °C·min^{-1} for *c*-PNIPAM (1.0 g·L^{-1}) in methanol/water mixtures. Right: an enlargement of the region in the red square.

2.3.2 Phase separation of cyclic PNIPAM in water/methanol mixtures

To investigate the effect of different chain architectures on the phase transition of PNIPAM in methanol/water mixture without the interference of end groups, *c*-PNIPAM and its linear precursor *l*-PNIPAM-N_3 was employed and their T_c in water/methanol was recorded as shown in **Figure 2.1**. The T_c of *c*-PNIPAM is much higher than that of its linear precursor *l*-PNIPAM-N_3 at all solvent compositions. The closed ring structure of the *c*-PNIPAM prohibits intermolecular interaction, which shifts the T_c to higher temperature. The more flat phase diagram of *c*-PNIPAM than that of its precursor polymer suggests lower cooperativity and higher association constant of hydrogen bond with methanol for the former in its water/methanol mixture due to the less flexibility of the cyclic structure. The onset phase transition temperature of *c*-PNIPAM decreases gradually as methanol fraction increases, while the ending temperature of the phase transition is almost constant in the region with methanol volume fraction 0–25% (molar fraction 0–0.13) as shown in **Figure 2.1**. In the right part of the phase diagram for *c*-PNIPAM (methanol molar fraction 0.17–0.25), the starting points of the transmittance curves were nearly constant (~ 26 °C) and the ending temperatures of the transmittance curves increase with molar fraction as shown in **Figure 2.4**. The wider

transmittance curves for solutions with higher methanol fractions correlated with the rigid ring structure of the *c*-PNIPAM. In the solution with high methanol volume fraction of 42%, the transmittance cannot decrease below 50% for the *c*-PNIPAM mixture. The low turbidity of the *c*-PNIPAM/water/methanol mixture at high methanol volume fraction implied small size of aggregates in this solution. The faster transitions of *s*-PNIPAM and *c*-PNIPAM in solutions with high methanol volume fraction as shown in **Figure 2.2** and **Figure 2.4**, compared with that of *l*-PNIPAM-Cl in the same condition (**Figure 2.3**), suggests lower cooperativity of the two polymers. The minimum T_c at lower methanol molar fraction around 0.18 for the *c*-PNIPAM and *s*-PNIPAM, compared with that for their linear counterparts at 0.24, correlates with the higher association constant for the hydrogen bond of methanol in the former two polymer solutions. It could be reasonably explained by Tanaka's theory. For the *s*-PNIPAM, the cooperativity in the hydration between polymer-methanol is even smaller than its linear counterpart, considering the "car parking effect" and the shorter sequence of monomer units per arm in the *s*-PNIPAM. For the *c*-PNIPAM, more hydrogen-bonding sites are wasted because of the constraints in the cyclic rings and the bigger size of methanol molecules compared with water.

The T_c of the *c*-PNIPAM is higher than that of the *s*-PNIPAM at all methanol compositions when T_c is defined as the inflection point of the turbidity curve. However, the T_c values of the two polymers are very close when T_c is defined as the temperature corresponding to 90% transmittance. The difference is mainly due to the relatively wider phase transition region of the *c*-PNIPAM as shown in **Figure 2.4**. The phase transition region of *c*-PNIPAM is wider than that of the *s*-PNIPAM at all methanol compositions studied, which reflects a higher degree of cooperativity for the *s*-PNIPAM than the *c*-PNIPAM.

2.3.3 Phase transition of PNIPAMs in water

DSC studies

The effect of chain architecture on the phase transition of PNIPAM in water/methanol mixtures is a combined result of the polymer chain architecture and solvent compositions. To simply examine the effect of different architectures, we study the phase separation process of *s*-PNIPAM, *c*-PNIPAM and their linear counterparts in water. The thermo properties of the phase transition of *s*-PNIPAM, *l*-PNIPAM-Cl and PNIPAM-arm were investigated by HP-

DSC. The heating rate and the concentration of polymer were kept constant at 1 ºC·min^{-1} and 1.0 g·L^{-1} for all polymers. The thermograms of the three polymers are presented in **Figure 2.5**. The phase transition enthalpy change (ΔH) of the *s*-PNIPAM is lower than its linear counterparts, suggesting that the star architecture affects the strength of hydrogen bonding between PNIPAM and water. The clathrate-like water cages surround the isopropyl groups of *s*-PNIPAM are less structured and water molecules are more mobile due to high local chain density. The steric constraints in the star PNIPAM restrict its hydration. The loss of conformational entropy for the star PNIPAM is smaller than that for its linear counterpart. The overall entropy changes for star PNIPAM is more positive. So a lower phase transition temperature is enough to render the demixing temperature to be negative. For the *s*-PNIPAM, the thermogram exhibits single transition peak around 40 °C. A unimodal endothermic peak was observed for 21-arm star PNIPAM with DP of each arm equalled to 20 by Liu et al.[32]

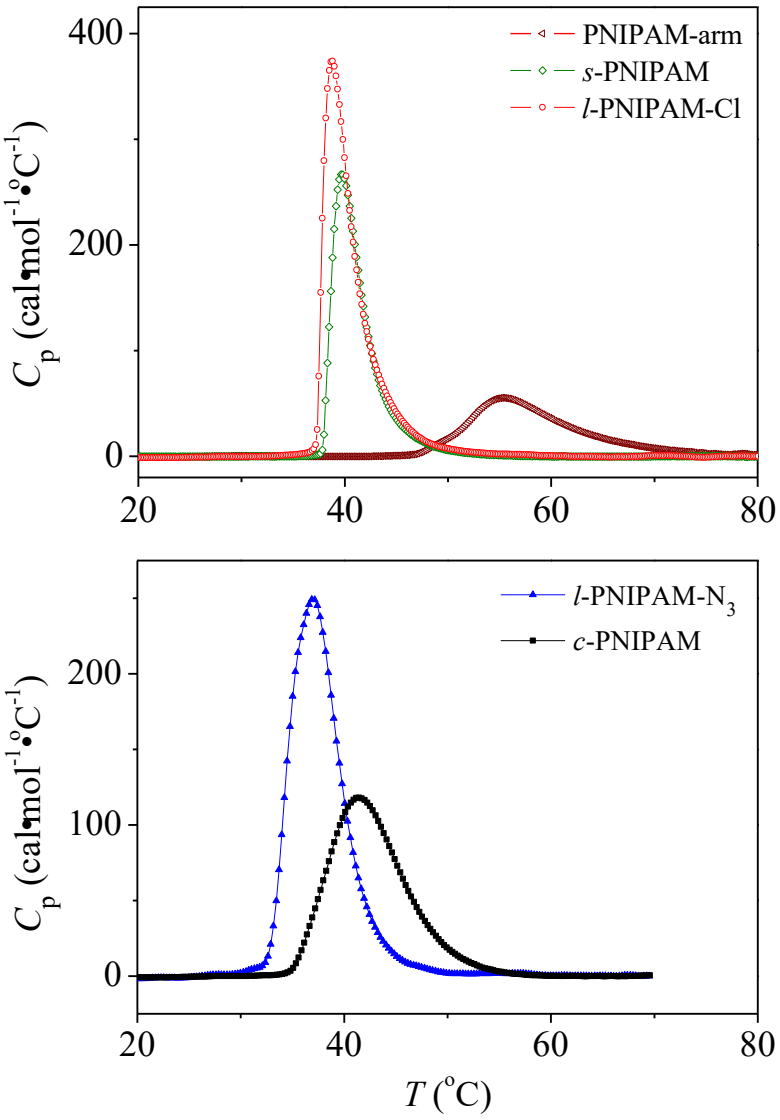

Figure 2.5 Heat capacities of *s*-PNIPAM, *l*-PNIPAM-Cl, and PNIPAM-arm (top); and *c*-PNIPAM and *l*-PNIPAM-N_3 (bottom) in water (1.0 g·L^{-1}) at a heating rate of 1.0 ºC·min^{-1}.

Information about the cooperativity in dehydration can also be obtained from DSC measurement. To determine the cooperativity of the phase transition quantitatively for the PNIPAMs with different architectures, we compare the thermodynamic parameters (ΔH^{VH}, ΔH, T_m, n_{CU} and $\boldsymbol{n}$) of the coil-globule transition using Tiktopulo's method as shown in **Table 2.1**. The ΔH^{VH} was estimated by the expression

$$\Delta H^{VH} = 4RT^2 \frac{C_p(T_m)}{\Delta H} \quad (2.4)$$

where $C_p(T_m)$ is the specific heat capacity of a polymer at temperature T_m of the absorption maximum. The n_{CU} is the number of monomer residues in a cooperative unit, and is determined by comparing the heat absorbed ΔH^{VH} by transferring 1 mole of cooperative units from the coil to the globule state with the transition enthalpy ΔH of the whole polymer. The n_{CU} is a quantitative measure of the strength of cooperativity. This model assumes the coil-to-globule phase transition involves two states; θ and 1- θ are the amounts of chains in each state. The ΔH^{VH} was estimated by assuming that θ = 1/2 in the middle of the transition ($T = T_m$). The monomers belonging to the same cooperative unit display a correlated behavior when the coil-to-globule phase transition takes place. The dependence of the size of the cooperative unit on the polymer architecture is shown in **Table 2.1**. The n_{CU} value of a PNIPAM with M_w of 11,200 g·mol^{-1} was reported to be 99 by Tiktopulo et al.[46], which is close to the n_{CU} value for the linear PNIPAM-arm. However the short PNIPAM-arm chain containing only 0.28 cooperative unit (***n*** =0.28) cannot support cooperative dehydration. The abnormally large n_{CU} value for the *s*-PNIPAM implies that the Tiktopulo's method does not apply for s-PNIPAM, as the assumption of θ = 1/2 in the middle of the transition may not be fulfilled. The middle of the transition may not correspond to transferring half mole of *s*-PNIPAM to globule state since the chemical environment from the core to the free end of the *s*-PNIPAM is not uniform. The slightly higher n_{CU} value for the *l*-PNIPAM-Cl than the conventional PNIPAM may be related to the hydrophilic end group Cl. The ***n*** value for *l*-PNIPAM-Cl suggests an "all-in-one" dehydration process in which the polymer chain undergoes coil-to-globule transition cooperatively. The DSC results consistent with the turbidity measurement of the studied polymers in water/methanol mixture. The cooperativity of the phase transition for the *c*-PNIPAM and *l*-PNIPAM-N_3 was determined by the n_{CU} and ***n*** values from their thermograms as well. The phase transition enthalpy change (ΔH) and the T_m values were cited from a previous publication of our group[41] as shown in **Table 2.1**. For *c*-PNIPAM and *l*-PNIPAM-N_3 with M_n 12,700 g·mol^{-1}, unimodal thermograms were observed as shown in the bottom of **Figure 2.5**. The lower ΔH^{VH} and n_{CU} of *c*-PNIPAM than that of the *l*-PNIPAM-N_3 indicates a lower cooperativity and a lower degree of hydrogen bonding of the former. The length of a

sequence of cooperatively bonded water molecules is arrested because of the rigid cyclic structure.

LS studies

The phase transition of PNIPAMs was studied by monitoring the scattering intensities of their aqueous solutions as a function of temperature. The solutions were equilibrated for an hour at each temperature before measurement. The scattering intensities were very low at this low concentration (0.09 $g \cdot L^{-1}$) below T_c as shown in **Figure 2.6**. The two linear PNIPAMs underwent phase transition first, followed by the *s*-PNIPAM. The inset shows a magnification of the onset of scattered intensity of the *c*-PNIPAM. The onset temperature of phase transition for *c*-PNIPAM is close to that of PNIPAM-arm, indicating a great concentration effect on the T_c of *c*-PNIPAM compared with other PNIPAMs of different architectures and a low inter-polymer interactions between *c*-PNIPAM chains at this low concentration.

The size of the PNIPAMs aggregates were examined by DLS. The R_H values of all the polymers in water at room temperature are only indicative, due to the low scattering intensity from dilute solutions (0.09 $g \cdot L^{-1}$) of short PNIPAM chains (3300–14,700 $g \cdot mol^{-1}$). This concentration was chosen to ensure clarity of the solutions above T_c, necessary for reliable LS data. **Figure 2.7** presents the R_H for the polymers studied at different temperatures. The R_H values of the *l*-PNIPAM-Cl aggregates are larger than that of the *s*-PNIPAM above corresponding T_c. The hydrophilic Cl groups preferentially locate on the surface of aggregates which hinder the interactions between aggregated *s*-PNIPAM chains. As a result, the surface tensions of aggregated mesoglobules are increased, leading to repulsive interactions between the mesoglobules. Thus, smaller R_H is expected for the *s*-PNIPAM aggregates, since the molar content of Cl group in the *s*-PNIPAM is four times higher than that of the *l*-PNIPAM-Cl. The preferential absorption of surfactant residuals and ions on the aggregated PNIPAM globules has been reported.[50, 51] A concomitant increase of the N_{agg} was observed for the two polymers as well. The N_{agg} value of *s*-PNIPAM increased gradually and reached a plateau ~ 2.1×10^5 at 65 ºC. A slightly larger value of $N_{agg} \sim 3 \times 10^5$ was obtained for the *l*-PNIPAM-Cl aggregates at 50 ºC, indicating a higher tendency of inter-globular interactions. The N_{agg} and R_H values reflect the influence of the end group and chain architecture on the stability of mesoglobules above the phase transition temperatures of PNIPAMs. The existence of hydrophilic end group

and the star-shaped architecture enhance the stability of PNIPAM mesoglobules by preferential orientation of Cl groups on the surface of mesoglobules. Much smaller R_H values were observed for the *c*-PNIPAM after phase transition, which was related to the repulsive forces between PNIPAM rings as a result of the topological prohibition of intermolecular linking and the absence of end groups. The N_{agg} value of *c*-PNIPAM increased gradually and reached a plateau ~ 0.5×10^5 at 62 ºC, which was in the same magnitude as the N_{agg} value (~ 0.45×10^5) reported by Wu et al.[42] for a cyclic PNIPAM. The ring architecture depresses the coalescence of mesoglobules. The R_H and N_{agg} values of *s*-PNIPAM were observed to be larger than that for the *c*-PNIPAM, suggesting a stronger structural constraint in the latter.

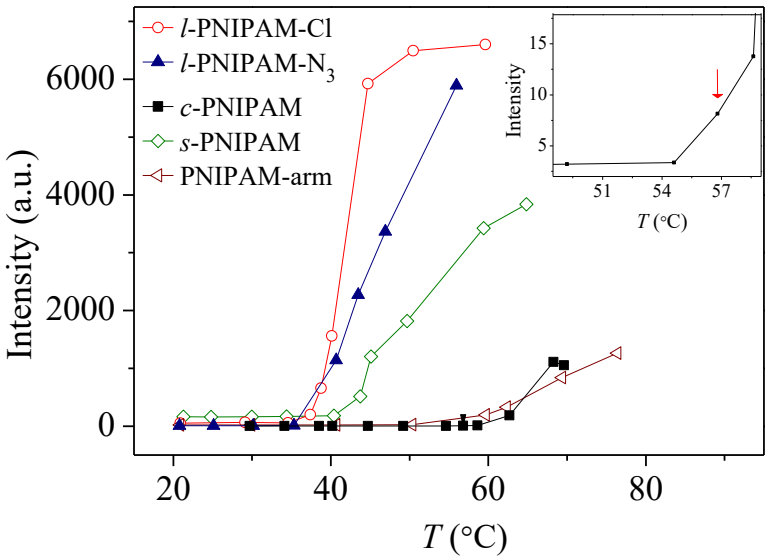

Figure 2.6 Temperature dependence of light scattering intensity for the studied polymers at concentrations of 0.09 g·L^{-1}. The inset indicates the onset temperature of intensity increase at 57 °C for *c*-PNIPAM.

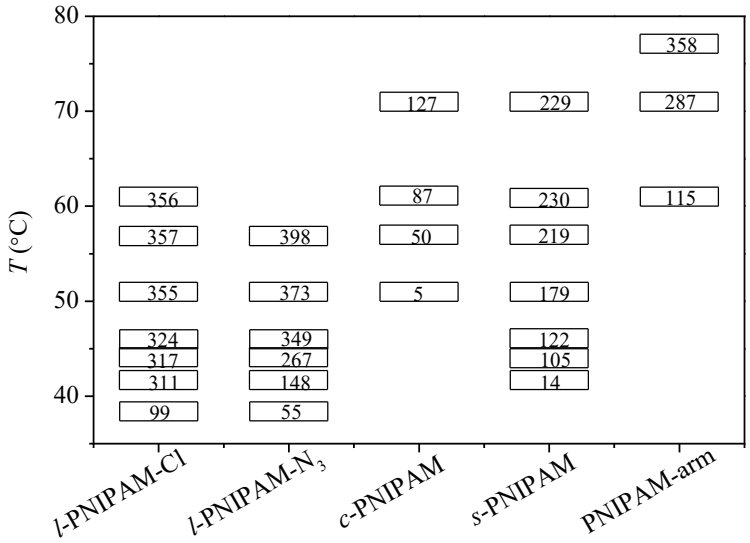

Figure 2.7 The R_H of aggregates for the polymers in water at a concentration of 0.09 $g \cdot L^{-1}$. The R_H values of polymers at certain temperature are denoted in the floating bar.

2.4 Conclusions

The effect of chain architecture on the phase transition behaviour of PNIPAM in water was evaluated by comparing the dehydration process of a star-shaped and cyclic PNIPAM with that of their linear analogues. Turbidity, light scattering and DSC measurements were employed. Tethering PNIPAM arms to a core greatly reduced the T_c. The T_c of the star-shaped PNIPAM is only slightly higher than that of the linear PNIPAM analogue. Much smaller sized aggregates and lower aggregation numbers after phase transition were observed for the *c*-PNIPAM and the *s*-PNIPAM compared with their linear analogues, reflecting topological constraint in the two polymers. A monomodal thermogram of the *s*-PNIPAM aqueous solution was obtained. A larger number of residues per cooperative unit was obtained for *s*-PNIPAM compared to its linear analogue, possibly relating to the higher content of Cl group. The lower cooperativity of the phase transition of *c*-PNIPAM was caused by topology constraint induced by its ring structure. Larger gap was observed between the T_c of the *s*-PNIPAM and that of the *l*-PNIPAM-Cl, when methanol compositions in the water/methanol mixture were increased. The phase transition region of *c*-PNIPAM is wider than that of the *s*-

PNIPAM at all methanol compositions studied, suggesting a higher degree of cooperativity for the *s*-PNIPAM than for the *c*-PNIPAM.

2.5 References

1. Asher, S. A.; Weissman, J. M.; Sunkara, H. B. WO9820388A1, **1998**.
2. Leipzig, N.; Wijekoon, A. WO2013112863A1, **2013**.
3. Mikos, A. G. WO2013086523A2, **2013**.
4. Samain, H. WO2013093773A1, **2013**.
5. Folan, M.; Horgan, F.; Turkington, M. US20130018258A1, **2013**.
6. Pelton, R. *Adv. Colloid Interface Sci.* **2000,** 85, 1-33.
7. Kikuchi, A.; Okano, T. *Adv. Drug Delivery Rev.* **2002,** 54, 53-77.
8. Stile, R. A.; Healy, K. E. *Biomacromolecules* **2001,** 2, 185-94.
9. Schild, H. G. *Prog. Polym. Sci.* **1992,** 17, 163-249.
10. Shibayama, M.; Mizutani, S.-y.; Nomura, S. *Macromolecules* **1996,** 29, 2019-24.
11. Ono, Y.; Shikata, T. *J. Am. Chem. Soc.* **2006,** 128, 10030-1.
12. Ye, X.; Lu, Y.; Shen, L.; Ding, Y.; Liu, S.; Zhang, G.; Wu, C. *Macromolecules* **2007,** 40, 4750-2.
13. Tanaka, F.; Koga, T.; Kaneda, I.; Winnik, F. M. *J. Phys. Condens. Matter* **2011,** 23, 284105.
14. Tanaka, F.; Koga, T.; Kojima, H.; Xue, N.; Winnik, F. o. M. *Macromolecules* **2011,** 44, 2978-89.
15. Zhang, Y.; Furyk, S.; Bergbreiter, D. E.; Cremer, P. S. *J. Am. Chem. Soc.* **2005,** 127, 14505-10.
16. Meewes, M.; Ricka, J.; De Silva, M.; Nyffenegger, R.; Binkert, T. *Macromolecules* **1991,** 24, 5811-6.
17. Hao, J.; Cheng, H.; Butler, P.; Zhang, L.; Han, C. C. *J. Chem. Phys.* **2010,** 132, 154902.
18. Dalkas, G.; Pagonis, K.; Bokias, G. *Polymer* **2006,** 47, 243-8.
19. Zhang, G.; Wu, C. *J. Am. Chem. Soc.* **2001,** 123, 1376-80.
20. Pang, J.; Yang, H.; Ma, J.; Cheng, R. *J. Phys. Chem. B* **2010,** 114, 8652-8.
21. Tanaka, F.; Koga, T.; Winnik, F., Competitive Hydrogen Bonds and Cononsolvency of Poly(N-isopropylacrylamide)s in Mixed Solvents of Water/Methanol. In *Gels: Structures, Properties, and Functions*, Springer Berlin / Heidelberg: **2009**; Vol. 136, pp 1-7.
22. Walter, J.; Sehrt, J.; Vrabec, J.; Hasse, H. *J. Phys. Chem. B* **2012,** 116, 5251-9.
23. Gao, H.; Matyjaszewski, K. *Prog. Polym. Sci.* **2009,** 34, 317-50.
24. Khanna, K.; Varshney, S.; Kakkar, A. *Polym. Chem.* **2010,** 1, 1171-85.
25. Kuckling, D.; Wycisk, A. *J. Polym. Sci. A Pol. Chem.* **2013,** 51, 2980-94.
26. Etrych, T.; Kovář, L.; Strohalm, J.; Chytil, P.; Říhová, B.; Ulbrich, K. *J. Control. Release* **2011,** 154, 241-8.
27. Zhang, M.; Xiong, Q.; Chen, J.; Wang, Y.; Zhang, Q. *Polym. Chem.* **2013,** 4, 5086-95.
28. Fukae, K.; Terashima, T.; Sawamoto, M. *Macromolecules* **2012,** 45, 3377-86.
29. Yang, K.; Liang, H.; Lu, J. *J. Mater. Chem.* **2011,** 21, 10390-8.

30. Cho, H. Y.; Averick, S. E.; Paredes, E.; Wegner, K.; Averick, A.; Jurga, S.; Das, S. R.; Matyjaszewski, K. *Biomacromolecules* **2013,** 14, 1262-7.
31. Gao, Z.; Liang, J.; Tao, X.; Cui, Y.; Satoh, T.; Kakuchi, T.; Duan, Q. *Macromol. Res.* **2012,** 20, 508-14.
32. Xu, J.; Liu, S. *J.Polym. Sci. A Pol. Chem.* **2009,** 47, 404-19.
33. Plummer, R.; Hill, D. J. T.; Whittaker, A. K. *Macromolecules* **2006,** 39, 8379-88.
34. Lyngsø, J.; Al-Manasir, N.; Behrens, M. A.; Zhu, K.; Kjøniksen, A.-L.; Nyström, B.; Pedersen, J. S. *Macromolecules* **2015,** 48, 2235-43.
35. Zhang, K.; Tew, G. N. *React. Funct. Polym.* **2014,** 80, 40-7.
36. Chen, B.; Jerger, K.; Fréchet, J. M. J.; Szoka Jr, F. C. *J. Control. Release* **2009,** 140, 203-9.
37. Honda, S.; Yamamoto, T.; Tezuka, Y. *J. Am. Chem. Soc.* **2010,** 132, 10251-3.
38. Zhu, X.; Zhou, N.; Zhang, Z.; Sun, B.; Yang, Y.; Zhu, J.; Zhu, X. *Angew. Chem. Int. Ed.* **2011,** 50, 6615-8.
39. Zhang, H.; Zhou, N.; Zhu, X.; Chen, X.; Zhang, Z.; Zhang, W.; Zhu, J.; Hu, Z.; Zhu, X. *Macromol. Rapid Commun.* **2012,** 33, 1845-51.
40. Prasad, A. V.; Biying, A. O.; Ling, W. Y.; Stubbs, L. P.; Zhu, Y. *J. Polym. Sci. A Pol. Chem.* **2013,** 51, 4167-74.
41. Qiu, X.-P.; Tanaka, F.; Winnik, F. M. *Macromolecules* **2007,** 40, 7069-71.
42. Ye, J.; Xu, J.; Hu, J.; Wang, X.; Zhang, G.; Liu, S.; Wu, C. *Macromolecules* **2008,** 41, 4416-22.
43. Xu, J.; Ye, J.; Liu, S. *Macromolecules* **2007,** 40, 9103-10.
44. Liu, B.; Wang, H.; Zhang, L.; Yang, G.; Liu, X.; Kim, I. *Polym. Chem.* **2013,** 4, 2428-31.
45. Chen, Y.; Xiao, N.; Fukuoka, M.; Yoshida, K.; Duan, Q.; Satoh, T.; Kakuchi, T. *Polym. Chem.* **2015,** 6, 3608-16.
46. Tiktopulo, E. I.; Uversky, V. N.; Lushchik, V. B.; Klenin, S. I.; Bychkova, V. E.; Ptitsyn, O. B. *Macromolecules* **1995,** 28, 7519-24.
47. Qiu, X.; Koga, T.; Tanaka, F.; Winnik, F. *Sci. China Chem.* **2013,** 56, 56-64.
48. Xia, Y.; Burke, N. A. D.; Stöver, H. D. H. *Macromolecules* **2006,** 39, 2275-83.
49. Satokawa, Y.; Shikata, T.; Tanaka, F.; Qiu, X.-p.; Winnik, F. o. M. *Macromolecules* **2009,** 42, 1400-3.
50. Balu, C.; Delsanti, M.; Guenoun, P.; Monti, F.; Cloitre, M. *Langmuir* **2007,** 23, 2404-7.
51. Chan, K.; Pelton, R.; Zhang, J. *Langmuir* **1999,** 15, 4018-20.
52. Luxenhofer, R.; Jordan, R. *Macromolecules* **2006,** 39, 3509-16.
53. Duclos, S.; Stoeckli-Evans, H.; Ward, T. R. *Helv. Chim. Acta* **2001,** 84, 3148-61.

2.6 Appendix

2.6.1 Experimental details for synthesis of star and linear PNIPAM

Materials. Copper (I) chloride (CuCl, 99.995%) and pentaerythritol (99+ %) were purchased from Sigma Aldrich Chemical Co. Inc. and used as received. *N*,*N*,*N*′,*N*″,*N*″-pentamethyldiethylenetriamine (PMDETA, > 98.0%) was purchased from Tokyo Kasei Kogyo Co., Ltd. (TCI) and used without further purification. 4-dimethylaminopyridine (DMAP, 99+ %) were purchased from Wako Pure Chemical Industries, Ltd. and used as received. *N*-isopropylacrylamide (NIPAM) was provided by Kohjin Co., and recrystallized twice from hexane/toluene (10/3, v/v) prior to use. Tris [2-(dimethylamino)ethyl]amine (Me_6TREN) was donated by Mitsubishi Chemical Co., and distilled over calcium hydride under reduced pressure. Azido end-functionalized poly(*N*-isopropylacrilamide) (N_3-PNIPAM) [41], 5-hexynoyl chloride[52] and ethyl 5-hexynoate (2)[53] were prepared according to their literature procedures. Deionized water and methanol of analytical grade (Sigma-Aldrich) were used for thermoresponsivity measurement. All other reagents not mentioned were of synthetic grade and used without further purification. A linear PNIPAM (*l*-PNIPAM) carrying an azide and a propargyl group at each end and a cyclic PNIPAM (*c*-PNIPAM) prepared by ring closure of the *l*-PNIPAM precursor were synthesized and characterized elsewhere.[41] The M_n of the two polymers was determined to be 12,700 g·mol^{-1} by GPC.

Characterization. The ^{1}H and ^{13}C NMR spectra were recorded using a JEOL JNM-EX 270 and a JEOL JNM-A 400II instrument. The IR spectra were recorded using a Perkin-Elmer Paragon 1000 FT-IR instrument. Size exclusion chromatography (SEC) was performed at 40 °C using a Jasco high performance liquid chromatography (HPLC) system (PU-980 Intelligent HPLC pump, CO-965 Column oven, RI-930 Intelligent RI detector, and Shodex DEGAS KT-16) equipped with a Shodex Asahipak GF-310 HQ column (linear, 7.6 mm × 300 mm; pore size, 20 nm; bead size, 5 μm; exclusion limit, 4×10^4) and a Shodex Asahipak GF-7M HQ column (linear, 7.6 mm × 300 mm; pore size, 20 nm; bead size, 9 μm; exclusion limit, 4×10^7) in DMF containing lithium chloride (0.01 M) at the flow rate of 0.4 mL·min^{-1}. The number-average molecular weight (M_n) and dispersity (M_w/M_n) of the polymers were calculated on the basis of a polystyrene calibration. The weight-average intrinsic viscosity

([η]) and weight-average hydrodynamic radius (R_H) of the polymer solution were determined by SEC in THF (1.0 mL·min^{-1}) at 40 °C using an Agilent 1100 series instrumentation equipped with two Shodex KF-804L columns (linear, 8 mm × 300 mm; exclusion limit, 4 × 10^5), viscosity detector (Wyatt, Viscostar), and refractive index detector (Wyatt, Optilab rEX), and estimated by the software ASTRA 5.1.6.0 (Wyatt). The preparative SEC was performed in THF (3.5 mL·min^{-1}) at 23 °C using a JAI LC-9201 equipped with a JAI JAIGEL-3H column (20 mm × 600 mm; exclusion limit, 7 × 10^4) and a JAI RI-50s refractive index detector. The turbidimetry analysis in water was performed using a Jasco V-550 spectrophotometer equipped with an EYELA NCB-1200 temperature controller. Transmittances of the PNIPAM aqueous solutions at 500 nm were recorded versus the increasing temperature at a heating rate of 1.0 °C·min^{-1}. The elemental analysis was performed using a MICRO CORDER JM10 (Center of the Instrumental Analysis, Hokkaido University).

Synthesis of Pentaerythrityl tetra-5-hexynoate (1). Under a nitrogen atmosphere, 5-hexynoyl chloride (1.00 g, 7.66 mmol) was added into a solution of pentaerythritol (220 mg, 1.62 mmol) and DMAP (0.786 g, 6.43 mmol) in dry dichloromethane (18 mL). The reaction mixture was allowed to stir at ambient temperature for 7 h. The reaction mixture was then filtered and evaporated. The resulting crude residue was then purified via chromatography on a silica gel column using a hexane/ethyl acetate (3/1, v/v, R_f = 0.26) solution as eluent. The solvent was removed by rotary evaporation, and the final product was dried under vacuum for 1 day to yield coupling agent 1 as shown in **Scheme A2.1**. Yield, 0.410 g (50.0 %). ^{1}H NMR (DMSO-d_6, 400 MHz): δ (ppm) 1.69 (tt, J = 7.3 Hz, J = 14.5 Hz, ($CH_2CH_2CH_2$, 8H), 2.19 (dt, J = 7.1 Hz, J = 2.6 Hz, ($CH_2C\equiv CH$, 8H), 2.41 (t, J = 7.5 Hz, $COCH_2$, 8H), 2.80 (t, J = 2.7 Hz, CH, 4H), 4.09 (s, CH_2O, 8H). ^{13}C NMR (DMSO-d_6, 100 MHz): δ (ppm) 17.01 ($CH_2C\equiv CH$), 23.35 ($CH_2CH_2CH_2$), 32.32 ($COCH_y$), 41.73 ($C(CH_2)_4$), 62.09 (CH_2O), 71.71 (CH), 83.53 ($C\equiv CH$), 171.94 (C=O). Anal. Calcd for $C_{29}H_{36}O_8$ (512.59): C, 67.95; H, 7.08. Found: C, 67.69; H, 7.21.

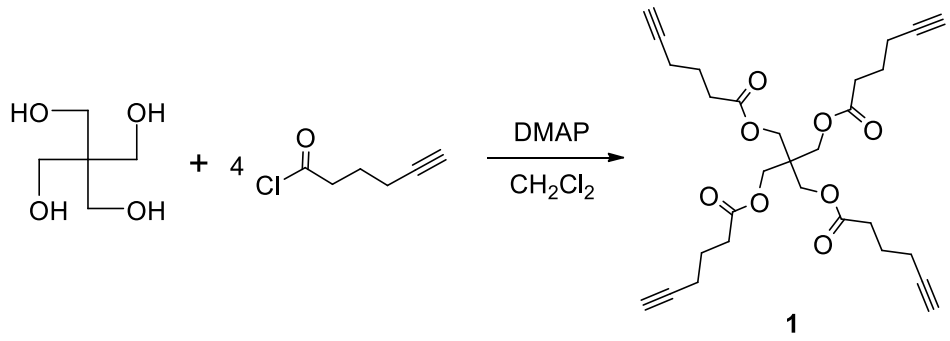

Scheme A2.1 Synthesis of pentaerythrityl tetra-5-hexynoate (**1**).

Synthesis of Star-PNIPAM. Compound 1 (59.5 mg, 0.116 mmol, 1 eq), N_3-PNIPAM$_{3300}$ ($M_{n,NMR}$ = 3300, 2.00 g, 0.116 mmol, 8 eq), and CuCl (276 mg, 2.79 mmol, 24 eq) were stirred in dry THF (7 mL) under an argon atmosphere. Into the reaction mixture was added PMDETA (964 mg, 5.57 mmol, 48 eq) and then stirred at room temperature for 24 h. The reaction mixture was exposed to air, diluted with THF, and passed through neutral silica gel column to remove the copper catalyst. The solvent was removed by rotary evaporation, and the residue was purified dialysis successively in methanol and in water (Spectra/Por 6 membrane; MWCO: 1000). Further purification via preparative SEC in THF afforded star-PNIPAM$_{14700}$ as a white powder. Yield, 65.0 mg (61.3 %). $M_{n,NMR}$ = 14,700, M_w/M_n = 1.17 (THF).

Synthesis of linear-PNIPAM Compound 2 (63.8 mg, 0.455 mmol, 3 eq), N_3-PNIPAM$_{3300}$ ($M_{n,NMR}$ = 3300, 500 mg, 0.152 mmol, 1 eq), and CuCl (90.0 mg, 0.91 mmol, 6 eq) were stirred in dry THF (1.5 mL) under an argon atmosphere. PMDETA (158 mg, 0.91 mmol, 6 eq) was added into the reaction mixture and stirred for 40 h at room temperature. The reaction mixture was exposed to air, diluted with THF, and passed through neutral silica gel column to remove the copper catalyst. The solvent was removed by rotary evaporation and the purification via preparative SEC in THF afforded linear-PNIPAM$_{3800}$ as a white powder. Yield, 225 mg (48.8 %). $M_{n,NMR}$ = 3800, M_w/M_n = 1.13 (THF)

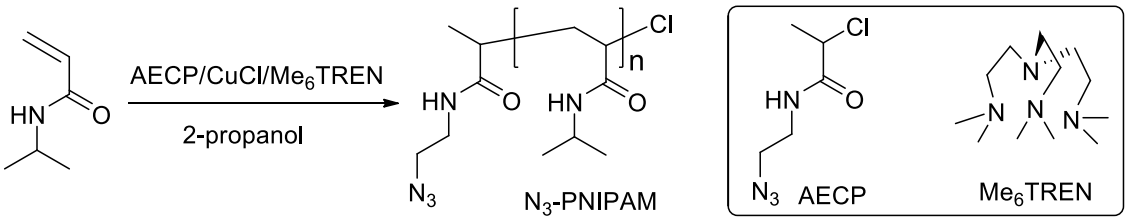

Scheme A2.2 Synthesis of azido end-functionalized poly(*N*-isopropyl acrylamide) (N_3-PNIPAM).

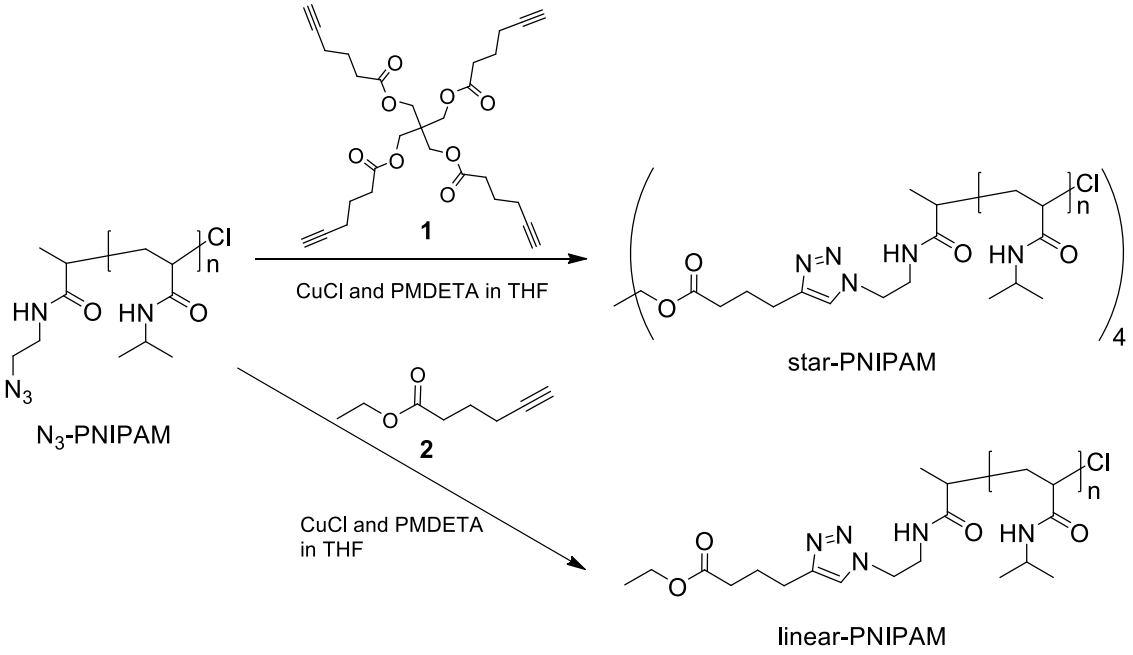

Scheme A2.3 Syntheses of star- and linear-PNIPAMs by the reactions of clickable N_3-PNIPAM with pentaerythrityl tetra-5-hexynoate (**1**) and ethyl 5-hexynoate (**2**), respectively.

4-arm star PNIPAM (star-PNIPAM) was synthesized via arm-first strategy in two steps. Firstly, azido end-functionalized PNIPAM (N_3-PNIPAM) with varying molar mass was prepared by ATRP of N-isopropylacrylamide. The star-PNIPAM was produced by a subsequent click reaction of N_3-PNIPAM with pentaerythrityl tetra-5-hexynoate. The linear-PNIPAM with identical structure as the arm of star-PNIPAM was prepared as well via click coupling of N_3-PNIPAM with ethyl 5-hexynoate.

2.6.2 Synthesis of N_3-PNIPAM

Table A2.1 Results of ATRP of NIPAM using *N*-(2-azidoethyl)-2-chloropropionamide (AECP) as an initiator in 2-propanol[a].

Polymer	[NIPAM]/[AECP]	conv. (%) [c]	$M_{n,th}$ [d] (kDa)	$M_{n,NMR}$ [e] (kDa)	$M_{n,SEC}$ [f] (kDa)	M_w/M_n [f]
N_3-PNIPAM$_{2100}$	15	93.8[e]	1770	2100	3000	1.24
N_3-PNIPAM$_{3300}$	25	97.1	2900	3300	5300	1.18
N_3-PNIPAM$_{5800}$	50	92.1	5390	5800	11,000	1.12
N_3-PNIPAM$_{11000}$ [b]	100	69.1[e]	8000	11,000	20,000	1.11
N_3-PNIPAM$_{13700}$	150	68.5	11,800	13,700	25,700	1.23

[a.] [AECP]/[CuCl]/[Me_6TREN] = 1/1/1; $[NIPAM]_0$/solvent = 0.5 (w/w); temp., 20 °C; for 4 h.
[b.] Reaction time was for 3 h.
[c.] Determined by ^{1}H NMR spectrum in $CDCl_3$.
[d.] $M_{n,th} = 113.16 \times (conv.)/100 \times [NIPAM]_0/[AECP]_0 + 176.61$.
[e.] Determined by ^{1}H NMR spectrum in D_2O.
[f.] Determined by SEC in DMF containing 0.01 mol·L^{-1} LiCl.

The azido end-functionalized poly(*N*-isopropylacrylamide) (N_3-PNIPAM) with varying molecular weight was prepared by ATRP of NIPAM with CuCl and tris[2-(dimethylamino)ethyl]amine (Me_6TREN) was carried out using *N*-(2'-azidoethyl)-2-chloropropionamide (AECP) as a initiator in 2-propanol (**Scheme A2.2**). The results were summarized in **Table A2.1**. For the polymerization using the [AECP]/[CuCl]/[Me_6TREN] of 1: 1: 1 and NIPAM/2-propanol of 1: 1 (w/w) at 20 °C, the number-average molecular weight (M_n) of the obtained polymers can be controlled by [NIPAM]/[AECP] ratio. The N_3-PNIPAMs with the $M_{n,NMR}$ in the range of 2100 to 13,700 g·mol^{-1} were obtained in good yield and the $M_{n,NMR}$ values were in good agreement with the theoretical molecular weight ($M_{n,th}$). SEC traces of the obtained N_3-PNIPAMs (**Figure A2.1a**) showed a symmetric mono-disperse distribution with narrow dispersity ($Đ$) in the range of 1.11 to 1.24. In the ^{1}H NMR spectrum of N_3-PNIPAM in D_2O (**Figure A2.2a**), the signals assignable to the protons of the PNIPAM appeared in the range from 0.6 to 2.4 ppm and from 3.8 to 4.2 ppm. The peak at 3.4 ppm was attributed to the methylene protons adjacent to the azido group. The attachment of the azide end group was ascertained by the peak at 2102 cm^{-1} in the IR spectrum of N_3-PNIPAM

(**Figure A2.3a**). The SEC, IR, and NMR results indicated that the polymerization proceeded in living manner with a high efficiency for end functionalization.

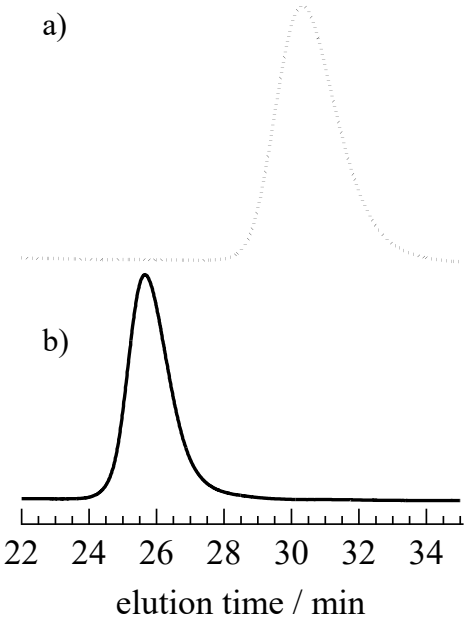

Figure A2.1 SEC traces of a) N_3-PNIPAM$_{3300}$ and b) star-PNIPAM$_{14700}$ measured in DMF containing 0.01 mol·L^{-1} LiCl.

2.6.3 Syntheses of star- and linear-PNIPAMs

Well-defined 4-arm star PNIPAM (star-PNIPAM) was obtained via arm-first strategy. The core of the polymer—the tetraalkyne-functionalized precursor, i.e., pentaerythrityl tetra-5-hexynoate (**1**), was prepared by reacting pentaerythritol with 5-hexynoyl chloride, as shown in **Scheme A2.1**. The ^{1}H NMR spectrum of the product **1** in DMSO-d_6 showed the complete disappearance of the hydroxyl proton of pentaerythritol at 4.2 ppm and the shift of the hydroxymethyl proton signal from 3.4 ppm to 4.1 ppm (*b* in **Figure A2.4a**). The complete esterification was also proved by a shift of the hydroxymethyl carbon ^{13}C NMR signal from 47.1 ppm to 62.1 ppm (*b* in **Figure A2.4b**).

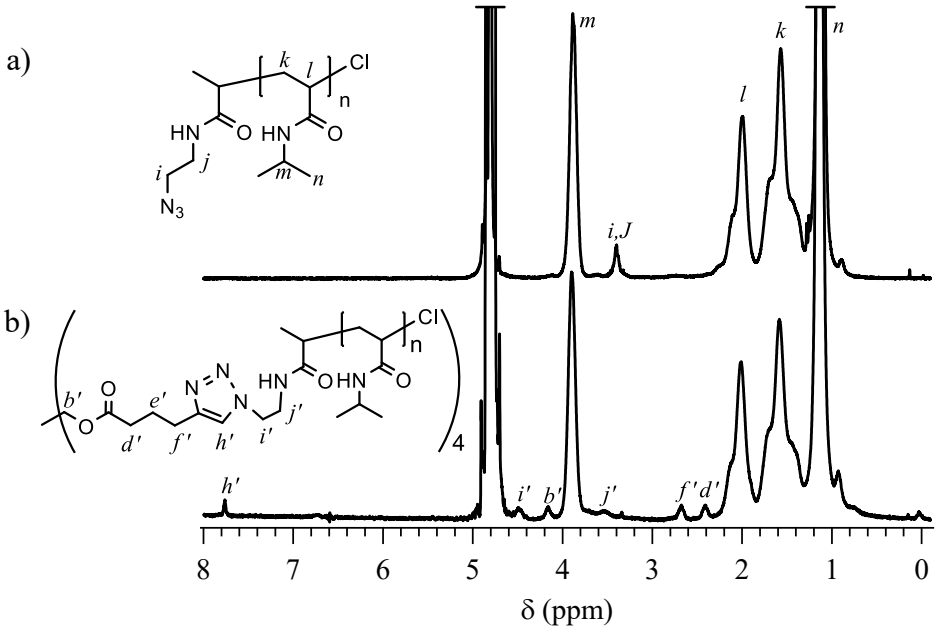

Figure A2.2 The ^{1}H NMR spectra of a) N_3-PNIPAM$_{5800}$ and b) star-PNIPAM$_{25000}$ in D_2O.

To obtain well-defined 4-arm star-PNIPAM, the "click" reaction of N_3-PNIPAM with **1** was carried out in THF at room temperature for 24 h in the presence of CuCl and PMDETA, as shown in **Scheme A2.2**. To ensure complete consumption of alkyne residues in **1**, excess N_3-PNIPAM was used, i.e., [alkyne]/[azide]/[CuCl]/[PMDETA] molar ratio was 1:2:3:6. The obtained products were purified by dialysis in methanol followed by water and preparative SEC in THF to afford star-PNIPAM as a white powder. **Figure A2.2** shows ^{1}H NMR spectra of N_3- and star-PNIPAMs. In the spectrum of star-PNIPAM (**Figure A2.2b**), the signals of the methylene protons (*i* in **Figure A2.2a**) adjacent to the azido group of N_3-PNIPAM and the methine protons (*h* in **Figure A2.4a**) of **1** completely disappear. Alternatively, the signals of the methylene protons (*i'*) shifted to 4.5 ppm and the signal of the methine proton (*h'*) in the triazole ring was observed at 7.8 ppm. The star-PNIPAMs were characterized by IR as shown in **Figure A2.3**. The complete disappearance of the characteristic azido absorbance at 2102 cm^{-1} for N_3-PNIPAM proved the success of the click reaction. The SEC trace of star-PNIPAM in **Figure A2.1b** was monomodal and symmetric, and shifted to higher molecular weight side compared to that of N_3-PNIPAM. These results confirmed that the "click" reaction proceeded qualitatively.

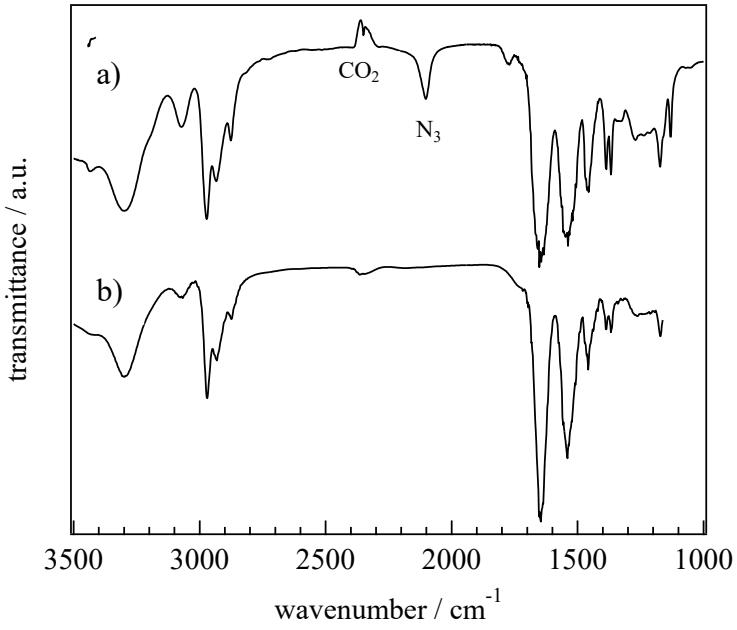

Figure A2.3 IR spectra of a) N_3-PNIAPM$_{3300}$ and b) star-PNIPAM$_{14700}$.

To compare the solution properties of the star-PNIPAM, a linear-PNIPAM having the same end groups as the star-PNIPAM was also prepared by the "click" reaction of N_3-PNIPAM with ethyl 5-hexynoate (**2**), as shown in **Scheme A2.3**. Based on the NMR and IR results of the obtained linear-PNIPAM (See **Figure A2.5** and **Figure A2.6**), the "click" reaction was also qualitatively complete and the linear-PNIPAMs with varying molecular weight were obtained.

Table A2.2 presents the $M_{n,NMR}$, dispersity, intrinsic viscosity ([η]), and hydrodynamic radius (R_H) of linear- and star-PNIPAMs, which were measured by the ^{1}H NMR analysis in water and the size exclusion chromatography (SEC) equipped with a viscosity detector in THF. Based on the ^{1}H NMR measurements, the $M_{n,NMR}$ value of star-PNIPAM were about four times greater than that of the corresponding linear-PNIPAM. Narrow dispersities in the range of 1.02 to 1.26 for the linear- and star-PNIPAMs were obtained. The [η] values increased with molecular weight. For linear-PNIPAMs with $M_{n,NMR}$ of 2600–13,800 g·mol^{-1}, [η] of 3.8–9.3 mL·g^{-1}; for star-PNIPAMs with $M_{n,NMR}$ of 8300–46,700 g·mol^{-1}, [η] of 5.9–9.2 mL·g^{-1}. Smaller [η] values were obtained for star-PNIPAM than that for linear-PNAIPAM with similar $M_{n,NMR}$ value, e.g., the [η] values were 6.5 and 9.3 mL·g^{-1} for star-PNIPAM$_{14700}$ and linear-

$PNIPAM_{13800}$, respectively. The result revealed less physical entanglement for star-PNIPAM based on the branched structure

Table A2.2 Physical properties of linear-PNIPAM and star PNIPAM.

linear-PNIPAM			star-PNIPAM		
$M_{n,NMR}$[a] (kDa)	M_w/M_n[b]	$[\eta]$[b] (mL·g^{-1})	$M_{n,NMR}$[a] (kDa)	M_w/M_n[b]	$[\eta]$[b] (mL·g^{-1})
2,600	1.26	3.8	8,300	1.10	5.9
3,800	1.13	4.5	14,700	1.17	6.5
6,100	1.05	6.3	25,000	1.02	8.3
11,300	1.13	7.8	46,700	1.14	9.2
13,800	1.07	9.3	---	---	---

[a.] Determined by ^{1}H NMR spectrum in D_2O.
[b.] Determined by SEC-viscometer in THF.

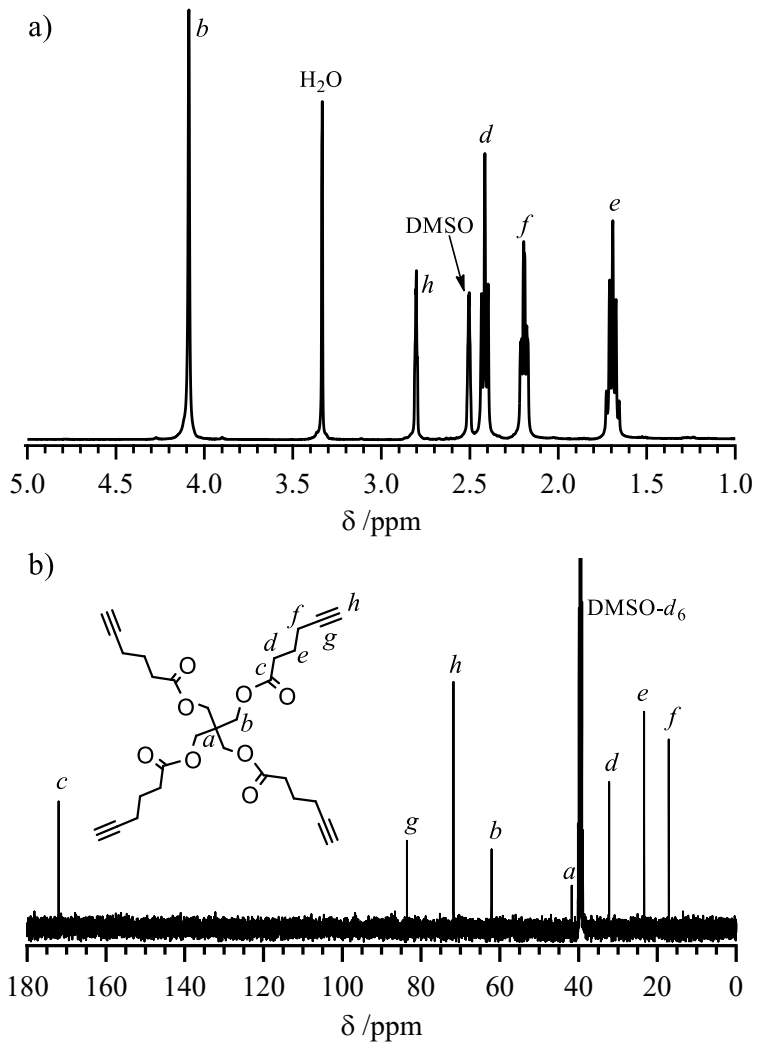

Figure A2.4 The a) ^{1}H and b) ^{13}C NMR spectra of pentaerythrityl tetra-5-hexynoate (**1**) in DMSO-d_6.

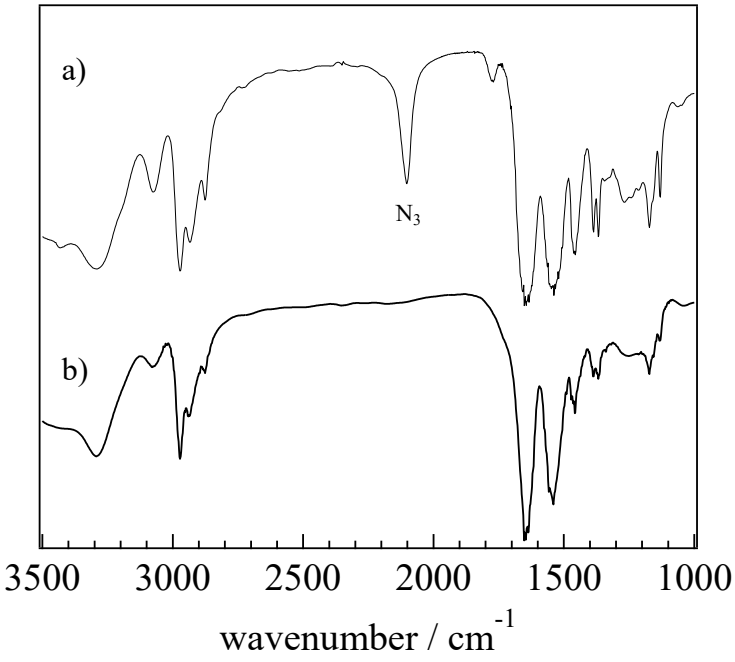

Figure A2.5 IR spectra of a) N_3-PNIAPM$_{2100}$ and b) linear-PNIPAM$_{2600}$.

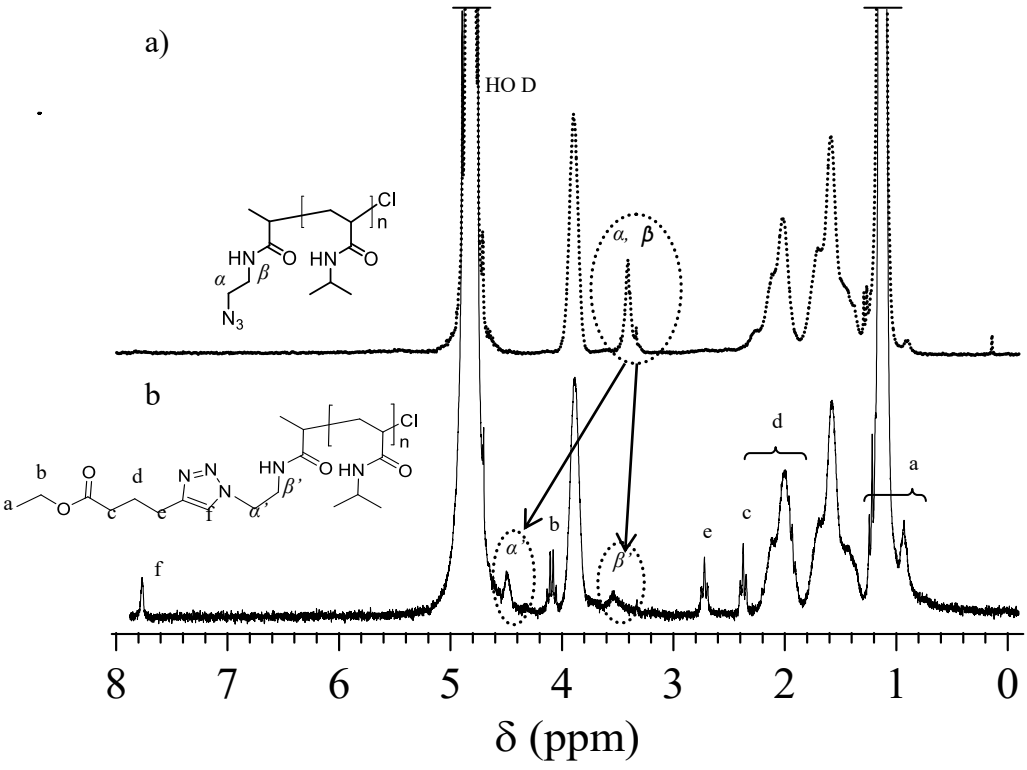

Figure A2.6 ^{1}H NMR spectra of a) N_3-PNIAPM$_{2100}$ and b) linear-PNIPAM$_{2600}$ in D_2O.

2.6.4 Phase separation of star PNIPAM in water

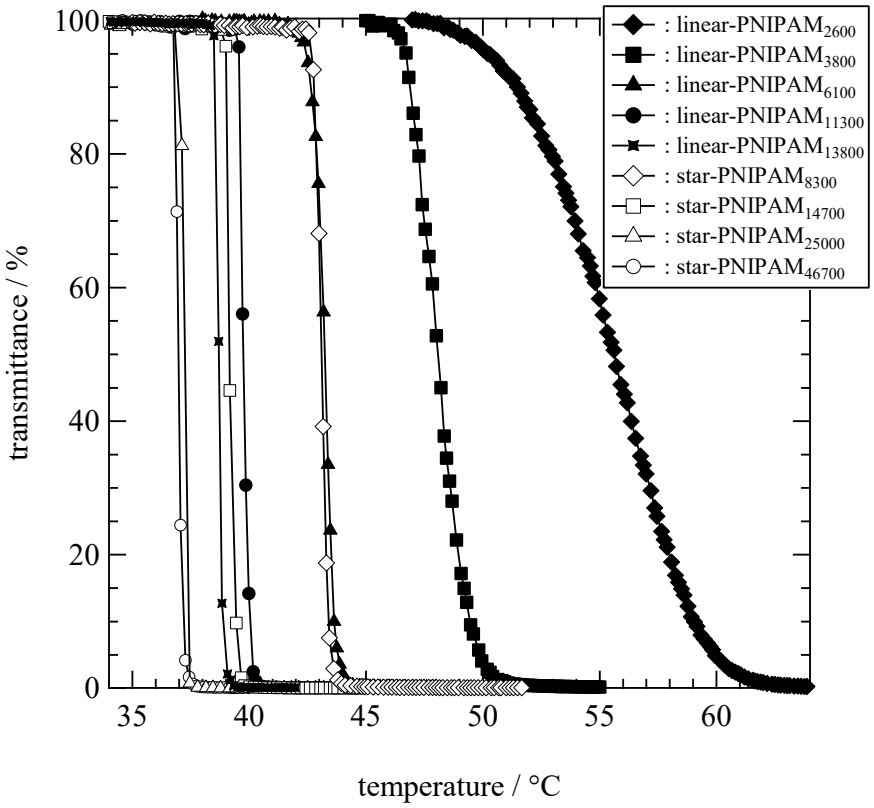

Figure A2.7 Optical transmittance of linear and star-PNIPAMs in water (2.0 $g \cdot L^{-1}$).

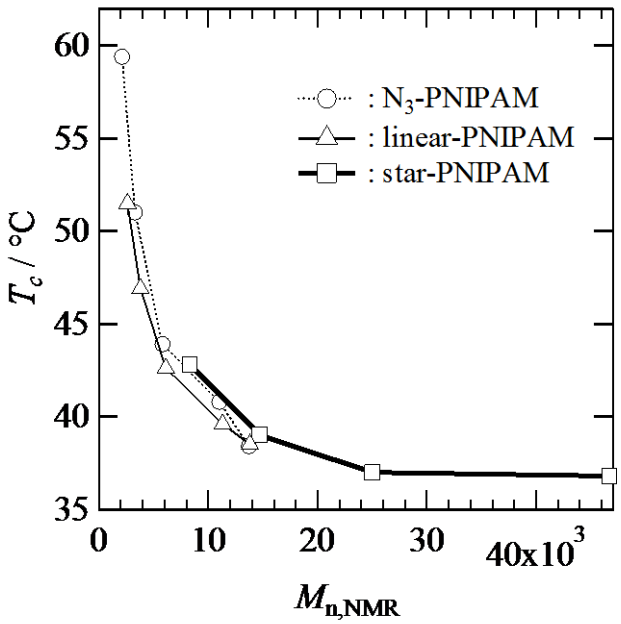

Figure A2.8 The critical phase separation temperature (T_c, 90 % transmittance at 500 nm) versus molecular weight ($M_{n,NMR}$) of N_3-PNIPAM, linear-PNIPAM and star-PNIPAM in H_2O. The transmittance of a 2.0 $g \cdot L^{-1}$ solution was measured versus the increasing temperature using a heating rate of 0.1 ºC min^{-1}.

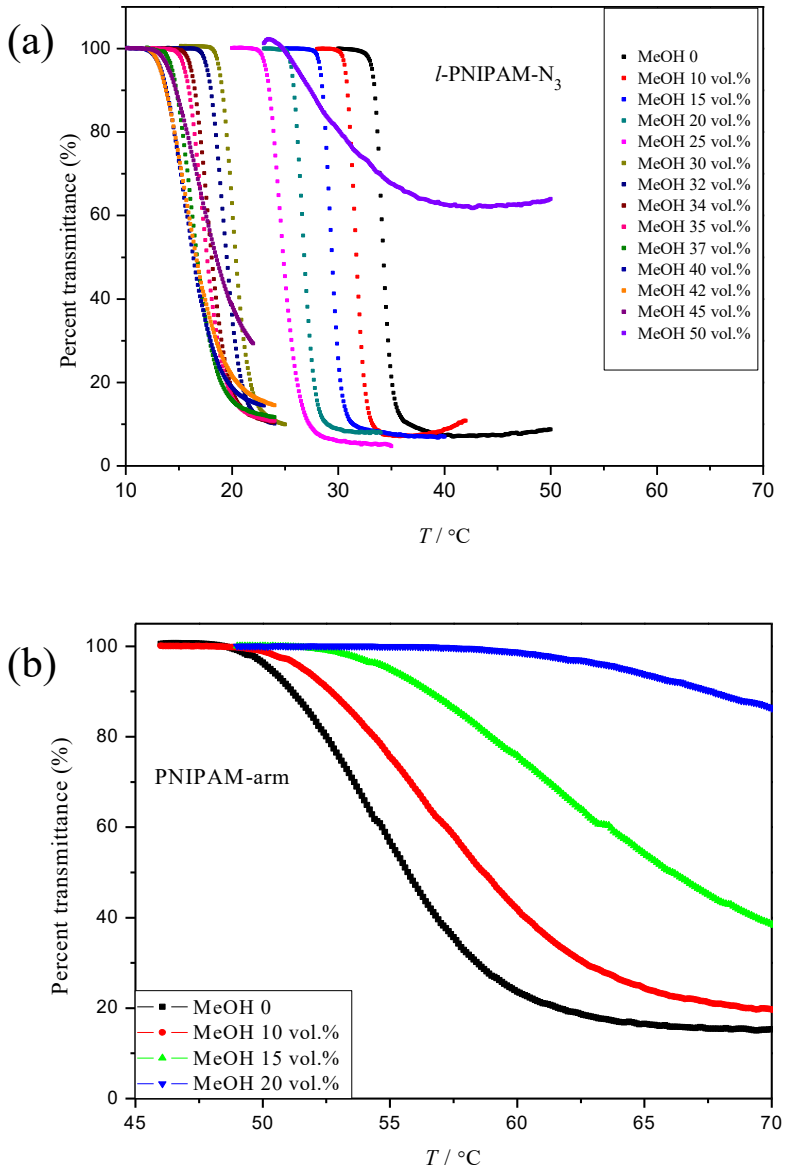

Figure A2.9 Temperature dependence of the turbidity at a heating rate 0.2 °C·min^{-1} for (a) *l*-PNIPAM-N_3, and (b) PNIPAM-arm (1.0g·L^{-1}) in methanol/water mixtures at various methanol volume fractions.

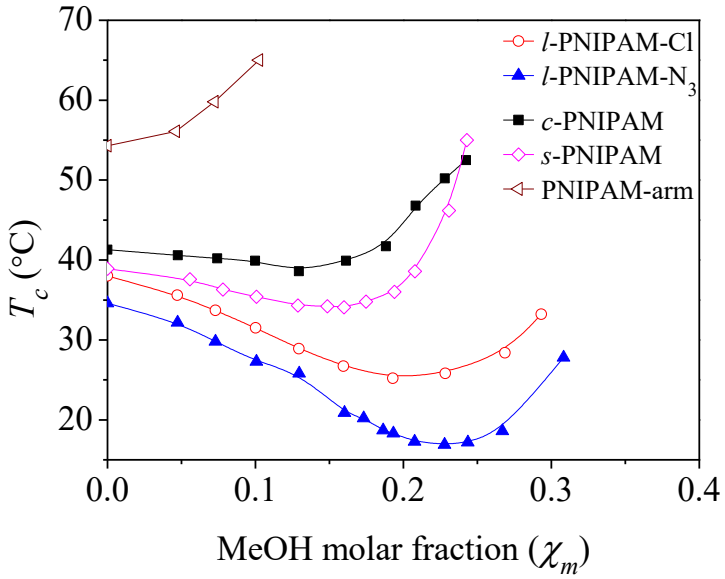

Figure A2.10 Phase diagram of PNIPAM (1.0 g·L^{-1}) as a function of solvent composition in methanol-water mixtures expressed in methanol (MeOH) molar fraction. T_c identified as the temperature corresponding to the inflection point in the turbidity curve.

Chapter 3. Liquid liquid phase separation in poly(*N*-isopropylacrylamide)/water/methanol mixture

3.1 Introduction

PNIPAM exhibits a LCST in water around 32 °C. The PNIPAM chain goes through a coil-globule phase transition above its LCST, and a stable turbid solution was observed. Addition of a water miscible solvent such as THF, DMSO and alcohol etc., into the PNIPAM aqueous solution results in a turbid solution, a phenomenon known as cononsolvency. The competition in hydrogen bond formation between the water and the cononsolvent molecules to the polymer results in a depressed LCST. Recently, the macroscopic liquid-liquid phase separation (MLLPS) of PNIPAM/water/consolvent system was reported by Young et al.[1], who studied the cononsolvency of PNIPAM in methanol and water in concentrated solutions. The solution mixture phase separated into two coexisting liquid phases including a polymer rich phase and polymer poor phase at given compositions of the solvent mixtures and the maximum polymer concentration used was 15 wt%. However, unfortunately a complete phase diagram was not obtained since the polymer concentrations used in their study were too high and the polymer gelled. By introducing a polymer-methanol-water ternary parameter, the calculated binodal line (miscibility-limit curve) matched the experimental data properly. The authors claimed that the demixing occurred where a sufficient number of solvent-solvent contacts happened in the vicinity of polymer chain.

The MLLPS was also observed in other mixed systems. The liquid liquid demixing in polymer solvents ternary systems has been studied by Berghmans et al.[2] and Shaw et al.[3] Berghmans' study[2] examined the phase separation of PVDM in the mixture of THF and water. Three coexisting liquid phases were observed. Changing of temperatures shifted the miscibility area in their ternary phase diagram. Shaw et al.[3] studied the phase behavior of PMMA in cosolvent of water and 2-propanol (individually nonsolvents) and observed liquid–liquid demixing regions separated by a miscible region as a result of a joint effect of the nonsolvents. Ganachaud et al.[4] studied the phase behavior of PMMA in water and acetone or THF. Depending on PMMA concentration and acetone concentration in the mixture, PMMA

particles of different size and morphologies were formed in the solutions. The compositions boundary between the ouzo region (PMMA nanoparticles) and the non-Ouzo region (nano- and microparticles) was reported to have nothing to do with the spinodal decomposition line of the ternary solutions. The nanoparticles formed through a nucleation-aggregation mechanism when the nonsolvent water was in abundance and PMMA concentration was low. When water was in a small fraction, the growth of PMMA nanoparticles followed a nucleation-and-growth mechanism. The schematic representation of the ouzo region is shown in **Scheme 3.1**. The ouzo effect occurs when solutions are rapidly brought from the one phase region into the metastable region between the binodal line and spinodal line. In the phase diagram, the binodal curve traces the thermodynamic Gibbs free energy minima. The spinodal curve traces the limit of thermodynamic stability.

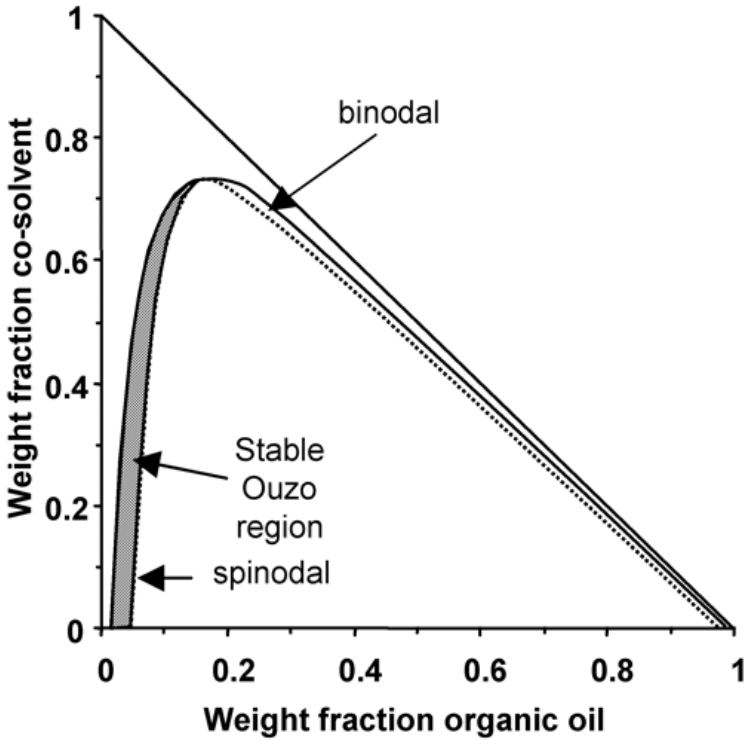

Scheme 3.1 Right triangle three-component phase diagram. (Reprinted with permission from Ref 5. Copyright (2003) American Chemical Society.)

The aim of this work is to study the demixing of the PNIPAM in water/methanol mixtures taking into account the effect of polymer concentration. A PNIPAM bearing two *n*-Butyl end groups with M_w 45,000 g·mol^{-1} and narrow dispersity was employed in the study. A PNIPAM with high molecular weight (M_n = 180,000 g·mol^{-1}) and high dispersity, synthesized

by the radical polymerization was used to test the effluence of molecular weight and dispersity on the phase separation of PNIPAM. The demixing kinetics during the MLLPS will be studied. The ternary phase diagram of the polymer constructed based on experimental data will supply a foundation for a better understanding the nature of the coil-to-globule phase separation.

3.2 Experimental section

3.2.1 Materials

The α, ω-di(*n*Butylpropionate)-poly(*N*-isopropylacrylamide) (*n*Bu-PNIPAM) and α,ω-di(2-chloroethyl propionate)-PNIPAM (Cl-PNIPAM) with the same M_n = 44,500 g·mol^{-1} ($Đ$ = 1.10) was synthesized and characterized as described elsewhere.[6] The poly(*N*-isopropylacrylamide) (PNIPAM-180K) with M_n = 180,000 g·mol^{-1} was obtained by radical polymerization. A PNIPAM bearing amine groups at both ends (PNPAM-NH_2) was employed for approximating the density of the condensed phase after MLLPS. Deionized water (deionized by a Millipore Milli-Q system) and analytical grade methanol (Sigma-Aldrich) were used for solution preparation. Trimethylsilyl propionic acid sodium salt (TMPS, 98%) and deuterium oxide (99.9%) were purchased from Sigma-Aldrich Chemicals.

3.2.2 Characterization methods

Composition measurements. The solutions for macroscopic liquid-liquid phase separation were prepared by weighing and mixing the stock aqueous solutions of *n*Bu-PNIPAM (10 g·L^{-1}) and methanol solutions of *n*Bu-PNIPAM (10 g·L^{-1}) at proper ratios in an s inverted conical vial made from a glass pipette. After macroscopic liquid-liquid phase separation (about 1 day), the compositions of the upper dilute and the bottom viscous phase were determined by NMR spectroscopy. The recovered separated phases were dissolved in D_2O (with a certain amount of TMPS added as standard), and ^{1}H NMR spectra of the resulting solutions were recorded on a Bruker AV400 MHz NMR spectrometer. The intensities of the peak at δ = 3.36 ppm (CH_3 of methanol), δ = 0 ppm ($(CH_3)_3$ in TMPS), δ = 1.16 ppm (CH_3 in PNIPAM) and δ = 4.80 ppm (H_2O) in the NMR spectra (**Figure 3.2**) were measured to calculate the compositions of the samples.

The methanol volume fractions in the initial mixtures ϕ were calculated according to the following equation

$$\phi = \frac{m_{Me}/\rho_{Me}}{m_{Me}/\rho_{Me} + m_W/\rho_W} \tag{3.1}$$

where m_{Me} is the mass of the stock methanol solution of *n*Bu-PNIPAM, ρ_{Me} is the density of methanol, m_W is the mass of the stock water solution of *n*Bu-PNIPAM, and ρ_W is the density of water.

The polymer volume fractions in the condensed phase ϕ_P after the macroscopic liquid-liquid phase separation were calculated by the following equation,

$$\phi_P = \frac{X * D}{\rho_P} \tag{3.2}$$

where X is the weight percent of *n*Bu-PNIPAM in the condensed phases (NMR results), ρ_P is the density of pure PNIPAM (1.0 g·mL^{-1})[7] and D is the density of the condensed phase after the MLLPS.

The methanol volume fractions in the condensed phases after the MLLPS were calculated as below,

$$\phi = (1 - \phi_P) * \phi' \tag{3.3}$$

where ϕ' is the volume ratio of methanol calculated from the NMR results according to equation (3.1).

Density measurement. The solutions for density measurement of the viscous condensed phase were prepared by weighing and mixing the stock aqueous solutions of PNIPAM (10 g·L^{-1}) and methanol solutions of PNIPAM (10 g·L^{-1}) at proper ratios inside 25 mL or 10 mL volumetric flasks. (V is the volume of the volumetric flask.) After macroscopic liquid-liquid phase separation happened (about 2.5 days), the upper dilute was removed carefully with a glass pipette. Govern amount of n-hexane was added to the volumetric flask until the total volume of n-hexane and the remained condensed phase reached the marked line. The mass of *n*-hexane and condensed phase was weighted to be m_H and m_p respectively. The

density of *n*-hexane was determined to be 0.67 g·mL^{-1} using a 25 mL volumetric flask. The density of the polymer condensed phase D was then calculated according to the following equation:

$$D = \frac{m_P}{V - m_H/0.67} \tag{3.4}$$

Solution preparation. Stock solutions of polymer in water (10 g·L^{-1}) and polymer in methanol (10 g·L^{-1}) were prepared one day before mixing. The polymer/water/methanol mixed solutions were prepared by mixing the polymer/water and the polymer/methanol stock solutions with proper volume ratio. All mixed solutions were prepared this way unless otherwise stated.

Microscopic observations. Given amounts of the mixed methanol/water solutions of *n*Bu-PNIPAM or PNIPAM-180K (10 g·L^{-1}) was dropped on a glass slide, covered with a small round glass slide and sealed with epoxy glue. The solution spread between the two glass slides and form a circular area about 3 mm in diameter. The thickness of the solution was ~ 1mm estimated from the solution volume and the area of the spread solution. After preparation the samples were immediately viewed by an Axioskop 2 Carl Zeiss Microscope and the Image-Pro-Plus software at room temperature (21 ºC). Images of the samples were taken from time to time and calibrated by a standard scale under the same conditions. The sizes of the droplets in a calibrated image were measured by manually counting each of the droplets in the image and a number averaged radius of the droplets was calculated and defined as the radius of the droplets about 700–2000 droplets were counted in each image.

In order to observe the macroscopic liquid-liquid phase separation in bulk solutions, the samples filled in capillaries were prepared and subjected to microscopy examination as well. The capillaries filled with water/methanol mixed solutions of Bu-PNIPAM45K (10 g·L^{-1}, prepared from the same stock solutions as for composition measurements) were flame-sealed at both ends together with certain amount of air inside the capillaries. After macroscopic liquid-liquid phase separation (about 1 day), the capillaries placed on top of a glass slide were examined by microscopy at room temperature (21 ºC).

Phase separation boundary. Given amounts of the methanol stock solution of *n*Bu-PNIPAM (10 $g \cdot L^{-1}$) were placed in glass vials immersed in water bath kept at constant temperature (21 ºC). The proper amounts (tenths or hundreds of microliters) of the aqueous stock solution of *n*Bu-PNIPAM (10 $g \cdot L^{-1}$) were added into the vials with a syringe and weighted. The composition of the solutions was calculated from the weight of the methanol solutions of *n*Bu-PNIPAM and the weight of total *n*Bu-PNIPAM aqueous solutions added. The solutions were stirred for 30 s and rested for ~10 min. The changes in the appearance of the solution in the glass vial were then observed. The time interval between each addition was ~15 min. Experiments showed that a maximum of 5 min was enough for the temperature of the mixed solutions to gain equilibration. Addition of aqueous solutions of *n*Bu-PNIPAM was stopped until the solution become clear again.

Temperature responses of the condensed phase. The methanol/water mixed solutions of *n*Bu-PNIPAM (10 $g \cdot L^{-1}$) with methanol molar fraction 0.100, 0.267, 0.308 and 0.421 were prepared in glass vials and sealed by parafilms. The solutions were placed in an ethylene glycol/water bath. The temperature of the solutions controlled by Julabo F12 Circulator was gradually increased from room temperature until 45 ºC and kept at each temperature for one day. At temperatures above 50 ºC, the solution was placed in a water bath with IKATRON ETS-D4 fuzzy temperature controller.

3.3 Results and discussion

3.3.1 Phase diagram

We observed a MLLPS of PNIPAM in water/methanol mixture at polymer concentration above 10 $g \cdot L^{-1}$. The phase separation accelerated because of the combined effect of methanol addition and concentration increase, since no MLLPS was observed in the same system at polymer concentration of 1 $g \cdot L^{-1}$, as shown in **Figure 3.1**. The properties of end groups were also observed to play a role in the stability of PNIPAM mesoglobules. MLLPS has been observed for both *n*Bu-PNIPAM and PNIPAM-180K, but not for Cl-PNIPAM in methanol and water mixed solutions. Balu et al.[8] suggested that “residual ions” was adsorbed on the surface of the mesoglobules. The strong hydrophilic Cl groups

preferentially located on the surface of mesoglobules in the Cl-PNIPAM solutions and increased their surface tension, leading to repulsive globule-globule interactions.

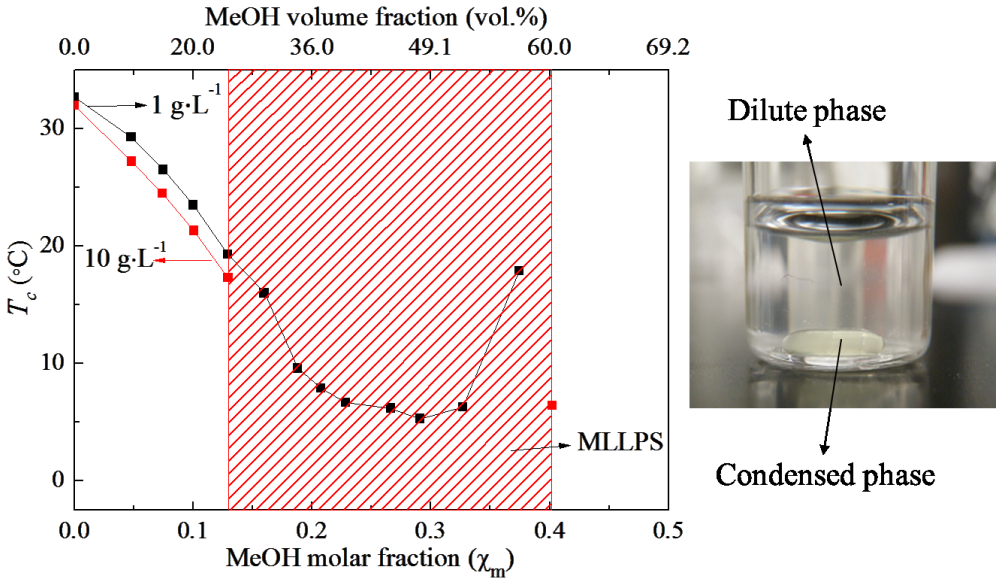

Figure 3.1 Phase diagram of *n*Bu-PNIPAM in methanol/water with polymer concentrations of 1.0 g·L^{-1} and 10 g·L^{-1}. The shaded area indicates the region where MLLPS happened at polymer concentration of 10 g·L^{-1}. The photo on the right shows an example of the MLLPS of *n*Bu-PNIPAM. Two liquid phases (a dilute solution phase and a viscous condensed phase) coexist in the solution after MLLPS.

At 21 °C, the MLLPS of PNIPAM-180K occurred in the region with methanol volume fraction of 57–65% approximately determined by vision observation. (A series of PNIPAM-180K/water/methanol mixtures were prepared with methanol volume fraction close to 50%. The demixing region was determined where MLLPS did not occur below 57% and above 65% methanol volume fraction.) It was much narrower than the MLLPS region for *n*Bu-PNIPAM (methanol volume fraction ranging from 25% to 60%).

The solution compositions of the condensed polymer rich phase and the dilute solution phase after MLLPS of *n*Bu-PNIPAM/methanol/water mixtures were measured by ^{1}H NMR as presented in **Table 3.1**. The number average standard error was about 11%. The polymer volume fraction in the condensed phase was around 0.2. **Figure 3.2** shows an example of the ^{1}H NMR spectra of the condensed phase and the dilute solution phase after MLLPS.

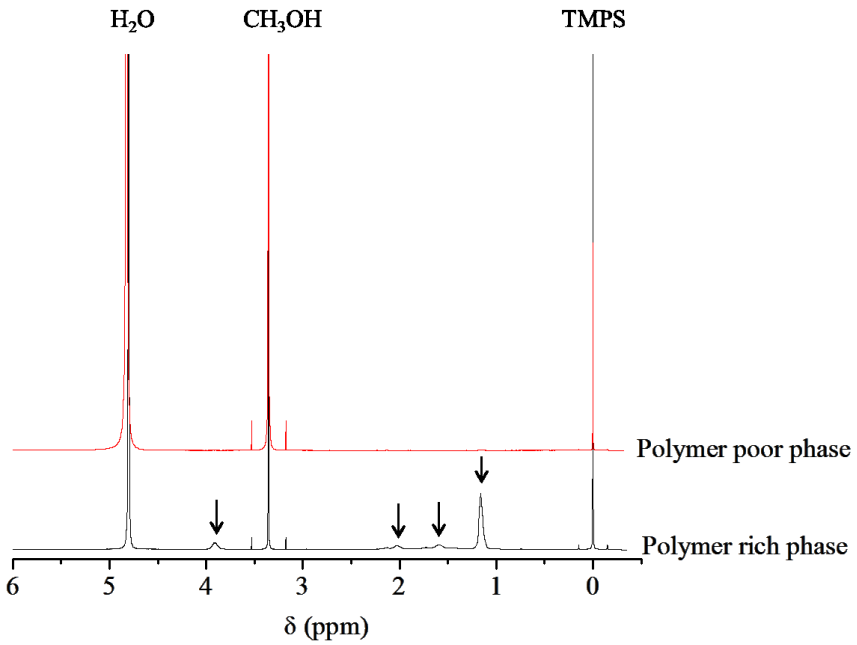

Figure 3.2 ^{1}H NMR spectrum of the polymer poor phase and the polymer rich phase in D_2O of *n*Bu-PNIPAM/water/methanol mixed solution after MLLPS. (Arrows indicate the PNIPAM signals: 1.16 ppm C*H*$_3$, 1.60 ppm -C*H*$_2$CH-, 2.03 ppm –CH$_2$C*H*(CO)-, 3.86ppm –CH-(CH$_3$)$_2$.)

Table 3.1 The methanol volume fractions ϕ in both polymer rich phase and polymer poor phase after MLLPS of *n*Bu-PNIPAM in methanol/water mixtures and the volume fractions of *n*Bu-PNIPAM in the polymer phase ϕ_P.

ϕ (initial solution)	ϕ_P (condensed phase)	ϕ (condensed phase)	ϕ (polymer poor phase)
0.350	0.163	0.202	0.238
0.386	0.227	0.194	0.325
0.452	0.249	0.243	0.389
0.498	0.266	0.244	0.423

The density of the polymer phase was measured and calculated to be 0.814 g·mL^{-1} (± 0.055 g·mL^{-1}) in methanol/water mixtures with methanol molar fraction 0.4. The density of polymer rich phase was necessary to calculate the ϕ_P. We only determined the density of the polymer phase in the mixed solutions with methanol molar fraction 0.4 and assumed it did not

vary much as composition in the MLLPS region studied, since the measurement required a big amount of polymers. The experimental detailed were presented in **Table A3.1**.

Based on the data of the compositions of the condensed phase and dilute solution phase, the phase diagram of *n*Bu-PNIPAM in water/methanol mixtures at 21 °C is shown in **Figure 3.3**. The binodal boundaries for the MLLPS are denoted by the red cycles in **Figure 3.3**. The dash blue line denotes a linear relationship of the phase separation boundary based on cloud point measurements for *n*Bu-PNIPAM in dilute water/methanol mixtures (1.0 $g \cdot L^{-1}$). As shown in **Figure 3.3**, the binodal boundaries does not always fall inside or outside the supposed phase separation region, suggesting a nonlinear relationship between the phase separation boundary and the polymer concentration. The results revealed that the condensed phase was both polymer rich phase and water rich phase. The dilute solution phase was polymer poor phase (polymer molar fraction ~ 0.01) and water poor phase.

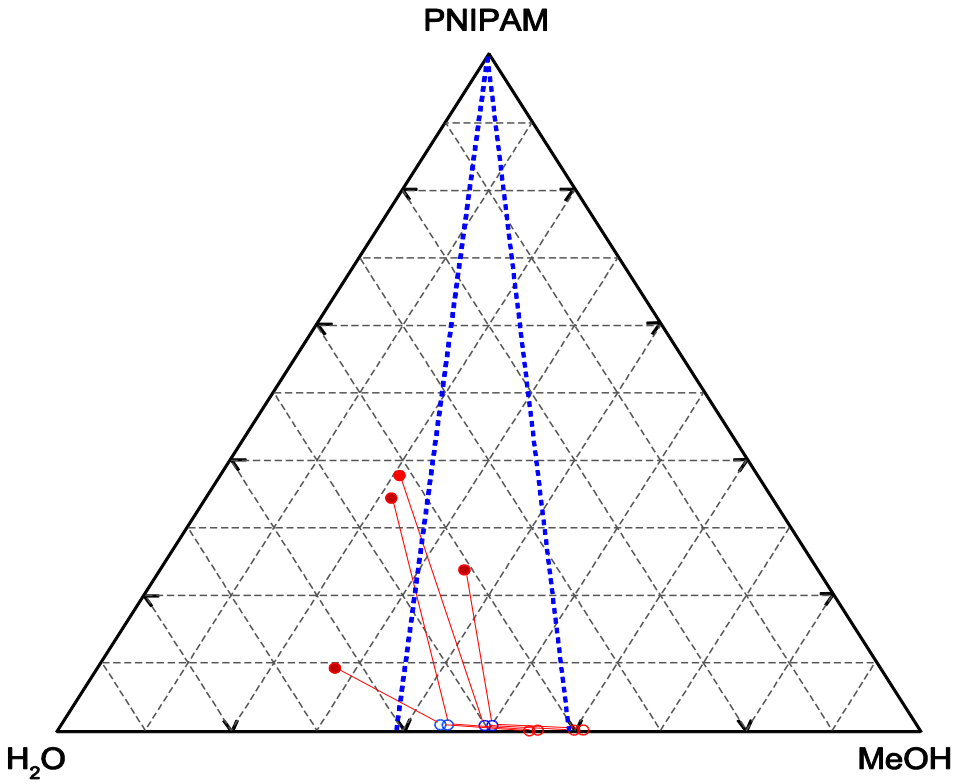

Figure 3.3 Phase diagram of *n*Bu-PNIPAM/water/methanol at 21 °C. The data points, denoted by filled cycles, represent the composition of the binodal boundary data points.

3.3.2 MLLPS at room temperature

In order to investigate the kinetics of the MLLPS, mixtures with various methanol compositions were observed by optical microscopy immediately upon mixing. The methanol/water mixed solutions of *n*Bu-PNIPAM (and PNIPAM-180K) sealed between two glass slides were photographed by optical microscopy as a function of time. **Figure 3.4** shows the phase separation process as a function of time in the *n*Bu-PNIPAM/methanol/water solution with methanol molar fraction of 0.308. Droplets emerged from the mixed solutions within a few minutes after mixing as shown in **Figure 3.4a**. The droplets coalesced with each other and grew in size with time. The size of droplets remained constant after a certain time as indicated in **Figure 3.8**. The coalescence was arrested duo to potential barrier. After 2 days, deformed large droplets were observed for the solution mixture with methanol molar fraction of 0.308. For the solution mixtures with methanol molar fraction 0.127, 0.177 and 0.4, the nearly spherical droplets connected by thin necks were observed after two days with no sing of coalescence, as shown **Figure 3.5**. The stability of the droplets depends on methanol fraction. In the case of mixtures with higher methanol molar fraction of 0.421, isolated spherical droplets were observed. Network of connected small droplets was observed for the *n*Bu-PNIPAM/methanol/water mixture with methanol volume fraction of 0.1.

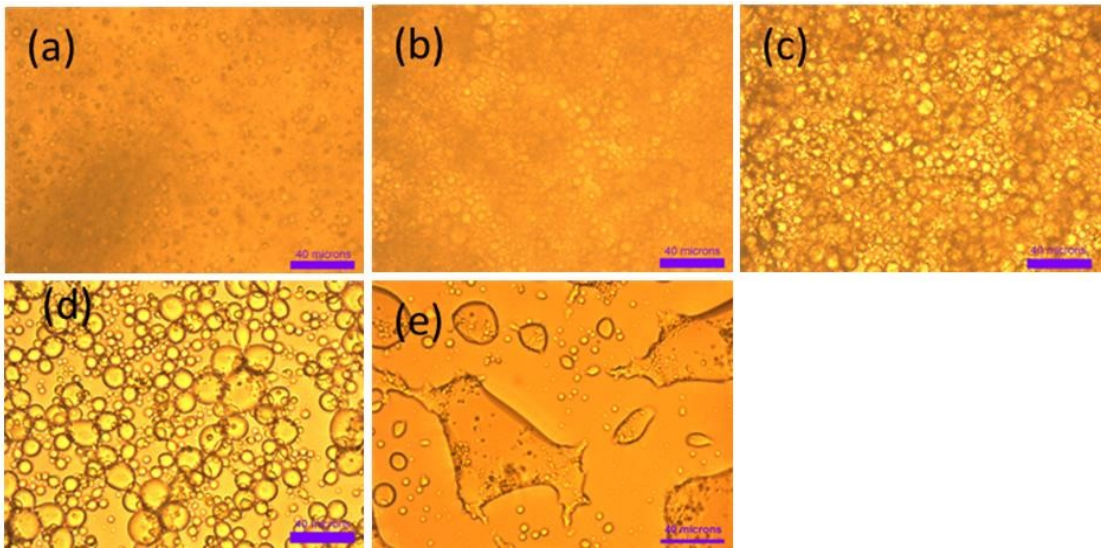

Figure 3.4 Microscopy images of *n*Bu-PNIPAM methanol/water solution with methanol molar composition 0.308 as a function of time: 1 min (a), 18 min (b), 52 min (c), 8 h (d), 2 d (e). (Scale bar: 40 μm).

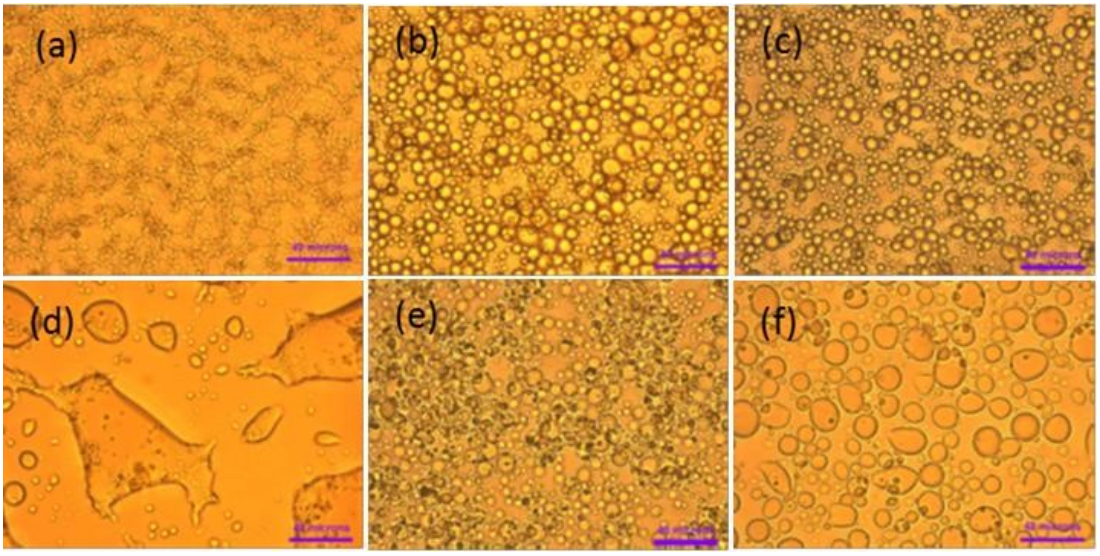

Figure 3.5 Microscopy images of *n*Bu-PNIPAM/MeOH/H_2O solution with MeOH molar fraction 0.100 (a), 0.127 (b), 0.177 (c), 0.308 (d), 0.400 (e), and 0.421 (f) after 2 d. (Scale bar: 40 μm).

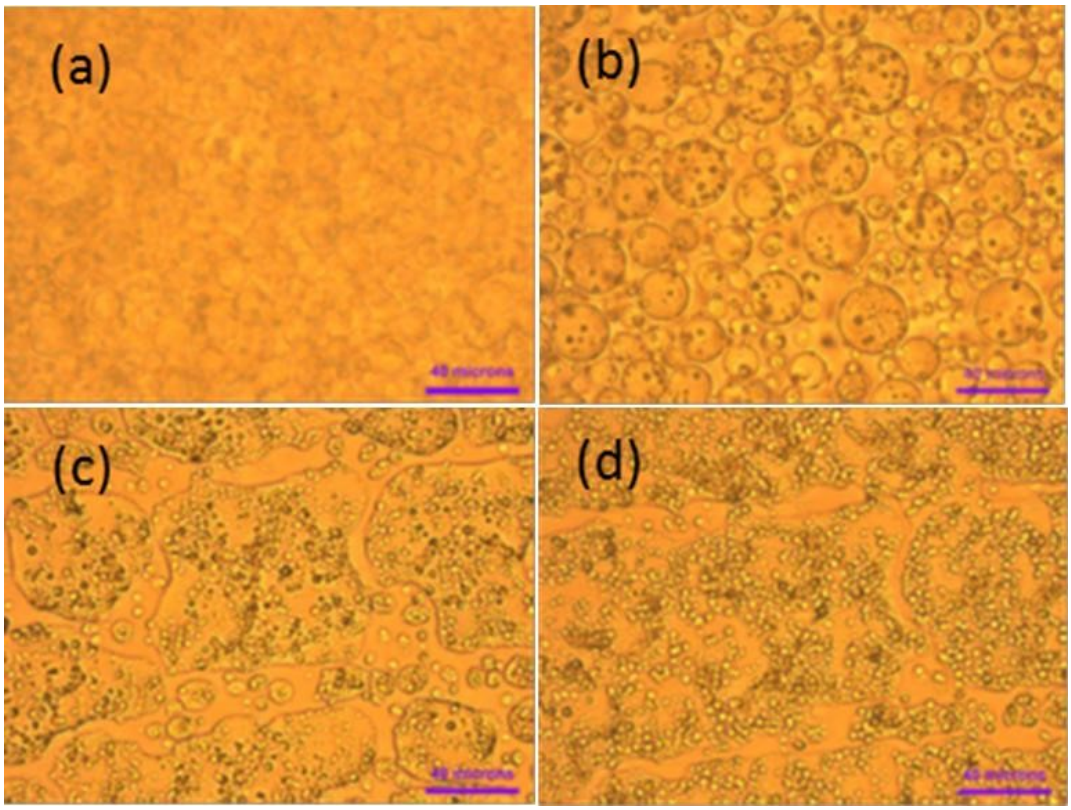

Figure 3.6 Microscopy images of PNIPAM-180K MeOH/H_2O solution with MeOH molar composition 0.453 as a function of time: 7 min (a), 20 min (b), 114 min (c), 2 d (d). (Scale bar: 40 μm)

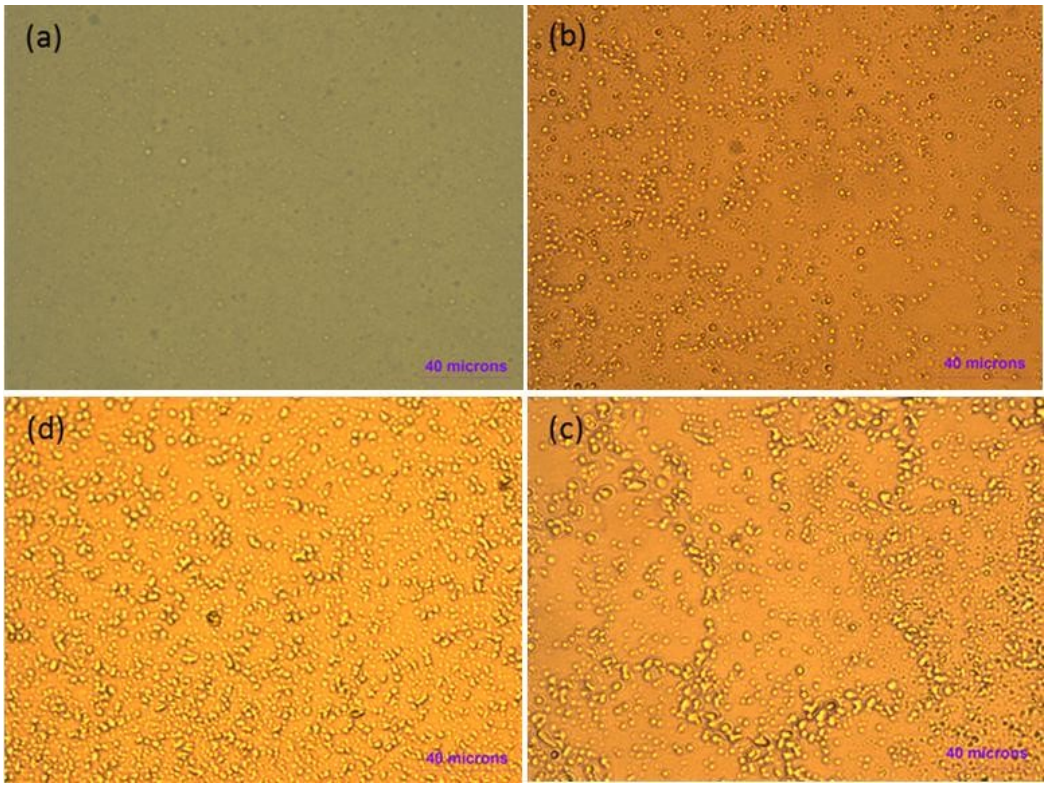

Figure 3.7 Optical images of PNIPAM180K methanol/water solution with methanol molar composition 0.308 (a), 0.371(b), 0.400 (c) and 0.509 (d) after 2 d. (Scale bar: 40 μm)

The situation was somewhat different in the case of PNIPAM-180K. **Figure 3.6** shows an example of PNIPAM-180K in mixed methanol/water with methanol molar fraction of 0.453. The images of the samples with different methanol compositions for PNIPAM-180K in methanol/water mixtures are depicted in **Figure 3.7**. Small droplets emerged immediately from the water/methanol solutions upon mixing, which grew in size by coalescence. Finally a continuous phase was formed coexisting with small droplets. The size of small droplets remained constant with time. The coexistence of metastable aggregates and the macroscopic polymer phase with different radius are predicted by Semenov et al.[9] The coexistence of small droplets and the macroscopic polymer phase was observed for PNIPAM-180K in all the studied solutions with methanol molar fractions of 0.308 to 0.509 as shown in **Figure 3.7**. A slight increase in the size of small droplets was observed with methanol molar fraction increases, indicating a reduced surface tension of the droplets when methanol fraction increased.

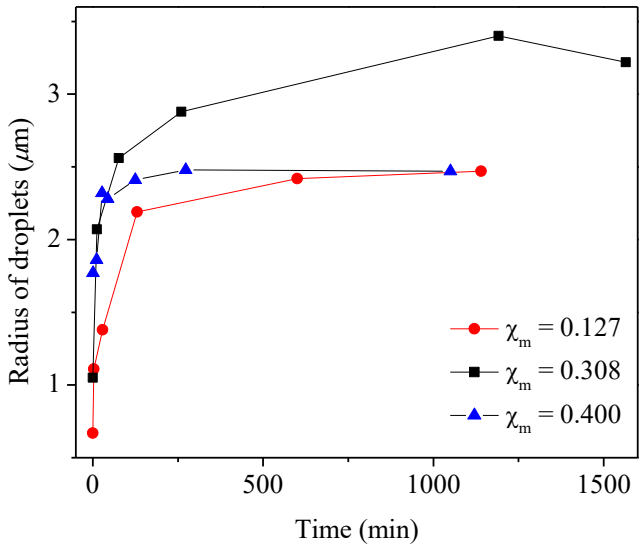

Figure 3.8 Radius of droplets in *n*Bu-PNIPAM methanol/water solutions as a function of time. Methanol molar fraction χ_m = 0.127, 0.308 and 0.400.

In the case of *n*Bu-PNIPAM water/methanol mixtures, both the size of the droplets and the size growing speed depend on the solvent compositions as show in **Figure 3.8**. The faster initial growing speed and final size of droplets for the solution with methanol molar fraction of 0.308 indicated lower surface tension at this composition. For the *n*Bu-PNIPAM/water/methanol system with polymer concentration 1.0 $g \cdot L^{-1}$, the minimum of LCST occurred in the solution with methanol molar fraction around 0.38. These results suggest that the methanol molecules influence the morphologies of the macroscopic polymer dense phase by interacting with the amide groups on the surface of droplets and thus changing the surface tension by altering their orientations.

The shape of droplets of the condensed phase showed methanol composition dependence after equilibration was obtained. In reality, the change would be continuous, thus the optical observations for solutions on the glass slides did not indicate a clear phase separation boundary. Moreover, the confinement of samples seemed to affect the phase transition boundary. When placed on a glass slide, the mixed solutions with the methanol compositions near the boundaries were slightly turbid for the two polymers studied, while the samples with the same composition prepared in a glass vial were transparent. As an example,

*n*Bu-PNIPAM/methanol/water mixture with methanol molar fraction 0.104 (near the boundary) was clear. However, small droplets formed were observed on the glass slide and the solution was little turbid with methanol molar fraction 0.100, as shown **Figure 3.4a**.

To rule out the effect of space confinement, the *n*Bu-PNIPAM water/methanol mixtures inside a capillary was subjected to microscopy measurements, and the images of the samples taken under 10 times of magnification were shown in **Figure 3.9**. In **Figure 3.9a**, small amount of little droplets were observed on the wall of the capillary, while the solution was still macroscopically homogeneous and transparent. For the solution with methanol molar fraction 0.421 shown in **Figure 3.9d** (same composition as in **Figure 3.5f**), similar observations were made. For the sample with methanol molar fraction 0.176 and 0.371, MLLPS were observed in the capillary. **Figure 3.9b** and **c** showed big droplets on the bottom of capillary. In **Figure 3.9b**, tiny droplets were observed diffusing in the dilute polymer poor phase on top of the condensed phase. Fusion and fission of droplets on the surface of the condensed phase were observed only in this solution, indicating a lower energy barrier for fusion in solutions with methanol molar fraction close to 0.176. Images of PNIPAM-180K/methanol/water solutions with the methanol molar fraction 0.371 and 0.453 (boundary of the MLLPS) were shown in **Figure 3.10**. Uniformed condensed polymer rich phases coexisting with small droplets were observed for both samples, which was consistent with the observations on glass slides.

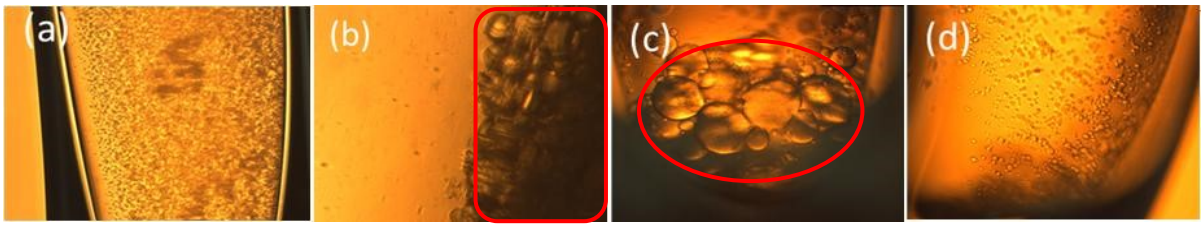

Figure 3.9 Microscopy images under 10 times magnification for *n*Bu-PNIPAM MeOH/H_2O solutions in capillaries incubated at 21 °C for 2 days. (Methanol molar fraction: 0.100 (a), 0.176 (b), 0.371 (c), 0.421 (d).) MLLPS occurred in the samples (b) and (c) where polymer condensed phase (the droplets inside the red square and circle) was clearly observed at the bottom of the capillary respectively.

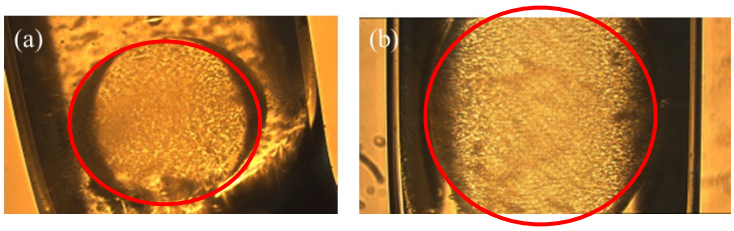

Figure 3.10 Microscopy images under 10 times magnification for PNIPAM-180K MeOH/H_2O solutions in capillaries incubated at 21 °C for 2 days. (Methanol molar fraction: 0.371 (a), 0.453 (b).) MLLPS occurred in the two samples where polymer condensed phase (the ball of polymer-rich droplets inside the red circle) was clearly observed at the bottom of the capillary respectively.

3.3.3 Temperature responses of the condensed phase

Figure 3.11 shows the images of the *n*Bu-PNIPAM/water/methanol mixture with χ_m 0.267 at different temperatures. The same tests were carried out on samples with χ_m 0.308, 0.421 and 0.100, respectively. A transparent homogenous solution was observed at 20.5 °C for the sample with χ_m 0.421, which separated into two liquid phases at 28.9 °C (± 0.5 °C). For the homogenous solution with χ_m 0.100 obtained at 20.5 °C, a cloudy suspension was observed upon increasing temperature, which underwent MLLPS at 24.6 °C. From these results, we can conclude that a narrow cloudy solution region exists between the one phase region and MLLPS region in the phase diagram.

Upon changing the temperature, the equilibrated mixture was disturbed and the transparent dilute phase became cloudy, which became clear again after a certain period of time. Temperature perturbation shifted the equilibrium between the two existing phases. In order to observe the changes happened to the solutions during temperature changes, we examined the *n*Bu-PNIPAM/water/methanol mixtures on a glass slide by microscopy.

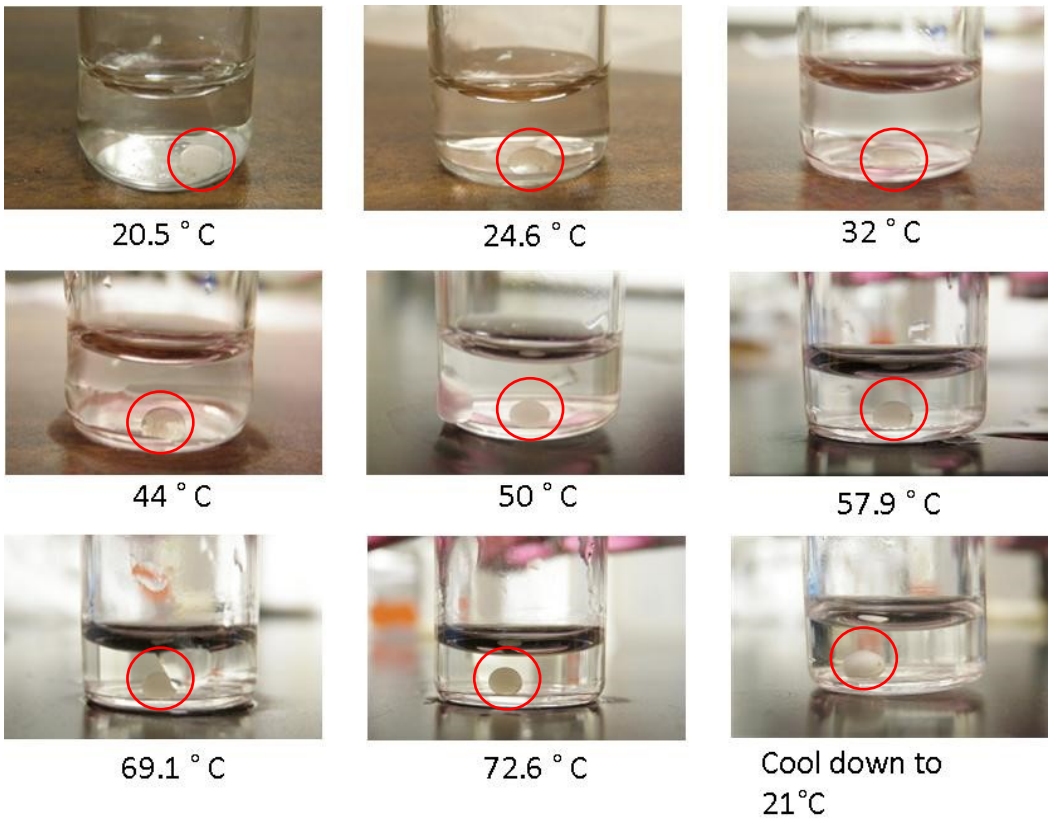

Figure 3.11 Microscopy images of *n*Bu-PNIPAM MeOH/H_2O mixture with MeOH molar fraction 0.267 at different temperatures. The polymer-rich phase in the red cirle changes in shape and transparency as temperature increases.

The temperature dependence of the patterns of the samples as a function of time is shown in **Figure 3.12**. The temperatures were chosen where patterns of the condensed phase changed. All the samples were equilibrated before measurements. New droplets emerged from the solutions for the samples in **Figure 3.12a-b** upon increasing temperature to the desired values. Then the droplets gradually settled down and integrated into the condensed phases at the bottom layer of the glass slides until finally a new equilibrium was obtained. **Figure 3.12c** presents the changes of the pattern for the sample with χ_m 0.421 at 50 °C. The uniform condensed phase observed at room temperature broke down upon heating. A bicontinuous structure appeared and slowly phased out through an Ostwald ripening process until a new uniform phase was obtained. No droplets were observed during the heating process. The temperature dependence of the patterns suggests that the volume of the condensed phase was affected by tempareture.

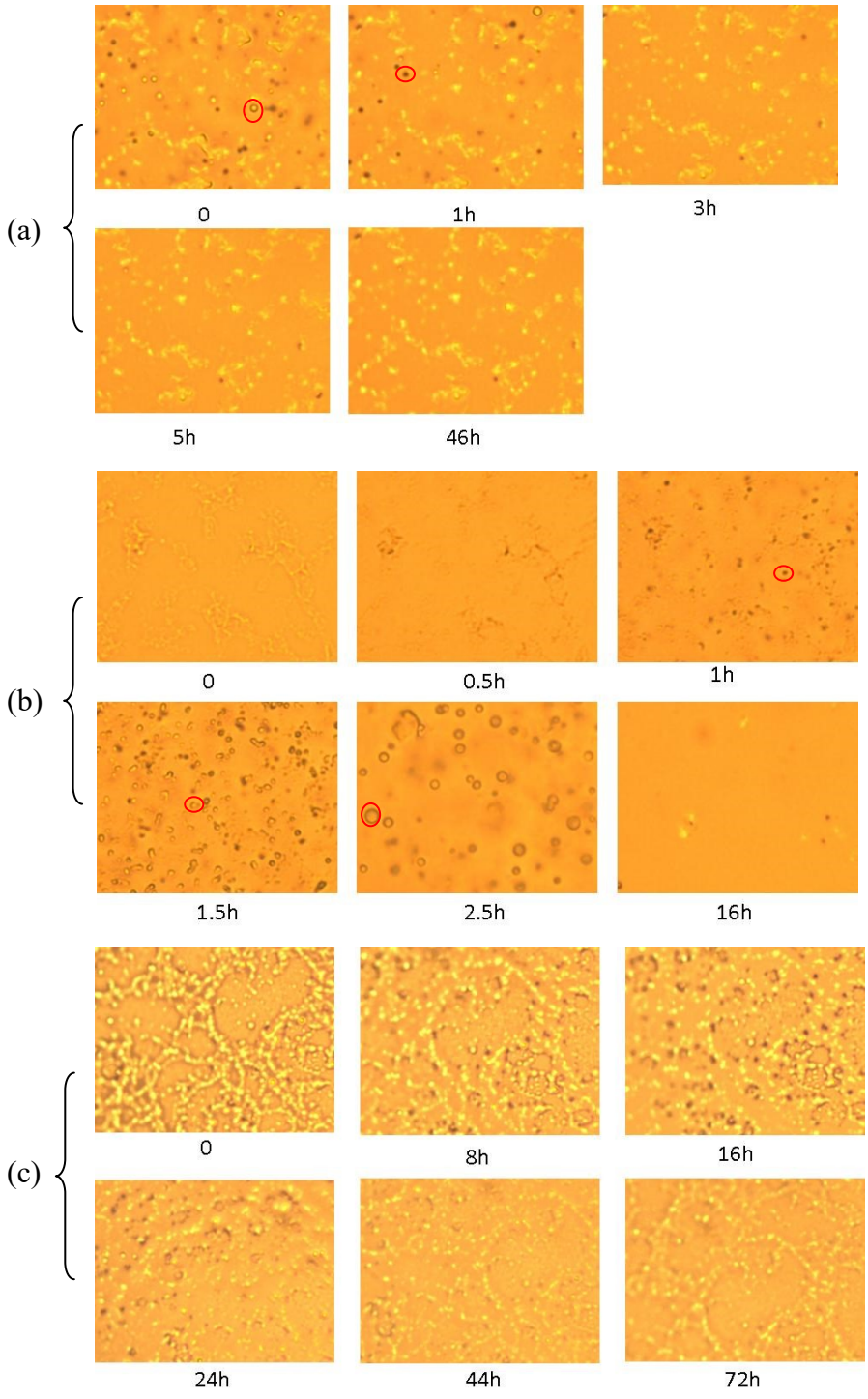

Figure 3.12 Microscopy images of *n*Bu-PNIPAM MeOH/H_2O solution with MeOH molar fraction 0.177 at 43 °C (a), 0.127 at 23 °C (b), and 0.421 at 50 °C (c) as a function of time. New droplets (spots in red circles) emerged from the solutions for the samples (a) and (b) upon increasing the temperature. Then the droplets gradually settled down to form the condensed phases at the bottom layer of the glass slides. In sample (c), the lamellae

structure of the condensed phase observed at room temperature broke down when heated. And a bicontinuous structure appeared which slowly swelled and became lamellae again.

3.4 Conclusions

The macroscopic liquid-liquid phase separation was observed for *n*Bu-PNIPAM in water/methanol mixtures at polymer concentration of 10 $g \cdot L^{-1}$. The phase diagram of the MLLPS for the *n*Bu-PNIPAM in water/methanol was constructed. The condensed phase was a polymer rich phase and water rich phase. The dilute solution phase was a polymer poor phase and methanol rich phase. The condensed phase after MLLPS was examined by optical microscopy. Droplets were observed and showed a dependence on methanol composition in the mixture. As methanol composition increases, the droplets gradually changes from a bicontinuous structure, to connected spheres, to isolated spheres, in the methanol composition range of 0.10 to 0.42. The surface tension of the droplets increases as the methanol volume fraction increases, leading to changes in the size and shape of the droplets. The MLLPS happened also in the PNIPAM-180K methanol/water mixtures too, in a narrow methanol composition region. A condensed polymer rich phase of PNIPAM-180K coexisting with droplets was observed after equilibration. The droplets emerged from the solutions upon mixing coalesced and form a uniformed macroscopic single phase coexisting with some small droplets. The concentration affects the stability of the PNIPAM droplets by increasing the number of effective collision of droplets. Together with effect of methanol on surface tension, the slow equilibrium kinetics of phase separation speed up and a macroscopic liquid-liquid phase separation is realized.

3.5 References

1. Tao, C.-T.; Young, T.-H. *Polymer* **2005,** 46, 10077-84.
2. Bergé, B.; Koningsveld, R.; Berghmans, H. *Macromolecules* **2004,** 37, 8082-90.
3. Cheng, L.-P.; Shaw, H.-Y. *J. Polym. Sci. Part B Polym. Phys.* **2000,** 38, 747-54.
4. Aubry, J.; Ganachaud, F.; Cohen Addad, J.-P.; Cabane, B. *Langmuir* **2009,** 25, 1970-9.
5. Vitale, S. A.; Katz, J. L. *Langmuir* **2003,** 19, 4105-10.
6. Qiu, X.; Koga, T.; Tanaka, F.; Winnik, F. *Sci. China Chem.* **2013,** 56, 56-64.
7. Schild, H. G.; Muthukumar, M.; Tirrell, D. A. *Macromolecules* **1991,** 24, 948-52.
8. Spěváček, J. i.; Hanyková, L.; Labuta, J. *Macromolecules* **2011,** 44, 2149-53.
9. Maresov, E. A.; Semenov, A. N. *Macromolecules* **2008,** 41, 9439-57.

3.6 Appendix

Table A3.1 Densities of the polymer rich phase after MLLPS in *n*Bu-PNIPAM MeOH/H_2O mixtures.

Density of polymer rich phase ($g \cdot mL^{-1}$)	MeOH molar fraction of initial solution	Volume of volumetric flask for measurement (mL)
0.820	0.388	10mL
0.836	0.397	10mL
0.860	0.401	25mL
0.791	0.403	10mL
0.761	0.405	10mL

Chapter 4. Synthesis and solution properties of telechelic poly(2-alkyl-2-oxazoline)s bearing perfluorodecanyl and octadecyl end groups

4.1 Introduction

Telechelic polymers consisting of a water soluble block linked to two hydrophobic end groups are referred to as associative polymers, as these polymers undergo hydrophobic association in water.[1, 2] In dilute aqueous solutions, such polymers tend to form "flower" micelles, whereas at higher concentration, extensive networks are formed by interconnection of flower micelles, yielding macroscopic gels.[3, 4] The rheological properties of associative polymers have found numerous applications in coatings,[5] oil production and transportation,[6] water treatment,[7] as well as thickeners for food, cosmetics and health care products.[8]

Poly(2-alkyl-2-oxazoline)s are a class of polymers with versatile properties.[9] Polyoxazolines with small alkyl groups such as methyl, ethyl, propyl, and isopropyl are water soluble, non-toxic, and biocompatible.[10] These polymers exhibit good protein repellent properties and are attractive for many biomedicinal applications as substitute of poly(ethylene oxide) (PEO).[11] Semitelechelic PIPOZs bearing hydrophilic and hydrophobic end groups have been synthesised by Huber et al.[12] The effect of end group polarity on the cloud point temperature (T_c) was studied. The T_c of the telechelic amphiphilic PIPOZ bearing C_9H_{19}- and C_9H_{19}-NH- at each end was 15 °C lower than that of the unmodified PIPOZ with the same polymerization degree (DP = 25). Telechelic PIPOZ bearing a $C_{18}H_{37}$- and $C_{18}H_{37}$NHCOO- group at each end were synthesized by Obeid et al.[13] The effect of hydrophobic modification on the phase transition of PIPOZ was studied, as well as the association behavior of the telechelic polymer in water. Fik et al.[14] synthesized telechelic poly(2-methyl-2-oxazoline) (PMOZ) end capped with a hydrophobic polymerizable group and a hydrophilic antimicrobial quaternary ammonium group at each end. The polymer was explored as an additive to a commercial dental adhesive and rendered the adhesive contact-active against streptococcus

mutans and helped prolonging longevity of dental composite restoration. So far, no study on the effect of fluorocarbon end modification on the solution properties of PIPOZ has been reported.

Fluorocarbon surfactants exhibit superb properties over their hydrocarbon counterparts because of their chemical and biological inertness, thermal stability, and oleophobicity. Fluorinated surfactants have been widely applied in different fields. They have been used in nonaqueous media of fluorocarbon solvents and supercritical carbon dioxide,[15] synthetic blood, liquid ventilation,[16] imaging agents,[17] and adhesive, antifogging and antistatic agents, cleaners, cosmetics, fire-fighting foams, herbicide formulations, and so forth. There have been many reports in which fluorocarbon segments are introduced onto polymer chains, obtaining a system with combined properties.[18,19] Fluorinated polymerizable hydrogels consisting of a chitosan mainchain and fluorinated side groups have been used for wound dressing that delivers dissolved oxygen or other small oxygenated molecules upon exposure to an environment of lower tension.[18] Fluorocarbon end-capped 2-acrylamido-2-methylpropanesulfonic acid polymers form gels in water that have a strong metal ion binding power and are used as potential inhibitors of HIV-1 replication in cell culture.[19] Among the fluorinated telechelics, telechelic PEOs were the most widely studied, due to their simple structure and the abundant studies of telechelic hydrocarbon end functionalized PEOs, as a foundation. Berret et al.[20] reviewed the studies on fluorinated telechelic polymers. Telechelic PEOs with fluorinated groups at each end have been reported to assemble into flower like micelles in dilute solutions.[21, 22] Most fluorinated telechelic PEOs contain bulky hydrophobic linkers, such as IPDU[23,22] or piperazine[24]. The ^{1}H and ^{19}F NMR studies of telechelic PEO[25] end capped with fluocarbons and HEUR linkers revealed that both hydrophobes and linkers are incorporated into the associating region of the micelles, thus the dual H/F characteristic. To rule out the influence of hydrocarbon on the association of telechelic fluorinated polymers, a short linker is needed.

The N_{agg} of telechelic PEO is one of the essential parameters for understanding the association behaviour of telechelic polymers in water. The reported values of the N_{agg} for telechelic PEOs end-capped with hydrocarbons varied between 10 and 33 depending on the examination method.[26-28] For telechelic fluorinated PEOs, the value was between 30 and 50 in

most studies.[21, 23] The N_{agg} value was found to be independent of the polymer concentration by some researchers.[21, 22] However some studies obtained different results. The N_{agg} of fluorinated PEOs determined by rheology and SANS was found to be dependent on the length of the fluorocarbon end groups and it was sensitive to polymer concentration and temperature.[29] A study of $C_{16}H_{33}$ end-capped PEO also reported a varying N_{agg} when the polymer concentration changed.[30] The N_{agg} was generally smaller for hydrocarbon end capped PEOs than for fluorocarbon end capped PEOs. However as far as we know, no one has compared the difference in the association of telechelic polymers with identical structure and chain length but end-capped with hydrocarbons and fluorocarbons, respectively. To study the effect of end group properties on the solution behavior of telechelics, we synthesized two telechelic PIPOZs with identical PIPOZ section but end-capped with hydrocarbons or fluorocarbons, respectively. The association and phase transition behaviour of the telechelic PIPOZs in water was studied by means of LS, DSC, fluorescence and microscopy.

4.2 Experimental section

4.2.1 Materials

All chemicals were from Sigma-Aldrich Chemicals Co. and used as received unless otherwise stated. 2-isopropyl-2-oxazoline was prepared from isobutyric acid and 2-aminoethanol following a known procedure.[31] Diethylene glycol di(*p*-toluenesulfonate) was synthesized according to a reported procedure and purified by recrystallization from methanol.[32] Acetonitrile was dried by reflux over CaH_2 under dry nitrogen atmosphere and distilled prior to use. Water was deionized with a Millipore Milli-Q system.

4.2.2 Instrumentation

^{1}H NMR spectra were recorded on a Bruker AMX-400 (400 MHz) spectrometer using chloroform-D as the solvent. FT-IR spectra were recorded on Bruker Vector-22 spectrometer. Gel permeation chromatography (GPC) was performed on a GPC-MALLS system consisting of an Agilent 1100 isocratic pump, a set of TSK-gel α-M (particle size 13 μm, exclusion limit 1×10^7 Dalton for polystyrene in DMF) and a TSK-gel α-3000 (particle size 7 μm, exclusion

limit 1×10^5 Dalton for polystyrene in DMF) (Tosoh Biosep) columns, a Dawn EOS multi-angle laser light scattering detector λ = 690 nm (Wyatt Technology Co.) and an Optilab DSP interferometric refractometer λ = 690 nm (Wyatt Technology Co.) under the following conditions: injection volume, 100 μL; flow rate, 0.5 mL·min^{-1}; eluent, DMF; temperature, 40 °C. The refractive index increment of poly(2-isopropyl-2-oxazoline) (PIPOZ, *dn/dc* = 0.084 cm^3·g^{-1}) was used.[26] The weight-average molecular weight M_w and the ratio of the weight- to number- average molecular weights M_w/M_n were determined by a routine procedure.

TEM images were observed on a FEI Tecnai 12 microscope at an accelerating voltage of 80 kV, equipped with a Gatan 1M Pixel digital camera and a field emission gun. The sample of α,ω-di-(1*H*,1*H*,2*H*,2*H*-perfluoro-1-decanyl)- poly(2-isopropyl-2-oxazoline) (FPIPOZ) (0.1 g·L^{-1}) was prepared by dilution from an aqueous solution with polymer concentration 1.0 g·L^{-1}. After equilibration for 1 day, the sample was prepared by placing a drop of the polymer aqueous solution on the copper grid, and stained by phosphotungstic acid (1 wt% in water).

The cac value was determined by fluorescence technique using pyrene as a probe. Steady-state fluorescence spectra were recorded on a Varian Cary Eclipse spectrometer equipped with a GRAMS/32 data analysis system. Slit widths were set at 10 and 1.5 nm for the excitation and emission monochromators, respectively. Pyrene fluorescence spectra were recorded from 345 to 600 nm using an excitation wavelength of 335 nm. Aqueous solutions containing pyrene (Py ~ 8×10^{-7} mol·L^{-1}) and of polymer concentration ranging from 3.0 to 10^{-4} g·L^{-1} were prepared by dilution of a polymer stock solution (3.0 g·L^{-1}) in pyrene. The aqueous solutions were prepared as follows: A solution of pyrene in ethanol (50 μL, 5×10^{-5} mol·L^{-1}) was added to an empty vial. The ethanol was evaporated with a stream of N_2 to form a thin film on the bottom of the vial. Polymer solutions were added to the vial and stirred for 60 hours at room temperature prior to measurement. The emission intensities measured at 373 nm (I_1) and 384 nm (I_3), the first and third vibronic peaks in the fluorescence emission spectrum of pyrene, were used to calculate the ratio I_1/I_3.

The cloud point temperature (T_c) of polymer was determined by turbidity measurement. Samples were prepared by dilution of a stock aqueous solution of 1.0 g·L^{-1}. The optical

transmittance at 550 nm of polymer solutions was recorded by UV-vis spectrophotometer at a heating speed of 0.2 ºC·min^{-1}. T_c is defined as the temperature corresponding to the inflection point in the turbidity curve.

The phase transition enthalpies of polymers were measured by VP-DSC microcalorimeter (MicroCal Inc.) at an external pressure of ca. 180 kPa. The reference cell and sample cell volumes were identical (0.517 mL). The solutions with polymer concentration of 10 g·L^{-1} were prepared one day before measurements. The samples were degassed at 10 °C for 20 mins before injection. The solutions were equilibrated at 10 °C for half an hour before initiation of the heating process. Three heating and cooling cycles were performed on each sample at a heating/cooling rate of 0.5 °C·min^{-1}. For each solution, the excess heat capacity curve was constructed by subtraction of a water vs water scan from the sample vs water scan.

The phase separation of telechelic FPIPOZ and C_{18}PIPOZ aqueous solutions were studied by optical microscopy. Samples of telechelic FPIPOZ and C_{18}PIPOZ solutions (0.5 g·L^{-1}) were prepared. A drop of the solution (10 μL) was deposited on a glass slide which was covered with a small round cover slip and sealed with epoxy glue. The solution spread between the two glass slides and formed a circular area about 3 mm in diameter. The thickness of the solution was ~0.35 mm estimated from the solution volume and the area of the spread solution. Images of the samples were taken by an Axioskop 2 Carl Zeiss Microscope and the Image-Pro-Plus software at variable temperatures. The sizes of the droplets in a calibrated image were measured by manually counting each of the droplets in the image and a number averaged radius of the droplets was calculated and defined as the radius of the droplets.

The size of the micelles and aggregates formed by FPIPOZ and C_{18}PIPOZ was determined by DLS and SLS measurements. The size of micelles formed by direct dissolution of telechelics in water solutions were measured at room temperature. The solutions examined were prepared by dilution of a stock solution (10 g·L^{-1}). They were filtered through 0.2 μm PVDF filter units prior to measurement. In DLS experiments, CONTIN analysis was applied to obtain the diffusion coefficient (D) of the scattering objects in solution. The corresponding hydrodynamic radii, R_H, were obtained via the Stokes-Einstein equation (4.1):

$$D = \frac{k_B T}{6\pi\eta_s R_H} \tag{4.1}$$

where k_B is the Boltzmann constant, η_s is the viscosity of the solvent (water), and T is the absolute temperature.

In SLS experiments, the apparent weight-average molar mass ($M_{w,app}$) and the *z*-average root-mean square radius of gyration (R_g) of scattering objects in dilute solution are evaluated according to the angular dependence of the excess absolute scattering intensity, known as the excess Rayleigh ratio $R_{(q,c)}$ given by equation (4.2):

$$\frac{K(c - c_{cac})}{R(q,c)} \cong \frac{1}{M_w P(q)} + 2A_2(c - c_{cac}) \tag{4.2}$$

where c is the polymer concentration, c_{cac} is the concentration of micellization onset, A_2 is the second virial coefficient, P(q) is the form factor, which reflects the size and shape of the particles. The optical constant $K = 4\pi^2 n^2 (dn/dc)^2 / N\lambda_0^4$, where n is the refractive index of the solvent, dn/dc is the specific refractive index increment, N_A is Avogadro's number, and λ_0 is the wavelength of the incident light in vacuum. The dn/dc of the telechelic PIPOZ in aqueous solutions were measured to be 0.1374 mL·g^{-1}, at 24 °C with the wavelength of 690 nm by GPC equipped with a refractometer.

For solutions below their phase transition temperature, data was analyzed according to the Zimm method, assuming that the macromolecules are in a swollen conformation. In this case, the particle scattering function is $P(q) = 1 - (q^2 R_g^2)/3$, where R_g is the radius of gyration. Since $qR_g << 1$, the following assumption is fulfilled $1/[1 - (q^2 R_g^2)/3] = 1 + (q^2 R_g^2)/3$. Thus, eq. (4.2) becomes

$$\frac{K(c - c_{cac})}{R(q,c)} \cong \frac{1}{M_w}\left(1 + \frac{R_g^{\,2}}{3} q^2\right) + 2A_2(c - c_{cac}) \tag{4.3}$$

The apparent molecular weight of a polymer (M_w) in a solution of concentration c is obtained by extrapolation of the scattered intensity $R(q,c)/(c - c_{cac})$ to $q = 0$, where $q = (4\pi n/\lambda_0)\sin(\theta/2)$ and θ is the scattering angle (30°–150°). The radius of gyration R_g of the scattering objects is obtained by a mean-square linear fit of the inverse of the scattered intensity versus q^2.

For solutions heated above 40 ºC, data was analyzed according to the Guinier method, assuming a hard sphere conformation of the particles. $qR_g \cong 1$, the radius of gyration can be approximated from the particle scattering function $P(q) = \exp[-(q^2R_g^2)/3]$. Thus, equation (4.2) becomes

$$\frac{K(c-c_{cac})}{R(q,c)} \cong \frac{1}{M_w \exp(-\frac{R_g^{\ 2}}{3}q^2)} + 2A_2(c-c_{cac}) \tag{4.4}$$

4.2.3 Synthesis

Synthesis of 1H,1H,2H,2H-perfluoro-1-decanyl propargyl ether. 1*H*,1*H*,2*H*,2*H*-perfluoro-1-decanol (4.6 g, 10 mmol) and propargyl bromide (1.8 g, 15 mmol) were dissolved in 10 mL of dry DMSO. To this solution, potassium hydroxide (KOH) (1.7 g, 30 mmol) was added. The mixture was stirred for 24 h at room temperature under nitrogen atmosphere. After that, DI water (30 mL) was added. The solution was extracted with diethyl ether twice. The organic extracts were mixed and washed by DI water three times and further passed through a short neutral alumina column. The product was obtained by evaporating the solvent. Yield 3.3 g, 66%. ^{1}H NMR ($CDCl_3$, δ) ppm: 2.45 (t, -C*H*$_2$CF$_2$-), 2.50 (s, *H*C≡CCH$_2$O-), 3.85 (t, -OC*H*$_2$CH$_2$CF$_2$-), and 4.20 (s, HC≡CC*H*$_2$O-).

Synthesis of n-octadecyl propargyl ether. *n*-octadecyl propargyl ether was prepared from 1-octadecanol using the same method as above. Yield 1.2 g, 23%. ^{1}H NMR ($CDCl_3$, δ) ppm: 0.82 (t, C*H*$_3$CH$_2$-), 1.19 (m, CH$_3$-(C*H*$_2$)$_{15}$CH$_2$-), 1.55 (m, CH$_3$-(CH$_2$)$_{15}$C*H*$_2$-), 2.35 (s, *H*C≡CCH$_2$O-), 3.45 (t, -OC*H*$_2$(CH$_2$)$_{16}$CH$_3$), and 4.07 (s, HC≡CC*H*$_2$O-).

Synthesis of N$_3$PIPOZ. α,ω-diazido poly(2-isopropyl-2-oxazoline) (N$_3$PIPOZ) was prepared according to the general procedure using diethylene glycol di(*p*-toluenesulfonate) as the initiator. In the example of N$_3$PIPOZ, typically, a round-bottom flask equipped with a N_2 filled condenser and a rubber stopper was charged with 2-isopropyl-2-oxazoline (5 mL, 44 mmol), acetonitrile (20 mL), and diethylene glycol di(*p*-toluenesulfonate) (248 mg, 0.6 mmol) via oxygen-free syringe at room temperature. After mixing, the flask was immersed in a pre-heated oil bath and the solution was stirred at 65 °C for 72 h. In order to monitor the kinetics

of the polymerization during the polymerization process, small amounts of solution were withdrawn from the polymerization solution at certain times for NMR measurement. The conversion of the monomer was calculated by comparing the resonances of methylene groups at 4.22 and 3.80 ppm of the monomer with the resonances at 3.40 ppm of the polymer backbone methylene groups. At the end of the polymerization, the polymerization solution was cooled to room temperature and sodium azide (0.40 g, 6.0 mmol) was added to quench the oxazolinium ions. The termination reaction was conducted at 65 °C for 8 h. After that, the solution was diluted with DI water to 100 mL and dialyzed against DI water for 3 days with a membrane MWCO of 3500 Dalton. The purified polymer was recovered by freeze-drying. Yield 4.0 g, 80%. ^{1}H NMR ($CDCl_3$, δ) ppm: 1.1 (br, $(CH_3)_2CH$-), 2.66 and 2.89 (br, $(CH_3)_2CH$-), 3.45 (br, -NCH_2CH_2-). FT-IR, 2976, 2934, 2873, 2105, 1646, 1474, 1431, 1205, 1160, 1089, and 755 cm^{-1}.

Synthesis of FPIPOZ and C_{18}PIPOZ. The copper(I)-catalyzed Huisgens 1,3-dipolar alkyne-azido cycloaddition was used for the end capping reaction of N_3PIPOZ with 1*H*,1*H*,2*H*,2*H*-perfluoro-1-decanyl propargyl ether in DMF.[33] 1-octadecanol was used for end capping reaction of N_3PIPOZ in the case of C_{18}PIPOZ. In the example of FPIPOZ, N_3PIPOZ (0.8 g, 0.2 mmol of N_3) and 1*H*,1*H*,2*H*,2*H*-perfluoro-1-decanyl propargyl ether (0.15 g, 0.3 mmol) were dissolved in 10 mL of DMF. To this solution, copper (I) bromide (15 mg, 0.1 mmol) and *N,N,N′,N″,N″*-pentamethyl diethylene triamine (PMDEMA, 21 μL, 0.1 mmol) were added. The mixture was stirred under N_2 for 12 h. After that, the solution was diluted with THF, and passed through a neutral alumina column to remove the copper catalyst. The eluent was further dialyzed against methanol for 1 day and against DI water for 2 days using a membrane with MWCO of 3500 Da. The polymer was recovered by freeze-drying. Yield 0.8 g, 90%. ^{1}H NMR ($CDCl_3$, δ) ppm: 1.1 (br, $(CH_3)_2CH$-), 2.66 and 2.89 (br, $(CH_3)_2CH$-), 3.45 (br, -NCH_2CH_2-), 3.85 (br, -OCH_2CH_2-), 4.66 (br, -OCH_2triazole). FT-IR, 2976, 2934, 2873, 1646, 1474, 1431, 1205, 1160, 1089, and 755 cm^{-1}.

4.3 Results and discussion

4.3.1 Synthesis of N_3PIPOZ

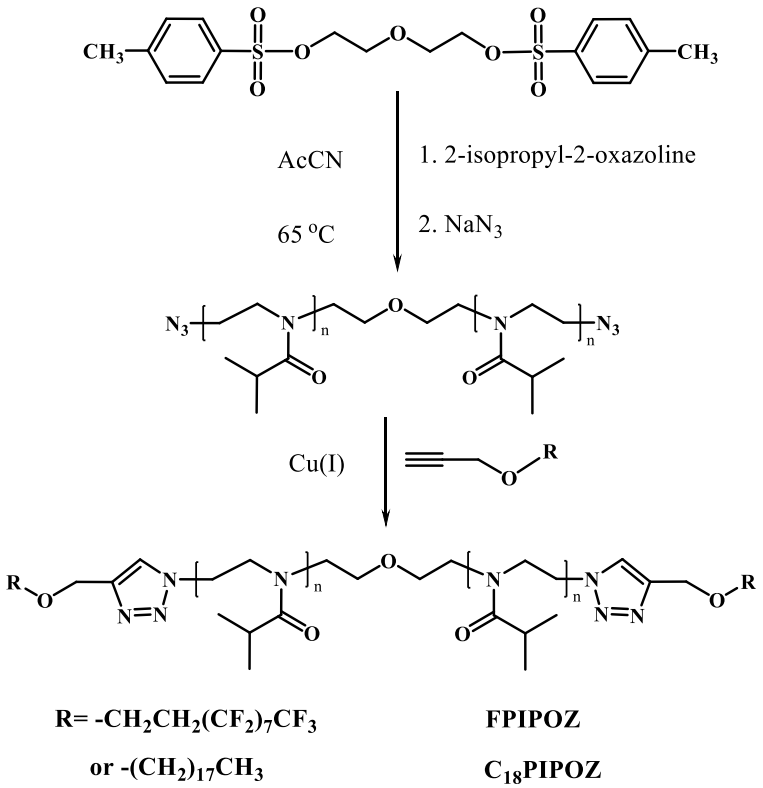

Scheme 4.1 Synthetic procedure of α, ω-diperfluorodecanyl poly(2-isopropyl-2-oxazoline) and α, ω-dioctadecanyl poly(2-isopropyl-2-oxazoline).

Scheme 4.1 depicts the synthesis procedure of the telechelic PIPOZ initiated by diethylene glycol di(*p*-toluenesulfonate). Using this bifunctional initiator, the polymerization was initiated from the two *p*-toluenesulfonate groups of the initiator, leading to a chain with propagating species at both ends.[34] Termination of the propagating oxazolinium ions by NaN_3 yielded α,ω-diazido-telechelic PIPOZ. Furthermore, 'click' reaction between the polymer azido termini with 1*H*,1*H*,2*H*,2*H*-perfluoro-1-decanyl propargyl ether generated the targeted α,ω-di-(1*H*,1*H*,2*H*,2*H*-perfluoro-1-decanyl)-PIPOZ (FPIPOZ). Accordingly, α,ω-di-(1-octadecanyl)-PIPOZ (C_{18}PIPOZ) was prepared with the same procedure. The kinetics of the polymerization was monitored by ^{1}H NMR and shown in **Figure A4.1**. For a typical living polymerization, the monomer conversion in terms of $\ln([M_0]/[M_t])$ increases linearly as a

function of polymerization time. The slightly upward curvature of the two curves indicates a relatively slow initiation process as compared to chain propagation.[35] The progressively increasing slope of the curve implies that polymerization rate is increasing with time owing to more initiators participating in the polymerization. In the late stage of the two polymerizations (last three points), a nearly linear relationship is observed, implying that the concentration of propagating species remained constant and termination reactions were absent in the system. The apparent polymerization rate of the polymerizations can be evaluated from the relationship of $\ln([M_0]/[M_t])$ versus time according to equation (4.5):

$$\frac{\ln([M_0])}{[M_t]} = K_{app} \times 2[I_0] \times t \tag{4.5}$$

The number 2 in front of $[I_0]$ is added because each bifunctional initiator generates two propagating species. As listed in **Table 4.1**, the k_{app} for IPOZ polymerizations in acetonitrile at 65 °C was calculated to be 2.6×10^{-4} $L \cdot mol^{-1} \cdot s^{-1}$. It should be mentioned that the polymerization degree (DP) of the polymer (**Table 4.1**) was in good agreement with the initial feeding ratio of monomer/initiator at the indicated conversion. This result supports our assumption that all the initiators were consumed in the late stage of the polymerization.

Table 4.1 Polymerization and molecular weight characterizations of N_3PIPOZ

Polymer	$[M_0]/[I_0]$	$[I_0]$ (M)	Time (hour)	Yield (%)	M_n (kDa)	DP	M_w/M_n	k_{app} $L \cdot mol^{-1} \cdot s^{-1}$
N_3PIPOZ	75	0.024	72	88	7.6	68	1.12	2.6

Because of the relatively slow initiation of the bifunctional initiator, it is anticipated that the dispersity of the telechelic polymers should be larger than the polyoxazolines obtained by standard living polymerizations. As expected, the dispersity (M_w/M_n) of N_3PIPOZ is measured to be 1.12, which are slightly larger than 1.10, the critical value for living polymerizations (**Table 4.1**). Such a phenomenon is usually encountered for less reactive alkyl (*p*-toluenesulfonate) initiated CROPs.[36] The M_w/M_n of these polymers is normally in the range of 1.10 to 1.30, depending on the activity of the initiator. Note that since termination is absent in the polymerization system, the end functionality of the polymers will not be affected

by the relatively slow initiation process. The successful azide termination is confirmed by FT-IR spectra with the moderate strong -N_3 vibration at 2105 cm^{-1} for N_3PIPOZ (**Figure 4.1**).

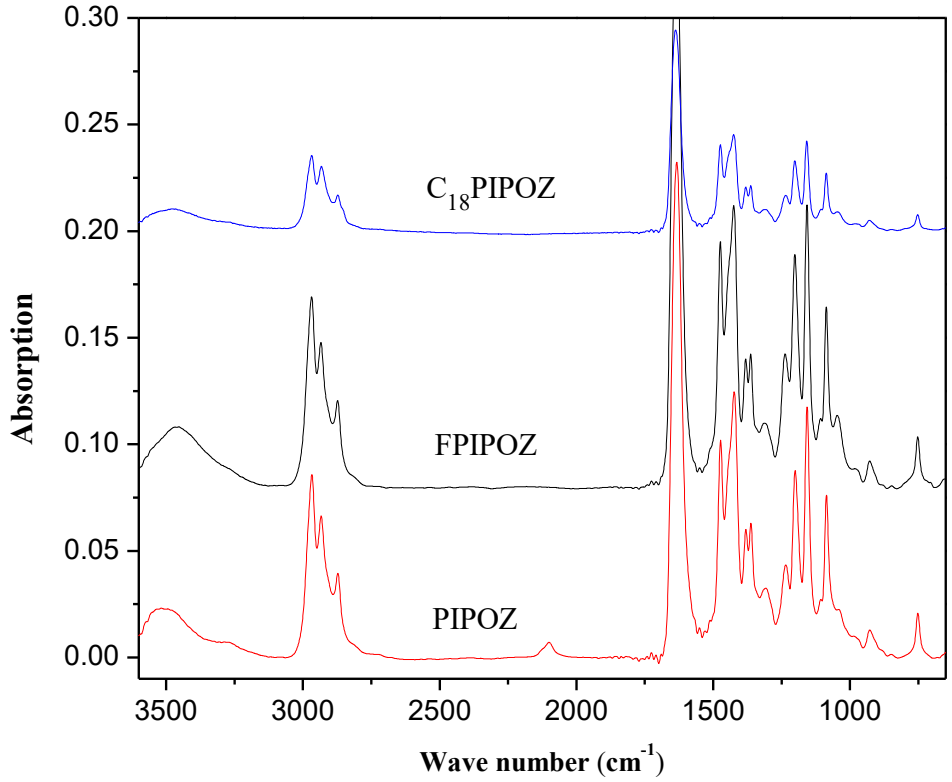

Figure 4.1 FT-IR spectra of telechelic FPIPOZ, C_{18}PIPOZ and N_3PIPOZ.

4.3.2 Synthesis of FPIPOZ and C_{18}PIPOZ

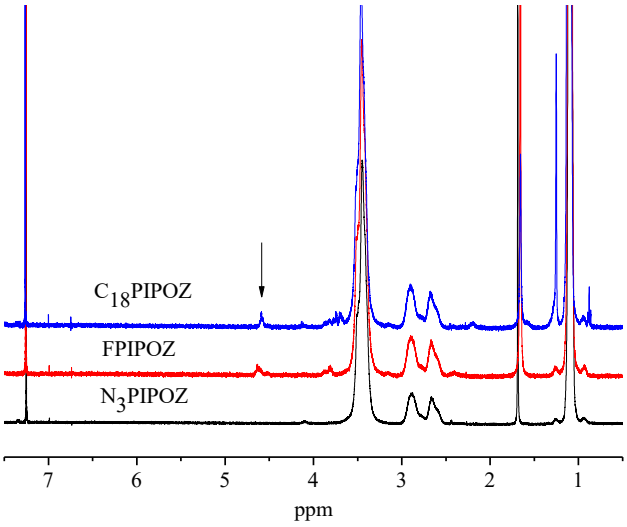

Figure 4.2 ^{1}H NMR spectra of N_3PIPOZ (lower panel), telechelic FPIPOZ (middle panel) and telechelic C_{18}PIPOZ (upper panel) in $CDCl_3$. The arrow indicate the signals (originating from the methylene groups of the 1*H*,1*H*,2*H*,2*H*-perfluoro-1-decanyl end groups and the methylene protons next to the triazole rings) used to calculate M_n.

The 'click' reaction between the terminal azido groups of the telechelic polyoxazolines and 1*H*,1*H*,2*H*,2*H*-perfluoro-1-decanol propargyl ether was performed in DMF at room temperature using Cu(I) as catalyst. The characterizations of the telechelic polymers and precursor polymer are presented in **Table 4.2**. The completion of this reaction was ascertained from the disappearance of the band at 2105 cm^{-1} due to the azide stretching in the FT-IR spectra of FPIPOZ as shown in **Figure 4.1**. In the ^{1}H NMR spectra (**Figure 4.2**), the 'click' reaction brought about two new resonances at 4.66 and 3.85 ppm originating from the methylene groups of the 1*H*,1*H*,2*H*,2*H*-perfluoro-1-decanyl end groups. The aromatic triazole ring undergo a downfield shift of the adjacent methylene protons resonance, originally at 4.21 ppm (-OCH_2C≡CH), to 4.66 ppm (-OCH_2-triazole). The ratio of the integrated values of the 4.66 ppm methylene resonance with respect to backbone methylene groups of PIPOZ yielded a similar polymerization degree of the two polymers measured by GPC-MALLS. This result implies that the two polymers have nearly quantitative hydrophobic end functionality. In addition, the near overlap of the GPC traces of PIPOZ before and after end capping reaction

also indicates that the 'click' ligation of the end groups did not affect the molecular weight and the dispersity of the precursors (**Figure A4.2**).

Table 4.2 Characterization of N_3PIPOZ, FPIPOZ and C_{18}PIPOZ

Polymer	M_n[a] (kDa)	M_w[a] (kDa)	$Đ$	M_n[b] (kDa)
N_3PIPOZ	7.6	8.5	1.12	
FPIPOZ	7.7	8.8	1.13	7.9
C_{18}PIPOZ	8.7	9.6	1.10	9.4

[a.] Determined by GPC.

[b.] Determined by NMR.

4.3.3 Association of FPIPOZ and C_{18}PIPOZ in water at room temperature.

cac of micelles formed by telechelic FPIPOZ and C_{18}PIPOZ

The two telechelic polymers are readily soluble in water at room temperature and clear solutions were obtained in the concentration ranging from 1.0 to 10.0 $g \cdot L^{-1}$. The critical aggregation concentration (cac) values of FPIPOZ and C_{18}PIPOZ are determined by fluorescence spectroscopy using pyrene as a probe. Pyrene is poorly soluble in water, and is preferentially solubilized within the hydrophobic microdomains of micelle solutions. The ratio I_1/I_3 of the intensities of the first and third bands of the pyrene emission decreases when pyrene goes from a polar to a nonpolar media. The onset concentration for which the I_1/I_3 value decreases gives an estimate of the cac. The plots of the changes in the ratio I_1/I_3 as a function of polymer concentration are presented in **Figure 4.3a** for C_{18}PIPOZ and FPIPOZ. The change of the ratio I_1/I_3 indicates three stages as indicated by the arrows in **Figure 4.3a**. For C_{18}PIPOZ, the ratio remains constant for solutions with polymer concentration below 0.006 $g \cdot L^{-1}$ in the first stage and decreases gradually with increasing polymer concentration. We took the polymer concentration corresponding to the onset (0.006 $g \cdot L^{-1}$) of the drop of I_1/I_3 as the cac of C_{18}PIPOZ, for which hydrophobic domains form by assembly of the end groups capable of hosting pyrene molecules. A previous research on telechelic PIPOZ end capped with octadecyl end groups with molecular weight of 7, 10, 13 $kg \cdot mol^{-1}$ revealed that the cac of these polymers was less than 0.1 $g \cdot L^{-1}$.[37] Despite the slight difference in polymer structure, the cac of the telechelic C_{18}PIPOZ in our study was the same as in the reference with similar

molecular weight measured by monitoring the I_1/I_3 ratio of pyrene. In the second stage, the ratio I_1/I_3 decreases gradually upon increasing C_{18}PIPOZ concentration until it reaches a plateau at 0.44 $g \cdot L^{-1}$ (C_m). Increasing polymer concentration above the cac, more octadecyl end groups participate in the hydrophobic microdomains, and micelles form progressively. The pyrene molecules sense the change in environmental polarity when they go from the hydrophobic microdomains to the core of micelles. The micellization process is also manifested by a decrease of emission intensity of pyrene and a shift of I_3 position (from 384 to 382.5 nm) when the polymer concentration decreases from 3.0 to 0.001 $g \cdot L^{-1}$ as shown in **Figure A4.3** for both telechelic polymers. For FPIPOZ solutions, the ratio I_1/I_3 decreased slightly from 1.93 to 1.67 over the entire concentration range (0.001–3.0 $g \cdot L^{-1}$). The reported value of the I_1/I_3 ratio of pyrene in the range of 1.5 to 1.7[38-40] in fluorocarbon surfactant solutions is consistent with our observation in FPIPOZ solution. The higher I_1/I_3 ratio of pyrene in fluorinated surfactant solutions compared with that in their hydrocarbon analogues is usually caused by (1) higher water penetration in micelles because of the bulkiness and rigidity of fluorocarbon chains; (2) the immiscibility between the hydrocarbons and fluorocarbons which results in less preferential partition of pyrene molecules into fluorocarbon micelles; (3) solubilized pyrene is located in the palisade layer (the region between the surface of the micelle and the micelle core) of the fluorinated core of micelles.[24] It is difficult to determine the cac of FPIPOZ by the minor change of the I_1/I_3 ratio of pyrene.

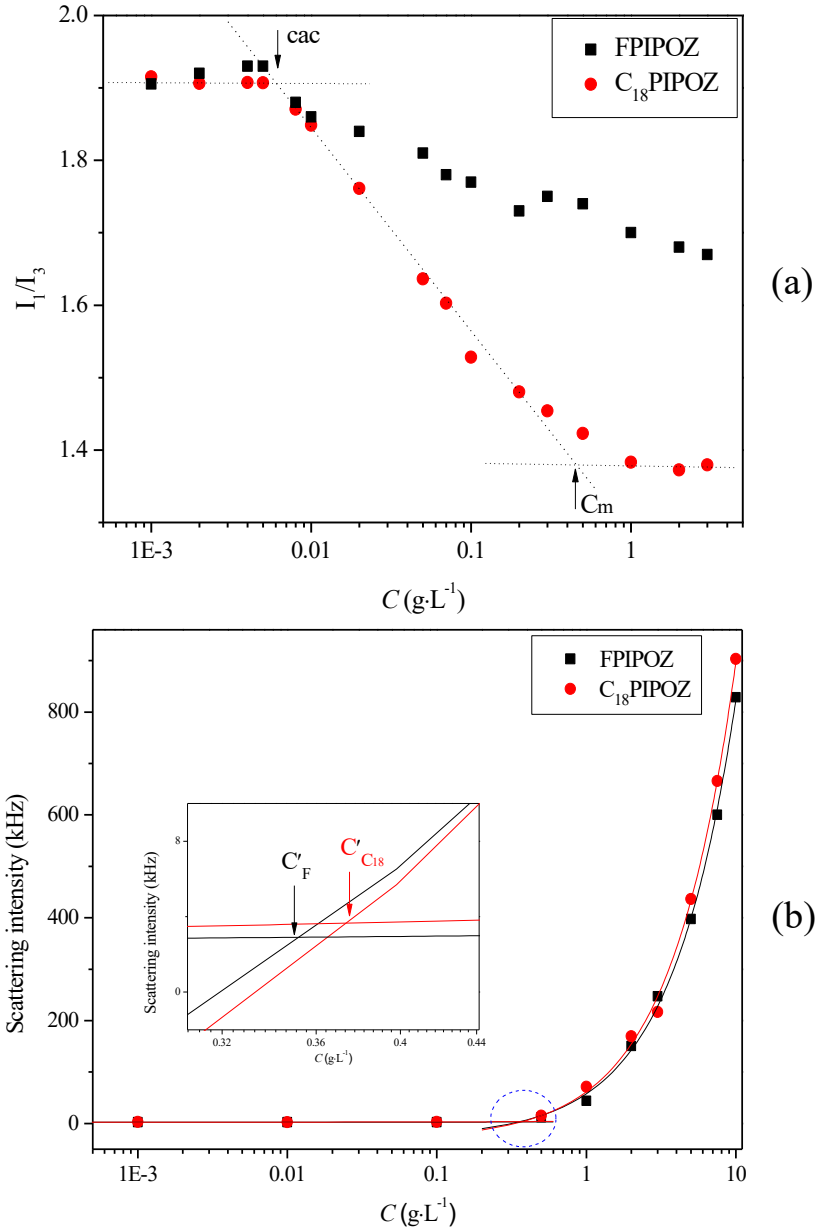

Figure 4.3 Changes in the ratio I_1/I_3 of the intensity of the first and third vibronic bands of pyrene (10^{-6} mol·L^{-1}) (a) and changes in the scattering intensity of assemblies (b) as a function of polymer concentration for solutions of C_{18}PIPOZ and FPIPOZ at 24 °C. The arrows indicate the critical concentrations in the micellization. The inset in (b) is an enlargement of the circled area.

Since the cac of FPIPOZ cannot be determined by pyrene fluorescence, we studied the micellization of the telechelic C_{18}PIPOZ and FPIPOZ in aqueous solutions by recording their light scattering intensity of their solutions as a function of concentration (**Figure 4.3b**). The scattering intensity remained constant with increasing polymer concentration up to a point C′,

beyond which it increased gradually. The increase in scattering intensity indicated the emergence of large assembles around C′. The C′ determined by the cross point of two extrapolated lines was 0.35 $g \cdot L^{-1}$ (C'_F) and 0.40 $g \cdot L^{-1}$ (C'_{C18}) for FPIPOZ and C_{18}PIPOZ, respectively. The C'_{C18} was close to C_m, implying that the C′ corresponds to the upper limit of the micellization process. In solutions where polymer concentration was above the corresponding C′, the telechelic polymers associate into micelles. Thus, in the aforementioned concentration range, FPIPOZ and C_{18}PIPOZ were expected to form flower-like micelles in water. Different cac values determined by fluorescence and light scattering techniques have been reported. Dai et al[30] reported a cac value of 0.2 $g \cdot L^{-1}$ for telechelic PEO end-capped with $C_{16}H_{33}$ groups based on the dependence of the scattering intensity on the polymer concentration. While Nicolai et al.[41] determined the cac for the telechelic PEO end-capped with $C_{16}H_{33}$ groups to be 0.05 $g \cdot L^{-1}$ by monitoring the ration I_1/I_3 of pyrene. The cac values of telechelic polymers measured by light scattering were usually larger than those obtained by fluorescence technique.

Size of micelles formed by telechelic FPIPOZ and C_{18}PIPOZ.

The sizes and shapes of the assemblies of the telechelic polymers obtained by the direct dissolution method were examined by light scattering. **Figure 4.4** represents the size distribution of FPIPOZ and C_{18}PIPOZ aqueous solutions in the concentration range from 1.0 to 10.0 $g \cdot L^{-1}$ at 20 °C measured by DLS. A uniform size distribution is observed for all solutions of FPIPOZ and C_{18}PIPOZ in the studied concentration range. The R_H value of C_{18}PIPOZ micelles is slightly larger (~ 1 nm) than that of FPIPOZ micelles, at the same concentration, as shown in **Table 4.3**. A study of the effect of the end group length on the association of telechelic PEOs end-capped with $C_{12}H_{25}$ and $C_{18}H_{37}$ groups, respectively, revealed a larger R_H of micelles formed by $C_{18}H_{37}$ end-capped PEO (6.1 nm) compared to $C_{12}H_{25}$ end-capped analogues (5.1 nm).[42] Considering the length of the end groups in this work, $C_2H_4C_8F_{17}$- and $C_{18}H_{37}$-, it is reasonable that the FPIPOZ micelles are slightly smaller than the C_{18}PIPOZ micelles. A study by Kim et al.[42] revealed that telechelic PEO end-capped with C_8H_{17} (polymerization degree 90) did not associate into micelles due to insufficient chain flexibility. The formation of micelles by the telechelic FPIPOZ with an even smaller degree

of polymerization (68), suggested stronger association ability for the fluorocarbon compared to the hydrocarbon analogue.

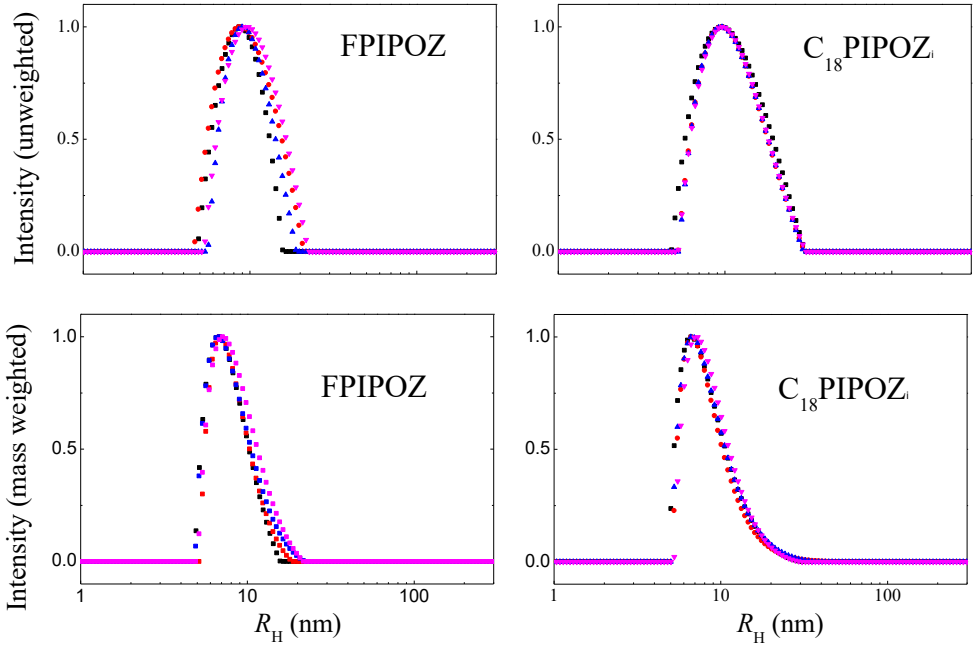

Figure 4.4 The R_H distribution of FPIPOZ and C_{18}PIPOZ micelles in aqueous solutions by dynamic light scattering at a scattering angle of 90° with polymer concentration 2.5 to 10.0 g·L^{-1} at 20 °C.

More information concerning the flower-like micelles was obtained by SLS measurements.[36] **Table 4.3** present the characters of associated micelles, the apparent weight-average molar mass $M_{w,app}$ of the micelles, the radius of gyration R_g, R_g/R_H and the aggregation number, N_{agg}, in terms of number of polymer chains per micelles for FPIPOZ and C_{18}PIPOZ flower-like micelles at different concentrations. The flower micelles consisted of approximately 10–35 chains and 9–38 chains for FPIPOZ and C_{18}PIPOZ, respectively, in the concentration range 0.5–10.0 g·L^{-1}. The N_{agg} of FPIPOZ was close to the reported value (17) of telechelic PEO (M_n = 10 kDa) end-capped with the same end group ($C_8F_{17}C_2H_4$-) by Tae et al.[29] using SANS. The N_{agg} values of C_{18}PIPOZ (28–38) were comparable to those of the micelles formed by the telechelic PNIPAM (M_n = 12 kDa) end-capped with $C_{18}H_{37}$- groups (N_{agg} = 27–39) in the concentration range 1.0–10.0 g·L^{-1} determined by the same technique.[36] The reported values and our observation of the N_{agg} of the two telechelic polymers suggest that the N_{agg} increases with polymer concentration in the studied concentration range. Obeid et

al.[37] determined the N_{agg} of telechelic PIPOZ (M_n = 7 kDa) end-capped with $C_{18}H_{37}$- groups to be 13 with polymer concentration 1.0 $g \cdot L^{-1}$ using the same technique. The discrepancy may be due to the difference in chemical structures of the two polymers — the linker of the end groups. The strongly hydrophilic triazole ring was introduced in the structure of the telechelic polymers in this work, whereas there was an amido linker at the ω- end in the polymer of Obeid's study. The concentration dependence of the N_{agg} value is insignificant in the concentration range of 2.5 to 10 $g \cdot L^{-1}$ for the telechelic C_{18}PIPOZ and FPIPOZ. The lower value of N_{agg} in solutions with 0.5 and 1.0 $g \cdot L^{-1}$ relates to the "unsaturated" nature of the micelles in growth for the telechelic FPIPOZ and C_{18}PIPOZ. The N_{agg} and size of micelles does not increase with increasing polymer concentration indicates the formation of micelles follows a closed association model.[43] On the contrary, an open association model[44] predicts increases of the size and aggregation number of micelles with polymer concentration. The near constant value of N_{agg} in the concentration range of 2.5 to 10 $g \cdot L^{-1}$ for the telechelic C_{18}PIPOZ and FPIPOZ suggests that the two telechelic polymers associate in water following a closed association model. It is known that the value of R_g/R_H, the so called shape factor, gives information of the conformation of polymer assemblies in solution. It takes a value of 0.77 for hard spheres, 1.3–1.5 for random coils in θ and good solvent, and above 2 for rodlike structures.[45] The values of R_g/R_H for FPIPOZ and C_{18}PIPOZ micelles fall between 1.32 to 1.77, indicating a disordered arrangement of the micelles loops. No clear concentration dependence of R_g/R_H is observed for either telechelic polymers. One should notice that for small particles with diameters lower than $\lambda/20$, due to the limit of instrument, the R_g/R_H value only provides an indicative, not unambiguous, determination of the particle shape. DLS measurements are conducted at different scattering angles (45, 90, and 135°), and no angular dependence was observed. The R_H values of these micelles at different angles are almost identical, indicating that the flower micelles are isotropic, possibly flexible spherical shapes.

Table 4.3 Physical data for FPIPOZ and C_{18}PIPOZ micelles in aqueous solution

Polymer	C (g·L^{-1})	R_H (nm)	$M_{w,app}$ (10^5 g·mol^{-1})	R_g (nm)	N_{agg}	R_g/R_H
FPIPOZ	0.5	8.8	0.76	11.6	10	1.32
FPIPOZ	1.0	8.6	1.4	12.1	19	1.41
FPIPOZ	2.5	8.8	2.1	15.1	28	1.72
FPIPOZ	5.0	8.9	2.5	15.8	33	1.77
FPIPOZ	7.5	9.3	2.6	14.3	34	1.54
FPIPOZ	10.0	10.3	2.7	14.5	35	1.41
C_{18}PIPOZ	0.5	8.9	0.80	13.0	9	1.46
C_{18}PIPOZ	1.0	8.9	2.4	12.5	27	1.40
C_{18}PIPOZ	2.5	9.0	3.0	15.1	34	1.68
C_{18}PIPOZ	5.0	9.9	3.0	14.9	34	1.50
C_{18}PIPOZ	7.5	10.7	3.1	15.1	36	1.41
C_{18}PIPOZ	10.0	11.2	3.3	18.9	38	1.69

The shapes of the flower micelles were assessed by TEM images of FPIPOZ. **Figure A4.4** shows that all the micellar particles are spherical or oval in shape and slightly polydisperse in size. The average radius of FPIPOZ micelle was evaluated to be 7.3 ± 1.5 nm, which is smaller than the hydrodynamic radius of the corresponding flower micelle in water. This is understandable because the hydrated PIPOZ corona of the micelles in aqueous solution was dehydrated after drying. Recently, Kadam et al.[46] reported the first TEM observation of hydrophobically end-capped PEO flower micelles. In their experiment, the hydrophobic cores of the flower micelles were locked by cross-linking. The bridged flower micelles were presented as stringed particles in TEM morphology. In our observation, the absence of stringed architectures may imply that there is no bridged flower micelles existing in a solution. This was consistent with light scattering observation.

4.3.4 Thermo responses of FPIPOZ and C_{18}PIPOZ micelles in water

Light Scattering and Optical Microscopy Studies

The thermo responses of telechelic FPIPOZ and C_{18}PIPOZ micelles in water were studied by UV, light scattering, optical microscopy and HS-DSC. Turbidity measurements of the telechelic polymers were employed to determine the phase transition temperature. Values of 30.3 °C and 30.1 °C were observed for FPIPOZ and C_{18}PIPOZ, respectively, at concentration of 1.0 g·L^{-1}. The turbidity curves of the two polymers and unmodified homopolymer (N_3PIPOZ) in water at different concentrations (1.0–0.05 g·L^{-1}) are shown **Figure 4.5**. T_c decreased with concentration for all three polymers studied. The lower the concentration, the wider the turbidity curves. The onset temperature of turbidity did not decrease as much as the polymer concentration decreased for FPIPOZ (0.8 ºC) and C_{18}PIPOZ (1.6 ºC) compared to that of N_3PIPOZ (5.7 ºC), in the concentration range studied. The near constant onset temperatures for FPIPOZ and C_{18}PIPOZ, at a polymer concentration as low as 0.05 g·L^{-1}, indicates that the telechelic polymers dehydrated in water as an entity of micelle.

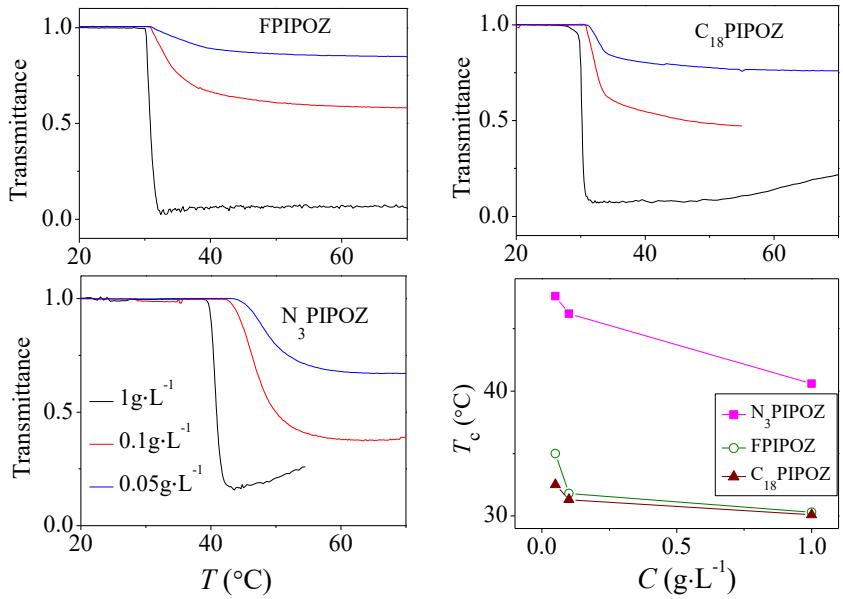

Figure 4.5 Optical transmittance of FPIPOZ, C_{18}PIPOZ and N_3PIPOZ aqueous solutions (polymer concentration 1.0–0.05 g·L^{-1})

The R_H values for FPIPOZ and C_{18}PIPOZ in water at a concentration of 0.5 g·L^{-1} were recorded upon gradually heating the solution from 10 °C to 60 °C. Both solutions became opalescent above their phase transition temperatures. **Figure 4.6** depicts the increase in R_H upon approaching the corresponding phase transition temperature of the telechelic polymers. Upon increasing the temperature above the corresponding T_c, micro-sized aggregates were

observed for both telechelic polymers as indicated by the shaded area in **Figure 4.6**. The size of the micro-sized objects was approximated by optical microscopy as shown in **Figure 4.8**. During the dehydration process at T_c, the corona of the telechelic polymer micelles collapsed. Large particles were formed through hydrophobic interaction between collapsed chains, exhibiting an increase in R_H. When the temperature of the solutions was gradually increased to 60 °C, constant R_H values of 140 nm and 60 nm, with very narrow size distribution, were observed for the telechelic FPIPOZ and C_{18}PIPOZ, respectively. The R_g values for the two telechelic polymers in aqueous solutions, showed the same temperature dependence as R_H. The R_g values remained constant for T < T_c; while they increased sharply as the temperature approached the T_c; and attained constant values above 40 °C. The ratio R_g/R_H for FPIPOZ and C_{18}PIPOZ decreased from ~1.5, below T_c, to ~ 0.81 at 60 °C, which was slightly larger than that for a hard sphere. The experimental plot (**Figure 4.7**) of $P(q)^{-1}$ vs q^2 recorded for C_{18}PIPOZ 0.5 $g \cdot L^{-1}$ at 60 °C, was in between the theoretical curves corresponding to hard sphere and random coil and closer to hard sphere. The same observation was also found for FPIPOZ under the same condition.

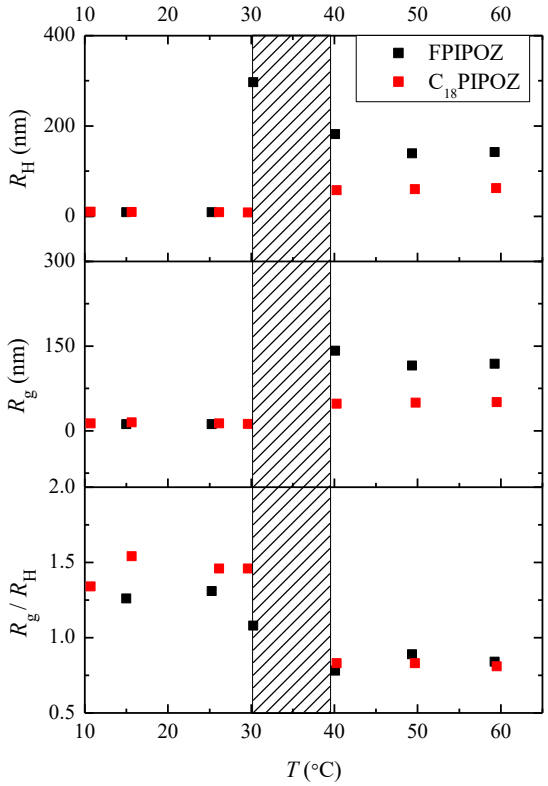

Figure 4.6 The R_H, R_g and R_g/R_H for FPIPOZ and C_{18}PIPOZ in water as a function of temperature (polymer concentration 0.5 $g \cdot L^{-1}$). The shaded area represents the temperature range in which micro-sized aggregates observed.

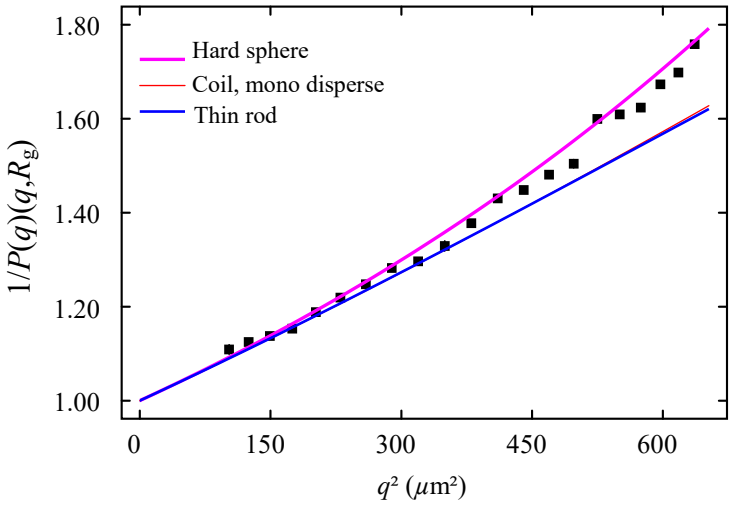

Figure 4.7 Reciprocal of the theoretical scattering functions for particles of basic shapes as a function of q^2. The full squares are the values obtained by an analysis assuming a spherical shape of experimental R_g values from a Guinier analysis of measurements carried out in aqueous solutions of C_{18}PIPOZ at 60 °C ($C_{polymer}$ = 0.5 g·L^{-1}).

To understand the disappearance of the micro-sized particles above 40 °C, for the two telechelic polymers, observed by light scattering studies, aqueous solutions of FPIPOZ and C_{18}PIPOZ with polymer concentration 0.5 g·L^{-1}, were monitored by optical microscopy upon heating. **Figure 4.8** presents images of the C_{18}PIPOZ 0.5 g·L^{-1} solution as an example. A Similar observation was found for the FPIPOZ solution (0.5 g·L^{-1}). **Figure 4.8a1-4** are images of the C_{18}PIPOZ solution in the bottom layer, between the two glass slides, and **Figure 4.8b1-4** shows the images of the FPIPOZ solution under the same conditions. Each image was taken after equilibration for 1 h at a given temperature. At 36 °C, droplets with diameters about 1 μm started to emerge from the C_{18}PIPOZ aqueous solution, and the droplets grew in size by coagulation and settled down on the bottom glass slide. Heating the solution to higher temperatures resulted in the disappearance of the droplets from the middle layer of the solution. More droplets coalesced and settled down to the bottom glass slide. Due to resolution limits, sizes of droplets smaller than 1 μm, remaining in the solution bulk could not be measured. Apparently, the size of droplets in the solution bulk reached a maximum near 36 °C and decreased thereafter, which is consistent with the light scattering results. The droplets on the bottom glass slide had a diameter between 1–3 μm, and did not increase significantly in size but did in number, as the temperature increased from 36 to 60 °C. For FPIPOZ, droplets with

diameters about 1 μm, started to immerge from the aqueous solution at 35 °C, and grew in size by coalescence and settled down on the bottom of the glass slide. The size of droplets on the bottom layer gradually increased to about 7 μm, as the temperature increased to 60 °C as shown in **Figure 4.8**. The much larger droplets (20−50 μm) observed by Katsumoto et al.[47] for unmodified PIPOZ at 50 °C must have been due to the much higher (300 times) polymer concentration they employed. Large droplets (2− 15 μm) was observed which emerged at 31 °C from FPIPOZ solution, with a polymer concentration of 1.0 $g \cdot L^{-1}$, as observed by optical microscope, which is an indication of the concentration dependent phase separation. A recent study of micelles formed by PS-PNIPAM-PS (polystyrene-b-poly(*N*-isopropylacrylamide-b-polystyrene) copolymer using SANS revealed that the micelle aggregate growths were governed by a diffusion-limited model for low concentration and shallow targeting temperature (just above T_c).[48] In our study, at the onset temperatures of phase separation of FPIPOZ and C_{18}PIPOZ, the almost constant small sizes of droplets were probably due to the low effective collision of droplets to coalesce in the low concentration regime (0.5 $g \cdot L^{-1}$). At even higher temperatures, bigger droplets were observed for FPIPOZ compared to C_{18}PIPOZ. Katsumoto's[47] study revealed that crystallization of unmodified PIPOZ beyond 50 °C required all-trans conformation which occurred at a lower temperature. The all-trans conformation of PIPOZ made the phase transition of PIPOZ irreversible. In the case of telechelic FPIPOZ and C_{18}PIPOZ, irreversible phase separation with no crystallization were observed in aqueous solutions at 0.5 $g \cdot L^{-1}$ after long time incubation at 60 °C. At this temperature, the PIPOZ backbones of telechelic polymers adopt an all-trans confirmation. However the constraint of micelle structure prevents the ordered packing of PIPOZ backbone. The growth in size of the FPIPOZ droplets may be stimulated by the fluorophilic property of the C_8F_{17}- end groups which favour staying together with their own kind and repelling all other segments.

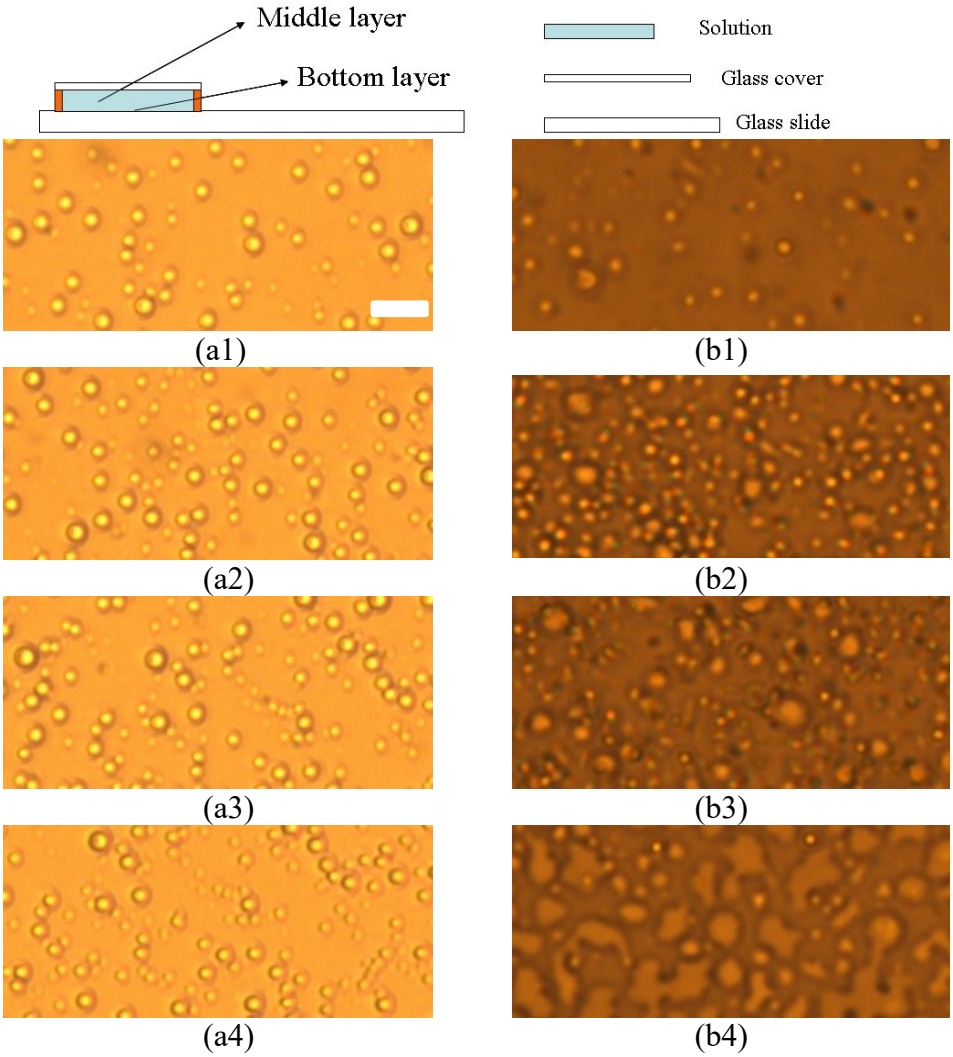

Figure 4.8 Optical images of C_{18}PIPOZ (column a) and FPIPOZ (column b) queous solutions ($C_{polymer}$ = 0.5 g·L^{-1}) in the bottom layer on glass slides at 36 ºC (1), 40 ºC (2), 50 ºC (3) and 60 ºC (4). (The scale bar in image (a1) stands for 10 μm. The magnifications in the images are the same. The schematic diagram on top indicates the middle layer and the bottom layer of the solution.)

Based on light scattering and microscopy results, we propose the following description of the events occurring in aqueous solutions of telechelic FPIPOZ and C_{18}PIPOZ, via the liquid-liquid phase separation mechanism for the phase separation of PIPOZ homopolymer solutions proposed by Katsumoto et al.[47] The numerous droplets emerged in the aqueous solution, for temperatures above the T_c, when the PIPOZ main chain experienced a sharp dehydration. The collapsed micelles with dehydrated PIPOZ shell associate with each other, and appear as large droplets of a polymer-rich phase corresponding to the big scatters shown

in **Figure 4.8**. Until the equilibrium is reached, the droplet sizes increase slowly through coalesces, depending on the surface tensions of the droplets and the concentrations in solution. By increasing the temperature, water becomes a worse solvent for the PIPOZ chains. More water molecules are expelled from the droplets, which present a decrease in size. So with time and temperature, the droplets become more compact, close to a hard sphere.

DSC studies

The thermodynamic properties of the phase transition of telechelic FPIPOZ and C_{18}PIPOZ, in aqueous solution, were investigated by means of DSC. The phase transition enthalpies for the telechelics, in aqueous solution, were determined to be ~ 4.61 kJ·mol^{-1} and ~ 4.69 kJ·mol^{-1} per isopropyloxazoline unit, for FPIPOZ and C_{18}PIPOZ, respectively, by DSC as shown in **Figure 4.9**. Significant decreases in the T_m (~ 6 °C) and ΔH (~ 1 kJ·mol^{-1}), and a much larger $T_{1/2}$ (increase about 4 °C), were observed for FPIPOZ and C_{18}PIPOZ compared to the N_3PIPOZ precursor polymer. The influence of the two types of end-group on the phase transition enthalpy of PIPOZ was quite similar.

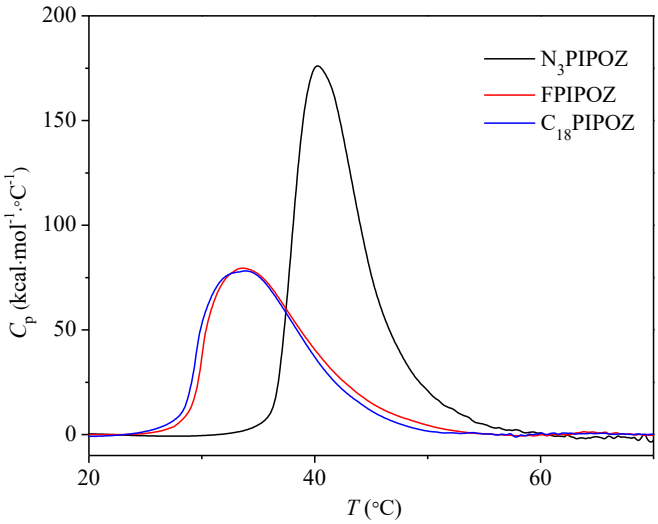

Figure 4.9 DSC results of FPIPOZ and C_{18}PIPOZ aqueous solution with a polymer concentration 10 g·L^{-1}.

The cooperative dehydration is an essential factor of the phase transition of PNIPAM in water. To determine the cooperativity of the phase transition quantitatively for the N_3PIPOZ and telechelic FPIPOZ and C_{18}PIPOZ, we compared the thermodynamic parameters

(ΔH^{VH}, ΔH, T_m and n_{CU}) of their phase transitions, using Tiktopulo's method, as shown in **Table 4.4**. The ΔH^{VH} was estimated by the expression:

$$\Delta H^{VH} = 4RT^2 \frac{C_P(T_m)}{\Delta H} \tag{4.6}$$

where $C_p(T_m)$ is the specific heat capacity of THE polymer at the temperature T_m of the absorption maximum. The n_{CU} is the number of monomer residues in a cooperative unit, and is determined by comparing the heat absorbed by transferring 1 mole of cooperative units from coil to aggregate state ΔH^{VH} with the transition enthalpy of the whole polymer ΔH. The n_{CU} is a quantitative measure of the strength of cooperativity. This model assumes the phase transition involves two states; θ and 1 - θ, which are the amount of chains in the two states respectively. The ΔH^{VH} was estimated by assuming that θ = 1/2 in the middle of the transition ($T = T_m$). The monomers belonging to the same cooperative unit, displayed correlated behavior when the phase transition took place. The effect of the end group modification on the size of the cooperative unit is shown in **Table 4.4**. The number of residues per cooperative unit n_{CU} was then calculated by the ratio of the van't Hoff enthalpy to the experimental specific transition enthalpy. The n_{CU} is determined to be 78, 54 and 52 for N_3PIPOZ, FPIPOZ, and C_{18}PIPOZ, respectively. Tiktopulo et al.[49] determined the n_{CU} of PNIPAM to be ~ 90, for short PNIPAM with M_w ~ 10 kDa. The short PNIPAM chain underwent the "all-or-none" transition with n_{CU}, equal to the total number of monomer unit in a chain. High molecular weight PNIPAMs behaved as if they consisted of quasi-independent "domains". In the reference, the van't Hoff enthalpy for each cooperative unit does not vary much with molecular weight, for PNIPAM chains with more than 1 cooperative unit. The value of n_{CU} for the N_3PIPOZ is a little larger than the total number of monomer units for individual polymer chains (68), which is probably due to the low molecular weight of the polymer. The value of n_{CU} for a N_3PIPOZ with a M_n = 10 kDa was calculated to be 78, same as for shorter chain N_3PIPOZ. So the N_3PIPOZ-8K unwent the "all-or-none" transition, while the polymer chain underwent the all-in-one cooperative dehydration. The van't Hoff enthalpies for FPIPOZ (247 kJ·mol^{-1}) and C_{18}PIPOZ (244 kJ·mol^{-1}) are greatly different from that of N_3PIPOZ (433 kJ·mol^{-1}), indicating that the degree of hydrogen bonding between polymer and water is reduced upon the formation of micelles. The lower van't Hoff enthalpies, thus the

lower degree of hydration, should be caused by the reduced interactions of PIPOZ segments with water molecules, resulting from the steric hindrance between polymer chain loops near the core of micelles. The increased stiffness of the main chain segments, close to the hydrophobic end groups, leads to a reduced degree of cooperativity, i.e. the n_{CU} values for FPIPOZ and C_{18}PIPOZ compared to that for N_3PIPOZ. A portion of monomer units in the telechelic polymers interact with each other instead of hydrogen bond with water, thus exhibiting an apparent lower phase transition enthalpy change. Whereas the telechelic polymer chains in the micelles phase separate together like an entity of higher molecular weight polymer at a lower phase transition temperature.

Table 4.4 Thermodynamic parameters of the phase transition of N_3PIPOZ and telechelic FPIPOZ and C_{18}PIPOZ

Polymer	T_m (ºC)	ΔH (kJ·mol^{-1})	ΔH^{VH} (kJ·mol^{-1})	n_{CU}
N_3PIPOZ	40.3	5.55	433	78
FPIPOZ	33.7	4.61	247	54
C_{18}PIPOZ	34.0	4.69	244	52

4.4 Conclusions

We have demonstrated that telechelic α,ω-diazido-polyoxazolines with nearly quantitative end functionality and narrow distribution can be readily synthesized by CROP using diethylene glycol di(*p*-toluenesulfonate) as a bifunctional initiator and NaN_3 as the terminating agent. The azido endgroups of the polymers are viable for further functionalization with the efficient alkyne-azide 'click' cycloaddition. As exemplified here, 1*H*,1*H*,2*H*,2*H*-perfluoro-1-decanyl propargyl ether and octadecyl ether were feasibly reacted with the azido endgroups, yielding the perfluorodecanyl end-functionalized telechelic polyoxazolines. The hydrocarbon and fluorocarbon end-capped PIPOZs form flower-like micelles in water at room temperature with R_H about 10 nm. No significant concentration dependence of the aggregation numbers was observed for the micelles formed by the two telechelic polymers above 1.0 g·L^{-1}. The upper limit concentration of the micellization process was lower for the fluorocarbon end-capped PIPOZ compared to the hydrocarbon end-capped PIPOZ. The effect of end group modification on the phase transition process of

PIPOZ was studied by turbidity measurement and static and dynamic light scattering. The two telechelic polymer solutions undergo phase separation above corresponding T_c with increased R_g and R_H and a reduced R_g/R_H value, close to that of a hard sphere. The R_g and R_H values of the FPIPOZ micelles are higher than that of the C_{18}PIPOZ micelles. An optical microscopy study revealed a liquid-liquid phase separation of the telechelic polymers, similar to that of the PIPOZ homopolymer. Large droplets were observed in FPIPOZ solutions compared to C_{18}PIPOZ solutions, after heating to 60 °C, probably because of fluorophilic properties of fluorinated end groups in FPIPOZ. DSC measurements indicated that the degree of cooperativity for the telechelic FPIPOZ, C_{18}PIPOZ was lower than that for N_3PIPOZ. Each polymer chain contained only one cooperative unit for all three polymers studied. Lower values of van't Hoff enthalpy change and n_{CU} of the telechelic polymers were caused by the steric hindrance between polymer chain loops near the core of the micelles. No significant difference in the solution behaviour was observed between the FPIPOZ and C_{18}PIPOZ, which is a bit of surprising. To further investigate the influence of end group properties on the solution behavior of telehelic PIPOZ, NMR relaxation techniques will be employed to study the association of the telechelic polymers on molecular level in Chapter 5 of this thesis.

4.5 References

1. Semenov, A. N.; Joanny, J. F.; Khokhlov, A. R. *Macromolecules* **1995,** 28, 1066-75.
2. Borisov, O. V.; Halperin, A. *Langmuir* **1995,** 11, 2911-9.
3. Borisov, O. V.; Halperin, A. *Macromolecules* **1996,** 29, 2612-7.
4. Wang, Y.; Winnik, M. A. *Langmuir* **1990,** 6, 1437-9.
5. Maestro, A.; González, C.; Gutiérrez, J. M. *J. Colloid Interface Sci.* **2005,** 288, 597-605.
6. Taylor, K. C.; Nasr-El-Din, H. A. *J. Pet. Sci. Eng.* **1998,** 19, 265-80.
7. Agarwal, P. K.; Garner, R. T.; Lundberg, R. D. *Macromolecules* **1984,** 17, 2794-9.
8. Tonge, S. R.; Tighe, B. J. *Adv Drug Deliv Rev.* **2001,** 53, 109-22.
9. Adams, N.; Schubert, U. S. *Adv Drug Deliv Rev.* **2007,** 59, 1504-20.
10. Zalipsky, S.; Hansen, C. B.; Oaks, J. M.; Allen, T. M. *J. Pharm. Sci.* **1996,** 85, 133-7.
11. Luxenhofer, R.; Sahay, G.; Schulz, A.; Alakhova, D.; Bronich, T. K.; Jordan, R.; Kabanov, A. V. *J. Controlled Release* **2011,** 153, 73-82.
12. Huber, S.; Jordan, R. *Colloid Polym. Sci.* **2007,** 286, 395-402.
13. Obeid, R.; Tanaka, F.; Winnik, F. o. M. *Macromolecules* **2009,** 42, 5818-28.
14. Eastoe, J.; Downer, A.; Paul, A.; Steytler, D. C.; Rumsey, E.; Penfold, J.; Heenan, R. K. *PCCP* **2000,** 2, 5235-42.
15. Wang, X.; Zhang, J.; Li, X.; Liu, Y.; Yang, H.; Zhao, X.; Xie, L.; Yin, L. *Clin Respir J* **2014,** 160-6.

16. Weigel, J. K.; Steinmann, D.; Emerich, P.; Stahl, C. A.; Elverfeldt, D. v.; Guttmann, J. *Physiol. Meas.* **2011,** 32, 251.
17. Leipzig, N.; Wijekoon, A. WO2013112863A1, 2013.
18. Sawada, H.; Katayama, S.; Ariyoshi, Y.; Kawase, T.; Hayakawa, Y.; Tomita, T.; Baba, M. *J. Mater. Chem.* **1998,** 8, 1517-24.
19. Berret, J.-F.; Calvet, D.; Collet, A.; Viguier, M. *Curr. Opin. Colloid Interface Sci.* **2003,** 8, 296-306.
20. Séréro, Y.; Aznar, R.; Porte, G.; Berret, J. F.; Calvet, D.; Collet, A.; Viguier, M. *Phys. Rev. Lett.* **1998,** 81, 5584.
21. Séréro, Y.; Jacobsen, V.; Berret, J. F.; May, R. *Macromolecules* **2000,** 33, 1841-7.
22. Calvet, D.; Collet, A.; Viguier, M.; Berret, J.-F.; Séréro, Y. *Macromolecules* **2002,** 36, 449-57.
23. Weberskirch, R.; Preuschen, J.; Spiess, H. W.; Nuyken, O. *Macromol. Chem. Phys.* **2000,** 201, 995-1007.
24. Zhou, J.; Zhuang, D.; Yuan, X.; Jiang, M.; Zhang, Y. *Langmuir* **2000,** 16, 9653-61.
25. Gourier, C.; Beaudoin, E.; Duval, M.; Sarazin, D.; Maı; amp; x; tre, S.; François, J. *J. Colloid Interface Sci.* **2000,** 230, 41-52.
26. Pham, Q. T.; Russel, W. B.; Thibeault, J. C.; Lau, W. *Macromolecules* **1999,** 32, 2996-3005.
27. Kadam, V. S.; Badiger, M. V.; Wadgaonkar, P. P.; Ducouret, G.; Hourdet, D. *Polymer* **2008,** 49, 4635-46.
28. Tae, G.; Kornfield, J. A.; Hubbell, J. A.; Lal, J. *Macromolecules* **2002,** 35, 4448-57.
29. Dai, S.; Sio, S. T.; Tam, K. C.; Jenkins, R. D. *Macromolecules* **2003,** 36, 6260-6.
30. Seeliger, W.; Aufderhaar, E.; Diepers, W.; Feinauer, R.; Nehring, R.; Thier, W.; Hellmann, H. *Angew. Chem. Int. Ed.* **1966,** 5, 875-88.
31. Schwabacher, A. W.; Lane, J. W.; Schiesher, M. W.; Leigh, K. M.; Johnson, C. W. *J. Org. Chem.* **1998,** 63, 1727-9.
32. Gao, H.; Matyjaszewski, K. *Macromolecules* **2006,** 39, 4960-5.
33. Luxenhofer, R.; Bezen, M.; Jordan, R. *Macromol. Rapid Commun.* **2008,** 29, 1509-13.
34. Fijten, M. W. M.; Haensch, C.; van Lankvelt, B. M.; Hoogenboom, R.; Schubert, U. S. *Macromol. Chem. Phys.* **2008,** 209, 1887-95.
35. Kujawa, P.; Tanaka, F.; Winnik, F. M. *Macromolecules* **2006,** 39, 3048-55.
36. Obeid, R.; Maltseva, E.; Thünemann, A. F.; Tanaka, F.; Winnik, F. M. *Macromolecules* **2009,** 42, 2204-14.
37. Kalyanasundaram, K. *Langmuir* **1988,** 4, 942-5.
38. Asakawa, T.; Amada, K.; Miyagishi, S. *Langmuir* **1997,** 13, 4569-73.
39. Muto, Y.; Esumi, K.; Meguro, K.; Zana, R. *J. Colloid Interface Sci.* **1987,** 120, 162-71.
40. Laflèche, F.; Nicolai, T.; Durand, D.; Gnanou, Y.; Taton, D. *Macromolecules* **2003,** 36, 1341-8.
41. Kim, M.; Choi, Y.-W.; Sim, J.-H.; Choo, J.; Sohn, D. *J. Phys. Chem. B* **2004,** 108, 8269-77.
42. Yekta, A.; Xu, B.; Duhamel, J.; Adiwidjaja, H.; Winnik, M. A. *Macromolecules* **1995,** 28, 956-66.
43. Beaudoin, E.; Borisov, O.; Lapp, A.; Billon, L.; Hiorns, R. C.; François, J. *Macromolecules* **2002,** 35, 7436-47.

44. Bhatt, M.; Jamieson, A. M. *Macromolecules* **1988,** 21, 3015-22.
45. Kadam, V. S.; Nicol, E.; Gaillard, C. *Macromolecules* **2011,** 45, 410-9.
46. Katsumoto, Y.; Tsuchiizu, A.; Qiu, X.; Winnik, F. M. *Macromolecules* **2012,** 45, 3531-41.
47. Adelsberger, J.; Grillo, I.; Kulkarni, A.; Sharp, M.; Bivigou-Koumba, A. M.; Laschewsky, A.; Muller-Buschbaum, P.; Papadakis, C. M. *Soft Matter* **2013,** 9, 1685-99.
48. Tiktopulo, E. I.; Uversky, V. N.; Lushchik, V. B.; Klenin, S. I.; Bychkova, V. E.; Ptitsyn, O. B. *Macromolecules* **1995,** 28, 7519-24.

4.6 Appendix

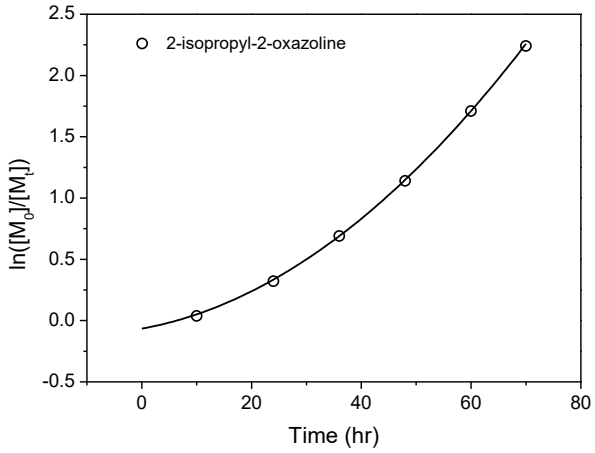

Figure A4.1 Kinetic plot of IPOZ polymerization initiated by diethylene glycol di(*p*-toluenesulfonate) in acetonitrile at 65 °C.

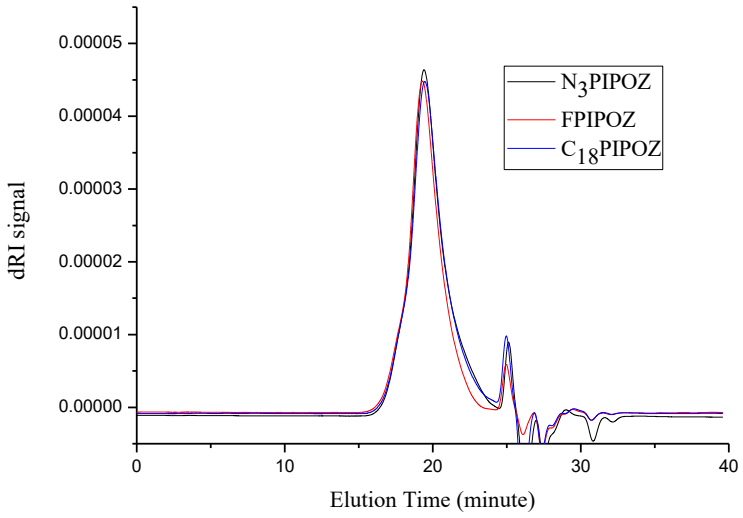

Figure A4.2 GPC traces of N_3PIPOZ, FPIPOZ and C_{18}PIPOZ in DMF.

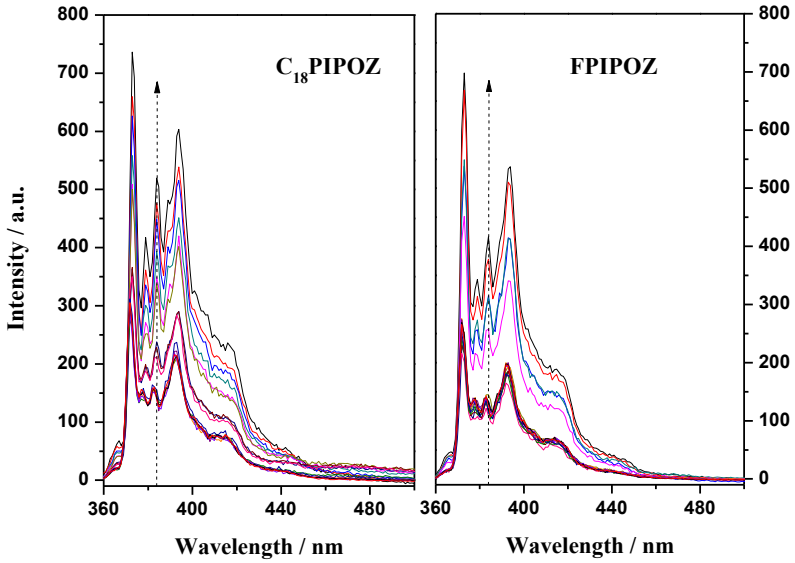

Figure A4.3 Emission spectra of pyrene as a function of polymer concentration in FPIPOZ and C_{18}PIPOZ aqueous solutions. The concentrations of polymer are 0.001–3.0 g·L^{-1}. The arrows indicate the increase of fluorescence intensity as polymer concentration increases.

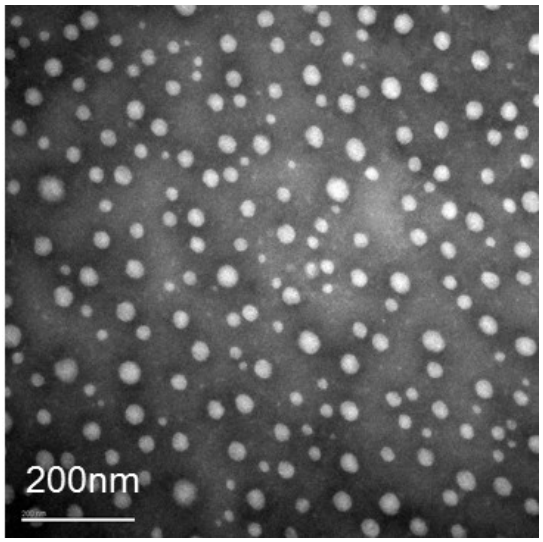

Figure A4.4 TEM micrograph of telechelic FPIPOZ (polymer concentration 0.1 g·L^{-1}).

Chapter 5. Studies of the influence of end group modification on the phase separation of poly(2-isopropyl-2-oxazoline) in D_2O solutions by NMR Spectroscopy

5.1 Introduction

Aqueous solutions of PIPOZ underwent a phase transition around 40 °C. The effect of end group modification on the association properties of PIPOZ has been studied previously by means of light scattering, differential scanning calorimetry (DSC), fluorescence and microscopy. In order to obtain more detailed knowledge of the solution and association properties of telechelic PIPOZ, a better understanding of the molecular dynamics and structure is necessary.

NMR studies have been employed to investigate polymer association in solutions through analysis of line shapes, peak intensities and relaxation times, etc. The association state of polymer chains reflected in terms of molecular dynamic parameters was detected and characterized by NMR spectroscopy, which provided a convenient and direct method for understanding polymer solution behaviour. Relaxation NMR techniques have been applied to study binding of biological macromolecules[1, 2] and association of polymers and surfactant in solutions.[3, 4]

A ^1H NMR study of PNIPAM solutions and gels was reported by Tokuhiro et al.[3] The methylene and methine protons in the PNIPAM gels exhibited no appreciable change throughout the phase transition, but the signal intensity of the methyl protons in the isopropyl acrylamide group decreased substantially with increasing temperature even beyond of the temperature of the collapse of the gel. Proton T_1 relaxation times of PNIPAM in D_2O solution (35 $mg \cdot L^{-1}$) were determined as well. Temperature dependence of ^1H T_1 for PNIPAM in D_2O solution exhibited difference between the side chain and the main chain protons. The T_1 values for the methyl and methine protons in the isopropyl group increase with increasing temperature. The temperature dependence of the T_1 values for the main chain methylene and

methine protons exhibited the opposite trend. Ohta et al[4] measured the T_1 and T_2 relaxation times for PNIPAM as a function of temperature and pressure. Another study by Zeng[5] and coworkers on PNIPAM solutions revealed a decrease in T_1 relaxation times of methylene and methine protons and an increase for the methyl protons with increasing temperature, which indicated difference in mobility of the methyl groups on the side chains and methylene group on the main chains. The phase separation in PNIPAM/water system was investigated by ^{13}C and ^{1}H NMR in this study. ^{1}H T_1 and T_2 values of the polyampholyte hydrogel poly(methylacrylic acid acryloyloxyethyl trimethylammonium chloride) were determined by Lu et al. under different conditions.[6] The molecular mobility of polyampholyte hydrogel was characterized by changes in T_2. The mobility of the main chain methylene protons of PNIPAM and the protons of different end groups was investigated for D_2O solutions of PNIPAM end-capped with different groups.[7] The kinetic behaviour of the phase transition of PNIPAM was studied by ^{1}H NMR. The chain mobility, as revealed by T_2, the mobile fraction of PNIPAM chain, as revealed by signal intensity, and the self-diffusion coefficient were examined as a function of temperature and time by Yushmanov et al.[8] A faster collapse and intermolecular aggregation and a slower redistribution of the individual chains among and within the globular and mobile states were suggested. The mobility of PNIPAM protons for PNIPAM microgels in SDS solutions was studied by Andersson,[9] by monitoring ^{1}H NMR relaxation times of different groups in PNIPAM.

In addition to the ^{1}H NMR studies, ^{19}F and ^{13}C NMR may also be employed in studies of polymer molecular motions. The high sensitivity and high natural abundance of ^{19}F in nature make ^{19}F NMR a useful technique for basic studies of fluorinated molecules, and for MRI of fluorinated imaging agents. Fluorocarbons are well-known to be more hydrophobic than their hydrocarbon analogues, one CF_2 groups equals ca. 1.7 CH_2 groups. Many studies have taken advantage of the super-hydrophobicity of fluorocarbons to form various structures of micelles and study their association properties by ^{19}F NMR. Fluorocarbon end-capped PEGs have been studied by many research groups. Different techniques have been employed to study their association properties, such as pulse-gradient spin-echo (PGSE) NMR,[10] ^{19}F relaxation NMR as a function of temperature and concentration,[11] ^{19}F chemical shift,[12, 13] electron-spin induced ^{19}F relaxation NMR,[14] etc. ^{19}F NMR spectroscopy has been reported to

examine the association and network formation of telechelic fluorinated PEG with C_6F_{13} and C_8F_{17} end groups.[15] Temperature dependent ^{19}F NMR spectra were recorded to study the aggregation of the polymers. A study of amphiphilic copolymer of water soluble poly(sodium acrylate) grafted by 8% hydrophobic C_7F_{15}-CH_2- side chains by ^{19}F NMR spectroscopy revealed a slow exchange of the polymer chains among different states of aggregation and a fast exchange of individual side chains among aqueous and hydrophobic environments within the same aggregate.[16]

In this work, we studied the phase transition of PIPOZ and telechelic PIPOZs by monitoring the spin-lattice relaxation time T_1 and the spin-spin relaxation time T_2 of the ^1H, ^{13}C and ^{19}F nuclei of PIPOZ and telechelic PIPOZ as a function of temperature.

5.2 Experimental Section

5.2.1 Materials

The synthesis of N_3PIPOZ and telechelic FPIPOZ and C_{18}PIPOZ were described in Chapter 4. **Scheme 5.1** shows the structures of the telechelic FPIPOZ and C_{18}PIPOZ. D_2O and TMS were purchased from Sigma-Aldrich.

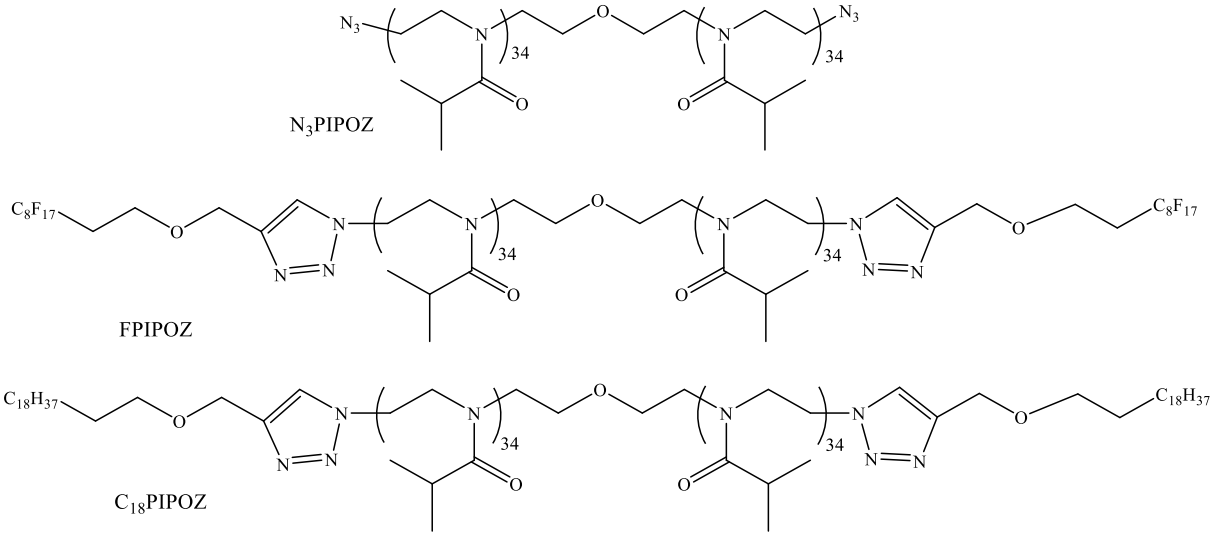

Scheme 5.1 Structures of N_3PIPOZ, FPIPOZ and C_{18}PIPOZ.

5.2.2 Instrumentation

^{1}H NMR T_1, T_2 relaxation times at various temperatures. The ^{1}H NMR experiments of the polymers were performed on a Bruker Advance 500MHz spectrometer. Temperature was calibrated using ethyleneglycol prior to the measurement. ^{1}H NMR T_1 relaxation time was measured by inversion-recovery pulse sequence. A recycling of 8 s and typically 16 scans were used. The integrals of peaks were collected and the relaxation decays were fitted with the exponential function

$$I = I_0(1 - k * \exp(-\tau / T_1) \tag{5.1}$$

where τ is delay time, and k and I_0 are constants. The T_2 relaxation time was measured by a CPMG sequence. The relaxation decay was fitted to a biexponential function (5.2) to obtain a $T_{2,\text{long}}$ and a $T_{2,\text{short}}$ beyond the transition temperature. Only one T_2 was obtained for samples below the phase transition temperature.

$$I = I_1 \exp(-2\tau * n / T_{2,short}) + I_2 \exp(-2\tau * n / T_{2,long}) \tag{5.2}$$

where n is the number of loops (the number of spin-echo blocks), and I_1 and I_2 are constants. The samples of polymers in D_2O solutions were prepared one day before the measurements. After loading the samples into the spectrometer, the temperature was set to a desired value and kept for 15 min to equilibrate. The NMR experiments were then started at 10 ºC and finished at 70 ºC.

Time dependence of ^{1}H NMR T_1, T_2 at 60 ºC. The FPIPOZ and N_3PIPOZ D_2O solutions with polymer concentration 10 g·L^{-1} were heated to 60 ºC from room temperature directly. The ^{1}H NMR T_1, T_2 times were measured as a function of time for one day using the same method described previously.

^{13}C NMR T_1, T_2 relaxation times. The ^{13}C NMR experiments of the polymers were performed on a Bruker Advance 700 MHz spectrometer. ^{13}C NMR T_1 relaxation time was measured by inversion-recovery method. And T_2 relaxation times were measured by a CPMG method. The concentrations of polymers in the D_2O solutions were kept at 10 g·L^{-1} and prepared one day before the measurements. After loading the sample into the spectrometer, the temperature was set to a desired value and kept for 15 min to equilibrate. The temperature of the sample started from 10 ºC and increased to 55 ºC (the temperature at which the intensity

of the peak is very low) stepwise at each desired value, followed by a gradual decrease to 25 ºC. At each temperature, T_1 and T_2 relaxation time were measured. The duration of the total measurement at each temperature was kept within 4 h.

5.3 Results and discussion

5.3.1 ^{1}H NMR of N_3PIPOZ and telechelic PIPOZs at different temperatures

The phase transition of the polymers can be followed by monitoring the changes in peak shape and intensity with temperature. In **Figure 5.1**, the methine and methyl protons of N_3PIPOZ and telechelic FPIPOZ and C_{18}PIPOZ broaden and are attenuated at elevated temperatures, indicating reduced mobility of these groups. The line shape broadening effect induced by strong nuclear magnetic dipole-dipole interactions among protons overcomes the motional narrowing effect, causing the broadening of the NMR signals of the polymer solution experiencing a phase transition. This is especially pronounced for the broadening of the CH_3 signals, as depicted in **Figure 5.1**. In the case of main chain methylene protons, the motional narrowing effect was more prominent as temperature increased. The intensities of methyl and methylene protons normalized to the intensity of the methyl protons at 5 ºC were recorded and plotted as a function of temperature in **Figure 5.2**. The decrease in peak intensities and the broadening of signals were more pronounced for the solution at 1.0 g·L^{-1} than for the one at 10 g·L^{-1}. The values of the phase transition temperature T_c defined as the 50% peak intensity were different for the three polymers depending on the positions of protons on the polymer chain. The T_c values of FPIPOZ and C_{18}PIPOZ regarding the mainchain methylene proton signals (T_c (CH_2)) were almost the same (~33.5 ºC) with no polymer concentration dependence. The T_c value of FPIPOZ (33.7 ºC) determined by side chain methyl proton intensity (T_c (CH_3)) was slightly lower than that for C_{18}PIPOZ (34.7 ºC) at polymer concentration 10 g·L^{-1}. However the T_c (CH_3) values rose to 37.5 ºC for FPIPOZ and 36.0 ºC for C_{18}PIPOZ when the polymer concentration decreased to 1.0 g·L^{-1}. These results implied that for the two telechelic PIPOZs the hydrophilic-to-hydrophobic state transition was more concentration dependent for the side chain methyl groups than for the main chain methylene groups. The T_c (CH_3) values and T_c (CH_2) values for the N_3PIPOZ rose from 38.1 and 37.7 ºC to 44.0 and 42.9 ºC respectively. The T_c (CH_2) values for the N_3PIPOZ increased with polymer concentration

decreasing, which is opposite to that for telechelic polymers, probably relating to the difference in mobility of main chain methylene groups in the N_3PIPOZ and in the telechelics. The difference in the T_c (CH_2) and T_c (CH_3) values were most significant for FPIPOZ (33.5 and 37.5 ºC respectively), and least significant for N_3PIPOZ (42.9 and 44 ºC).

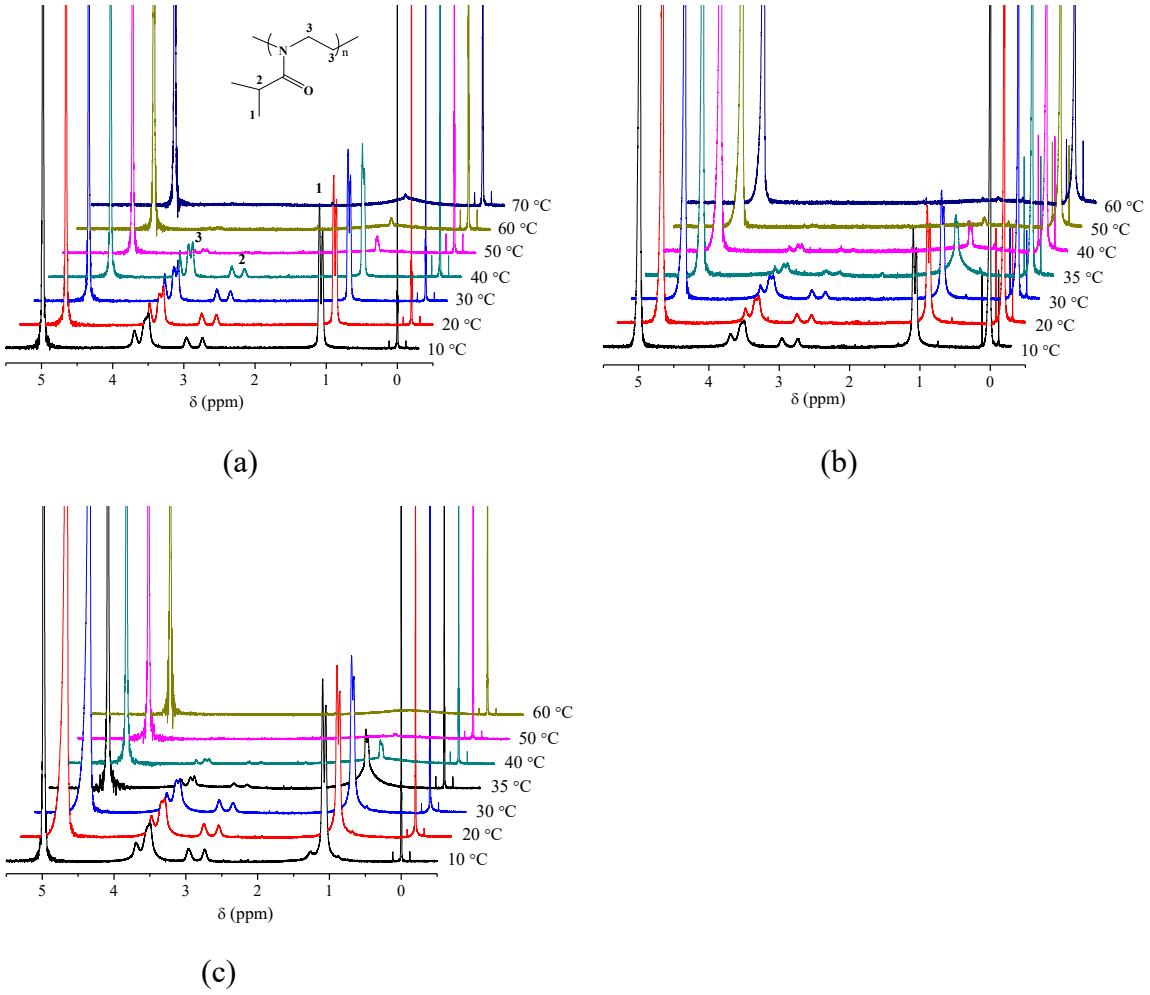

Figure 5.1 ^{1}H NMR spectra of N_3PIPOZ (a), FPIPOZ (b) and C_{18}PIPOZ (c) in D_2O solutions with polymer concentration 1.0 g·L^{-1} at 5–70 ºC.

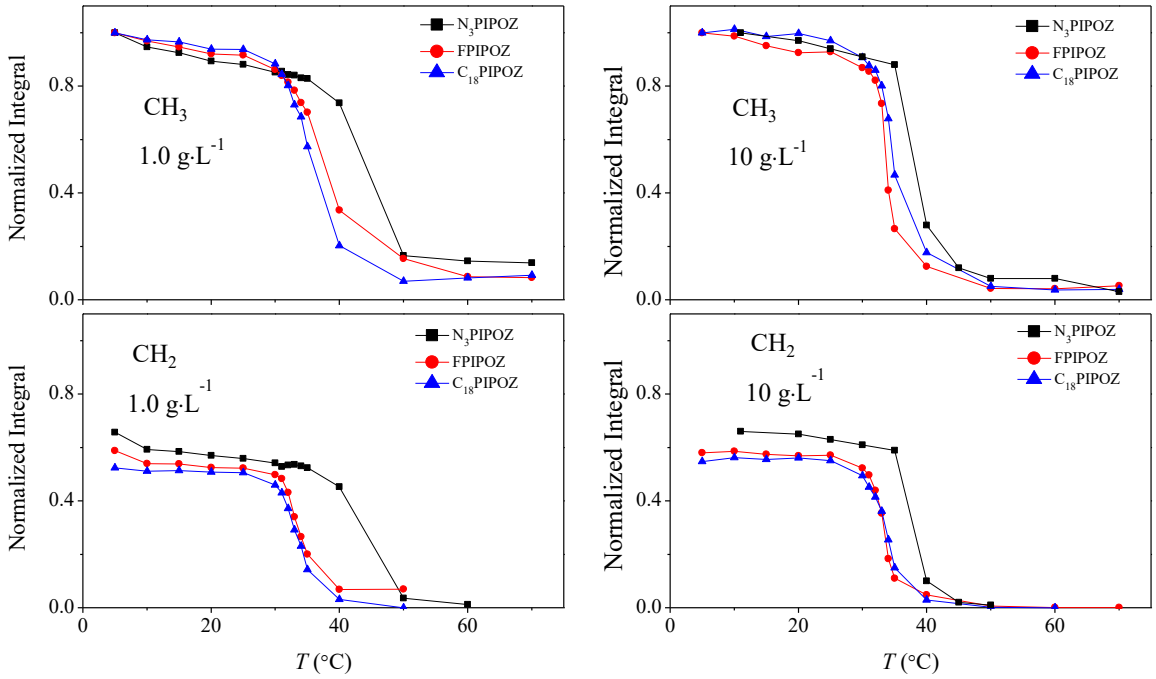

Figure 5.2 ^{1}H NMR integrals of side chain methyl group and main chain methylene group of N_3PIPOZ, FPIPOZ and C_{18}PIPOZ in D_2O solutions with polymer concentration 1.0 and 10 g·L^{-1} as a function of temperature.

The phase transition can be investigated more quantitatively by monitoring the changes of the proton spin-lattice (T_1) and spin-spin (T_2) relaxations. As shown in **Figure 5.3a**, the temperature dependence of ^{1}H T_1 exhibited distinct differences between chemical groups of N_3PIPOZ. The T_1 value for the methyl protons in the isopropyl groups increased with rising temperature. These results are consistent with the findings of Zeng et al.[5] and of Tanaka et al.[3] for the temperature dependence of the T_1 values for the side chain methyl protons in poly(*N*-isopropylacrylamide). On the other hand, the temperature dependence of the methylene protons in the main chain exhibited a minimum at 50 °C. The temperature dependence of the T_1 value for the methylene proton decreased with rising temperature before phase transition occurred, which is consistent with the observations for main chain methylene protons in PNIPAM below corresponding phase transition temperature.[3, 5] The T_1 value for the methine proton slightly decreased below the phase transition temperature and increased after 40 °C. Above the LCST of N_3PIPOZ (40 °C), the T_1 values of the methyl and methine protons in the N_3PIPOZ side chain increased with temperature. However, the ^{1}H T_1 for methylene groups

kept decreasing until 60 °C. A strong increase of T_1 was observed when temperature reached 60 °C, where the crystallization of the N_3PIPOZ is reported to occur. The N_3PIPOZ was reported to have a T_g ~ 68 °C measured by TGA.[17] The segmental mobility of this polymer in the liquid droplets is still relatively high and makes it possible to detect the broad lines corresponding to the N_3PIPOZ units after phase separation. The inversion-recovery experimental data and CPMG experimental data are shown in the Appendix.

The temperature dependence of T_1 varied for different resonances in the telechelic FPIPOZ and C_{18}PIPOZ solutions as shown in **Figure 5.3b-c**. The T_1 values for the methyl protons of telechelic FPIPOZ and C_{18}PIPOZ increased with rising temperature. Opposite temperature dependence of T_1 was observed for methine and methylne protons compared with methyl protons in the telechelic FPIPOZ and C_{18}PIPOZ. The ^{1}H T_1 of methine and methylene groups for telechelic FPIPOZ and C_{18}PIPOZ generally decreased with temperature, especially when temperature went above corresponding T_c. For both telechelic polymers, a local maximum was observed at 32 °C (FPIPOZ) and 33 °C (C_{18}PIPOZ) as shown in **Figure 5.3b-c**. In the transition region (30–33 °C for FPIPOZ and 30–34 °C for C_{18}PIPOZ), the ^{1}H T_1 values of methyl, methine and methylene groups followed the same trend. In hot aqueous solutions (above 50 °C), the formation of micelles prevented the conformation changes of PIPOZ backbone of the telechelics from a mixture of trans and gauche to all trans, manifested by low T_1 values instead of the abrupt increase of T_1 for N_3PIPOZ. The T_1 value of methine protons for FPIPOZ (~ 0.5 s) at 60 °C is higher than that for C_{18}PIPOZ (~ 0.1 s).

The near constant T_1 value of methine and methylene protons below the phase transition temperatures of the telechelic polymers is due to the restrained mobility of the methylene groups brought in close proximity by micelle assemblies of telechelic polymers in aqueous solutions. The hydrogen bond in the micelle assembies was less structured compared to that in the free coil of the unmodified N_3PIPOZ. Lower T_1 values were observed for CH_3 protons than that of CH_3 and CH protons at 10 °C for all three polymers, suggesting lower flexibility of methyl groups due to stronger water cages surrounds polymer chains at this low temperature.

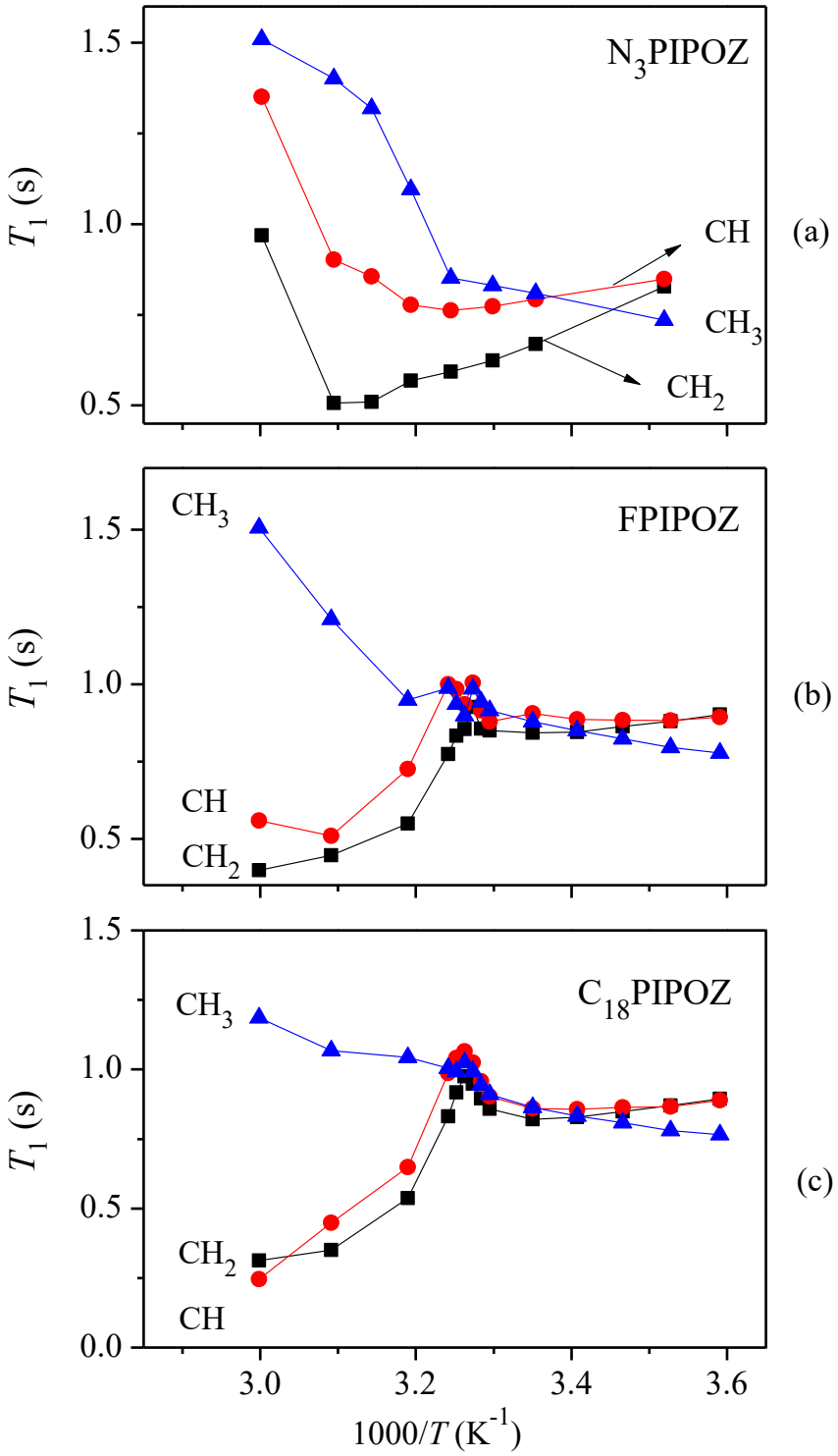

Figure 5.3 ^{1}H NMR T_1 times of CH_2, CH and CH_3 of isopropyl acrylamide groups of N_3PIPOZ (a), FPIPOZ (b), and C_{18}PIPOZ (c) in D_2O solution ($C_{polymer}$ = 10 g·L^{-1}) at different temperatures.

In order to obtain knowledge of the general nature of molecular motions, we analyzed the temperature dependence of T_1 by applying the rudimentary BPP theory

$$\frac{1}{T_1} = K\left(\frac{\tau_c}{1+\omega_0^2\tau_c^{\,2}} + \frac{4\tau_c}{1+4\omega_0^2\tau_c^{\,2}}\right) \tag{5.3}$$

$$\frac{1}{\tau_c} = \frac{1}{\tau_0}\exp\left(-\frac{E_a}{kT}\right) \tag{5.4}$$

where ω_0 is the Larmor frequency, τ_c is the correlation time, E_a is the Arrhenius activation energy, k is the Boltzmann constant, and T is the absolute temperature. K in equation (5.3) is a constant only depending on the structures. In this study, ω_0 is a fixed, thus the value of T_1 depends only on the parameter τ_0 and E_a. And the location of T_1 depends solely on the chemical environment of the specific proton. The T_1 curve was divided into high- and low-temperature side by the minimum point. With increasing temperature, the relaxation of methyl protons in N_3PIPOZ falls into the high- temperature side of the T_1 curve. The relaxations of the methine proton and methylene protons pass through their minimum respectively when temperature increases. For N_3PIPOZ, the location of the minimum in T_1 curve follows the order: $CH_3 < CH < CH_2$. With rising temperature, the relaxation of the side chain methyl protons slows down, while that of the methylene and methane protons speeds up in the beginning and slows down probably due to the conformational change in hot water. In the case of the two telechelic polymers, the behavior of methyl groups follows the T_1 curve on the high-temperature side, and that of methylene and methine protons follows the T_1 curve on the low-temperature side. The conformational change of polymer chains is hindered by the micellization of the telechelics, reflected by the absence of the turning in the T_1 curves.

Figure 5.4 Shows the theoretically calculated T_1 by equation (5.3) and (5.4) and experimental values of protons in N_3PIPOZ, FPIPOZ, and C_{18}PIPOZ, and the parameters are summarized in **Table 5.1**. These values are typical for polymers in solutions. The correlation times for T_1 are calculated by equation (5.4) using the same fitting parameters as shown in **Figure 5.5**. Similar temperature dependences of the τ_c values are obtained for the three polymers below their corresponding T_c. The smallest τ_c is found for side chain methyl groups, indicating the highest mobility among the three different groups. The τ_c values of methyl protons are larger in the telechelic polymers than in N_3PIPOZ, indicating a reduced mobility

of side chain methyl protons in the telechelic micelles compared with that in the free coil of N_3PIPOZ. The mobility of methylene protons on the contrary is higher in the telechelic polymers than in N_3PIPOZ as reflected by the lower τ_c values of the former.

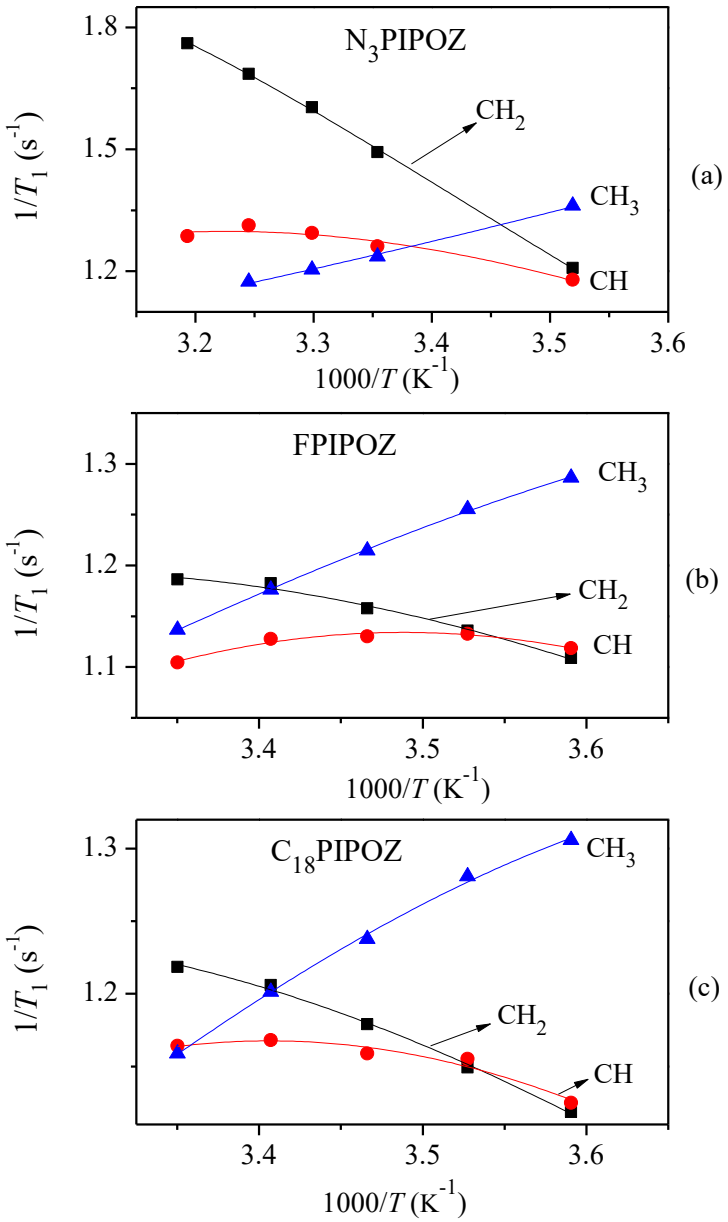

Figure 5.4 Theoretical calculated (lines) and experimental ^{1}H NMR T_1 times (filled symbols) of CH_2, CH and CH_3 of isopropyl acrylamide groups of N_3PIPOZ (a), FPIPOZ (b), and C_{18}PIPOZ (c) in D_2O solution ($C_{polymer}$ = 10 g·L^{-1}) at different temperatures.

Table 5.1 Fitting parameters for ^{1}H T_1 using equation (5.3) and (5.4) for N_3PIPOZ, FPIPOZ, and C_{18}PIPOZ.

Polymer/group	$\tau_0 \times 10^{-12}$ (s)	E_a (kJ·mol^{-1})	$K \times 10^9$ (s^{-2})
N_3PIPOZ			
CH_2	0.786	15.9	4.41
CH	0.786	14.2	2.86
CH_3	2.25	4.61	17.3
FPIPOZ			
CH_2	2.31	11.3	2.63
CH	0.37	15.0	2.50
CH_3	1.77	9.98	3.02
C_{18}PIPOZ			
CH_2	3.07	10.8	2.73
CH	0.80	13.4	2.57
CH_3	1.02	11.5	2.98

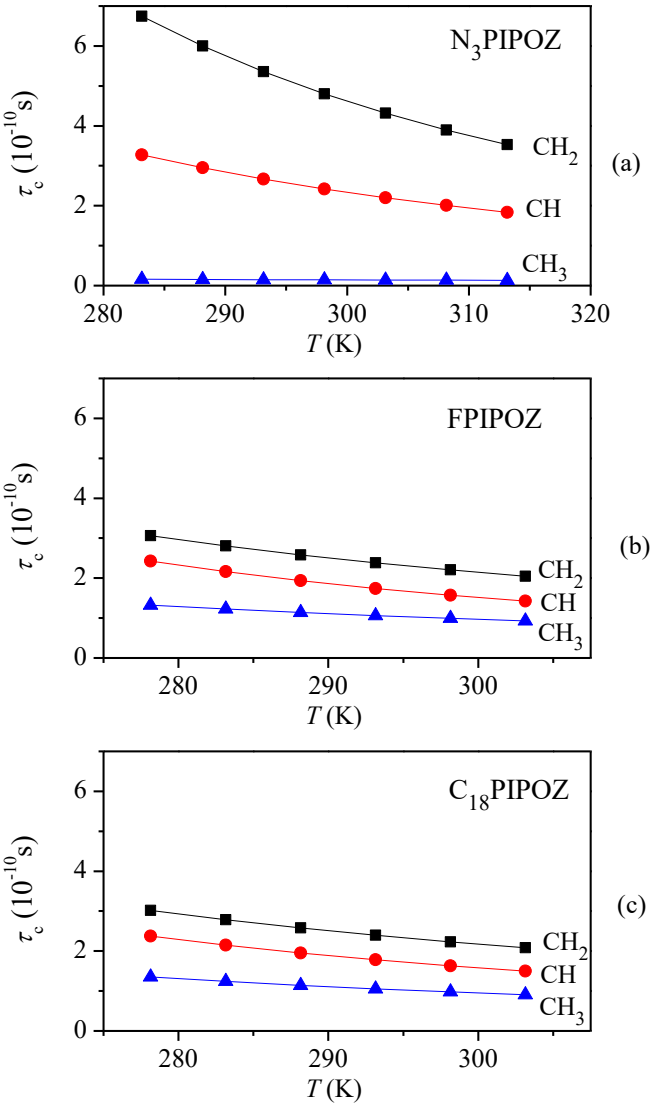

Figure 5.5 Temperature dependence of the correlation time τ_c calculated using the τ_0 and E_a obtained from fitting of T_1.

The T_2 relaxation of proton linked to polymer chains is strongly affected by the local rigidity. Faster T_2 relaxation was observed for protons in constrained environment, compared to identical protons in free environment. Consequently, the loss of segmental mobility upon micellization and upon phase transition is manifested by the changes in T_2 relaxation. By fitting the relaxation decays to a one or two exponential function, T_2 of one or two components was obtained as shown in **Figure 5.6**.

Lower ^{1}H T_2 values were obtained for protons in the telechelic polymers compared with that in the N_3PIPOZ, indicating reduced tumbling rate of the telechelic polymer chains in the micelle assembles. Higher ^{1}H T_2 values of the chemical groups in the FPIPOZ was observed, compared to that for the chemical groups in the C_{18}PIPOZ, suggesting a higher mobility of the chain segments in FPIPOZ. The higher mobility of the chain segments in the corona of the FPIPOZ micelles than those of the C_{18}PIPOZ micelles indicates less constraint in the former. Although the ^{1}H T_2 value of the methyl groups in the side chain of FPIPOZ is higher at room temperature, it decreases to almost the same value as that of C_{18}PIPOZ, when the temperature reached 30 °C.

Short T_2 relaxation times (2–16 ms) are obtained above 40 °C as expected for protons corresponding to segments in the polymer-rich phase ("collapsed" phase) of N_3PIPOZ. The same trend was observed for telechelic polymers above their phase transition temperatures. A significant loss of signals was revealed for all three polymers above their T_c values, especially for methine and methylene protons in the aggregated state. As a result, the short T_2 relaxation times for the methine and methylene protons cannot be detected above 40 °C. The protons in the chemical groups that remained in the polymer-lean phase (solution phase) after liquid-liquid phase transition exhibit an increase in T_2 relaxation times, indicating an increase of mobility because of thermo effect. For the main chain methylene protons in the N_3PIPOZ, a short T_2 relaxation time ~ 2.5 ms was observed at 60 °C where crystallization of PIPOZ homopolymer in water was supposed to occur.

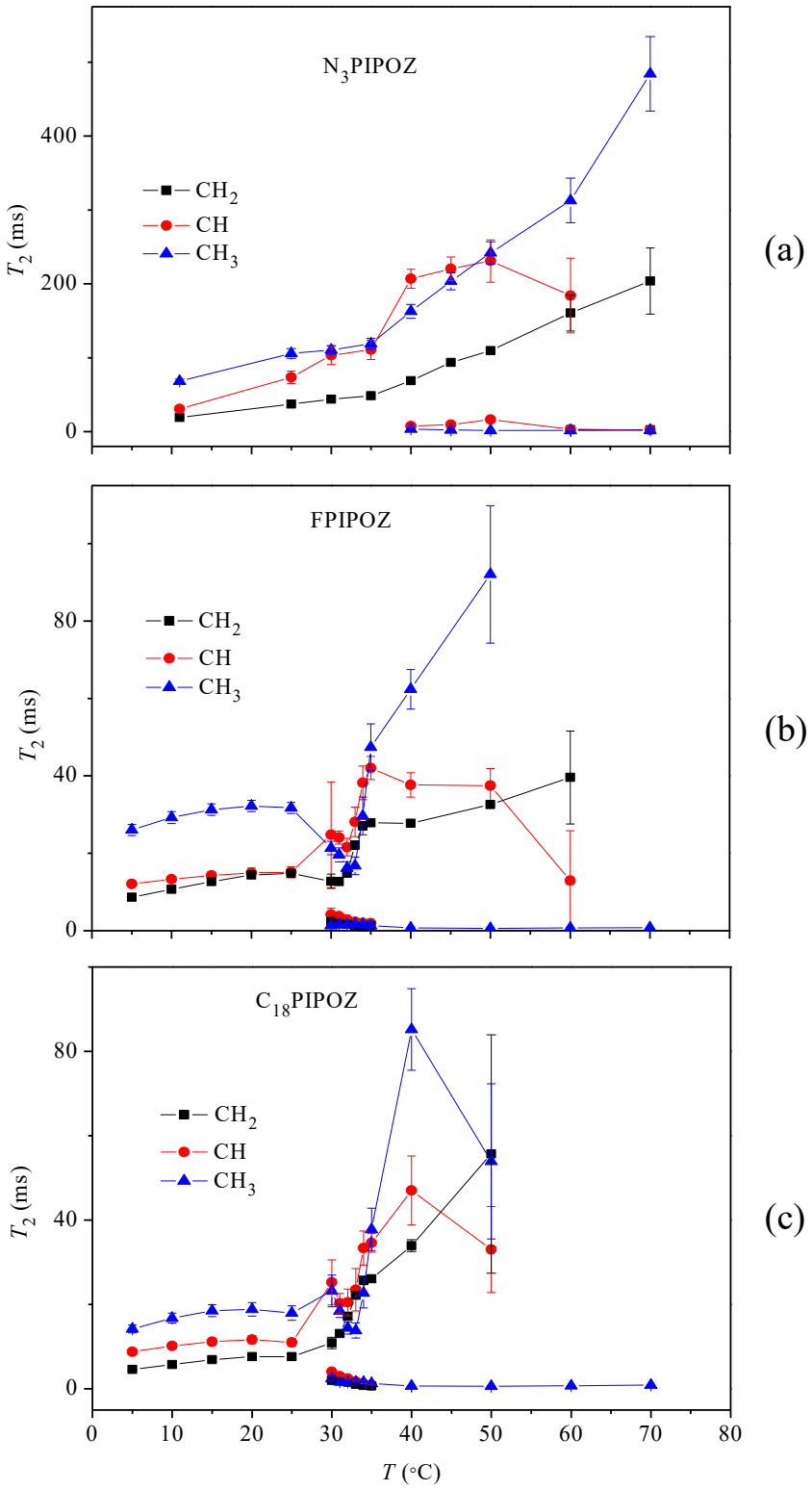

Figure 5.6 ^{1}H NMR T_2 times of N_3PIPOZ (a), FPIPOZ (b), and C_{18}PIPOZ (c) in D_2O solution ($C_{polymer}$ = 10 g·L^{-1}) at different temperatures.

The temperature dependence of ^1H T_2 relaxation times for FPIPOZ and C_{18}PIPOZ shows some difference from that of unmodified N_3PIPOZ as shown in **Figure 5.6**. A short T_2 relaxation time was observed for the three types of protons at 30 °C. Above 35 °C, only long T_2 relaxation times (T_{2long}) existed only for the methine and methylene protons. Beyond 35 °C, the short T_2 (T_{2short}) for methyl protons was nearly constant at about 1 ms. Though the data scattered above the phase transition temperature, the T_{2long} tended to increase with temperature. The disappearance of the T_{2short} values for the methylene and methine protons above 35 °C indicated a sedimentation process of the phased separated liquid droplets, which was consistent with previous LS and microscopy studies in Chapter 4 of this thesis. The T_{2short} values decrease with temperature implying an increase of local rigidity. A relatively stronger signal was obtained for the methyl protons compared with that of the methylene and methane protons at all studied temperatures, which was attributed to the higher flexibility of the methyl groups. **Figure 5.7** presents the amplitude of $T_{2,\,short}$ ($f_{T2,\,short}$) expressed as the ratio of $I_1/(I_1 + I_2)$. As the temperature reaches the LCST of the polymer solution, two components of different mobility appeared suddenly and $T_{2,\,short}$ gradually became the dominant component ($f_{T2,\,short} > 0.5$) in a narrow temperature range. The $f_{T2,\,short}$ decreased rapidly for the CH_2 and CH protons at even higher temperatures because of the loss of signal intensities due to sedimentation of liquid droplets. The detectable proton resonances originate from the polymer chains in the polymer poor phase and the weak signals from polymers in the polymer-rich phase which remains mobile. The low T_g value of PIPOZ gave certain mobility of PIPOZ segment in the polymer-rich phase above the phase transition temperature.

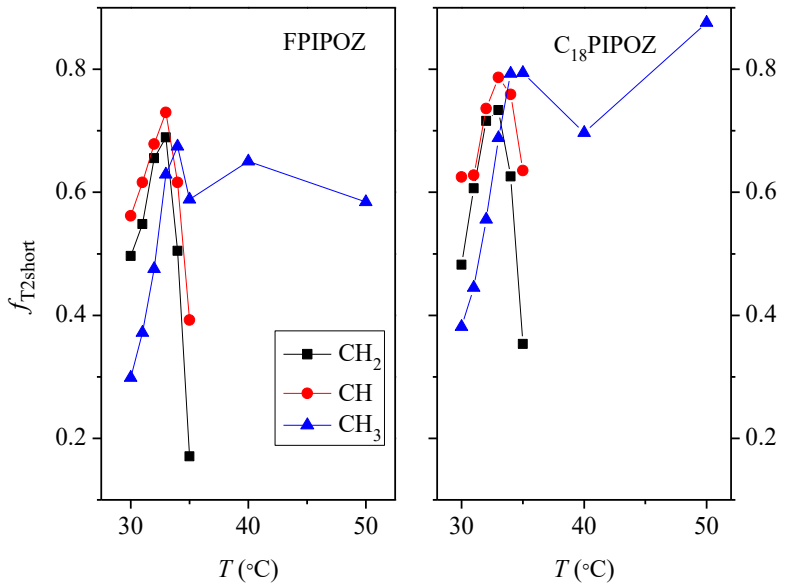

Figure 5.7 The amplitude of short ^{1}H T_2 times in FPIPOZ and C_{18}PIPOZ solutions ($C_{polymer}$ = 10 g·L^{-1}) as a function of temperature.

5.3.2 ^{13}C NMR spectra of N_3PIPOZ and telechelic PIPOZs

The ^{13}C NMR spectra of N_3PIPOZ, FPIPOZ and C_{18}PIPOZ in D_2O solutions are presented in **Figure 5.8**. The assignment of each resonance peak is based on previous reports for PNIPAM.[5, 18] The doublet at 18.6 ppm is assigned to the resonance of the methyl carbon in the side chain. The signal at 30 ppm is attributed to the side chain methine carbon, and the signal at 45 ppm is assigned to the main chain methylene carbon. The resonance of the C=O group is detected as at 180.7 ppm. The small signals at 14 ppm and 22.6 ppm in the C_{18}PIPOZ spectra are assigned to the carbon in the octadecyl groups.

Rising the temperature from 10 to 50 ºC, attenuated the intensity of signals gradually for the three polymers. In **Figure 5.8a**, one observes a new peak at 19.6 ppm, which appears at 40 ºC, whereas the intensity of the methyl peak at 18.6 ppm decreased as temperature increased. When the temperature reached 60 ºC, only one broad peak centered at 19.6 ppm is observed. The peak at 19.6 ppm disappeared once the sample was cooled down to below 35 ºC. Similar observation was found in FPIPOZ and C_{18}PIPOZ solutions at 35 and 33 ºC respectively. The new peak at 19.6 ppm must be related to the methyl groups in the polymer-

rich phase as a result of the dehydration of PIPOZ chain. The structure restriction, induced by the loop structure formation of telechelic FPIPOZ and C_{18}PIPOZ in D_2O solutions, rendered the telechelic polymer chains more mobile and dehydrated at a lower temperature than in the case of the unmodified N_3IPOZ. To study the solution behaviour of the telechelic polymers, ^{13}C NMR relaxation times of carbons from different chemical groups were determined as a function of temperature.

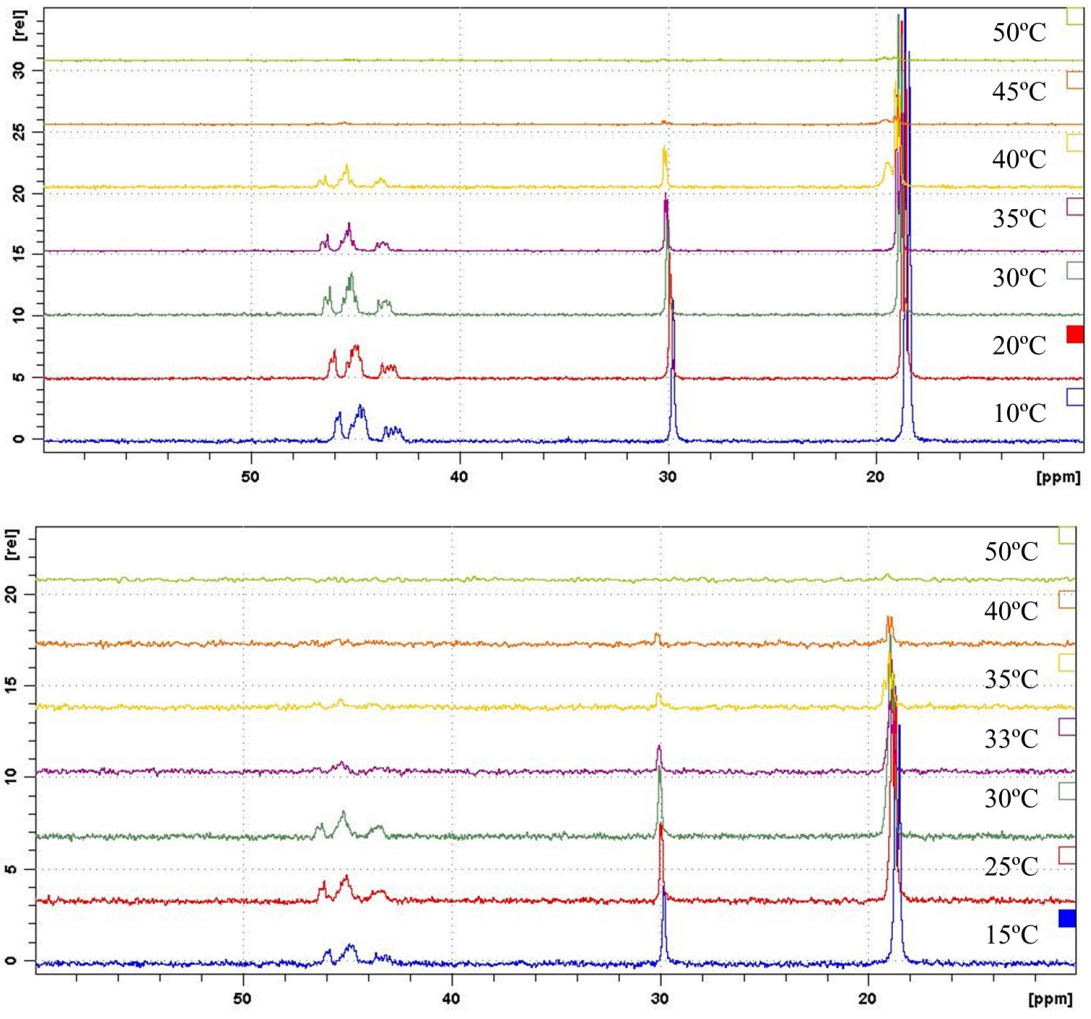

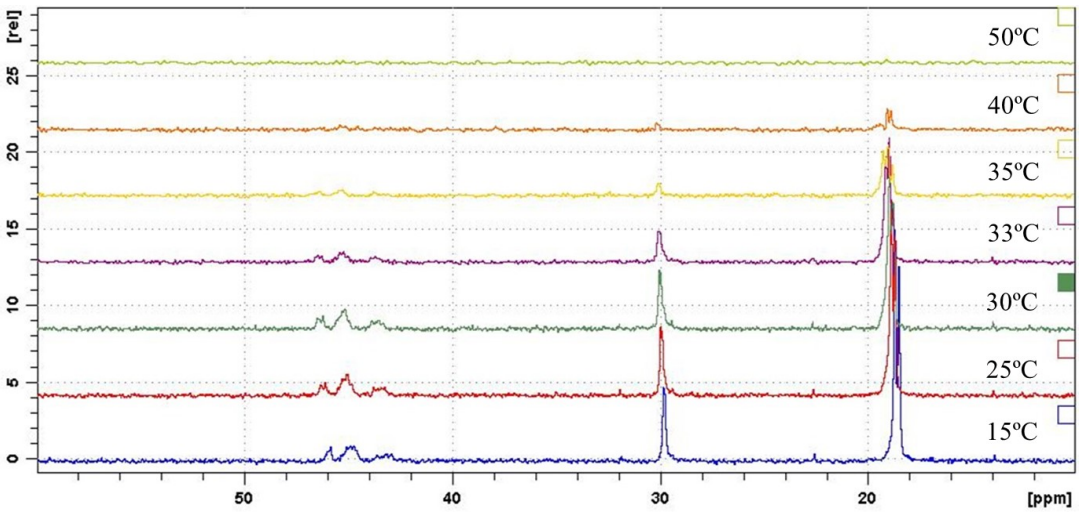

(c)

Figure 5.8 ^{13}C NMR spectra of N_3PIPOZ (a), FPIPOZ (b) and C_{18}PIPOZ (c) in D_2O solution ($C_{polymer}$ = 10 g·L^{-1}) at different temperatures.

5.3.3 ^{13}C NMR T_1, T_2 of PIPOZ and FPIPOZ

Figure 5.9 presents the T_1 and T_2 values for carbons from different chemical groups of N_3PIPOZ, FPIPOZ and C_{18}PIPOZ. Though the data is scattered due to low sensitivity of ^{13}C NMR, the temperature dependence of ^{13}C T_1, T_2 relaxation times of methine and methylene carbons showed clear upwards tendency. The T_2 relaxation time of methyl carbon in the isopropyl group increased with temperature below the corresponding LCST of each polymer. A faster T_2 relaxation mode is detected for methyl carbon in the telechelic polymer solutions after the phase transition of PIPOZ, with a typical ^{13}C T_2 relaxation time in the range 10–50 ms as shown in **Figure 5.9b-c**. In the N_3PIPOZ solution before the phase transition, longer ^{13}C T_1 values were observed for the side chain methine and methyl carbons than the main chain methylene carbons due to faster motions of the former. However, in the FPIPOZ and C_{18}PIPOZ solutions, a great increase of ^{13}C T_1 for the main chain methylene carbons was obtained, while the ^{13}C T_1 values for the side chain methine and methyl carbons decreased only slightly.

The increase of the ^{13}C T_2 values of all three chemical groups with temperature, confirmed that these chemical groups in the polymer poor phase experience a speeding up process upon increasing temperature after the phase transition. A second component of methyl carbons with short T_2 appeared for all three polymers at a certain temperature,

indicating a less mobile part of the methyl group in the aggregated polymer chains which enabled the detection of the polymers in both "solid" like and "liquid" like states. The ^{13}C T_2 values of side chain methine and methyl carbons were greatly decreased for the telechelic polymer, compared with that of N_3PIPOZ, an indication of a decreased mobility of the side chain in a constrained structure. However, the ^{13}C T_2 values of the main chain methylene carbons do not change much before and after end group modification in solutions below phase transition temperature. **Figure 5.10** shows an example of the comparison of the ^{13}C T_1 and T_2 relaxation times of CH_3 groups between the three polymers. No noticeable difference was observed between the fluorocarbon and hydrocarbon modified telechelics.

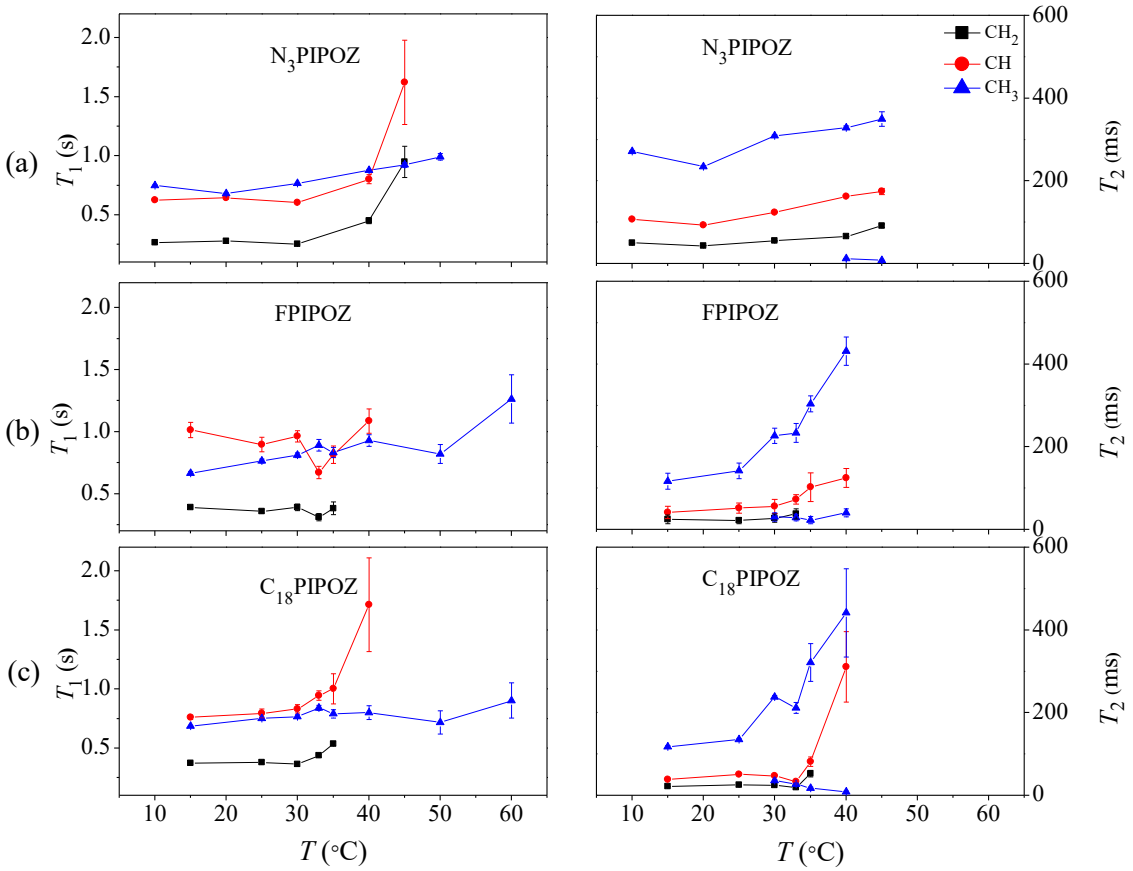

Figure 5.9 ^{13}C NMR T_1 (left) and T_2 (right) times of N_3PIPOZ (a), FPIPOZ (b) and C_{18}PIPOZ (c) in D_2O solutions ($C_{polymer}$ = 10 g·L^{-1}) as a function of temperature.

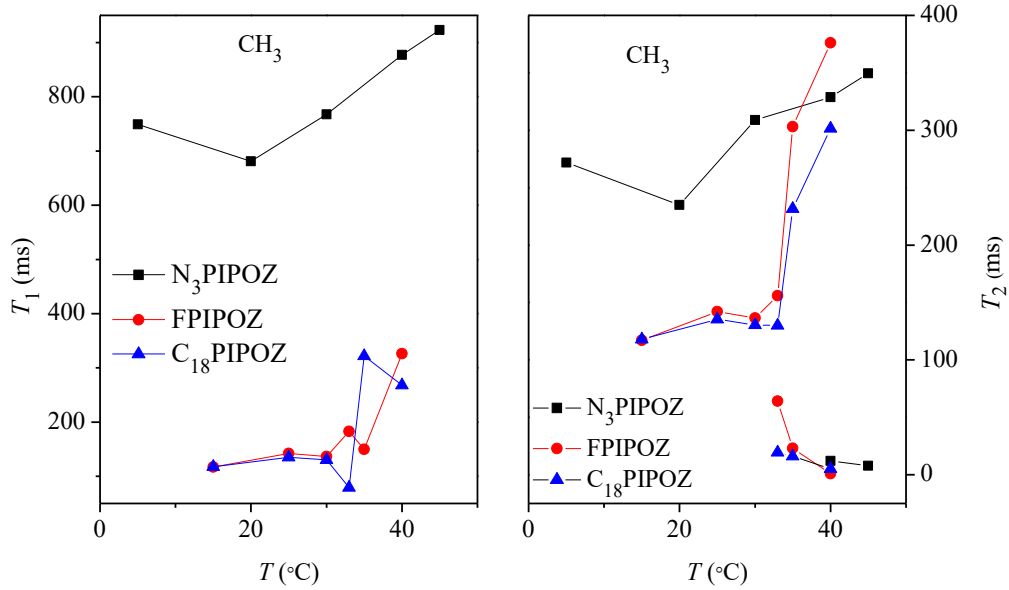

Figure 5.10 ^{13}C NMR T_1 (left) and T_2 (right) times of CH_3 in N_3PIPOZ, FPIPOZ and C_{18}PIPOZ D_2O solutions ($C_{polymer}$ = 10 g·L^{-1}) at different temperatures.

5.3.4 ^{19}F NMR spectra of the FPIPOZ in D_2O solutions

To investigate the assembly behaviour of the hydrophobic end groups, we recorded the ^{19}F NMR spectra of the FPIPOZ in D_2O and monitored the temperature dependence of the ^{19}F relaxation behaviour of the fluorinated end groups. **Figure 5.11** presents the ^{19}F NMR spectra of telechelic FPIPOZ in D_2O with polymer concentration 10 g·L^{-1}. The resonance peaks were assigned following Preuschen et al.[19] The chemical shift of ^{19}F in CF_3 shifted to lower field when temperature increased, accompanied by the line shape broadening and intensity decrease. A shift of 1.55 ppm for the CF_3 peak was observed at 70 ºC. The normalized peak area of ^{19}F at different positions of the end group is plotted against temperature. It showed a convex curvature (**Figure 5.12**). After reaching a minimum (40 ºC for CF_3 and 35 ºC for the other CF_2), the peak areas slowly increased upon further increase of the temperature. The temperature region 30–35 ºC corresponds to the area where the PIPOZ backbone goes through a demixing process exhibiting big changes in the ^{1}H T_1 and T_2 relaxation rates. When temperature goes beyond 35 ºC, the ^{19}F peak intensity increases again, indicating a reduced shielding effect of the dehydrated corona of the FPIPOZ micelles at this temperature region. As previously found out by ^{1}H NMR studies, the FPIPOZ chains do change their conformations above LCST although no crystallization is observed in water solutions above

60 ºC. The increase of the ^{19}F signal after the steep decrease must be a combined action of the fluorophilic property of the end groups and reordering of the PIPOZ backbone.

The association behaviour of the fluorinated end groups was studied by monitoring the ^{19}F T_1 and T_2 relaxation times of the fluorinated end groups. **Figure 5.13** shows the ^{19}F T_1 and T_2 relaxation times as a function of temperature. The ^{19}F T_1 relaxation time of CF_3 group increases with temperature. ^{19}F T_1 relaxation time of CF3 (F1) in D2O solution with higher concentration was slightly larger than that in dilute solutions. The ^{19}F T_2 relaxation times of the F4, F2/3 decrease with temperature and T_2 of F1 increase slightly above 60 ºC. The decrease of ^{19}F T_2 relaxation time could be explained by the difference in the packing density inside a micelle core and in dehydrated aggregates. Between the fluorine atoms in the end group, the ones in the CF_3 groups experienced the biggest decrease of the ^{19}F T_2 relaxation time and signal intensity. For one thing, the CF_3 terminal group has larger mobility. On the other hand, fluorinated alkyl chains have less rotational freedom due to the bulky fluorine atoms at neighbouring carbon.

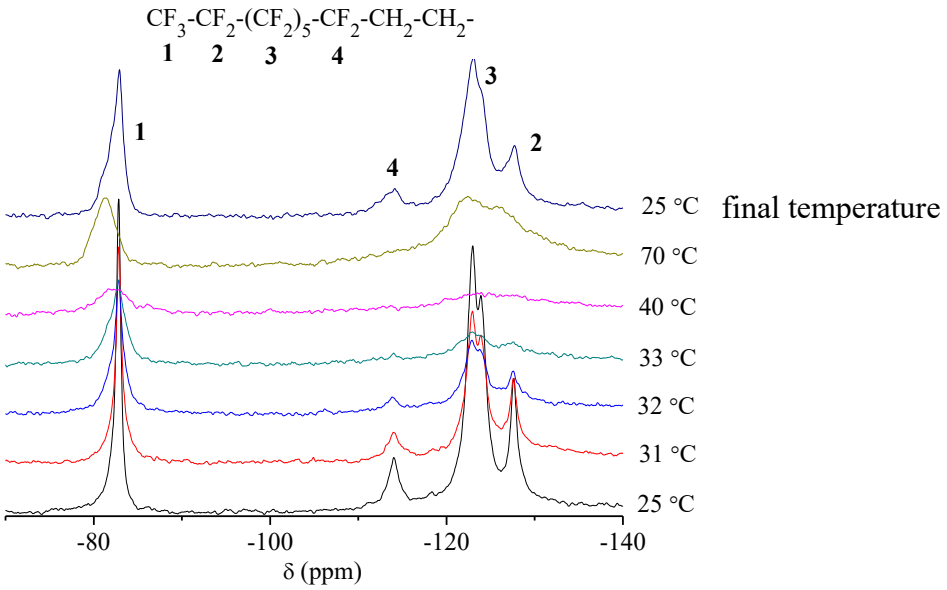

Figure 5.11 ^{19}F NMR spectra of telechelic FPIPOZ in D_2O ($C_{polymer}$ = 10 g·L^{-1}).

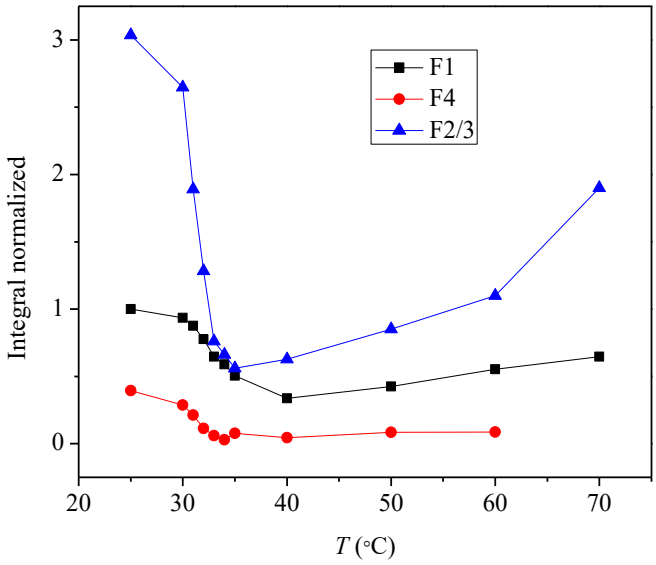

Figure 5.12 Integrals of peaks in the ^{19}F NMR spectra of telechelic FPIPOZ in D_2O ($C_{polymer}$ = 10 g·L^{-1}).

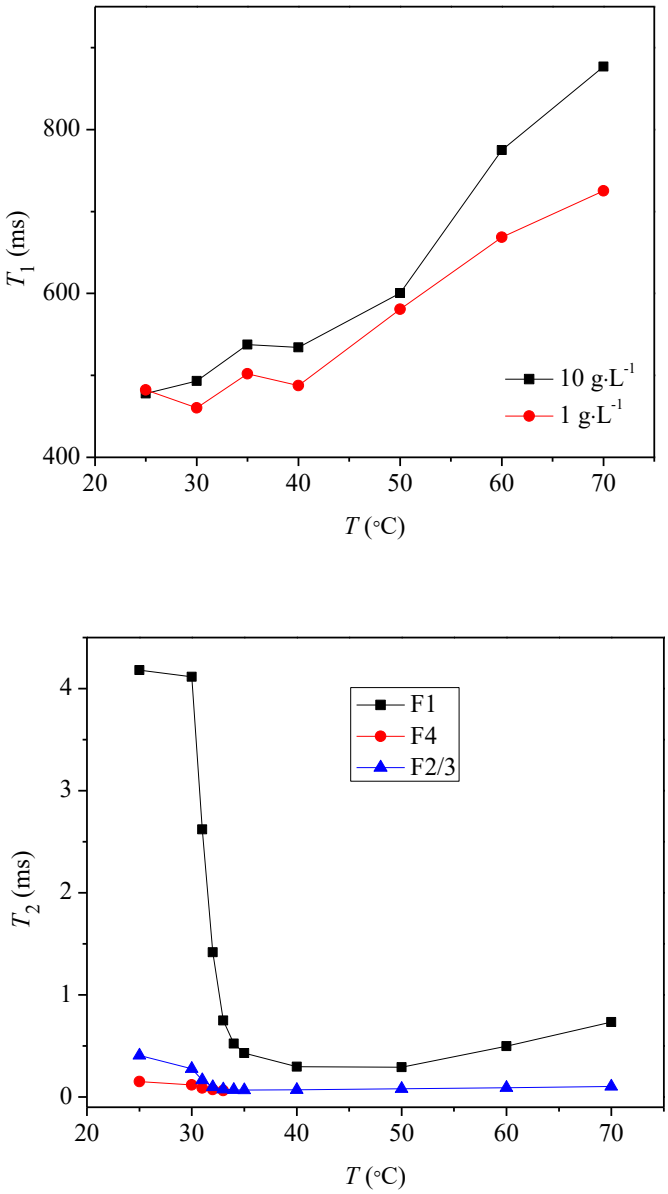

Figure 5.13 ^{19}F NMR T_1 of CF_3 and T_2 of fluorinated end groups for FPIPOZ in D_2O solutions ($C_{polymer}$ = 10 g·L^{-1}).

5.4 Conclusions

In this work, the conformation changes of polymers were monitored by ^{1}H NMR resonance intensity and T_1 and T_2 relaxation times, which is a convenient way to study molecular motions in polymer solutions. The ^{1}H T_1 relaxation of the main chain methylene

groups in N_3PIPOZ increases sharply at T_g and decreases slowly until reaching a stable value, which is not observed for telechelic FPIPOZ and C_{18}PIPOZ. The ^{1}H T_1 and T_2 of main chain methylene groups and the side chain methyl group exhibit opposite trend towards temperature, indicating different molecular motions in solutions. The association behavior of the telechelic polymers was studied by ^{13}C NMR and ^{19}F NMR as well. Carbon spectra are sensitive to changes in the chemical environment and thus a powerful way to study the structure changes of polymers. The assembly behavior of the telechelic polymer was studied by examining the solution behavior of the end groups in solution by ^{19}F NMR technique. ^{19}F NMR T_2 of perfluorodecyl group in FPIPOZ decreases from end to the middle of the polymer chain. Both the ^{19}F NMR spectra and the relaxation studies were proved to be a powerful way as a supplement to ^{1}H NMR routine.

5.5 References

1. Igumenova, T. I.; Frederick, K. K.; Wand, A. J. *Chem. Rev.* **2006,** 106, 1672-99.
2. Kay, L. E. *J. Magn. Reson.* **2005,** 173, 193-207.
3. Tokuhiro, T.; Amiya, T.; Mamada, A.; Tanaka, T. *Macromolecules* **1991,** 24, 2936-43.
4. Ohta, H.; Ando, I.; Fujishige, S.; Kubota, K. *J. Polym. Sci., Part B: Polym. Phys.* **1991,** 29, 963-8.
5. Zeng, F.; Tong, Z.; Feng, H. *Polymer* **1997,** 38, 5539-44.
6. Lu, C.-g.; Xu, K.; Li, W.-b.; Li, P.-c.; Tan, Y.; Wang, P.-x. *Chem. Res. Chin. Univ.* **2013,** 29, 1203-7.
7. Ru, G.; Feng, J. *J. Polym. Sci., Part B: Polym. Phys.* **2011,** 49, 749-55.
8. Yushmanov, P. V.; Furó, I.; Iliopoulos, I. *Macromol. Chem. Phys.* **2006,** 207, 1972-9.
9. Andersson, M.; Maunu, S. L. *Colloid Polym. Sci.* **2006,** 285, 293-303.
10. Xu, B.; Li, L.; Yekta, A.; Masoumi, Z.; Kanagalingam, S.; Winnik, M. A.; Zhang, K.; Macdonald, P. M.; Menchen, S. *Langmuir* **1997,** 13, 2447-56.
11. Preuschen, J.; Menchen, S.; Winnik, M. A.; Heuer, A.; Spiess, H. W. *Macromolecules* **1999,** 32, 2690-5.
12. Zhou, J.; Zhuang, D.; Yuan, X.; Jiang, M.; Zhang, Y. *Langmuir* **2000,** 16, 9653-61.
13. Hoang, K. C.; Mecozzi, S. *Langmuir* **2004,** 20, 7347-50.
14. Mathias, E. V.; Liu, X.; Franco, O.; Khan, I.; Ba, Y.; Kornfield, J. A. *Langmuir* **2007,** 24, 692-700.
15. Rzaev, Z. M. O.; Dinçer, S.; Pişkin, E. *Prog. Polym. Sci.* **2007,** 32, 534-95.
16. Filali, M.; Aznar, R.; Svenson, M.; Porte, G.; Appell, J. *J. Phys. Chem. B* **1999,** 103, 7293-301.
17. Diehl, C.; Černoch, P.; Zenke, I.; Runge, H.; Pitschke, R.; Hartmann, J.; Tiersch, B.; Schlaad, H. *Soft Matter* **2010,** 6, 3784.
18. Diez-Pena, E.; Quijada-Garrido, I.; Barrales-Rienda, J. M.; Wilhelm, M.; Spiess, H. W. *Macromol. Chem. Phys.* **2002,** 203, 491-502.

19. Preuschen, J.; Menchen, S.; Winnik, M. A.; Heuer, A.; Spiess, H. W. *Macromolecules* **1999,** 32, 2690-5.

5.6 Appendix

The ^{1}H NMR T_1 relaxation data of CH_2, CH and CH_3 protons of N_3PIPOZ, FPIPOZ and C_{18}PIPOZ in D_2O were presented in **Figure A5.1**, **Figure A5.2** and **Figure A5.3** respectively.

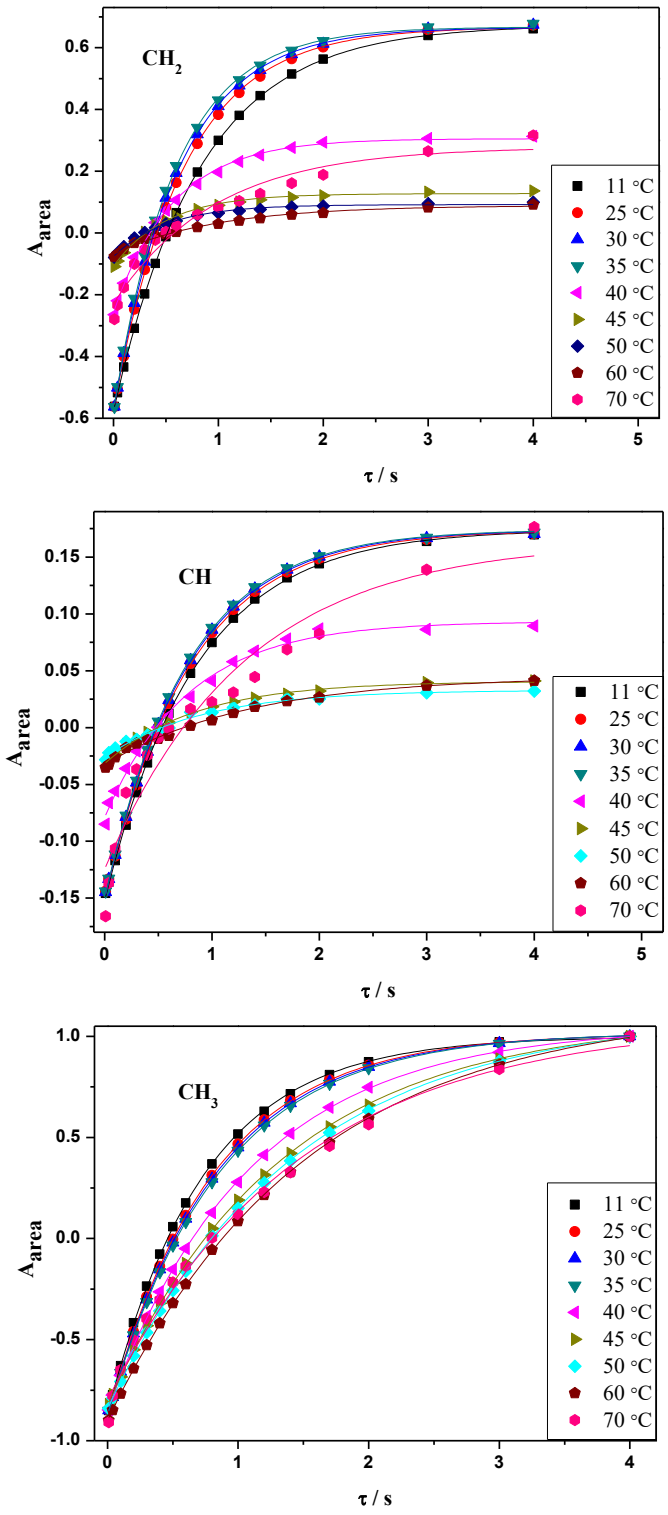

Figure A5.1 ^{1}H NMR T_1 relaxation decays of CH_2, CH and CH_3 of isopropyl acrylamide group of N_3PIPOZ in D_2O solution ($C_{polymer}$ = 10 g·L^{-1}) at different temperatures.

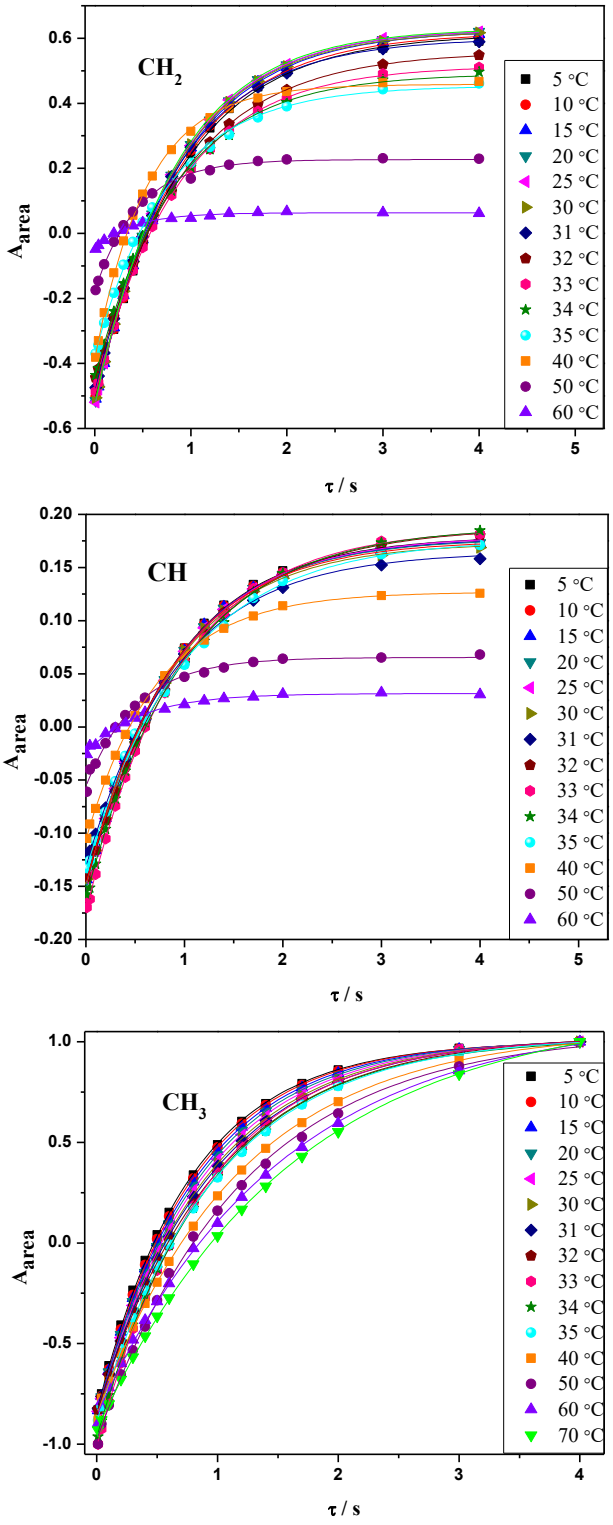

Figure A5.2 ^{1}H NMR T_1 relaxation decays of CH_2, CH and CH_3 of isopropyl acrylamide group of FPIPOZ in D_2O solution ($C_{polymer}$ = 10 g·L^{-1}) at different temperatures.

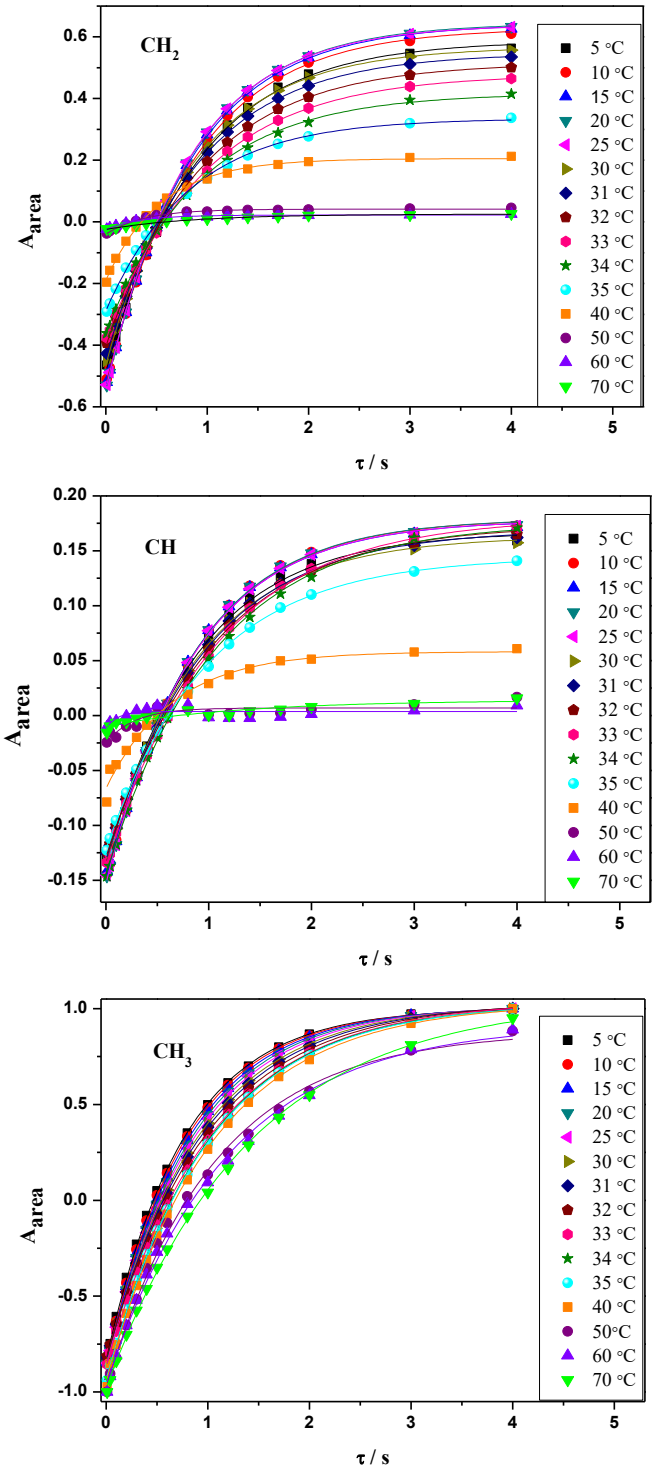

Figure A5.3 ^{1}H NMR T_1 relaxation decays of CH_2, CH and CH_3 of isopropyl acrylamide group of C_{18}PIPOZ in D_2O solution ($C_{polymer}$ = 10 g·L^{-1}) at different temperatures.

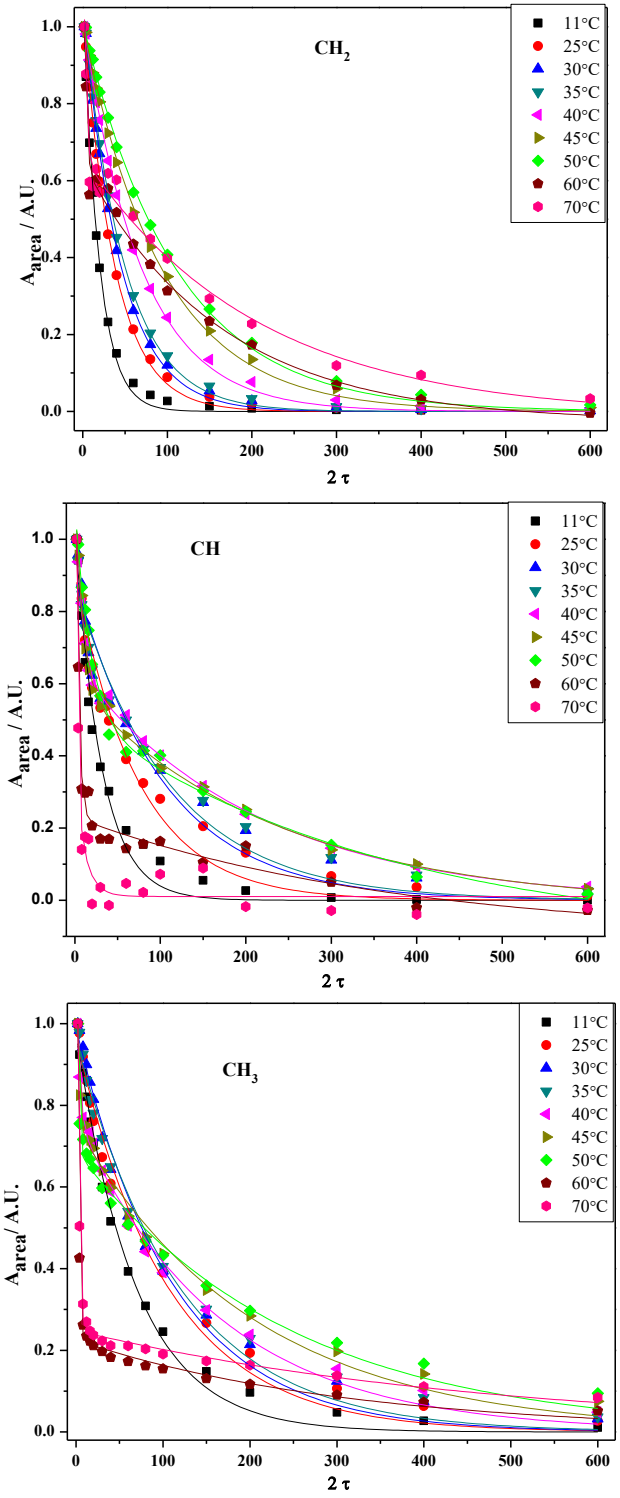

Figure A5.4 ^{1}H NMR T_2 relaxation decays of CH_2, CH and CH_3 of isopropyl acrylamide group of N_3PIPOZ in D_2O solution ($C_{polymer}$ = 10 g·L^{-1}) at different temperatures.

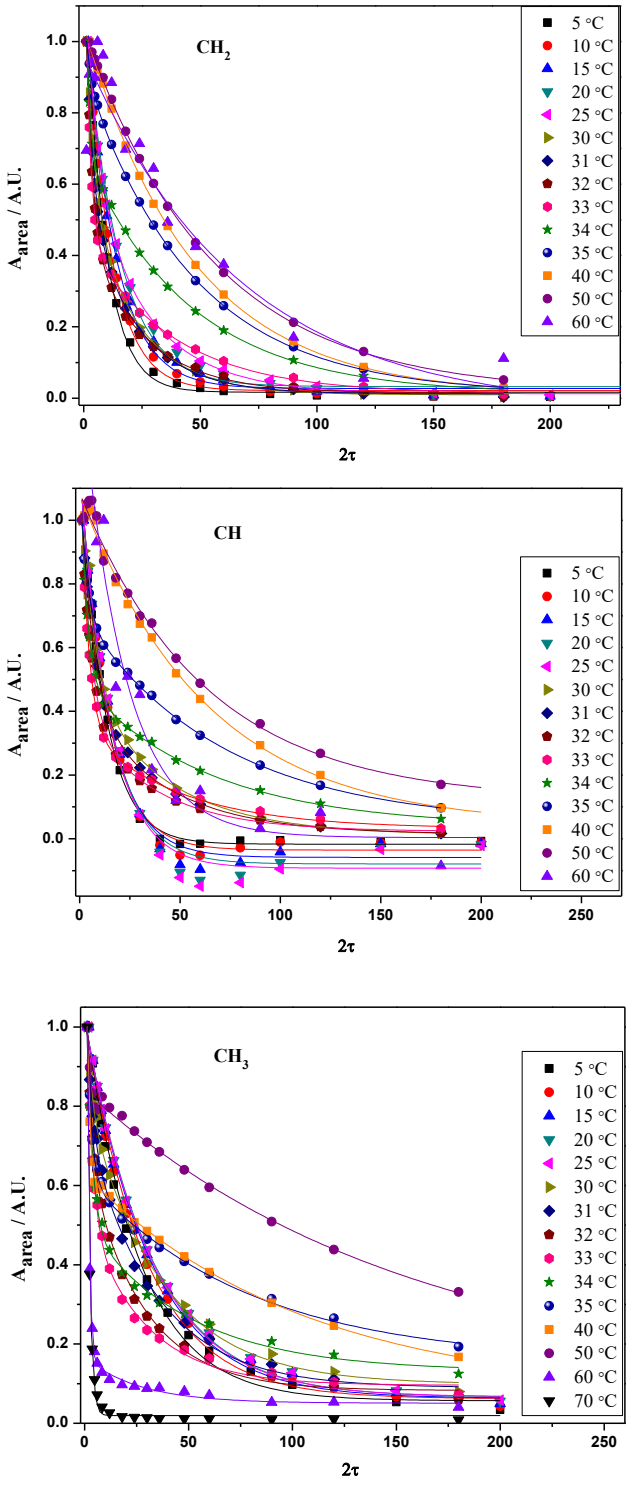

Figure A5.5 ^{1}H NMR T_2 relaxation decays of CH_2, CH and CH_3 of isopropyl acrylamide group of FPIPOZ in D_2O solution ($C_{polymer}$ = 10 g·L^{-1}) at different temperatures.

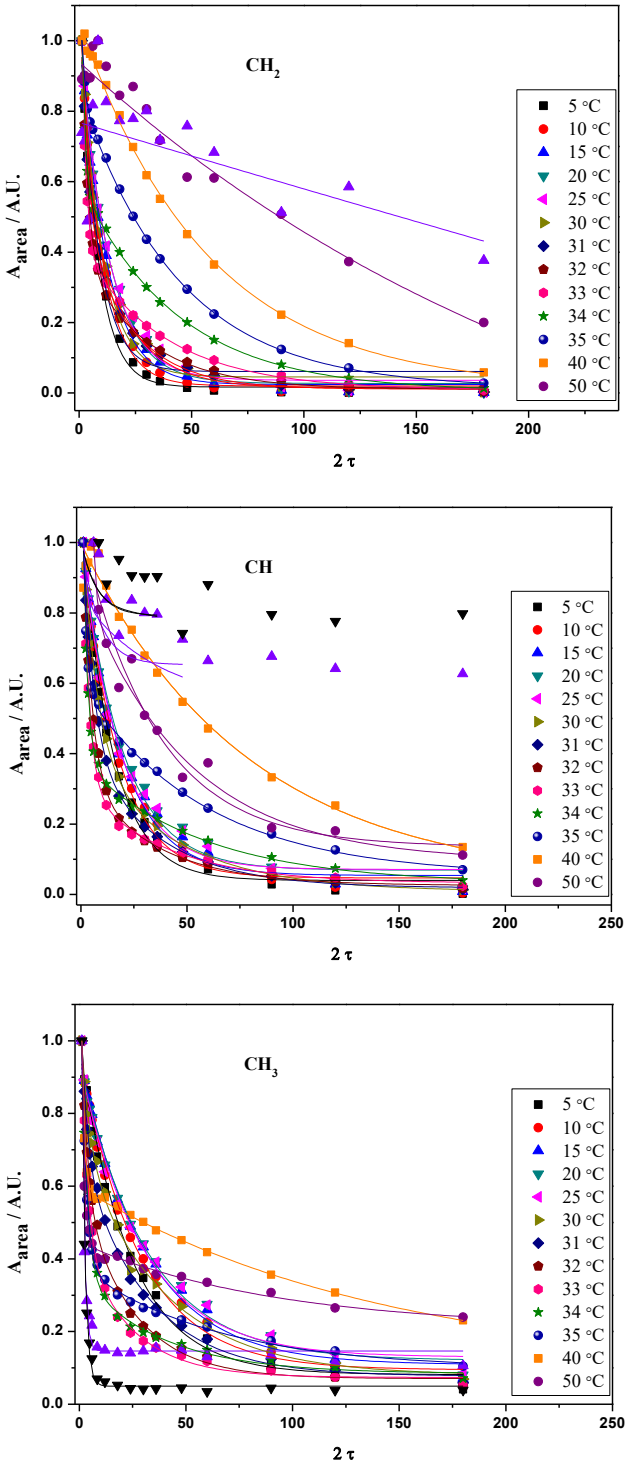

Figure A5.6 ^{1}H NMR T_2 relaxation decays of CH_2, CH and CH_3 of isopropyl acrylamide group of C_{18}PIPOZ in D_2O solution ($C_{polymer}$ = 10 g·L^{-1}) at different temperatures.

The ^{1}H NMR T_1 relaxation times for FPIPOZ and C_{18}PIPOZ determined in a solution with polymer concentration of 1.0 g·L^{-1} was shown in **Figure A5.7** and **Figure A5.8**. **Figure A5.9** and **Figure A5.10** presents the ^{1}H NMR T_2 relaxation times for FPIPOZ and C_{18}PIPOZ determined in a solution with polymer concentration of 1.0 g·L^{-1}.

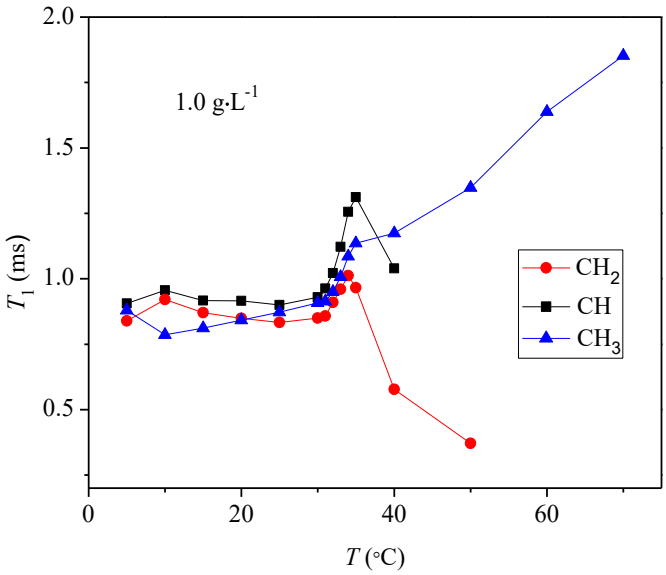

Figure A5.7 ^{1}H NMR T_1 relaxation times of CH_2, CH and CH_3 of isopropyl acrylamide groups of FPIPOZ in D_2O solution ($C_{polymer}$ = 1.0 g·L^{-1}) at different temperatures.

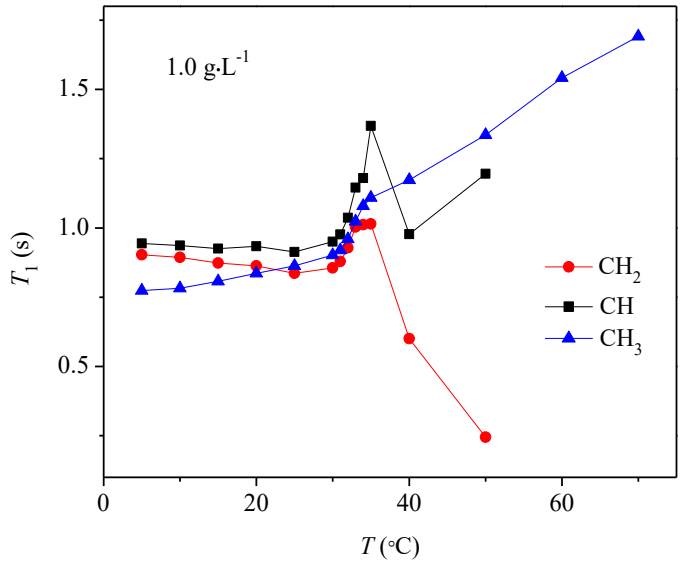

Figure A5.8 ^{1}H NMR T_1 times of CH_2, CH and CH_3 of isopropyl acrylamide groups of C_{18}PIPOZ in D_2O solution ($C_{polymer}$ = 1.0 g·L^{-1}) at different temperatures.

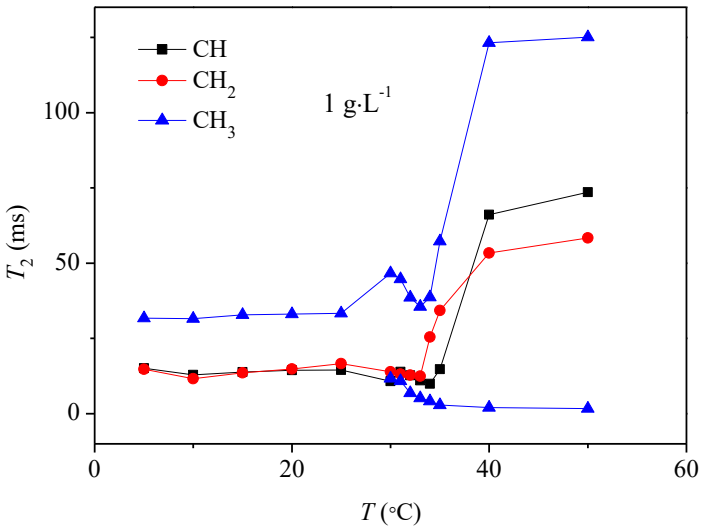

Figure A5.9 ^{1}H NMR T_2 times of CH_2, CH and CH_3 of isopropyl acrylamide groups of FPIPOZ in D_2O solution ($C_{polymer}$ = 1.0 g·L^{-1}) at different temperatures.

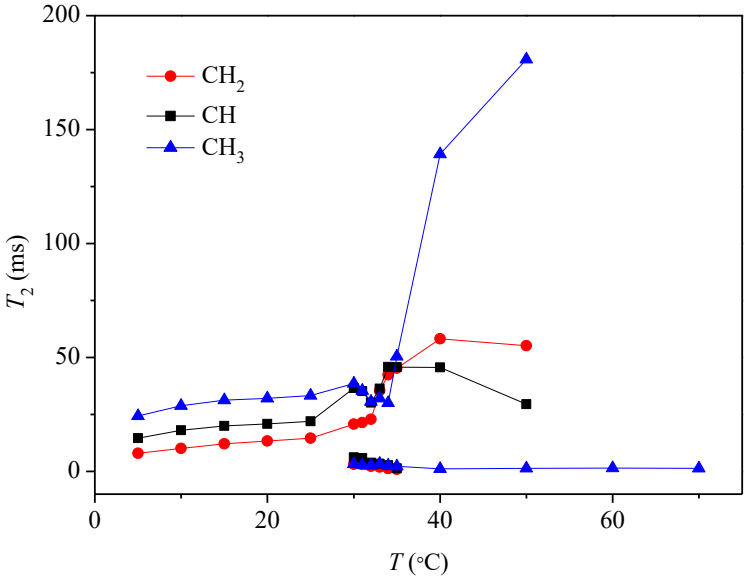

Figure A5.10 ^{1}H NMR T_2 times of CH_2, CH and CH_3 of isopropyl acrylamide groups of C_{18}PIPOZ in D_2O solution ($C_{polymer}$ = 1.0 g·L^{-1}) at different temperatures.

Time dependence of ^{1}H NMR T_1, T_2 at 60 ºC

To examine the effect of end group modification on the phase transition behaviour of PIPOZ, time dependent relaxation experiments were performed at 60 ºC for 1 day. ^{1}H T_1 and T_2 relaxation times of the main chain methylene groups and side chain methyl groups in N_3PIPOZ and FPIPOZ were determined as a function of time as shown in **Figure A5.11** and **Figure A5.12**. Significant changes of ^{1}H T_1 and T_2 values occurred for methyl and methylene protons in N_3PIPOZ incubated at 60 ºC for 2 h. T_1 values increased and T_2 values decreased until they reached a plateau. The changes began at a point where irreversible conformational change of PIPOZ (packing of aligned PIPOZ chains) is expected to start, accompanied by morphology changes (from liquid droplets to fiber meshes). In the case of FPIPOZ, no significant changes were observed for the T_1 and T_2 values of main chain methylene protons, indicating the packing of the PIPOZ segments was eliminated by introduction of end groups. The ^{1}H T_1 slightly decreased and T_2 increased with time in the beginning until equilibrium for the methyl groups in FPIPOZ.

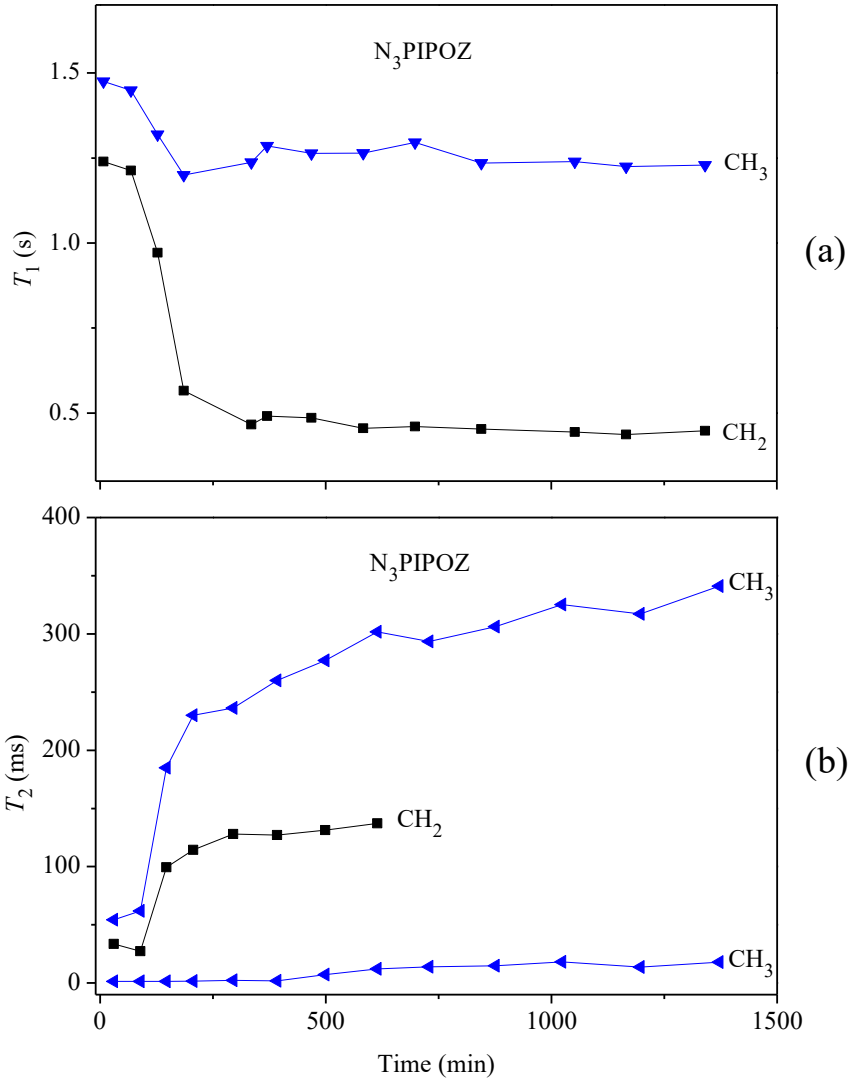

Figure A5.11 ^{1}H NMR T_1 (a), T_2 (b) times of N_3PIPOZ in D_2O solution ($C_{polymer}$ = 10 g·L^{-1}) at 60 ºC as a function of time.

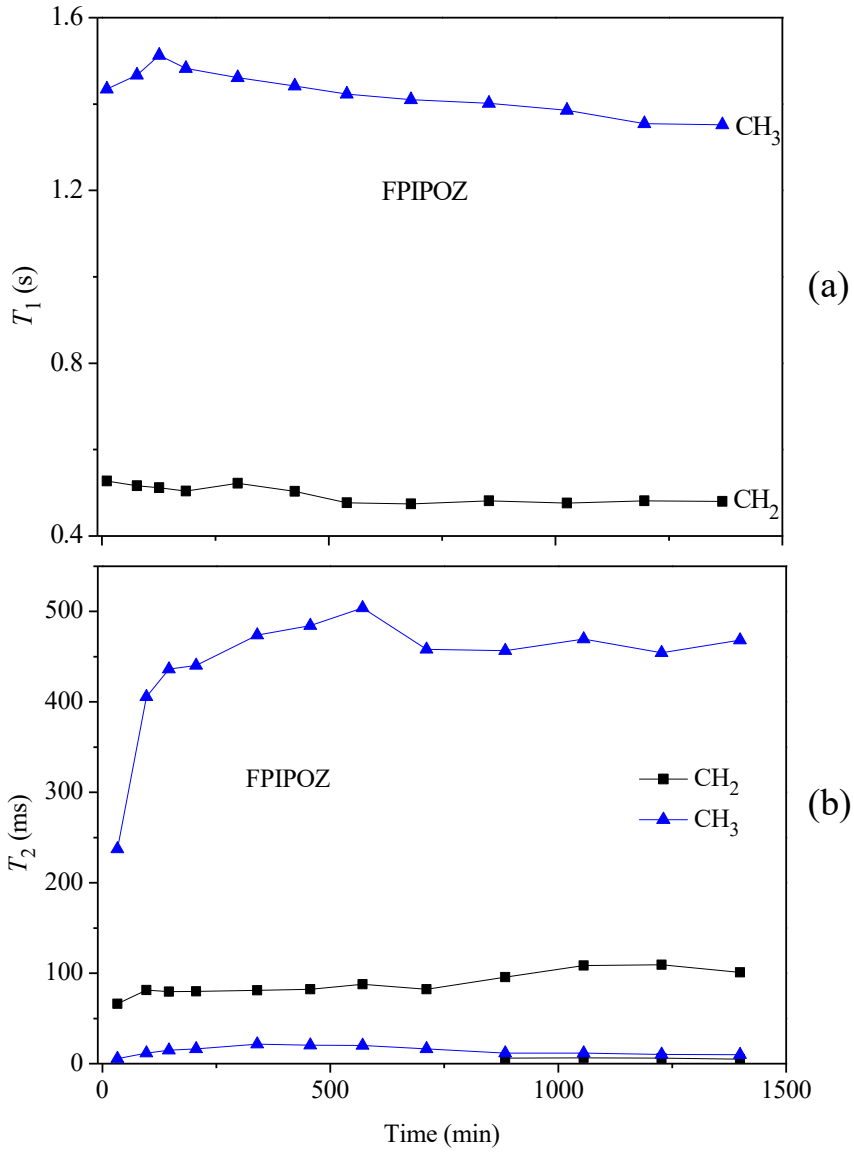

Figure A5.12 ^{1}H NMR T_1(a), T_2(b) relaxation times of FPIPOZ in D_2O solution with $C_{polymer}$ = 10 g·L^{-1} at 60 ºC as a function of time.

Chapter 6. Conclusions and future work

6.1 Conclusions

This thesis focused on the phase transition of two thermo-responsive polymers — PNIPAM and PIPOZ in water. The influences of an added water miscible solvent —methanol, the polymer concentration, and the polymer chain architecture have been studied. Moreover, the effect of end group modification of the polymer chain has been assessed by spectroscopic methods.

6.1.1 Influence of chain architetecture on the phase separation of PNIPAM

The coil-to-globule phase transition of PNIPAM in water has been extensively studied and different models were proposed to explain the phenomenon. Among them, most studies focused on linear PNIPAM. PNIPAM as a thermo-sensitive, smart material has many potential applications as thermosensor or surface coating material. There have been numerous reports on PNIPAM copolymers and PNIPAM grafted nanoparticles[1, 2] or surfaces, where the LCST values of PNIPAM changed because of the hydrophobic/hydrophilic balance or special chain architecture. It is thus important to understand how these factors influence the phase transition process of PNIPAM, so as to supply experimental bases for practical applications.

The effect of chain architecture on the phase transition behaviour of PNIPAM has been studied in Chapter 2 of this thesis. A series of 4-arm star-PNIPAM and linear-PNIPAM with identical end groups were synthesized. The T_c of PNIPAM was greatly depressed by attaching to a hydrophobic core. A reverse molecular weight dependence of T_c and a unimodal thermo phase transition were observed for the star-PNIPAMs, which suggested that no n-cluster formed in the star-PNIPAM. The strong *n*-cluster of PNIPAM segments in Liu's study,[3] was due to the high local chain density in the densely grafted 7-arm and 21-arm PNIPAM. The phase transition behavior of the star-PNIPAM was compared with its linear analogue quantitatively by determine the number of cooperative units $\boldsymbol{n}$ in a single chain. The $\boldsymbol{n}$ value for star PNIPAM was determined to be 0.66, which was higher than that for the "arm" and

lower than that for its linear analogue. The mediate value of ***n*** suggests a lower cooperativity in hydration for star PNIPAM over its linear analogue due to the constraint of the star structure, and a higher cooperativity than the short "arm" due to increased molecular weight. The effect of chain architecture on the hydration cooperativity was examined by comparing linear PNIPAM with cyclic PNIPAM. An n_{CU} value of 84 for *c*-PNIPAM (DP = 112) was obtained, indicating low degree of cooperativity for the *c*-PNIPAM. The large number of NIPAM segments per cooperative unit for star-PNIPAM and the "arm", described the required number of monomer units for a cooperative dehydration to happen. The lower degree of cooperativity in dehydration process for star-PNPAM and its "arm" PNIPAM was also obtained by the relatively flat curvatures of their phase diagrams in water/methanol mixtures.

As a summary, tethering PNIPAM chain to a hydrophobic core depresses the T_c of PNIPAM. The molecular weight effect plays an important role in tuning the T_c of PNIPAM. The lower degree of cooperativity in dehydration for star PNIPAM compared to the linear analogue of an arm with similar molecular weight is manifested by a rather flat phase diagram when methanol is added. The hydrophobic/hydrophilic end groups also affect the T_c to some extent.

6.1.2 Influence of polymer concentration on the phase separation of PNIPAM in water/methanol mixture

The LCST of PNIPAM in water was reported to decrease monotonically with an increase of PNIPAM concentration[4]. A slight molecular weight and concentration dependence of the LCST for linear PNIPAM in water has been reported.[5,6,7] In all these studies, stable suspensions were observed above the LCST of PNIPAM in water for polymer concentration up to 700 $g \cdot L^{-1}$. The phase transition of PNIPAM in water/methanol mixture has been widely studied, and turbid solutions have been observed above LCST. No one has studied systematically the stability of the PNIPAM/water/methanol mixture above LCST. In our previous study about the phase transition of a PNIPAM with n-butyl end groups (*n*Bu-PNIPAM), stable suspensions of the polymer/water/methanol mixtures were observed. What is the effect of concentration on the stability of the ternary system? What are the influencing factors? Chapter 3 addressed these questions using *n*Bu-PNIPAM as a model polymer, and

described their phase transition behavior in water/methanol mixtures. Macroscopic liquid-liquid phase separation (MLLPS) was observed for *n*Bu-PNIPAM with all studied molecular weight range (6–45 kDa) in solutions with polymer concentration of 10 $g \cdot L^{-1}$ or higher.

The MLLPS was affected by the end group of PNIPAM. No MLLPS was observed for PNIPAM bearing Cl groups at both ends. Stable suspensions were observed for months in case of Cl-PNIPAM. However, for a PNIPAM with molecular weight 180 $kg \cdot mol^{-1}$ prepared by standard radical polymerization and a PNIPAM bearing NH_2 at both ends, MLLPS was observed in polymer/water/methanol mixtures. The MLLPS was not affected by the dispersity of samples. The MLLPS of PNIPAM180K happened in a narrow solvent composition region than that of *n*Bu-PNIPAM.

The compositions of both phases after MLLPS of *n*Bu-PNIPAM45K methanol/water solutions were measured by ^1H NMR. And the condensed phase is found to be polymer rich phase and water rich phase. Optical microscopy studies of the *n*Bu-PNIPAM45K methanol/water solutions with different methanol fractions reveals that droplets of different sizes form in the condensed phase after MLLPS. In the mixture with methanol molar fraction of 0.3, droplets coalesce and large droplets of hundreds of microns in diameter were observed in the capillary. For the PNIPAM180K, a network of the condensed phase was observed. The stability of the *n*Bu-PNIPAM after MLLPS was tested and the mixtures behaved differently depending on methanol composition. As a summary, addition of methanol increases the surface tension of droplets, leading to enhanced coalescence of droplets. By increasing the polymer concentration in the ternary mixture, effective collision between droplets is increased. So MLLPS happens when the polymer concentration is above a threshold value, and the methanol volume fraction is in the two phase region.

6.1.3 Influence of end group properties on the phase separation of PIPOZ in water

The phase transition of PIPOZ in water occurs at a higher temperature compared to its structural isomer, PNIPAM. The lower degree of chain hydration, due to the inefficient hydrogen bonding with water for the tertiary amine in the PIPOZ main chain which acts only

as a proton receptor, is reflected by the lower phase transition enthalpy change of PIPOZ compared with that for PNIPAM.

A commonly used method to tune the phase transition temperature of PNIPAM or PIPOZ is hydrophobic modification. In this thesis, we functionalized the PIPOZ chains by attaching either alkyl groups or fluorinated alkyl groups to the chain ends. The LCST of PIPOZ was reduced after end group modification as shown in Chapter 4. The end capped PIPOZs, named here FPIPOZ and C_{18}PIPOZ, self-assembled into stable micelles in aqueous solutions, as revealed by LS and TEM measurements. We studied the association process and thermo responses of the FPIPOZ and C_{18}PIPOZ in water and found that: 1) Monomodal size distribution of micelles for both the FPIPOZ and C_{18}PIPOZ in water in the concentration range of 1–10 $g \cdot L^{-1}$; 2) The association process of the two telechelic polymers follows a closed-association model; 3) Liquid-liquid phase separation occurs above the LCST. Larger droplets were observed in phase separated solutions of FPIPOZ, compared to that observed in the C_{18}PIPOZ solution, possibly due to the fluorophilic properties of the former. **Scheme 6.1** represents the phase separation process for the two telechelic polymers in water.

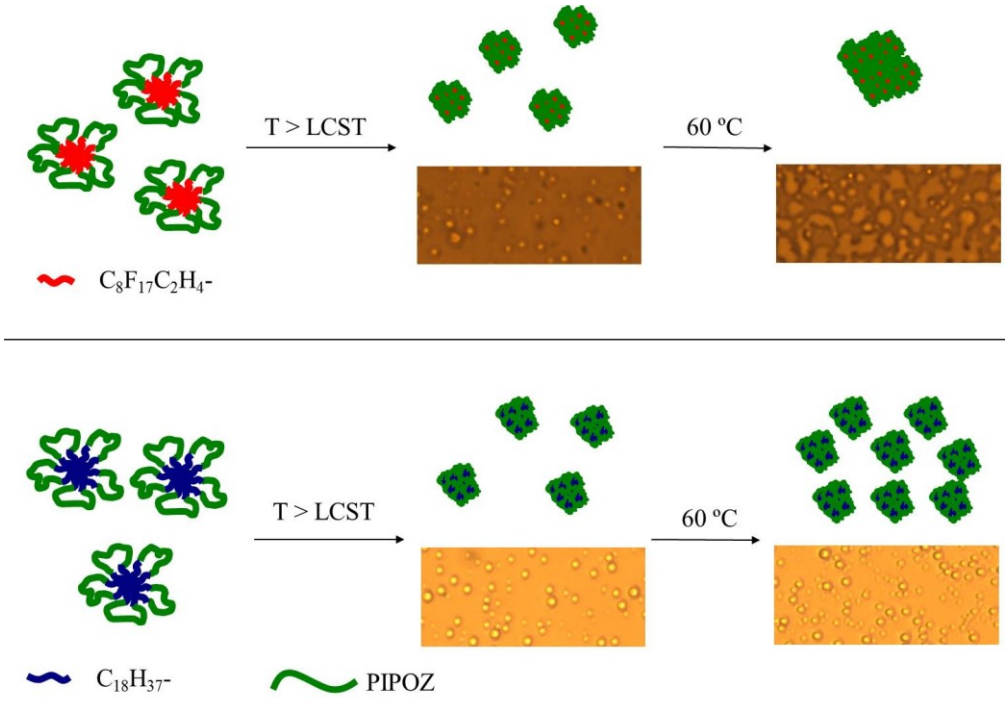

Scheme 6.1 Phase separation of FPIPOZ and C_{18}PIPOZ aqueous solutions.

A lower degree of cooperativity for the dehydration of PIPOZ was observed compared with PNIPAM. The number of monomers per cooperative unit n_{CU} is 78, much lower than that for PNIPAM ~100. So, it is not surprising to see the monotonic increase of LCST with methanol composition in the PIPOZ/water/methanol mixture as shown in **Figure 6.1**. No cononsolvency is observed for PIPOZ in water/methanol mixture. As we already concluded in Chapter 2, PNIPAM with a low n_{CU} value or too short chain exhibits rather flat phase diagram in polymer/water/methanol system.

The phase separation of PIPOZ in water is irreversible if the solution is heated for long time (more than 2 hours) as reported by Schlaad et al.[8] The chain conformation changes from a mixture of gauche and trans to all trans during the heating process. Prolonged heating results in crystallization of PIPOZ. In Chapter 5, we studied the conformation changes of N_3PIPOZ and telechelic FPIPOZ and C_{18}PIPOZ in D_2O by NMR spectroscopy and T_1 and T_2 relaxation technique.

The ^{1}H T_1 and T_2 of the main chain methylene groups and the side chain methyl groups in FPIPOZ and C_{18}PIPOZ exhibited opposite tendencies towards temperature, indicating different molecular motions. The ^{1}H T_1 relaxation of the main chain methylene groups in N_3PIPOZ increases sharply at T_g (glass transition temperature) and decreases slowly until reaching a stable value. No such observation was recorded for telechelic FPIPOZ and C_{18}PIPOZ, indicating no crystallization in the aqueous solutions of the two telechelic polymers. The ^{13}C T_2 values of side chain methine and methyl carbons were greatly decreased for the telechelic polymer compared with N_3PIPOZ, an indication of the decreased mobility of the side chain in a constrained structure. However, the ^{13}C T_2 value of the main chain methylene carbons does not change much before and after end group modification in solutions below phase transition temperature, which suggests that the mobility of the main chain carbons are affected by the assembly of the telehelic polymers. The assembly behavior of the telechelic polymer was studied by examining the changes in motions of the end groups by ^{19}F NMR technique. ^{19}F T_2 of fluorine in FPIPOZ varied depend on the position of the fluorine on the carbon chain. The ^{19}F, ^{1}H and ^{13}C NMR spectroscopy and the relaxation technique were proved to be a powerful to analyze the properties of the polymer on a molecular level.

6.2 Future work

The macroscopic liquid-liquid phase separation of PNIPAM in methanol/water mixture has been observed in semi-dilute solutions in the current work. Whether or not the macroscopic liquid-liquid phase separation will also happen to PNIPAM in other water miscible mixed solutions remains to be tested. Detection of the concentration and temperature limit of the MLLPS was necessary to construct a complete 3D phase diagram of PNIPAM in cononsolvent mixtures. Such a study would help to understand the governing mechanism during the MLLPS. The properties of end group have been shown to affect the stability of the demixed suspensions of PNIPAM/water/methanol. As we know, the long hydrophobic end groups of PNIPAM induce the formation of micelles in aqueous solution. What is the phase diagram of PNIPAM bearing long alkyl end groups in the water/methanol mixture? The effect of the length of end groups and hydrophobicity on the MLLPS process of PNIPAM in mixed solvents needs to be studied for a better understanding of the phenomenon.

No cononsolvency was observed for PIPOZ homopolymer. And no cononsolvency was reported for poly(*N*, *N*-diethylacrylamide) either. However, we observed a significant decrease of the LCST for telechelic FPIPOZ in water/methanol mixture as shown in **Figure 6.1**. The cononsolvency seems to be affected not only by the terminology of nitrogen, but also the structure of the thermo-sensitive polymer chain. The phase separation of the telechelic PIPOZ/water/methanol mixtures will help to clarify the determinant factors of the phase separation of polyacrylamide in mixed solvent, taking into account of the hydrophobicity of end groups and properties of different water-miscible solvents. Whether the MLLPS happens to telechelic PIPOZ under certain condition? A study of the stability of the phase separated telechelic PIPOZ/water/methanol mixtures will help to gain a comprehensive understanding of the phase separation of the two structural isomers (PNIPAM and PIPOZ).

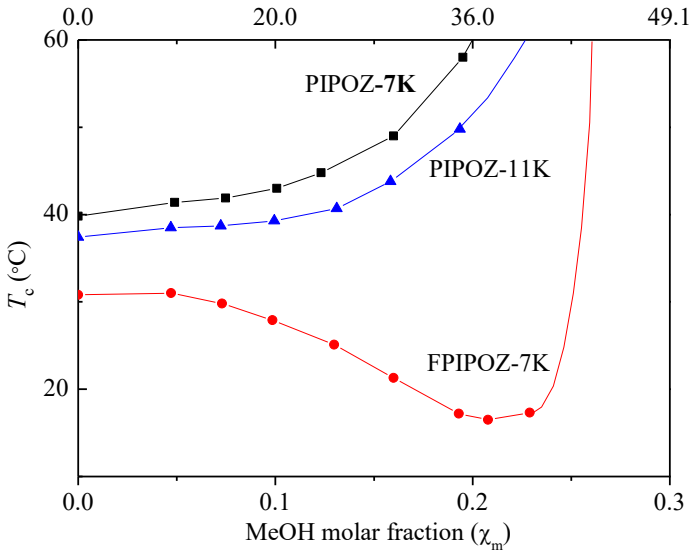

Figure 6.1 Phase diagram of N_3PIPOZ-7K, N_3PIPOZ-11K, and FPIPOZ-7K in water/methanol mixtures ($C_{polymer}$ = 1.0 g·L^{-1}) as a function of methanol molar fraction.

The effect of star shape chain architecture has been studied in this thesis with a 4-arm star-PNIPAM. No n-cluster was observed in this polymer, unlike in the reported 7-arms and 21-arms PNIPAM tethered to a β-CD core. The n-cluster formation was claimed to be caused by high local chain density in the 7-arms and 21-arms PNIPAM. To verify the proposition and examine the phase transition behavior of PNIPAM, star shape PNIPAMs with various arms are necessary.

NMR relaxation technique has been proved to be an efficient way to monitoring the chain segment motions in solutions. Future studies of polymer solutions may consider employing NMR spectroscopy.

6.3 References.

1. Shan, J.; Chen, J.; Nuopponen, M.; Tenhu, H. *Langmuir* **2004,** 20, 4671-6.
2. Shan, J.; Tenhu, H. *Chemi. Commun.* **2007**, 4580-98.
3. Xu, J.; Liu, S. *J. Polym. Sci., Part A: Polym. Chem.* **2009,** 47, 404-19.
4. Wohlfarth, C., *Thermodynamic Data of Coploymer Solutions*. CRC: Boca Raton, FL, 2000.
5. Tong, Z.; Zeng, F.; Zheng, X.; Sato, T. *Macromolecules* **1999,** 32, 4488-90.
6. Otake, K.; Inomata, H.; Konno, M.; Saito, S. *Macromolecules* **1990,** 23, 283-9.
7. Van Durme, K.; Van Assche, G.; Van Mele, B. *Macromolecules* **2004,** 37, 9596-605.

8. Demirel, A. L.; Meyer, M.; Schlaad, H. *Angew. Chem. Int. Ed.* **2007,** 46, 8622-4.